UNIVERSIDADE DE SÃO PAULO
Instituto de Ciências Matemáticas e de Computação

Machine learning and complex network approaches for mental disorder classification

Loriz Francisco Sallum

Tese de Doutorado do Programa Interinstitucional de Pós-Graduação em Estatística (PIPGEs)

ICMC USP SÃO CARLOS

Loriz Francisco Sallum

Machine learning and complex network approaches for mental disorder classification

Thesis submitted to the Institute of Mathematics and Computer Science – ICMC-USP and to the Department of Statistics – DEs-UFSCar – in accordance with the requirements of the Statistics Interagency Graduate Program, for the degree of Doctor in Statistics. *FINAL VERSION*

Concentration Area: Statistics

Advisor: Prof. Dr. Francisco Aparecido Rodrigues
Co-advisor: Dra. Caroline Lourenço Alves

USP – São Carlos
July 2025

Ficha catalográfica elaborada pela Biblioteca Prof. Achille Bassi
e Seção Técnica de Informática, ICMC/USP,
com os dados inseridos pelo(a) autor(a)

S169m

Sallum, Loriz Francisco
Machine learning and complex network approaches for mental disorder classification / Loriz Francisco Sallum; orientador Francisco Aparecido Rodrigues; coorientadora Caroline Lourenço Alves. -- São Carlos, 2025.
206 p.

Tese (Doutorado - Programa Interinstitucional de Pós-graduação em Estatística) -- Instituto de Ciências Matemáticas e de Computação, Universidade de São Paulo, 2025.

1. Redes complexas. 2. Aprendizado de maquina. 3. Diagnostico automático. 4. Transtornos mentais. I. Rodrigues, Francisco Aparecido, orient. II. Alves, Caroline Lourenço, coorient. III. Título.

Bibliotecários responsáveis pela estrutura de catalogação da publicação de acordo com a AACR2:
Gláucia Maria Saia Cristianini - CRB - 8/4938
Juliana de Souza Moraes - CRB - 8/6176

Loriz Francisco Sallum

Abordagens de aprendizado de máquina e redes complexas na classificação de transtornos mentais

Tese apresentada ao Instituto de Ciências Matemáticas e de Computação – ICMC-USP e ao Departamento de Estatística – DEs-UFSCar, como parte dos requisitos para obtenção do título de Doutora em Estatística – Programa Interinstitucional de Pós-Graduação em Estatística. *VERSÃO REVISADA*

Área de Concentração: Estatística

Orientador: Prof. Dr. Francisco Aparecido Rodrigues
Coorientador: Dra. Caroline Lourenço Alves

USP – São Carlos
Julho de 2025

UNIVERSIDADE FEDERAL DE SÃO CARLOS

Centro de Ciências Exatas e de Tecnologia
Programa Interinstitucional de Pós-Graduação em Estatística

Folha de Aprovação

Defesa de Tese de Doutorado da candidata Loriz Francisco Sallum, realizada em 30/05/2025.

Comissão Julgadora:

Prof. Dr. Francisco Aparecido Rodrigues (USP)

Prof. Dr. João Luis Garcia Rosa (USP)

Prof. Dr. Thomas Kauê Dal'Maso Peron (USP)

Profa. Dra. Angélica Nardo Caseri (USP)

Prof. Dr. Eduardo Ponde de Sena (UFBA)

O Relatório de Defesa assinado pelos membros da Comissão Julgadora encontra-se arquivado junto ao Programa Interinstitucional de Pós-Graduação em Estatística.

ACKNOWLEDGEMENTS

I would like to express my deepest gratitude to my supervisor, Prof. Dr. Francisco Aparecido Rodrigues, for his valuable guidance, patience, and support throughout my PhD journey. I am truly grateful for the opportunity to be part of his research group, where I have grown both academically and professionally. His insightful opinions and continuous encouragement have been fundamental in this work. Beyond the academic sphere, I deeply appreciate his human side—his understanding of the moments of stress and anxiety that inevitably come with this journey and his ability to provide reassurance and help me regain balance during challenging times.

I am also immensely grateful to my co-supervisor, Dra. Caroline Lourenço Alves, whose support has been essential throughout this work and beyond. Despite being in a different time zone and managing many responsibilities, she always found time to discuss results, provide thoughtful feedback, and offer her friendship. Her guidance has been essential not only for this research but also in my academic and professional path, and I am deeply grateful for her support and mentorship.

I would also like to thank the professors I had during my PhD for sharing their knowledge and for their patience in answering my questions.

I am also immensely thankful to my friends from the PhD program, who have made this journey more enriching and bearable. The discussions, shared frustrations, and moments of laughter have been a source of motivation and strength.

I also want to express my gratitude to the employees of ICMC/USP and DEs/UFSCar, who were always willing to help, promptly answering my questions and providing assistance whenever needed.

I want to express my sincere gratitude to my parents, who have always been by my side, no matter what. Their unconditional love, support, and belief in me have been a foundation of strength throughout this journey.

I am profoundly grateful to my husband, Éder, for his love, patience, and encouragement. Even in the face of difficult times, he has always stood by my side, offering strength and support to help me keep going and not lose motivation.

Also, a special thanks to my beloved cat, Maia, for being my constant companion through long nights of writing and research. Her presence, warmth, and occasional interruptions provided comfort and moments of joy during long working hours.

Finally, I would like to thank my financial support, Coordenação de Aperfeiçoamento de Pessoal de Nível Superior - Brasil (CAPES) - 88887.645667/2021-00, for making this research possible. This support has been crucial in allowing me to fully dedicate myself to my studies and complete this work.

RESUMO

SALLUM, L. F. **Abordagens de aprendizado de máquina e redes complexas na classificação de transtornos mentais**. 2025. 206 p. Tese (Doutorado em Estatística – Programa Interinstitucional de Pós-Graduação em Estatística) – Instituto de Ciências Matemáticas e de Computação, Universidade de São Paulo, São Carlos – SP, 2025.

A ciência de redes complexas emergiu como uma ferramenta poderosa para estudar a organização estrutural e funcional do cérebro, tanto em condições normais quanto em contextos patológicos. Recentemente, métodos baseados em redes complexas têm sido amplamente utilizados para entender como os transtornos mentais e do neurodesenvolvimento influenciam a organização cerebral e alteram sua funcionalidade. A integração entre teoria dos grafos, técnicas de neuroimagem funcional e métodos computacionais possibilita a reconstrução de redes cerebrais e contribui para a compreensão dos impactos de diferentes transtornos em nível individual. Além disso, avanços no diagnóstico automatizado utilizando aprendizado de máquina têm demonstrado resultados promissores na previsão e caracterização de diversos transtornos a partir da análise da conectividade funcional derivada de séries temporais de atividade cerebral. Este projeto tem como objetivo classificar diferentes transtornos mentais por meio da reconstrução de redes complexas a partir de séries temporais extraídas de dados de neuroimagem. Busca-se avaliar qual métrica de conectividade é mais adequada para a reconstrução da topologia da rede cerebral associada a diferentes transtornos mentais, assim como a que apresenta a melhor performance na classificação. Modelos de aprendizado de máquina foram utilizados para analisar matrizes de conectividade funcional com o intuito de caracterizar a topologia cerebral associada a cada condição e identificar padrões específicos na conectividade da rede. Para o transtorno depressivo maior (TDM), a correlação de Spearman foi a métrica mais adequada para reconstrução da rede cerebral. Os resultados sugerem que alterações na conectividade estão relacionados com déficits em atenção, memória e tomada de decisão. Para o transtorno do espectro autista (TEA) e transtorno do déficit de atenção e hiperatividade (TDAH), a transferência de entropia foi utilizada para construir a matriz de conectividade, revelando padrões alterados em regiões do cérebro associadas à atenção e controle dos impulsos no TDAH, e a comprometimento de áreas sociais e cognitivas no TEA. Padrões de conectividade cerebral foram analizados para entender a progressão da doença de Parkinson (DP). Nos estágios iniciais, os padrões foram semelhantes aos de indivíduos saudáveis, enquanto nos estágios avançados, observou-se uma redução na sincronização entre regiões do cérebro. Assim, os resultados deste estudo colaboram para diagnósticos mais precisos e para a formulação de estratégias de intervenção personalizadas, promovendo avanços na compreensão e no tratamento dessas condições.

Palavras-chave: redes complexas, transtornos mentais, conectividade funcional, aprendizado de máquina, diagnóstico automático.

ABSTRACT

SALLUM, L. F. **Machine learning and complex network approaches for mental disorder classification**. 2025. 206 p. Tese (Doutorado em Estatística – Programa Interinstitucional de Pós-Graduação em Estatística) – Instituto de Ciências Matemáticas e de Computação, Universidade de São Paulo, São Carlos – SP, 2025.

Complex network science has emerged as a powerful tool for studying the structural and functional organization of the brain under normal conditions and in pathological contexts. In recent years, network-based approaches have been widely used to understand how mental and neurodevelopmental disorders influence brain organization and alter its functionality. The integration of graph theory, functional neuroimaging techniques, and computational methods enables the reconstruction of brain networks and contributes to understanding the impacts of various disorders at the individual level. Moreover, advances in automated diagnosis using machine learning have shown promising results in predicting and characterizing a range of disorders based on the analysis of functional connectivity obtained from time series of brain activity. This project aims to classify different mental disorders through the reconstruction of complex networks from time series extracted from neuroimaging data. The goal is to assess which connectivity metric is most suitable for reconstructing the brain network topology associated with each mental disorder, as well as the one that achieves the best classification performance. Machine learning models were used to analyze functional connectivity matrices in order to characterize the brain topology associated with each condition and to identify disorder-specific connectivity patterns. For major depressive disorder (MDD), Spearman correlation was the most suitable metric for reconstructing brain networks. The results suggest that alterations in connectivity are related to deficits in attention, memory, and decision-making. For autism spectrum disorder (ASD) and attention-deficit hyperactivity disorder (ADHD), transfer entropy was used to build the connectivity matrix, revealing altered patterns in brain regions associated with attention and impulse control in ADHD, and impairments in social and cognitive areas in ASD. Connectivity patterns were also analyzed to understand the progression of Parkinson's disease (PD). In its early stages, the patterns resembled those of healthy individuals, while in later stages, a reduction in synchronization between brain regions and disease progression was observed. Therefore, the findings of this study contribute to more accurate diagnoses and to the development of personalized intervention strategies, promoting advances in the understanding and treatment of these conditions.

Keywords: complex networks, mental disorders, functional connectivity, machine learning, automated diagnosis.

CONTENTS

CHAPTER

1

INTRODUCTION

Complex systems are composed of discrete parts that interact with each other (BOCCALETTI *et al.*, 2006; COSTA *et al.*, 2007). The primary goal of studying complex systems is to understand and control collective dynamics. Unlike individual elements, collective behavior emerges from the intricate relationships between these parts and their environment. These systems are ubiquitous and are studied across a wide range of fields, from sociology to biology. Examples of complex systems include social interactions, the brain, ecosystems, and the economy (COSTA *et al.*, 2011). In recent decades, research on complex systems has gained significant attention, resulting in the Nobel Prize in Physics in 2021 (GUPTA *et al.*, 2022). This recognition is expected to drive further studies in this field, contributing to solutions for pressing challenges of humanity, including climate change, social inequality, epidemics, and the treatment of diseases such as cancer (COSTA *et al.*, 2011; MIGUEL *et al.*, 2012).

A powerful approach to representing complex systems is through complex networks (BOCCALETTI *et al.*, 2006; COSTA *et al.*, 2007), which play a crucial role in analyzing their dynamic properties. Understanding the interplay between a network's topological structure and its diverse dynamical behaviors is essential for effectively characterize and control complex systems. Real-world complex networks can generally be classified into two categories. In the first category, network structures are explicitly available, such as city transportation networks, protein interaction networks, airline networks (BARRAT *et al.*, 2004), and Wikipedia (COSTA *et al.*, 2011). In these networks, vertices and connectivity maps are well-defined. In the second category, vertices are known, but connections must be inferred (ANGULO *et al.*, 2017). This challenge arises in cortical networks, where electroencephalography (EEG) signals are recorded from different brain regions (ALVES *et al.*, 2022b; ALVES *et al.*, 2022a; ALVES *et al.*, 2022c), as well as in financial markets (PERON; COSTA; RODRIGUES, 2012) and climate networks (TSONIS *et al.*, 2011). Since most real-world complex networks do not have readily available connectivity structures, reconstructing network topology and dynamics from data is essential for understanding and controlling their behavior (TIMME; CASADIEGO, 2014; ANGULO *et al.*,

2017; FREILICH *et al.*, 2020).

Despite network science emerged in the late 20th century (WATTS; STROGATZ, 1998; BARABÁSI; ALBERT, 1999), many fundamental questions remain unresolved, particularly regarding how network structure influences system dynamics (MIGUEL *et al.*, 2012). One critical issue is how to infer the structure of a network — essentially, how to uncover its topology based on time series data reflecting interactions between its components (ANGULO *et al.*, 2017). From a mathematical perspective, inferring network connectivity constitutes a high-dimensional inverse problem. This problem is increasingly relevant, as algorithms capable of reconstructing networks can help recover missing information, eliminate false interactions, and improve the prediction and control of system dynamics (LÜ; ZHOU, 2011). Network reconstruction has applications in various domains, such as modeling the spread of diseases in social networks (SHEN *et al.*, 2014) and diagnosing neurological disorders (STAM, 2014; YAN *et al.*, 2024).

In complex networks, three primary types of connections can be inferred: structural connectivity (SC), related to the physical structure of the network; functional connectivity (FC), reflecting statistical dependencies between different network components (TURNBULL *et al.*, 2018); and effective connectivity (EC), describing causal or directed influences between network elements (FRISTON, 1994). The structure of a network always lays a crucial role in its collective dynamics and therefore its functionality (STROGATZ, 2001; TIMME; CASADIEGO, 2014). However, the reverse is not necessarily true, as functional or effective connections do not always indicate structural links.

The ability to accurately reconstruct networks from observed data is a significant challenge that impacts various fields (ANGULO *et al.*, 2017; ARICI; TUNCBAG, 2021; MUNGO *et al.*, 2024). In neuroscience, inferring brain network structures from EEG signals or other functional neuroimaging data is crucial for understanding cognitive function and diagnosing disorders. Several methods have been employed to infer brain network connectivity, ranging from simple correlation measures as Spearman or Pearson correlation (ALVES *et al.*, 2022c) to more sophisticated causality-based techniques such as Granger causality (DING; CHEN; BRESSLER, 2006). The choice of inference method directly influences diagnostic accuracy, since many neurological and psychiatric disorders are associated with altered brain connectivity (BASSETT; BULLMORE, 2009).

The study of brain networks is particularly relevant for understanding mental disorders, which are among the most pressing health challenges worldwide. In 2019, approximately 970 million people, or one in eight worldwide, were living with a mental disorder, with anxiety and depression being the most common (World Health Organization, 2023). Additionally, mental disorders accounted for 125.3 million disability-adjusted life years (DALYs) in 2019, representing 4.9% of the global total DALYs (COLLABORATORS *et al.*, 2022). It is estimated that half of the global population will develop at least one mental disorder by the age of 75 (MCGRATH *et al.*, 2023). These data highlight the urgency of research focused on accurately reconstructing brain

networks to advance the understanding, diagnosis, and treatment of mental disorders, supported by advances in network science.

In recent years, network science has emerged as a powerful framework for studying the brain's organization and function. However, the study of brain disorders presents many challenges (DU; FU; CALHOUN, 2018). Unlike structural brain diseases, such as tumors that can be directly visualized in brain scans, mental disorders often lack clear anatomical markers and rely on the patient's symptoms. Providing an accurate diagnosis and successful treatment is difficult and depends on medical expertise. Disorders such as depression (LUI *et al.*, 2011; FURMAN; HAMILTON; GOTLIB, 2011; KAISER *et al.*, 2015), schizophrenia (HEUVEL *et al.*, 2013; FORNITO *et al.*, 2011), and autism (WASS, 2011; KANA; LIBERO; MOORE, 2011) are related to altered brain network dynamics, which manifest at different levels, from individual neuronal connections to large-scale functional interactions. Also, they are characterized by disruptions in functional and effective connectivity (HEUVEL; SPORNS, 2019; HEUVEL *et al.*, 2013; BULLMORE; SPORNS, 2009), affecting neural communication between different brain regions. Understanding these phenomena and their relationship with the emergence and progression of brain disorders is crucial for developing effective diagnostic tools.

In this context, this work aims to explore state-of-the-art methods for reconstructing functional brain networks and assessing their effectiveness in analyzing data from individuals with mental disorders. We investigate several network reconstruction techniques, combining connectivity metrics, machine learning algorithms, and complex network measures to determine their potential use in the diagnosis of psychiatric conditions. By improving the classification performance, we hope to contribute to the development of more reliable tools or understanding and diagnosing mental health disorders.

1.1 Objectives

The main objective of this thesis is to reconstruct complex brain networks from time series data and apply these reconstructed networks to classify brain disorders. We aim to identify which connectivity metric and machine learning algorithm are the most suitable for the disorder under investigation. To achieve the primary objective, the following activities are proposed:

1. *Impact of reconstruction methods on disorder classification*

   This study aims to identify the most effective reconstruction methodology for the accurate diagnosis of mental disorders. To achieve this, a data matrix is constructed in which each entry represents the relationship between two time series, quantified using various connectivity metrics. Several machine learning algorithms are applied to optimize the classification accuracy. The best-performing model is then used to identify distinct patterns

associated with different brain disorders. This investigation contributes to improving classification techniques and enhancing diagnostic accuracy in mental health research.

2. *Identify disorder-specific brain connectivity patterns and improve classification methods*

   This objective analyzes brain network connectivity across various neurological and psychiatric disorders to uncover distinctive patterns that improve classification accuracy. Using machine learning techniques, the study focuses on refining diagnostic methods for mental health disorders, such as differentiating subtypes based on network dynamics. In addition, the research identifies potential biomarkers for the detection and progression of the disease, which contribute to more accurate diagnostics and personalized treatment strategies.

3. *Influence of network topology and dynamics on reconstruction accuracy*

   Mental disorders significantly impact brain dynamics and network topology. Understanding how network structure and underlying dynamics influence the choice of reconstruction measures is therefore essential.

   This study investigates how network topology and dynamical state influence the performance of network reconstruction using dynamical models such as coupled logistic maps. Networks with varying topologies, including Erdős-Rényi, Barabási-Albert, and Watts-Strogatz models, are generated while maintaining a fixed number of vertices and mean degree. The networks are then reconstructed using different metrics, including statistical correlation measures, information-theoretic measures, and phase synchrony measures. Reconstruction performance is evaluated for each method using metrics such as true positive rate, false positive rate, and F1-score. By analyzing how specific network topological features and dynamic states influence the reliability of reconstruction, this study provides a deeper understanding of the relationship between network structure, dynamics, and reconstruction methods.

1.2 Thesis organization

This thesis is organized into seven chapters, each addressing a specific aspect related to mental disorder classification.

Chapter 1 introduces the research topic and describes the objectives. Chapter 2 provides a review of the most classical network reconstruction methods in the literature. It introduces applications in brain networks, reviews functional connectivity measures, both undirected and directed, and discusses the analysis of reconstructed networks, particularly in the context of brain disorders and automatic diagnosis.

The following chapters present the findings of this thesis as a collection of research articles, each preceded by introductory sections outlining the context and contributions of the study. Chapter 3 applies machine learning and complex network methods to identify patterns

in Major Depressive Disorder (MDD). It highlights its contributions to understanding network alterations in MDD brain. Chapter 4 extends the analysis to multiclass classification of mental disorders, such as autism spectrum disorder (ASD), attention deficit hyperactivity disorder (ADHD), and typically developed individuals (TD), introducing methodologies and results that distinguish these different conditions using machine learning and network-based approaches. Chapter 5 explores the existing classification of autism spectrum disorder (ASD) and its limitations. It discusses how network-based methods and machine learning techniques can offer a more data-driven approach to redefining ASD subtypes. Chapter 6 focuses on brain connectivity in Parkinson's disease (PD) and explains how changes in functional connectivity over time can be used as indicators of disease progression. Chapter 7 examines how network topology and the underlying dynamical processes influence the reliability of network reconstruction. This analysis is based on simulations and exploratory analysis, distinguishing it from the previous chapters, which focus on data analysis.

CHAPTER

2

RECONSTRUCTION OF NETWORKS

2.1 Context

A considerable amount of research in the field of complex network dynamics has been dedicated to understanding how different network topologies influence the collective behavior that emerges from the interactions between interconnected nodes (BOCCALETTI *et al.*, 2006; NEWMAN, 2003; STROGATZ, 2001). However, in many real-world scenarios, only the time-evolving behavior of individual nodes is observable, while both the underlying network structure and the governing dynamical rules remain unknown.

The interest in the inverse problem, that is, inferring the underlying network topology and dynamical rules from observed data, has grown significantly in recent years, as reflected by the rapid increase in related publications. The main challenge in reconstructing complex networks from time series data lies in developing methods capable of indirectly recovering the original network structure with sufficient accuracy to allow understanding, prediction, and control of the system dynamics (EROGLU *et al.*, 2019; WANG; LAI; GREBOGI, 2016). This is a fundamental challenge across multiple disciplines, including network science (MAJDANDZIC *et al.*, 2014), biology (HERRGÅRD *et al.*, 2008), social sciences (ZHOU; XU; YEN, 2019), engineering (JIANG *et al.*, 2018), and economics (BARDOSCIA *et al.*, 2021), since connectivity between nodes is typically not directly observable and must be inferred from measurable data, often within a solution space of high dimensionality (HAN *et al.*, 2015).

Several methods have been proposed for the reconstruction of complex networks, which are generally categorized into model-based (ARRIDGE *et al.*, 2019) and model-free approaches (MENG; JIANG; WEI, 2020). Model-based methods are based on mathematical or statistical formulations to infer the underlying network structure. These approaches assume a specific model, or a family of models, and estimate their parameters based on prior knowledge about the dynamics governing the observed data. Examples include Boolean network models (BORNHOLDT, 2008),

Bayesian network models (MARCOT; PENMAN, 2019), and differential equation-based models (BRUNTON; PROCTOR; KUTZ, 2016; GAO; YAN, 2023).

On the other hand, model-free methods do not rely on predefined mathematical or statistical models to infer network connectivity. Instead, they analyze the temporal dynamics of observed data to estimate the presence and strength of interactions between nodes to reconstruct functional links (CASADIEGO *et al.*, 2017). In this context, a variety of techniques are employed, including correlation (RUBIDO *et al.*, 2014), mutual information (BUTTE; KOHANE, 1999; RUBIDO *et al.*, 2014), Granger causality (GRANGER, 1969), transfer entropy (SCHREIBER, 2000), among others. Both model-based and model-free methods have their strengths and limitations, and the choice of a specific approach depends on the research objectives, characteristics of the available data, and the specific nature of the network under investigation.

To effectively address the inference problem, it is essential to clearly define the specific information about the network system to be uncovered. Depending on the level of detail regarding the connection properties to be inferred, there are three main approaches to the reconstruction problem. An approach focuses on unraveling the structural connectivity of the network, which involves identifying direct interactions between individual units and mapping the configuration of their connections (TIMME; CASADIEGO, 2014).

Another approach involves recovering the functional connectivity of the network, a concept originally introduced by Friston (1994) in the context of neuroscience to describe the statistical relationships between the dynamic activities of neural units in different anatomical regions. Typically assessed using correlation or covariance, functional connectivity measures the similarity or statistical dependencies between node dynamics over time and is represented by a matrix of pairwise similarities (EROGLU *et al.*, 2020). While initially developed for brain networks, this concept has been extended to other complex systems. The study of functional connectivity provides a deeper understanding of the underlying mechanisms, dynamic interactions within the network, and functional relationships among its components.

The third approach involves recovering effective connectivity, which was originally defined as the directional influence that one neural unit exerts over another (FRISTON, 1994). Effective connectivity can be estimated using dynamic causal modeling (DCM), which provides a deterministic framework for modeling neural dynamics to describe causal mechanisms within brain networks (FRISTON; HARRISON; PENNY, 2003). Alternatively, it can also be inferred from time series data using methods such as Granger causality, which does not require prior knowledge of the structural organization of the network. In general, effective connectivity refers to directed influence or causal interactions between nodes in a network (BULLMORE; SPORNS, 2012), and is particularly useful to uncover how components interact and influence each other, thus helping to characterize the underlying dynamics and global behavior of the system.

Several studies suggest that disruptions in functional connectivity contribute to the development of several brain disorders (FORNITO; ZALESKY; BREAKSPEAR, 2015). Functional

connectivity has become a valuable tool for examining how how brain organization and communication between regions are affected by neurological and psychiatric conditions, contributing to earlier and more effective diagnoses (ALVES *et al.*, 2022a). Also, alterations in effective connectivity can reveal specific patterns of causal interactions that contribute to the manifestation of a disorder. The integration of functional and effective connectivity provides a more comprehensive understanding of brain dynamics and can improve the identification of biomarkers and mechanisms associated with mental health conditions.

Multiple techniques are available to reconstruct the connectivity in complex networks, and the choice of the most appropriate method depends on the specific research question, data availability, and the complexity of the network under study. An effective reconstruction method must select an optimal threshold to determine the presence or absence of links, retain weak but significant connections, and accurately classify whether the interaction between nodes is strong enough to establish a link.

For example, Rubido *et al.* (2014) examined discrete-time dynamical systems, such as logistic maps and circle maps, comprising $N = 16$ units with time series length of $T \approx 10^4$. These units interacted under various coupling topologies, including random and small-world networks, with homogeneous and heterogeneous weights. Their findings indicate that under a weak coupling regime, where the network is neither fully synchronized nor completely desynchronized, the network structure can be perfectly inferred. Moreover, mutual information generally outperforms cross-correlation by providing more robust and reliable results. Furthermore, they demonstrated that careful analysis of the distribution of similarity values enables the selection of optimal thresholds to infer direct links.

In another study, Tirabassi *et al.* (2015) conducted linear and non-linear statistical similarity analyzes in time series of length $T \approx 10^4$, derived from the dynamics of $N = 12$ nodes in two different systems of coupled oscillators: the Kuramoto and Rössler oscillators. The authors considered a fully random (Erdős–Rényi) structural network. Their results demonstrated that with an appropriate selection of the observed variable, a suitable interaction strength, and an optimal threshold applied to the similarity matrix, the network links could be inferred without errors. Contrary to findings in discrete-time maps, the cross-correlation measure outperformed mutual information in this context.

2.2 Brain networks

Brain disorders represent a major global health challenge and are one of the leading causes of disability and mortality worldwide (DILUCA; OLESEN, 2014; KOLAPPA; SEEHER; DUA, 2022). In recent years, the incidence of mental disorders, including depression, anxiety, and schizophrenia, has increased abruptly (WANG *et al.*, 2021). Neurological disorders such as epilepsy, dementia, Alzheimer's disease, multiple sclerosis, and Parkinson's disease remain

particularly difficult to diagnose accurately (SIULY; ZHANG, 2016). Research on brain diseases has shown that the brain network topology undergoes abnormal alterations, varying in extent depending on the specific disorder. Such changes have been observed in conditions like Alzheimer's disease (ZHANG *et al.*, 2010), schizophrenia (BASSETT; BULLMORE, 2009; BULLMORE; SPORNS, 2009), and during epileptic seizures (FROLOV; HRAMOV, 2021). Research on brain functional networks can improve the understanding of the pathological mechanisms underlying neurological and psychiatric disorders and offers the potential for earlier, more accurate, and cost-effective diagnoses.

In brain networks, nodes typically correspond to different brain regions or individual neurons, while links represent various types of connections, such as anatomical, functional, or effective connections, depending on the specific dataset being analyzed (FRISTON, 1994). Brain connectivity can be characterized at three hierarchical levels (ZENG, 2018): at the microscale, where individual synaptic connections link single neurons; at the mesoscale, where networks consist of connections between neuronal populations; and at the macroscale, where large groups of neurons and neuronal populations form distinct brain regions are interconnected, resulting in large-scale connectivity patterns.

Studying brain connectivity at the macroscale helps to elucidate how different brain regions interact and how disruptions in these connections can contribute to neurological and psychiatric disorders. This approach provides important information on the organization and integration of brain function, supporting research in fields such as neuroscience and brain mapping. On the macroscale, brain connectivity can be categorized into structural, functional, and effective connectivity.

Structural connectivity, often referred to as the brain connectome, describes the anatomical pathways that connect different brain regions (SPORNS, 2013). It involves examining the white matter tracts that physically connect these regions. Techniques such as diffusion tensor imaging (DTI) are commonly used to map and analyze these structural connections.

Functional connectivity captures the temporal correlations between neuronal activities and can occur between regions that are not anatomically connected or between widely dispersed neuronal units (FRISTON, 1994; SPORNS; TONONI, 2007). An important difference within functional connectivity lies in whether the dependencies are instantaneous or reflect an underlying dynamic process, where activity in one region consistently precedes and potentially influences activity in another. This leads to the differentiation between undirected and directed functional connectivity, depending on whether or not temporal precedence is considered (FRISTON; MORAN; SETH, 2013). Common measures used to assess undirected functional connectivity include synchrony, correlation, coherence, and mutual information. In contrast, directed functional connectivity is often assessed using methods such as Granger causality and transfer entropy.

Conversely, effective connectivity captures causal interactions between activated brain

areas, with measurements reflecting interactions among hidden neuronal states (FRISTON; MORAN; SETH, 2013). Effective connectivity is inherently directed and is based on parameterized models of causal influence, typically expressed through difference or differential equations (FRISTON; MORAN; SETH, 2013). It is used to understand how activity in one region influences activity in another, focusing on directional influences among segregated neuronal assemblies. Effective connectivity can be estimated by observing system perturbations or analyzing time series data (FRISTON; HARRISON; PENNY, 2003; SPORNS; TONONI, 2007). The most widely used approach to effective connectivity is dynamic causal modeling (DAVID *et al.*, 2006).

The human brain exhibits a highly complex and heterogeneous structure, which leads to a range of complex network properties that reflect the diverse and intricate organization of its connectivity (RUBINOV; SPORNS, 2010; BASSETT *et al.*, 2006; LYNN; BASSETT, 2019). The functional and anatomical connectivity of human brain is known to display large-scale network structures with non-trivial topological characteristics (LEE *et al.*, 2011). Studies suggest a close relationship between structural and functional networks: anatomically connected regions of the brain often exhibit stronger functional connectivity, suggesting that functional networks reflect dynamic patterns emerging from the underlying physical architecture (BULLMORE; SPORNS, 2009). However, functional connectivity can also be observed between brain regions lacking direct anatomical connections (MIJALKOV; PEREIRA; VOLPE, 2020), and the extent to which the anatomical structure shapes functional dynamics remains an open question (WEIN *et al.*, 2021).

Brain networks are characterized by several key topological features. They exhibit small-world properties, combining high local clustering with short average path lengths, and scale-free characteristics, where a few highly connected nodes (hubs) coexist with many sparsely connected nodes (EGUILUZ *et al.*, 2005). These networks also demonstrate modular or community organization, in which groups of nodes are more densely connected within themselves than with nodes outside their module, and a hierarchical organization, with connections spanning multiple spatial scales (HEUVEL; SPORNS, 2011). In addition, brain networks are known to be sparse, meaning that the number of actual connections is relatively small compared to the total number of possible connections (LEE *et al.*, 2011; WANG *et al.*, 2021; YU *et al.*, 2019).

To gain a deeper comprehension of the brain function, researchers have increasingly relied on non-invasive imaging techniques to measure functional connectivity on the macroscale (BASSETT; SPORNS, 2017). Common methods include electroencephalography (EEG) (ALVES *et al.*, 2022c), magnetoencephalography (MEG) (STAM, 2010), and functional magnetic resonance imaging (fMRI) (ALVES *et al.*, 2022a), each offering specific advantages and limitations.

EEG involves placing electrodes on the scalp to record electrical activity from populations of neurons located beneath each active area of the electrode for a certain amount of time (TIMME; CASADIEGO, 2014). While EEG provides excellent temporal resolution, its spatial resolution is limited, making it less effective in capturing whole brain activity patterns. Nonetheless, EEG is

relatively low cost and widely accessible in clinical and research settings (ALVES *et al.*, 2022c).

MEG, on the other hand, is a functional neuroimaging technique that uses arrays of superconducting quantum interference devices (SQUIDs) placed around the head to detect weak magnetic fields produced by neuronal currents (STAM, 2010; FORNITO; ZALESKY; BULLMORE, 2016b). It offers high temporal resolution and has the advantage of directly capturing neuronal activity throughout the brain. However, MEG systems are expensive and less widely available, and the measurements are highly sensitive to external noise (STAM, 2010).

Functional magnetic resonance imaging (fMRI) is one of the most widely used techniques to measure functional connectivity. It enables the investigation of neural activity in specific regions of the cerebral cortex by capturing physiological signals and acquiring a time series of brain images while participants rest inside the scanner, without performing any particular task (WANG *et al.*, 2021; BULLMORE; SPORNS, 2009). fMRI measures blood oxygenation level-dependent (BOLD) signals, producing a sequence of three-dimensional images over time. Although fMRI has relatively low temporal resolution, it provides high spatial resolution, making it well-suited for analyzing spatial aspects of brain dynamics (ALVES *et al.*, 2022a).

One important difference between these neuroimaging techniques lies in how network nodes are defined. In networks derived from fMRI data, nodes typically correspond to anatomically defined regions or individual voxels within the brain images. In contrast, networks derived from EEG or MEG data generally define nodes based on the location of recording electrodes or sensors on the scalp surface (FORNITO; ZALESKY; BULLMORE, 2016b). Regardless of the technique used, the network topologies can be obtained using graph theory combined with appropriate network reconstruction methods.

The data obtained from these imaging techniques enable the inference of both functional and effective connectivity across different spatial and temporal scales. Connections are typically represented by a matrix, commonly referred to as an adjacency or connectivity matrix, that quantifies the relationships between nodes. This matrix is derived through a variety of reconstruction approaches. The following section provides a detailed overview of the most commonly used network reconstruction techniques.

2.3 Methods for network reconstruction

Several methods have been proposed to reconstruct networks from time series data. The inverse problem of recovering the network adjacency matrix from observed dynamics remains a significant challenge, particularly in neuroscience, where it plays a crucial role in understanding brain disorders.

Functional connectivity inference methods can be broadly categorized based on whether they capture the directionality of interactions. Undirected metrics quantify statistical dependen-

cies between signals without indicating the direction of influence. In contrast, directed metrics aim to infer causal relationships, relying on the principle that causes precede and help predict their effects.

The following subsections provide an overview of the methodologies used in this thesis to reconstruct functional brain networks.

2.3.1 Undirected functional connectivity measures

In the study of functional brain networks, connectivity is often assessed by analyzing statistical correlations or similarities between the activity patterns of different brain regions (LYNN; BASSETT, 2019). Brain regions that exhibit similar temporal patterns are considered functionally connected (FORNITO; ZALESKY; BULLMORE, 2016a).

By systematically evaluating these statistical dependencies across all possible pairs of brain regions, it is possible to construct a network representation of brain connectivity. In this network, each brain region is represented as a node, and the strength of the statistical correlation between regions determines the presence and weight of the connections.

Functional connectivity is commonly measured in the time domain using metrics such as correlation and mutual information. However, these measures typically ignore the temporal structure within the data, treating time series as independent realizations of random variables (BASTOS; SCHOFFELEN, 2016). For instance, Pearson's correlation is a widely used metric in fMRI network analysis (LIANG *et al.*, 2012; ZALESKY *et al.*, 2012), although alternative measures such as covariance and coherence (which analyzes data in the frequency domain) are also used (MEDAGLIA; LYNALL; BASSETT, 2015).

2.3.1.1 Pearson's correlation coefficient

Pearson's correlation coefficient is the simplest and most interpretable metric used to evaluate functional connectivity (HRAMOV *et al.*, 2021). It quantifies the linear statistical relationship between two time series, indicating how much of the variability in one signal can be explained by changes in the other. Let the time series $X = \{x_1, x_2, \ldots, x_N\}$ and $Y = \{y_1, y_2, \ldots, y_N\}$ represent the neural activity recorded by the sensors x and y, respectively. The Pearson correlation coefficient is then defined as

$$r_{XY} = \frac{1}{N} \frac{\sum_{t=1}^{N} (x_t - \bar{x})(y_t - \bar{y})}{\sigma_X \sigma_Y} \tag{2.1}$$

where σ_X, σ_Y and $\bar{x}\,\bar{y}$ are mean square deviations and mean values of the time series X and Y.

Pearson's correlation values range from -1 to $+1$, with -1 indicating a perfect negative linear relationship (as one signal increases, the other decreases), and $+1$ indicating a perfect positive linear relationship (both signals increase or decrease together).

Despite its simplicity, this metric does not provide information about the direction or causality of interactions, nor does it capture nonlinear relationships. Furthermore, it tends to infer spurious connections between indirectly coupled nodes, often resulting in networks that are excessively dense, clustered, and modular (BASSETT; SPORNS, 2017). To address confounding effects in highly correlated networks, partial correlation is often used as a connectivity measure in brain networks (LEE *et al.*, 2011), which usually results in sparser networks. However, the resulting topologies can be difficult to interpret, may inadvertently remove true interactions, and require a large number of samples for stable estimation (BASSETT; SPORNS, 2017).

Typically, the correlation matrix is thresholded to determine the network edges. Any correlation value r_{ij} in the functional connectivity matrix greater than a specified threshold τ is retained as an edge, connecting regions i and j in the adjacency matrix; if $r_{ij} < \tau$, no edge is assigned between these regions. Thresholding at different τ values produces graphs with varying connection densities or costs, where connection density is defined as the number of edges in a graph with N nodes divided by the maximum possible number of edges $[(N^2 - N)/2]$.

2.3.1.2 Spearman's rank correlation

The Spearman correlation coefficient (ρ_S) is a nonlinear metric used to quantify the strength of the monotonic association between two random variables X and Y (MYERS; SIROIS, 2004). It consists of calculating the Pearson linear correlation between the ranked variables rX and rY, which are obtained by sorting the values of each variable in ascending order and assigning rank labels accordingly. The Spearman correlation coefficient is then defined as

$$\rho_{XY} = \frac{1}{N} \frac{\sum_{t=1}^{N} (rx_t - \bar{x})(ry_t - \bar{y})}{\sigma_{rX}\sigma_{rY}} \tag{2.2}$$

Spearman's correlation measures monotonic relationships and yields high values when the ranks of observations in both variables are similar, and low values when the ranks differ substantially (SPEARMAN, 1961). In the absence of equal ranks, a perfect Spearman correlation of $+1$ or -1 occurs if one variable is a perfect monotonic function of the other. This metric is particularly useful when the assumption of linearity is violated, providing a robust alternative to analyze nonlinear dependencies in complex brain networks.

The Spearman rank correlation has been widely applied for brain network reconstruction. For example, it has been used to quantify similarities in connectivity patterns across various neurological and psychiatric disorders, helping to identify distinct network features associated with specific conditions (THOMPSON; FRANSSON, 2015a; THOMPSON; FRANSSON, 2015b; BINNEWIJZEND *et al.*, 2014).

2.3.1.3 Mutual information

Mutual information is a nonlinear, model-independent measure used to investigate relationships between time series (TIMME; LAPISH, 2018). Based on concepts from information theory, it quantifies the entropy of a random variable, which represents the amount of information or uncertainty involved in describing or predicting the outcomes of that variable (NA *et al.*, 2002). This measure captures how knowledge of one system can uncover details about the state of another (HRAMOV *et al.*, 2021), enabling detection of linear and nonlinear dependencies between time series (IOANNIDES *et al.*, 2000; TIMME; LAPISH, 2018). By estimating the average amount of information (entropy) of a system, mutual information allows us to infer the state of that system solely on observations from another.

In information theory, the fundamental measure of uncertainty for a discrete random variable is its Shannon entropy, which quantifies the reduction in uncertainty achieved when the value of the variable is observed (SHANNON, 1948). Given only the state of system X, its Shannon entropy is defined as (COVER; THOMAS *et al.*, 1991):

$$H(X) = -\sum_{t=1}^{N} p_X(x_t) \log p_X(x_t), \tag{2.3}$$

where $p_X(x_t)$ denotes the probability that X takes the value x_t. f the log is to the base 2, the entropy is expressed in bits.

This concept extends naturally to pairs of variables. If, concurrently, another process Y assumes a state y_k, the joint entropy $H(X,Y)$, based on the joint distribution $p_{XY}(x_t, y_k)$, is given by (COVER; THOMAS *et al.*, 1991):

$$H(X,Y) = -\sum_{k=1}^{N} \sum_{t=1}^{N} p_{XY}(x_t, y_k) \log p_{XY}(x_t, y_k). \tag{2.4}$$

To quantify the uncertainty in X when the value of Y is known, the conditional entropy is calculated as:

$$
\begin{aligned}
H(X|Y) &= \sum_{k=1}^{N} p_Y(y_k) H(X|Y=y_k) \\
&= -\sum_{k=1}^{N} p_Y(y_k) \sum_{t=1}^{N} p_{X|Y}(x_t|y_k) \log p_{X|Y}(x_t|y_k) \\
&= -\sum_{k=1}^{N} \sum_{t=1}^{N} p_{XY}(x_t,y_k) \log p_{X|Y}(x_t|y_k) \\
&= -\sum_{k=1}^{N} \sum_{t=1}^{N} p_{XY}(x_t,y_k) \log p_{X,Y}(x_t,y_k) + \sum_{k=1}^{N} \sum_{t=1}^{N} p_{XY}(x_t,y_k) \log p_Y(y_k) \\
&= -\sum_{k=1}^{N} \sum_{t=1}^{N} p_{XY}(x_t,y_k) \log p_{X,Y}(x_t,y_k) + \sum_{k=1}^{N} p_Y(y_k) \log p_Y(y_k) \\
&= H(X,Y) - H(Y)
\end{aligned}
\tag{2.5}
$$

Mutual information, $I(X,Y)$, can then be expressed as the relative entropy between the joint distribution and the product of the marginals:

$$
\begin{aligned}
I(X,Y) &= \sum_{t=1}^{N} \sum_{k=1}^{N} p_{XY}(x_t,y_k) \log \frac{p_{XY}(x_t,y_k)}{p_X(x_t) p_Y(y_k)} \\
&= H(X) - H(X|Y).
\end{aligned}
\tag{2.6}
$$

This interpretation shows that mutual information represents the reduction in uncertainty about X due to knowledge of Y. Moreover, mutual information is symmetric: $I(X,Y) = I(Y,X)$, meaning that the information Y provides about X is equal to the information X provides about Y.

Within the context of functional brain networks, mutual information evaluates the similarity or coherence between activity patterns in different brain regions. It is used as a measure of dynamical coupling or information transfer between time series (NA *et al.*, 2002), quantifying how much observing the activity of one region reduces uncertainty about another.

Higher mutual information values indicate stronger functional connectivity and greater information exchange. Mutual information reaches its maximum (typically +1 bit) when two signals perfectly predict each other, that is, when the signals are identical. Conversely, if two regions behave independently, mutual information approaches zero (NA *et al.*, 2002; TIMME; LAPISH, 2018).

Mutual information can be estimated through various methods, including entropy estimation or binning approaches (BORST; THEUNISSEN, 1999; TIMME; LAPISH, 2018; ZBILI; RAMA, 2021). It is widely applicable to time series from neuroimaging techniques such as fMRI, EEG, or MEG (TIMME; LAPISH, 2018).

Using mutual information, researchers can identify patterns of information sharing and communication within functional brain networks (YIN *et al.*, 2017; DIMITRIADIS *et al.*, 2018).

This approach helps to better understand how different brain regions coordinate and integrate their activity during cognitive tasks (CHEN *et al.*, 2008), resting-state conditions (SAVVA; MITSIS; MATSOPOULOS, 2019), and in the presence of neurological disorders (JEONG; GORE; PETERSON, 2001; ABASOLO *et al.*, 2008).

2.3.1.4 Coherence

Coherence is a widely used for assessing functional connectivity between two signals, particularly in the context of brain networks and neural activity (BOWYER, 2016; FRENCH; BEAUMONT, 1984; SRINIVASAN *et al.*, 2007). It quantifies the extent of linear correlation between signals in the frequency domain, offering information about the stability of their phase relationship and amplitude correlation across different frequencies (BASTOS; SCHOFFELEN, 2016; DING *et al.*, 2000; SRINIVASAN *et al.*, 2007). Mathematically, the coherence between two signals $X(t)$ and $Y(t)$ is defined as (BENDAT; PIERSOL, 2011):

$$C_{XY}(f) = \frac{|S_{XY}(f)|^2}{S_{XX}(f)S_{YY}(f)} \tag{2.7}$$

where:

- $S_{XY}(f)$ is the cross-spectral density between signals $X(t)$ and $Y(t)$ at frequency f,
- $S_{XX}(f)$ and $S_{YY}(f)$ are the power spectral densities of $X(t)$ and $Y(t)$, respectively, at the same frequency.

The coherence function produces values between 0 and 1, where a coherence value of 1 indicates perfect linear dependence between the signals at a specific frequency, and a value of 0 suggests no linear association between them at that frequency (BASTOS; SCHOFFELEN, 2016; DING *et al.*, 2000). The coherence function is particularly useful for examining the relationship between oscillatory brain activity in different regions or between different brain states (BOWYER, 2016; NOLTE *et al.*, 2004; BRAZIER, 1972; GROSS *et al.*, 2001; GANZETTI; MANTINI, 2013).

One of the key advantages of coherence is that it provides a clear and interpretable representation of the coupling between signals at different frequencies. It is a relatively straightforward and computationally efficient method, making it widely used in both neuroscience and signal processing to investigate functional interactions between brain regions or other physiological systems. However, coherence has some limitations. Primarily, it captures only linear dependencies between signals and may not be sensitive to nonlinear interactions, which can be critical in many biological and physiological systems. In addition, coherence does not provide information about the directionality of interactions (BOWYER, 2016); it only quantifies the strength of the relationship without indicating which signal leads or lags the other. Additionally,

coherence estimation is most reliable when applied to sufficiently long time series, ensuring stable spectral estimates and reducing noise-related variability (BOWYER, 2016). Despite these limitations, coherence remains a valuable tool in functional connectivity analysis, especially when examining linear coupling between signals in the frequency domain.

2.3.1.5 Phase locking value

Phase Locking Value (PLV) is a widely used metric in neuroscience to assess phase synchronization between signals, especially in the context of functional connectivity (LACHAUX *et al.*, 1999). It is a method for quantifying the strength of phase synchronization between different brain regions (SAKKALIS, 2011). It assumes that two dynamic systems can exhibit phase synchronization even when their amplitudes are uncorrelated (MORMANN *et al.*, 2000).

Phase synchronization refers to the alignment of the phases of two signals, where the phase difference between them remains relatively stable over time. Mathematically, this can be expressed as (SAKKALIS, 2011):

$$|\phi_X(t) - \phi_Y(t)| = \text{constant} \tag{2.8}$$

where $\phi_X(t)$ and $\phi_Y(t)$ are the instantaneous phases of the signals $X(t)$ and $Y(t)$, respectively.

To estimate the instantaneous phase of a signal, the Hilbert transform is commonly applied to construct the analytic signal $H(t)$ (TASS *et al.*, 1998; ROSENBLUM; PIKOVSKY; KURTHS, 1996; PIKOVSKY *et al.*, 1997), given by (ROSENBLUM; PIKOVSKY; KURTHS, 1996):

$$H(t) = X(t) + i\tilde{X}(t) \tag{2.9}$$

where $X(t)$ is the original signal and $\tilde{X}(t)$ is its Hilbert transform. The Hilbert transform is defined as the Cauchy principal value of the integral (ROSENBLUM; PIKOVSKY; KURTHS, 1996):

$$\tilde{X}(t) = \frac{1}{\pi} \mathscr{P} \int_{-\infty}^{\infty} \frac{X(t')}{t - t'} dt' \tag{2.10}$$

where $\mathscr{P}$ denotes the Cauchy principal value, ensuring the integral is properly interpreted when the denominator $t - t'$ approaches zero.

The instantaneous phase of the signal is then obtained from the analytic signal as (SAKKALIS, 2011):

$$\phi_X(t) = \arctan\left(\frac{\tilde{X}(t)}{X(t)}\right) \tag{2.11}$$

Therefore, for two signals $X(t)$ and $Y(t)$ of equal time length, with instantaneous phases $\phi_X(t)$ and $\phi_Y(t)$, respectively, the Phase Locking Value (PLV) is defined as (LACHAUX *et al.*, 1999):

$$\mathrm{PLV}_{XY} = \left| \frac{1}{N} \sum_{t=1}^{N} \exp\left(i\left(\phi_X(t) - \phi_Y(t)\right)\right) \right| \tag{2.12}$$

where $\phi_X(t)$ and $\phi_Y(t)$ are the instantaneous phases of signals $X(t)$ and $Y(t)$, respectively, computed using the Hilbert transform and N is the number of time points considered in the analysis.

PLV provides a value between 0 and 1. If the phase difference between the signals remains stable over time, the PLV will approach 1, indicating exact phase synchronization. Conversely, if the phase difference varies randomly, the PLV will approach 0, suggesting no phase synchronization.

In neuroscience, PLV has been successfully applied to various studies of brain networks and functional connectivity (GHUMAN; MCDANIEL; MARTIN, 2011; SCHMIDT; GHUMAN; HUPPERT, 2014; PALVA; PALVA; KAILA, 2005; MARZETTI *et al.*, 2019; ZHANG *et al.*, 2016; LOWET *et al.*, 2016; CHAWLA; LUMER; FRISTON, 1999). For example, PLV has been used to assess the phase synchronization of neuronal activity in different regions of the brain, providing insights into how these regions interact during various cognitive tasks (LACHAUX *et al.*, 1999; SAUSENG; KLIMESCH, 2008; GYSELS; CELKA, 2004). One key application of PLV is in the study of epilepsy (SAKKALIS *et al.*, 2008; ABDELHALIM; SMOLYAKOV; GENOV, 2011; ELAHIAN *et al.*, 2017), where PLV measures can detect changes in phase synchronization during epileptic seizures, highlighting alterations in brain network connectivity. In addition to its utility in seizure detection, PLV is often employed to assess connectivity between brain regions (SCHMIDT; GHUMAN; HUPPERT, 2014; GLEREAN *et al.*, 2012; WANG *et al.*, 2020).

PLV offers several advantages, including its ability to provide a simple and intuitive measure of phase synchronization between signals, making it useful in fields like neuroscience and signal processing. It is robust to amplitude variation, as it is based solely on phase differences; thus, it remains unaffected by amplitude fluctuations, which can be advantageous in noisy data. However, PLV also has limitations. It is sensitive to the length of the signal, as the PLV estimates improve with longer signals. It can be affected by non-stationary signals or drift, as statistical properties change over time. Additionally, PLV does not account for amplitude information, which may be crucial in some contexts.

2.3.2 Directed functional connectivity measures

Understanding causal relationships between parts of the brain is of extreme importance. Therefore, quantifying the stimulus response relationship alone does not fully describe brain dynamics (VICENTE *et al.*, 2011). Efforts have been made to incorporate notions of causality in traditional metrics of functional connectivity that rely mostly on correlation analysis. Causality represents the directionality of information flow in a network and has motivated researchers to explore causal relationships among neurons and brain regions.

Directed functional connectivity refers to the analysis and quantification of the directed or causal interactions between different brain regions based on their time series data. Unlike undirected functional connectivity, which measures the statistical dependencies or correlations between brain regions without indicating the direction of influence, directed functional connectivity explicitly aims to identify the direction of information flow or causality between brain regions. In contrast with effective connectivity, directed functional connectivity does not use dynamical modeling to infer the causal interactions and information flow between brain regions (BARNETT *et al.*, 2020), i.e., it does not need the construction of mathematical models that describe the temporal dynamics of the system under investigation.

In contrast with time series analysis tools for undirected functional networks, measures of directed functional connectivity generates networks with directed edges that provide information about the extent to which the past of one time series can predict the future of another and it is very useful in neuroscience (BASSETT; SPORNS, 2017). Also, these measures have practical implications for controlling brain networks and intervening in the treatment of neurological disease and psychiatric disorders (LYNN; BASSETT, 2019).

2.3.2.1 Granger causality

Among the approaches that do not use mathematical modelling, the most popular is the Granger causality test, which was originally applied to time series data in the field of economics (GRANGER, 1969). Standard Granger-causality test is a statistical test of the hypothesis of whether the information about process X improves the prediction of process Y based on two principles: (1) the cause precedes the effect; (2) the cause has unique information about the future meanings of the effect (GRANGER, 1969). The linear relationship among the causes and effects are implemented by fitting autoregressive models.

Let X and Y be stationary time series. If the inclusion of lagged X values leads to better predictions of Y, then X is said to Granger-cause Y, suggesting a causal relationship from X to Y. Granger causality test if X (and lags of X) is helpful in explaining Y, and thereby help forecasting it. So it do not provide the true causal relationship between the time series.

For two variables X and Y, where X Granger causes Y (written as $X \rightarrow Y$), the unrestricted

regression model is given by:

$$Y(t) = \alpha_0 + \sum_{\Delta t=1}^{k} a_{\Delta t} Y(t-\Delta t) + \sum_{\Delta t=1}^{k} \beta_{\Delta t} X(t-\Delta t) + \varepsilon(t) \tag{2.13}$$

where $\varepsilon(t)$ is the residual error for time t, Δt denotes the lag interval, and $\alpha_{\Delta t}$ and $\beta_{\Delta t}$ are the coefficients of the regression model that are chosen via least squares regression. So, with this formulation, the values of $Y(t)$ is explained as a function of the lags of Y and lags of X variable.

This model is compared by a hypothesis test to the restricted model given by:

$$Y(t) = \alpha_0 + \sum_{\Delta t=1}^{k} \alpha_{\Delta t} Y(t-\Delta t) + \varepsilon_j(t) \tag{2.14}$$

This restricted model takes the position of the null hypothesis in the test. Thus, the null hypothesis is $H_0 : \beta_{\Delta t} = 0$, that is, X do not Granger cause Y and for a causal link to be detected the null hypothesis must be rejected. A popular choice for Granger analysis is the F test (CARLOS-SANDBERG; CLACK, 2021).

Neuroscientists have applied Granger causality methods in different sources of data, including EEG (ALVES *et al.*, 2022c), MEG (FRISTON; MORAN; SETH, 2013) and fMRI (ROEBROECK; FORMISANO; GOEBEL, 2005) to investigate functional neural systems at scales of organization from the cellular level to whole-brain network activity, under a range of conditions, including sensory stimuli, cognitive tasks, and pathological states. In such analyses, the time series data are interpreted to reflect neural activity from a particular source, and Granger causality is used to characterize the directionality and dynamics of influence between sources.

2.3.2.2 Transfer entropy

As discussed previously, mutual information quantifies the content of shared information between two time series but does not capture causal interactions, as it lacks both directionality and temporal asymmetry. To address these limitations, Schreiber (2000) introduced the concept of transfer entropy (TE) , which estimates the amount of information transferred from one signal to another. Its definition is based on the observational causality principle of Nobert Wiener, which states that a process X can be said to influence another process Y if incorporating the past of X in addition to the past of Y improves the prediction of future states of Y (WIBRAL *et al.*, 2012; VICENTE *et al.*, 2011).

Transfer entropy is an asymmetric, nonlinear, model-free measure of information flow, meaning that TE from X to Y is not necessarily equal to TE from Y to X (BARNETT; BOSSOMAIER, 2012; VICENTE *et al.*, 2011). It is particularly suited for identifying directed interactions and uncovering the temporal structure of information flow in complex systems.

Importantly, TE explicitly incorporates the temporal evolution of the target process by conditioning on its past. This allows for the construction of directed networks that reflect the

underlying causal relationships and system dynamics. This framework is especially valuable for exploring interactions among components in high-dimensional systems, such as brain networks (NOVELLI; LIZIER, 2021).

Formally, the transfer entropy from a source X to a target process Y is defined as (SCHREIBER, 2000)

$$\begin{aligned} T_{X\to Y}(t) &:= I(Y_{t+1}; X_t^m | Y_t^n) \\ &= \sum_{Y_{t+1}} \sum_{X_t^m} \sum_{Y_t^n} p(Y_{t+1}; X_t^m; Y_t^n) \log \frac{p(Y_{t+1}|X_t^m; Y_t^n)}{p(Y_{t+1}|Y_t^n)} \end{aligned} \tag{2.15}$$

where $X_t^m = (x_t, \ldots, x_{t-m+1})$ and $Y_t^n = (y_t, \ldots, y_{t-n+1})$ represent the embedding vectors (or past states) of X and Y, respectively. The integers m and n denote the orders (i.e., memory lengths) of the Markov processes X and Y. The term $I(Y_{t+1}; X_t^m \mid Y_t^n)$ is the conditional mutual information between the past of the source and the next state of the target, conditioned on the target's own past.

Transfer entropy has been applied in a variety of neuroscience contexts, including MEG and EEG recordings (VICENTE *et al.*, 2011), as well as fMRI data (LIZIER *et al.*, 2011), to uncover directed information flow and characterize causal brain network dynamics.

2.4 Analysis of the reconstructed network

The analysis of reconstructed networks has become an active area of research in various fields, as it allows a deeper understanding of both network structure and dynamics. These networks can be examined using tools and methods from graph theory, which offer a wide range of metrics, to assess the importance of individual nodes and the overall organization of the network (SPORNS, 2022; RUBINOV; SPORNS, 2010). Once the structural properties are understood, network dynamics, such as spreading processes and information flow, can also be investigated.

In the context of neuroscience, the analysis of reconstructed brain networks helps to understand the structural and functional organization of the brain (RUBINOV; SPORNS, 2010; STAM; REIJNEVELD, 2007). IIt provides information on how cognitive tasks reorganize brain connectivity and how dysfunctions arising from neurological disorders spread and influence interactions between brain regions (VENKATESH; JAJA; PESSOA, 2020; LYNN; BASSETT, 2019; STAM; STRAATEN, 2012). In addition, this analysis allows for comparative studies between groups, such as healthy individuals and patients with neurological conditions, helping to uncover alterations in functional connectivity patterns.

Moreover, several computational methods have been applied to detect and classify brain disorders using reconstructed connectivity matrices (DU; FU; CALHOUN, 2018). These include

machine learning, deep learning, and Bayesian modeling approaches, which aim to identify informative patterns and extract relevant features that support the diagnosis and prognosis of neurological conditions.

The following subsections present key aspects of network topology associated with brain disorders as documented in the literature. In addition, computational strategies used for diagnosing and classifying neurological conditions are discussed.

2.4.1 Network studies in brain disorders

Researchers use methods from network science to investigate the key organizational properties of functional brain networks. These studies have consistently shown that functional brain networks in healthy individuals exhibit large-scale modularity, small-world characteristics, heavy-tailed degree distributions, and metabolically constrained organization (HEUVEL; POL, 2010; HE *et al.*, 2009; ACHARD *et al.*, 2006).

Brain disorders can induce changes in brain connectivity and function (LIU *et al.*, 2017). Such changes may affect various aspects of neural communication, including the strength of connections between brain regions and patterns of information flow. These alterations reflect specific features of the underlying disorder and can affect cognitive processes, emotional regulation, and neurological functions. By examining these network alterations, researchers uncover critical aspects of the underlying mechanisms of brain disorders, which can contribute to improved diagnosis.

For example, EEG studies have demonstrated that functional brain networks in schizophrenia (SCZ) patients exhibit reduced clustering coefficients and shorter path lengths compared to healthy controls, indicating a shift towards a more random network topology (MICHELOYANNIS *et al.*, 2006; RUBINOV *et al.*, 2009). In childhood-onset schizophrenia (COS), a decrease in topological modularity has been reported, along with reductions in local clustering and an increase in global efficiency and robustness (ALEXANDER-BLOCH *et al.*, 2010). In addition, Alves *et al.* (2022) analyzed fMRI and EEG datasets from patients with schizophrenia (SCZ) and found that spectral entropy was the most relevant EEG feature, showing a positive association with SCZ, followed by Hjorth mobility and complexity, which were negatively correlated with the disorder. For the fMRI data, diameter and closeness centrality (CC) were identified as crucial measures, with low CC values associated with SCZ.

In the context of autism spectrum disorder (ASD), EEG studies have revealed that affected individuals show reduced clustering coefficients and increased path lengths compared to healthy controls, suggesting a deviation from small-world network organization and increased modularity (BARTTFELD *et al.*, 2011). Complementary findings based on fMRI time series analyses indicate that patients with ASD exhibit greater network segregation, reduced global information distribution, and lower overall connectivity compared to healthy individuals (ALVES

et al., 2023).

Major depressive disorder (MDD) is another widely studied brain disorder characterized by heterogeneity in both symptoms and underlying causes (LEISTEDT; LINKOWSKI, 2013). EEG sleep studies have shown that acutely depressed patients have significantly reduced path lengths, unchanged clustering coefficients, decreased global synchronization, and a loss of small-world network properties (LEISTEDT *et al.*, 2009). Similarly, resting-state fMRI studies have identified reduced global efficiency and clustering coefficients, along with increased global betweenness centrality and path length in MDD patients (MENG *et al.*, 2014; SINGH *et al.*, 2013).

In general, graph theoretical approaches have proven valuable for characterizing functional network alterations in a variety of brain disorders. Such studies not only improve the understanding of disorder-specific network dysfunctions, but can also support the development of improved diagnostic and therapeutic strategies.

2.4.2 Automated brain disorder diagnosis

Reconstructing functional brain networks and developing automated diagnosis are closely related in the context of understanding and diagnosing brain disorders. Reconstructed networks serve as essential input data for machine learning algorithms and provide crucial information on the topological and functional properties of brain connectivity. These networks capture patterns associated with specific neurological conditions, allowing automated systems to more accurately identify and classify brain disorders. By analyzing the characteristics of functional networks for different disorders, automatic diagnosis methods can effectively distinguish individuals with brain abnormalities from healthy controls.

Automatic diagnosis of brain disorders involves the application of algorithms and machine learning techniques to analyze medical data and assist in the detection, classification, and prognosis of neurological conditions. The objective is to develop robust and reliable models capable of integrating multiple data sources, such as brain imaging scans, physiological signals, clinical records, and reconstructed functional networks, in order to identify relevant biomarkers and characteristics associated with specific brain disorders.

Over the past few years, there has been a significant increase in the development of diagnostic tools based on neuroimaging techniques (JO; NHO; SAYKIN, 2019; ALVES *et al.*, 2022b; ALVES *et al.*, 2022a; ALVES *et al.*, 2022c; AOE *et al.*, 2019). Common approaches in automatic diagnosis combine neuroimaging analysis with machine learning algorithms. Various neuroimaging modalities such as magnetic resonance imaging (MRI), functional MRI (fMRI), positron emission tomography (PET), and electroencephalography (EEG) provide data that, along with reconstructed functional networks, are used as training datasets for algorithms to extract relevant features and identify patterns associated with specific disorders.

Deep learning models have proven particularly effective in analyzing complex, high-dimensional datasets, such as fMRI data. By applying nonlinear transformations to raw data, deep learning classifiers automatically address challenges related to feature selection, which is especially advantageous when dealing with high-dimensional data or when prior domain knowledge is limited (RASHID; CALHOUN, 2020). Consequently, several studies have applied deep learning techniques for the diagnosis and understanding of various neurological and neuropsychiatry disorders.

These topics and methodologies are reviewed in recent literature (NATU *et al.*, 2022; RASHID; CALHOUN, 2020; SU *et al.*, 2020; MYSZCZYNSKA *et al.*, 2020). For example, Alves *et al.* (2022) used machine learning and deep learning techniques to evaluate connectivity matrices and complex network measures to establish an automated diagnosis and understand the topology and dynamics of brain networks in patients with schizophrenia. Their results showed that EEG-derived features outperformed complex network metrics to capture brain alterations associated with schizophrenia. The proposed model achieved excellent classification performance, with an area under the curve (AUC) of 100% and accuracy of 98% for the fMRI dataset, and an AUC of 95% with 95% accuracy for the EEG dataset.

In another study, Alves *et al.* (2022c) proposed a method for the automatic diagnosis of mental disorders based on connectivity matrices derived from EEG time series and deep learning techniques. The connectivity matrices between brain regions were constructed using three different approaches: Granger causality, Pearson's correlation and Spearman's correlation. These matrices were the entries of a convolutional neural network, which was optimized using random search and Bayesian optimization methods. The authors demonstrated that their method can classify patients with Alzheimer's disease and schizophrenia with high accuracy, achieving superior precision compared to traditional approaches, even when working with relatively small datasets.

Automatic diagnosis systems have the potential to assist healthcare professionals by achieving more accurate, rapid and cost-effective diagnoses. Moreover, such systems can enhance early detection and intervention, as well as support personalized treatment planning. By providing data-driven information, these tools contribute to better patient outcomes through more informed clinical decisions and targeted therapeutic strategies. However, it is important to emphasize that automatic diagnosis systems are designed as decision support tools to complement, not replace, the expertise of medical professionals.

CHAPTER

3

REVEALING PATTERNS IN MAJOR DEPRESSIVE DISORDER

Revealing patterns in major depressive disorder with machine learning and networks. Loriz Francisco Sallum, Caroline L. Alves, Thaise G. L. de O. Toutain, Joel Augusto Moura Porto, Christiane Thielemann, and Francisco A. Rodrigues *Chaos, Solitons & Fractals*. Current status: Accepted.

3.1 Context

Major Depressive Disorder (MDD) is a widespread mental health condition that significantly affects individuals' quality of life and is a leading cause of disability globally (COLLABORATORS, 2021). Traditional MDD diagnostic methods, which are highly based on subjective clinical evaluations, face challenges in providing consistent and objective results (PALLAGROSI *et al.*, 2016; LI *et al.*, 2019a). The urgency for innovative diagnostic tools has led to the exploration of machine learning (SAEEDI; SAEEDI; MAGHSOUDI, 2020; MAHATO; PAUL, 2020; MOVAHED *et al.*, 2021; XIA *et al.*, 2023; ANIK *et al.*, 2024) and complex network analysis (SUN *et al.*, 2019; HASANZADEH; MOHEBBI; ROSTAMI, 2020; ZHANG *et al.*, 2020; NOBAKHSH *et al.*, 2024; CHEN *et al.*, 2024) to better understand the neural mechanisms underlying MDD and improve diagnostic accuracy.

3.2 Contributions

This study presents a machine learning approach to diagnosing Major Depressive Disorder (MDD) using electroencephalography (EEG) data, with a particular focus on altered brain connectivity patterns. By comparing different connectivity metrics and applying advanced machine learning algorithms, including support vector machine (SVM) classifiers, we achieved

high accuracy in distinguishing MDD patients from typically developing (TD) patients.

To address the challenge of small datasets in neuroscience, we introduced a sliding window data augmentation approach, which improved model performance and generalisation. In addition, we investigated the effect of different sliding window sizes on classification accuracy, an aspect that has not been explored in previous research.

To ensure the robustness of our findings, we performed a rigorous analysis to prevent overfitting, including careful model selection and hyperparameter tuning, which are often overlooked in similar studies. As a result, our methodology outperformed previous work in the literature, achieving higher classification accuracy in distinguishing MDD from TD. In particular, our analysis identified the right fronto-central connection (F8-C4) as a critical region associated with MDD, suggesting connectivity disruptions that may affect emotional regulation, cognitive processing, and social cognition.

In addition, we applied complex network measures to investigate the structure of functional brain networks, which revealed distinct alterations in the MDD brain. Our findings highlight assortativity as a key metric and identify it as a potential biomarker for MDD. These findings contribute to a deeper understanding of the neural connectivity patterns of the disorder, helping to improve diagnostic and therapeutic approaches.

Revealing patterns in major depressive disorder with machine learning and networks

Loriz Francisco Sallum,[1,*] Caroline L. Alves,[2] Thaise G. L. de O. Toutain,[3,4] Joel Augusto Moura Porto,[5] Christiane Thielemann,[3] and Francisco A. Rodrigues[1]

[1] *University of São Paulo (USP), Institute of Mathematical and Computer Sciences (ICMC), São Paulo, Brazil*
[2] *Laboratory for Hybrid Modeling, Aschaffenburg University of Applied Sciences, Aschaffenburg, Bayern, Germany*
[3] *BioMEMS lab, Aschaffenburg University of Applied Sciences, Aschaffenburg, Germany*
[4] *Federal University of Bahia (UFBA), Health Sciences Institute(HSI), Bahia, Brazil*
[5] *University of São Paulo (USP), Institute of Physics of São Carlos (IFSC), São Paulo, Brazil*

Keywords: major depressive disorder, EEG, machine learning, complex networks

Major depressive disorder (MDD) is a multifaceted condition that affects millions of people worldwide and is a leading cause of disability. There is an urgent need for an automated and objective method to detect MDD due to the limitations of traditional diagnostic approaches. In this paper, we propose a methodology based on machine and deep learning to classify patients with MDD and identify altered functional connectivity patterns from EEG data. We compare several connectivity metrics and machine learning algorithms. Complex network measures are used to identify structural brain abnormalities in MDD. Using Spearman correlation for network construction and the SVM classifier, we verify that it is possible to identify MDD patients with high accuracy, exceeding literature results. The SHAP (SHAPley Additive Explanations) summary plot highlights the importance of C4-F8 connections and also reveals dysfunction in certain brain areas and hyperconnectivity in others. Despite the lower performance of the complex network measures for the classification problem, assortativity was found to be a promising biomarker. Our findings suggest that understanding and diagnosing MDD may be aided by the use of machine learning methods and complex networks.

I. INTRODUCTION

Major depressive disorder (MDD) is a common mental condition that affects over 274 million people worldwide, according to information on depression provided by the Global Burden of Disease (GBD) study of 2019 [1]. It is ranked as the second most significant contributor to the worldwide disease burden, measured in disability-adjusted life years, spanning both developed and developing countries [2]. MDD is a disabling condition marked by the presence of at least one distinct depressive episode enduring for a minimum of 2 weeks [3]. It is characterized by a persistent and pervasive low mood, loss of interest or pleasure in most activities, and a range of other symptoms that significantly impact daily functioning [4, 5].

Previous work has shown that MDD is a multifaceted disorder involving complex neurobiological mechanisms, including the interplay of nerve growth factors, neurosecretory systems, biogenic monoamines and brain-derived neurotrophic factors [6, 7]. Despite advances in understanding its neurobiology, there is currently no established mechanism that explains all aspects of the disorder [3, 4].

The diagnosis of MDD currently relies on doctor-patient communication and scale analysis, which is prone to problems such as low sensitivity, subjective bias and inaccuracy [8, 9]. Therefore, there is an urgent need for an objective, automated method capable of predicting clinical outcomes in depression, ultimately improving the accuracy of depression detection and treatment.

Recently, a large amount of data has been generated from MDD [10, 11]. Researchers have used different techniques to study MDD, such as functional magnetic resonance imaging (fMRI) [10, 12, 13], positron emission tomography (PET) [14, 15], and electroencephalography (EEG) [11, 16–19]. Recently, EEG has emerged as an important non-invasive and cost-effective tool that reveals real-time electrical activity and provides insights into neural oscillations and connectivity patterns associated with MDD. In particular, researchers have identified specific patterns and changes in brainwave activity, such as changes in frequency, amplitude and connectivity, that are indicative of MDD [19–21].

These observed changes have allowed the neuroimaging community to consider analytical methods to facilitate the classification of patients for different disorders [21–24], such as autism [25], schizophrenia [26] and Alzheimer [27]. Similarly, machine learning methods have been applied to the diagnosis of MDD through the analysis of EEG data [21–24, 28, 29], recognising subtle and intricate patterns within large datasets and identifying distinct features or biomarkers [19, 30]. The application of machine learning to EEG analysis has provided a more objective and data-driven approach to diagnosis, paving the way for personalised and effective interventions.

In a recent study [24], three machine learning algorithms were used to classify individuals with MDD:

* loriz.sallum@usp.br

support vector machine (SVM), multilayer perceptron (MLP), and the extended K-nearest neighbours (E-KNN) model. The use of all features in conjunction with the linear SVM classifier resulted in an accuracy of 93.75%. The proposed E-KNN model showed an accuracy of 93.10%, while MLP achieved an accuracy of 92.18%. Subsequently, Movahed et al. [21] used different types of EEG features derived from MDD, including statistical, spectral, wavelet, functional connectivity and nonlinear analysis methods. The Radial Basis Function Kernel Support Vector Machine (RBFSVM) classifier, which combines all feature sets, showed the best performance of all classifiers used, resulting in an average accuracy of 99%, sensitivity of 98.4%, specificity of 99.6%, f1-score of 98.9% and a false discovery rate of 0.4%.

Deep learning methods have also been applied to MDD diagnosis [31–34]. For example, Anik et al. [31] proposed an extended 11-layer 1-D convolutional neural network (Ex-1DCNN) to classify signals from MDD patients and healthy subjects. They analyzed the entire range of brainwaves, as well as each specific brainwaves separately. They identified that the Gamma brainwave at a 15-second epoch duration was the most effective feature, achieving an accuracy of 99.60%, sensitivity of 100%, specificity of 99.21%, and an F1 score of 99.60%. Additionally, for all brainwaves, a 5-second epoch duration achieved an accuracy of 98.73%, sensitivity of 98.63%, specificity of 98.82%, and an F1 score of 98.73%.

In another work [35], the authors proposed an end-to-end integrated deep learning (DL) model for classifying MDD patients and healthy controls based on resting-state EEG data. The model first automatically learned the potential connectivity relationships among EEG channels through a multi-head self-attention mechanism, then extracted higher-level features using a parallel two-branch convolutional neural network module, and finally performed classification through a fully connected layer. Ultimately, using the full frequency band, the AUC of the proposed model reached 0.96, with an accuracy of 98.45%, sensitivity of 98.55%, and specificity of 98.35%.

Several other studies have been conducted on the classification of MDD using EEG-derived data. Table I provides a list of papers along with the respective results of each investigation, including details of the machine learning and deep learning classifiers, providing a comparative overview of their performance.

In addition to brain signal data, researchers have recently incorporated network science as an additional method for understanding the fundamental properties of functional brain networks associated with various disorders [25–27, 36–38]. Numerous studies in the literature have examined depression through the lens of brain networks [19, 39–44], providing valuable information on brain functionality in relation to this disorder. These studies use advanced methods to analyze intricate connectivity patterns within brain networks, with the aim of distinguishing people with MDD from healthy subjects. Some of these works and their results are summarized in Table II, which emphasizes the differences between the brain topologies of MDD and TD and the relevance of brain network metrics as potential biomarkers for MDD diagnosis.

For example, Chen et al. [39] used phase locking value to construct brain networks for MDD, identifying several network metrics as potential biomarkers for diagnosis. Their analysis revealed significant differences between MDD and healthy controls in the theta, alpha, and full frequency bands. Specifically, the MDD brain network showed a lower clustering coefficient, local efficiency, and degree, indicating reduced local information processing and connectivity. Additionally, the MDD network had higher path length and lower global efficiency, suggesting impaired global information transmission.

In another study [41], the authors observed that MDD increases the shortest path length and decreases the clustering coefficient, indicating that the small-world characteristics of the brain functional network in MDD patients are weakened and tend to become more randomized. Additionally, they reported a decrease in betweenness centrality and local efficiency. Nevertheless, the existence of conflicting findings underlines the need for additional studies and further investigation. In particular, regarding path length, some authors observed longer path lengths in depressed patients [44, 45], while others reported shorter path lengths [46, 47].

Table II provides an overview of the studies, their results and the specific complex network measures used to differentiate MDD from healthy controls.

Thus, previous studies have shown that the analysis of raw EEG data and the use of complex networks are promising approaches to improve the diagnosis of MDD. In this paper, unlike previous work, we investigate MDD using both machine learning and network science approaches into a unified framework. Using the connectivity metric that yielded the highest predictive power, we reconstructed the brain topology and employed complex network metrics to gain deeper insights into the connectivity patterns that may underlie MDD brain topology.

Our primary goal is to diagnose MDD and understand the distinctive brain topological properties associated with this condition. We investigate the influence of reconstruction methods and machine learning algorithms on the classification process to achieve an accurate diagnosis. We verify that the Spearman correlation coefficient emerges as the most effective connectivity metric for network construction. We compute complex network measures from the connectivity matrix to determine the brain differences in MDD compared to typical development (TD). Specifically, the functional MDD brain network is characterised by increased assortativity, decreased connectivity density, and a more randomised topology. Our analysis also complements previous studies by incorporating data enrichment through multiple time windows to analyse brain signals. By integrating these different methods, metrics and machine learning algorithms, we achieve more accurate results than those

TABLE I. Summary of results on the performance of machine learning and deep learning methods for MDD classification using EEG time series.

Reference	Year	Data	EEG data	Methods	AUC	Accuracy	Recall	Precision	f1-Score
[31]	2024	34 MDD 30 TD 19 channels	EEG time series/ Frequency bands	ex-1DCNN	-	98.73	98.63	98.82	98.73
[35]	2023	30 MDD 28 TD 19 channels	EEG time series	DL model	0.96	98.45	98.55	-	-
[21]	2021	34 MDD 30 TD 19 channels	Combining feature sets	RBFSVM	-	99.0	98.4	-	98.9
[23]	2020	34 MDD 30 TD 19 channels	Power of frequency bands/ Alpha asymmetry	SVM/ LR/ NB/ Decision tree	-	88.33/ 85.82/ 86.63/ 87.50	89.41/ 73.57/ 87.42/ 89.28	-	-
[24]	2020	34 MDD 30 TD 19 channels	Frequency bands	SVM/ MLP/ E-KNN	-	93.75/ 92.18/ 93.10	94.11/ 91.11/ 88.23	-	-

TABLE II. Overview of results related to network-based features. PL: Shortest Path-Length, CC: Clustering Coefficient, BC: Betweeness Centrality, GE: Global Efficiency, LE: Local Efficiency, NS: Node Strength, ND: Node Degree.

Reference	Year	Complex network features	Findings related to MDD group
[39]	2024	CC, LE, GE, PL, ND	Decreased CC, LE, GE, ND and increased PL
[40]	2024	ND, BC	Increased ND and BC
[41]	2021	PL, BC, CC, LE	Increased PL and decreased BC, CC, LE
[42]	2020	GE, LE, BC, ND, NS	Increased GE and BC, no changes in LE, ND and NS
[43]	2019	CC, BC	Decreased CC and decreased BC
[44]	2018	PL, CC, GE, NS	Increased PL and decreased CC, GE, NS

reported in previous studies.

II. DATA AND DATA PRE-PROCESSING

The MDD dataset used in this paper was obtained by [22]. It consisted of two groups of participants: 34 MDD patients (17 women and 17 men, mean age = 40.3 ± 12.9) and 30 age-matched healthy controls (9 women and 21 men, mean age = 38.2 ± 15.6). Participants were recruited from the outpatient clinic of the Hospital Universiti Sains Malaysia (HUSM), Malaysia. EEG signals were recorded with the eyes closed from 19 scalp channels including frontal (Fp1, Fp2, F3, F4, F7, F8, Fz), temporal (T3, T4, T5, T6), parietal (P3, P4, Pz), occipital (O1, O2) and central (C3, C4, Cz) regions. The Cz electrode used as a reference was removed, leaving a total of 18 electrodes. For further details see [22].

The EEG dataset was pre-processed according to the methodology described by Toutain et al. [48]. The cleaning process was performed using EEGLAB from MATLAB. A bandpass filter from 0.5 to 48 Hz was applied and the data were then segmented into 1.05 second epochs. A threshold of $\pm 70\,\mu V$ was used, and epochs containing artefacts above the threshold (such as those associated with eye movements or muscle activity) were removed. Only eye closed EEG data from 29 MDD patients and 28 TD subjects were used in this study.

III. METHODOLOGY

Our methodology is illustrated in Figure 1.

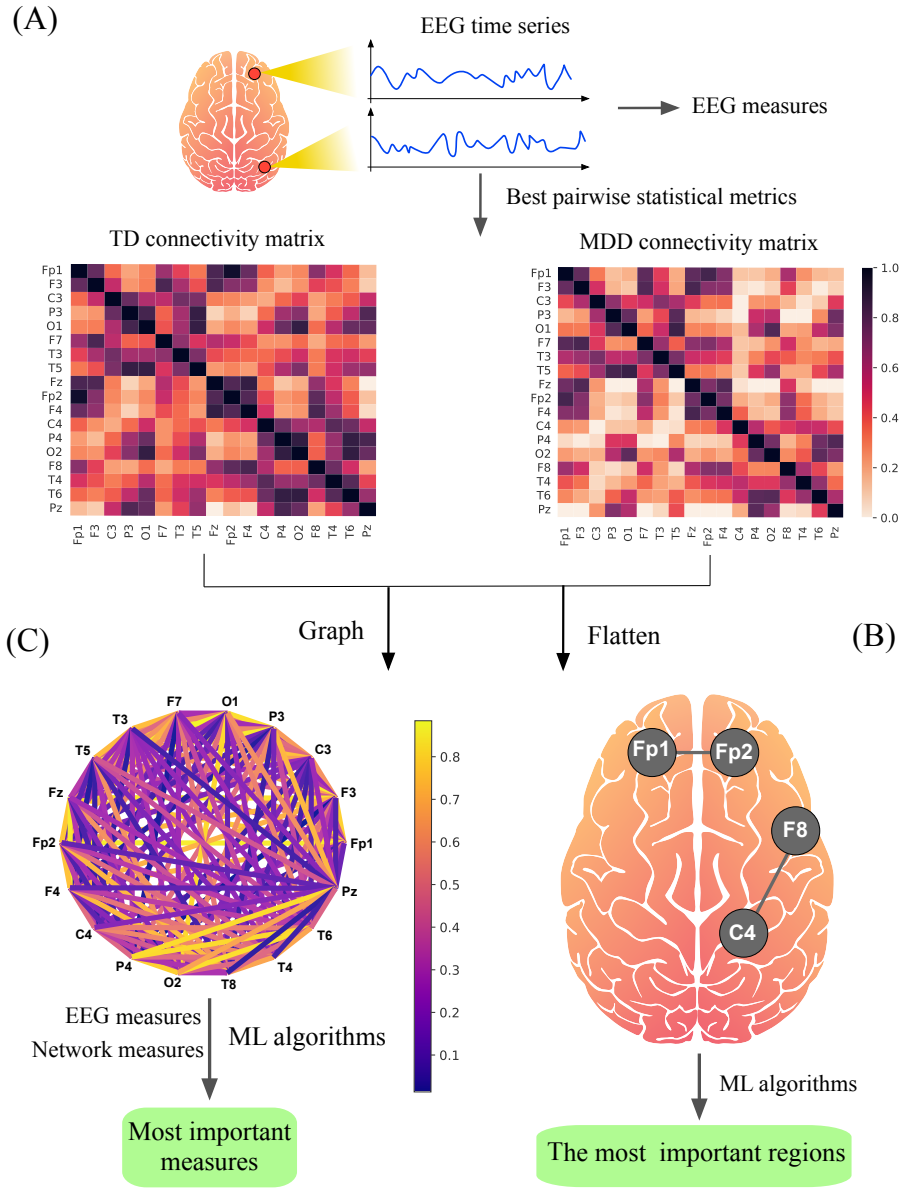

FIG. 1. The methodology for distinguishing MDD from TD patients. In (A), EEG signals are pre-processed and the most appropriate method for constructing the connectivity matrix is identified (see subsection III A). In (B), machine learning algorithms are used to find the most significant brain regions to discriminate between MDD and TD subjects. In (C), complex network measures quantify the main topological difference between TD and MDD brains (see subsection III B).

A. Connectivity matrices

From the 18-channel EEG time series, the connectivity matrix was constructed using Pearson Correlation (PC), Spearman Correlation (SC), Mutual Information (MI), Transfer Entropy (TE), Ledoit-Wolf Shrinkage (LW), Sparse Canonical Correlation Analysis (SCC) and Synchronization (Sync), as shown in Figure 1(A). These measures reflect the statistical dependence of activity between different brain regions. Each matrix was then reduced to vectors and used as input to the ML algorithm, as shown in Figure 1(B). The Support Vector Machine (SVM) algorithm was used to determine the most appropriate metric for constructing the connectivity matrices.

We used SVM because it has been widely employed in the literature to classify brain disorders [49]. Its relative simplicity and flexibility make it suitable for addressing various classification problems. In addition, SVM has a lower computational cost than other methods and is known to be robust to overfitting. Furthermore, it generally shows good predictive performance even with limited

sample size, which is common in neuroscience.

A 10-fold cross-validation procedure was employed for model selection and hyperparameter optimization, using the grid search method. The specific hyperparameters used for each machine learning method are detailed in Appendix A (Table VII).

Once the optimal brain connectivity metric was identified, the following machine learning classifiers were used: (i) Naive Bayes (NB), (ii) Random Forest (RF), (iii) Logistic Regression (LR), (iv) Multilayer Perceptron (MLP), and (v) Extreme Gradient Boosting (XGBoosting).

Accuracy was adopted as the standard performance metric for evaluating both connectivity metrics and machine learning and deep learning classifiers. Other common metrics such as AUC, precision and recall were also included. To evaluate the performance of the classifiers, we examined the confusion matrix, the receiver operating characteristic (ROC) curve and the learning curve. Using the best connectivity metric and the best machine learning classifier, the SHAPley additive explanation (SHAP) method was used to identify the differences between MDD and TD brain regions.

B. Complex network measures

An undirected binary graph was generated for each connectivity matrix to extract different complex network measures, as shown in Figure 1(C). The network connections are defined by functional connectivity, which refers to the temporal correlations between neurophysiological events in spatially distant brain regions. The complex network measures were stored in an attribute matrix, where each column represents a complex network measure and each row represents a subject.

The following complex network measures were calculated to describe brain structure Average Shortest Path Length (APL) [50], Betweenness Centrality (BC) [51], Closeness Centrality (CC) [52], Diameter [53], Assortativity Coefficient [54, 55], hub score [56], eccentricity [57], eigenvector centrality (EC) [58], average degree of k-nearest neighbours [59] (Knn), mean degree [60], entropy of the degree distribution (ED) [61], transitivity [62, 63], second moment of the degree distribution (SMD) [64], complexity, k-core [65, 66], density [67] and efficiency [68]. These 17 complex network measures were used in previous studies [25–27, 69, 70].

Additionally, the average path length within the largest community of each network was calculated, and the resulting value was incorporated into the attribute matrix. The community detection algorithms employed included FastGreedy (FC), Infomap (IC), Leading Eigenvector (LC), Label Propagation (LPC), Edge Betweenness (EBC), Spinglass (SPC), and Multilevel Community Identification (MC). To indicate the inclusion of the average path length, the abbreviations were modified by adding the letter "A" (for Average Path Length), resulting in the following notation: AFC, AIC, ALC, ALPC, AEBC, ASPC, and AMC.

The most accurate classifier algorithm, together with the most appropriate connectivity metric, was used to classify MDD patients. Performance evaluation included confusion matrix, ROC curve and learning curve. In addition, the SHAP method was used to identify the most relevant complex network measures to distinguish the topology of the MDD brain.

IV. RESULTS

A. Connectivity matrices

First, we conducted a performance analysis using the entire time series. To achieve this, connectivity matrices were constructed by applying connectivity-related metrics to compute the relationships between pairwise time series. The results are shown in Figure 2.

According to Figure 2, the AUC values of the training set were higher than 0.5, which is expected for a random classification. However, the accuracy of all metrics in the training set was poor, with values below 0.79. Furthermore, there were remarkably high errors in both AUC and accuracy and poor performance of the test set for almost all metrics. These results are indicative of overfitting, suggesting that the model may have learned to fit the training data too closely and was unable to generalize well to unseen data. Increasing the size of the datasets may be necessary to address this issue.

To overcome the problem of small data sets in neuroscience, in this paper we use a sliding window data augmentation approach, similar to what was done previously in [25]. The 300-second EEG time series was divided into non-overlapping segments with window sizes of 5, 10, 20, 30, 40, 50, 60, 80, 100, 120, and 150 seconds to increase the sample data. For each dataset generated with a specific window size, performance measures such as AUC and accuracy were calculated for both the training and test sets. For that, the window size was kept consistent across both the training and test sets during the experiment to ensure a fair evaluation of the model, with both sets being processed under the same temporal resolution conditions. This approach helped identify the optimal window size for each connectivity metric while maintaining consistency and fairness in performance evaluation. The AUC and accuracy results are illustrated in Figure 3.

To determine the optimal window size, we sought a balance between AUC and accuracy values for both the test and training sets. We also considered the error values associated with these metrics, giving preference to lower error rates.

After examining the results shown in Figure 3, it was evident that PC and SC exhibited superior performance compared to other metrics, with SC slightly outperforming PC. In particular, the most encouraging results were

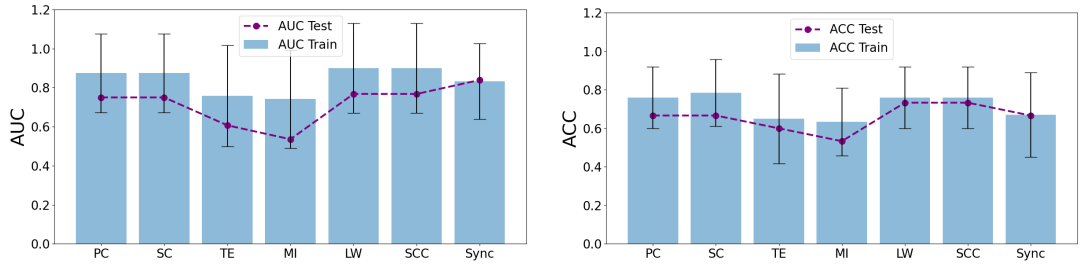

(a) (b)

FIG. 2. (a) AUC and (b) accuracy measures for each connectivity metric without using the sliding window.

observed for window sizes below 60 seconds, where both training and test sets showed excellent performance with minimal variance. Based on our analysis, the optimal window size for PC and SC data was determined to be $20s$ and $10s$ respectively. With a window size of 20 seconds, we obtained 435 connectivity matrices for the MDD class and 420 for the TD class. Similarly, a window size of 10 seconds corresponded to 870 connectivity matrices for the MDD class and 840 for the TD class.

The other connectivity metrics displayed significant variance across almost all window sizes. The performance of TE and MI data did not yield a satisfactory result for any of the window sizes tested, and there was no discernible trend between performance and window size. Therefore, a window size of $5s$ seconds was chosen, resulting in 1740 connectivity matrices for the MDD class and 1680 for the TD class. This window size was also chosen for LW and SCC, and a window size of $10s$ seconds was chosen for synchronisation.

Table III presents the results for each connectivity matrix constructed using each of the pairwise statistical metrics, along with their respective optimal window sizes. SVM was used to determine the most effective metric for classifying MDD and TD brains. The corresponding illustrations of the connectivity matrices for MDD and TD, for each metric, can be found in Appendix B (Figures 11 and 12).

Among the applied connectivity methods, PC (AUC = $1,000$, accuracy = 0.991) and SC (AUC = $1,000$, accuracy = 0.995) showed the best performance for the test set compared to the other metrics. However, SC was chosen over PC because of its ability to capture non-linear relationships and handle non-normally distributed data, which are common characteristics of brain connectivity data.

Three measures were used to evaluate the performance of classification models: (i) confusion matrix, (ii) ROC curve and (iii) learning curve. The results are shown in Figure 4.

After identifying the best connectivity metric, we compared different machine learning methods to determine the one that provides the most accurate classification. Table IV shows the results for each machine learning method using the connectivity matrices constructed using the Spearman correlation coefficient.

According to the table IV, all algorithms except the NB classifier showed high performance. Comparing the results for the test set, SVM gave the best performance (AUC = $1,000$, Accuracy = 0.995), closely followed by MLP (AUC = $1,000$, Accuracy = 0.991). However, SVM emerges as the preferred choice due to its ability to handle high-dimensional data efficiently, its robustness to overfitting, especially when dealing with small sample sizes, and its lower computational cost. In addition, SVM provides clear decision boundaries, which facilitates the interpretability and understanding of the classification process.

Our method achieved remarkable performance, surpassing the results found in the literature (see table I). In addition, we carefully examined potential overfitting problems and computed the AUC metric, a step not taken in other studies in the literature. The results of the confusion matrix, ROC curve and learning curve have already been shown in Figure 4.

As the performance reached almost 100%, we deliberately included random noise in the connectivity matrices of the MDD and TD groups to gain insight into the resilience of the model and its ability to recognise patterns even in the presence of perturbations, thus contributing to a more comprehensive understanding of its learning dynamics and performance under different conditions.

The noise was randomly generated from a Gaussian distribution with a mean of zero and a standard deviation ranging from 0.1 to 10. The response of the model's performance under these conditions was measured by the average AUC and average accuracy of the test set, and the results are shown in Figure 5.

Figure 5 shows that both AUC and accuracy values decrease as the error amplitude increases, roughly following a decreasing logarithmic function. This analogous trend was also observed in the autism study by Alves et al. [25], and suggests that the model can identify patterns even in the presence of noise.

SHAP values were then calculated to assess the importance of brain connections. To reduce the computational cost associated with calculating SHAP values without compromising the performance of the machine learning classification method, we first performed Recursive

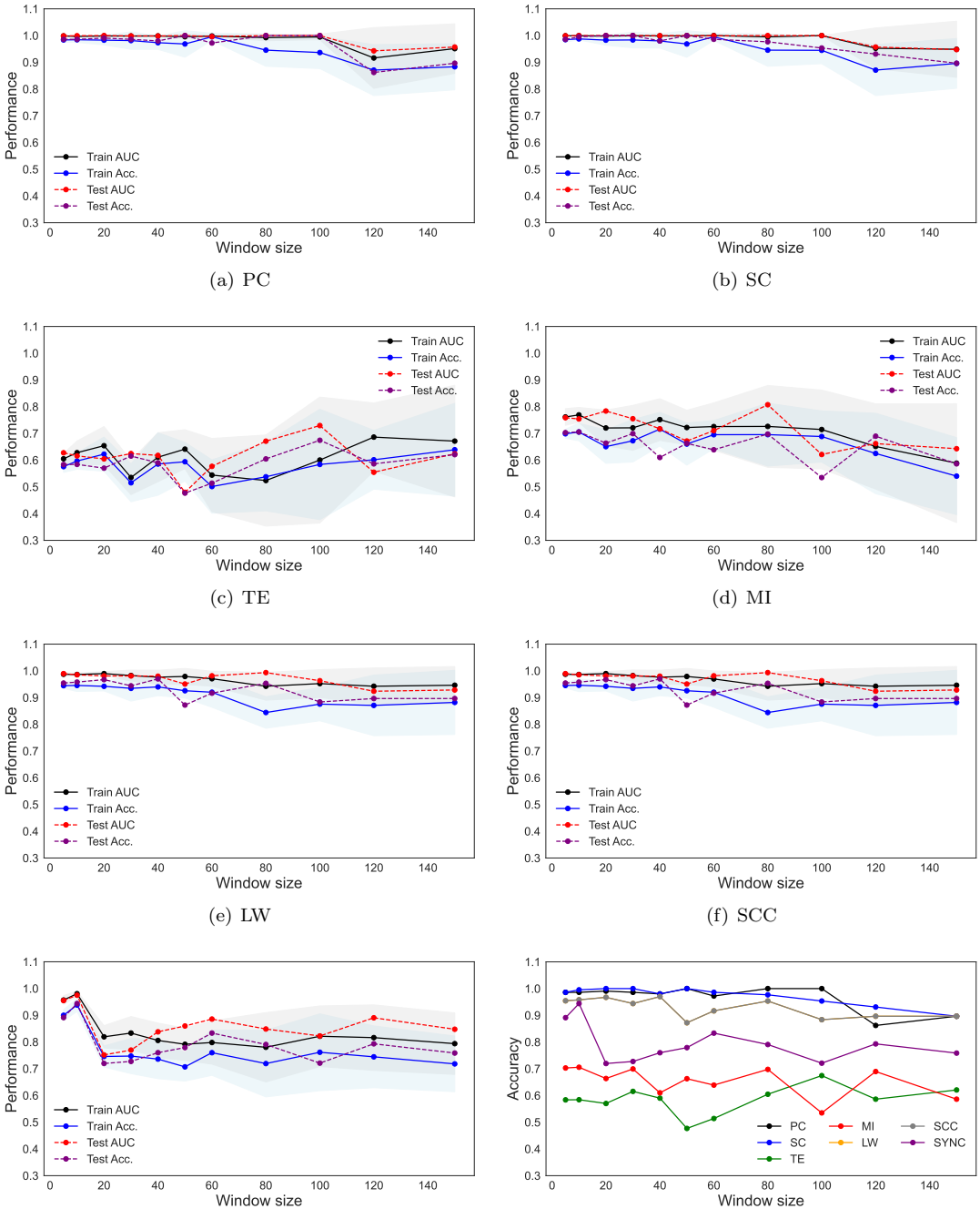

(a) PC (b) SC

(c) TE (d) MI

(e) LW (f) SCC

(g) Sync (h) Test accuracy

FIG. 3. Performance measures (AUC and accuracy) for the training and test set for all the connectivity metrics with different sliding window sizes.

Feature Elimination with Cross-Validation (RFECV) to identify the most relevant features. The RFECV analysis was conducted using an SVM model. As shown in Figure 6, the model achieved higher accuracy with a subset of 277 features, indicating that the entire feature set was not required for optimal efficiency. This approach ensures computational efficiency while preserving the performance of the classification model

As shown in Figure 6(b), maximum performance is achieved using the full data set. In addition, the gap between the validation curve and the training curve remained consistent with the results obtained using all features (see Figure 4(c)), as did the variability over the validation curve. As shown in Table V, the performance

TABLE III. Results obtained from SVM using different statistical methods to construct the brain network.

Method	Window size	Subset	AUC	Accuracy	Recall	Precision
PC	20s	Train	0.999 ± 0.002	0.983 ± 0.018	0.983 ± 0.018	0.984 ± 0.016
		Test	1.000	0.991	0.991	0.991
SC	**10s**	**Train**	$\mathbf{0.999 \pm 0.001}$	$\mathbf{0.988 \pm 0.004}$	$\mathbf{0.988 \pm 0.004}$	$\mathbf{0.988 \pm 0.004}$
		Test	**1.000**	**0.995**	**0.995**	**0.995**
TE	5s	Train	0.605 ± 0.020	0.576 ± 0.022	0.576 ± 0.022	0.576 ± 0.022
		Test	0.628	0.584	0.584	0.584
MI	5s	Train	0.762 ± 0.031	0.699 ± 0.017	0.699 ± 0.017	0.700 ± 0.017
		Test	0.759	0.703	0.703	0.703
LW	5s	Train	0.987 ± 0.006	0.945 ± 0.010	0.945 ± 0.010	0.945 ± 0.010
		Test	0.990	0.954	0.954	0.955
SCC	5s	Train	0.987 ± 0.006	0.945 ± 0.009	0.945 ± 0.009	0.948 ± 0.009
		Test	0.990	0.954	0.954	0.955
Sync	10s	Train	0.981 ± 0.010	0.938 ± 0.024	0.900 ± 0.021	0.900 ± 0.021
		Test	0.975	0.944	0.891	0.891

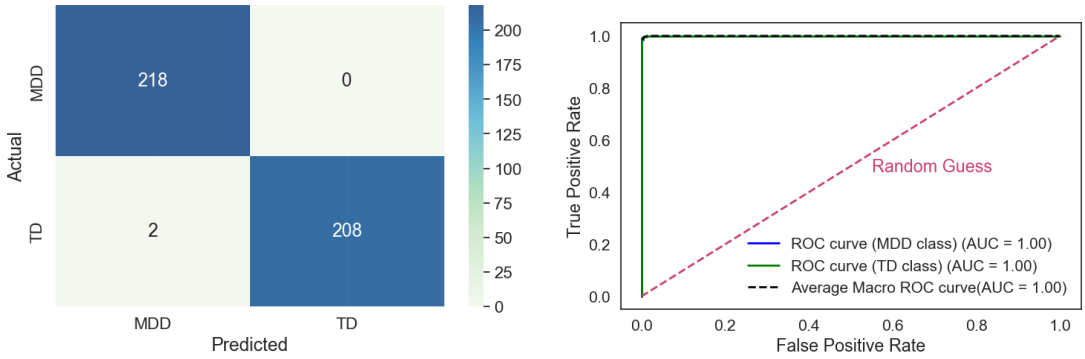

(a) Confusion matrix

(b) ROC curve

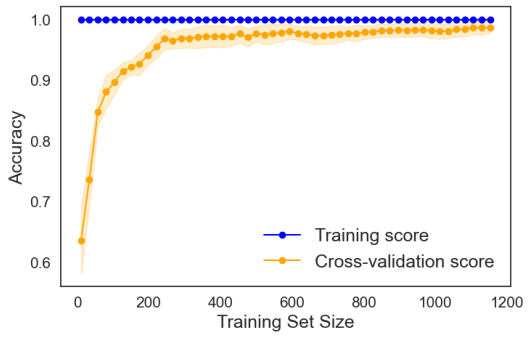

(c) Learning curve

FIG. 4. Results from the SVM classifier using as input the connectivity matrices constructed via SC and times series with a window size of 10s.

remained sufficiently high. Based on these results, we used the 277 features derived from the RFECV analysis to obtain SHAP values, as shown in Figure 7.

The most important brain connections that are crucial for distinguishing MDD patients from TD patients are ranked in Figure 7. The connection between region C4 and F8 emerged as the most important for distinguishing MDD patients from TD patients. Low PC values (blue dots) for this connection are indicative of the MDD group, whereas high PC values (red dots) are associated with the TD group. The second most important connection was between region Fp1 and Fp2. Low PC values (blue dots) for this connection characterise MDD individuals, while high correlation values (red dots) are

TABLE IV. Results obtained from machine learning classifiers using the connectivity matrices constructed by employing Spearman correlation coefficient and times series with a window size of $10s$.

ML methods	Dataset	AUC	Accuracy	Recall	Precision
SVM	**Train**	$\mathbf{0.999 \pm 0.001}$	$\mathbf{0.988 \pm 0.004}$	$\mathbf{0.988 \pm 0.004}$	$\mathbf{0.988 \pm 0.004}$
	Test	**1.000**	**0.995**	**0.995**	**0.995**
MLP	Train	0.998 ± 0.002	0.984 ± 0.007	0.984 ± 0.007	0.984 ± 0.007
	Test	1.000	0.991	0.991	0.991
RF	Train	0.991 ± 0.006	0.943 ± 0.018	0.943 ± 0.018	0.946 ± 0.017
	Test	0.995	0.944	0.944	0.949
NB	Train	0.762 ± 0.028	0.729 ± 0.020	0.729 ± 0.020	0.791 ± 0.021
	Test	0.783	0.743	0.743	0.810
LR	Train	0.995 ± 0.005	0.964 ± 0.016	0.964 ± 0.016	0.965 ± 0.015
	Test	0.995	0.974	0.974	0.974
XGBoost	Train	0.993 ± 0.004	0.963 ± 0.010	0.963 ± 0.019	0.964 ± 0.019
	Test	0.998	0.958	0.958	0.958

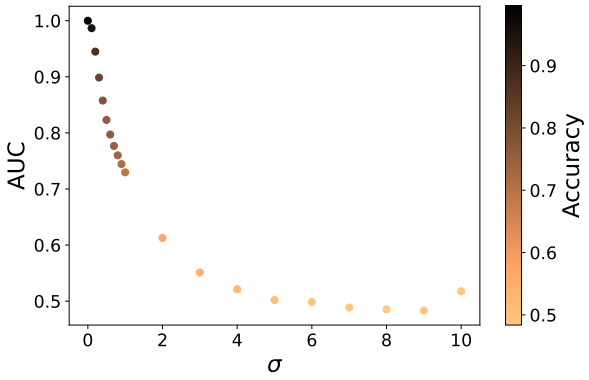

FIG. 5. Performance of the test set for the SVM model with random Gaussian noise with a mean equal to zero and a standard deviation that varies from 0.1 to 10.

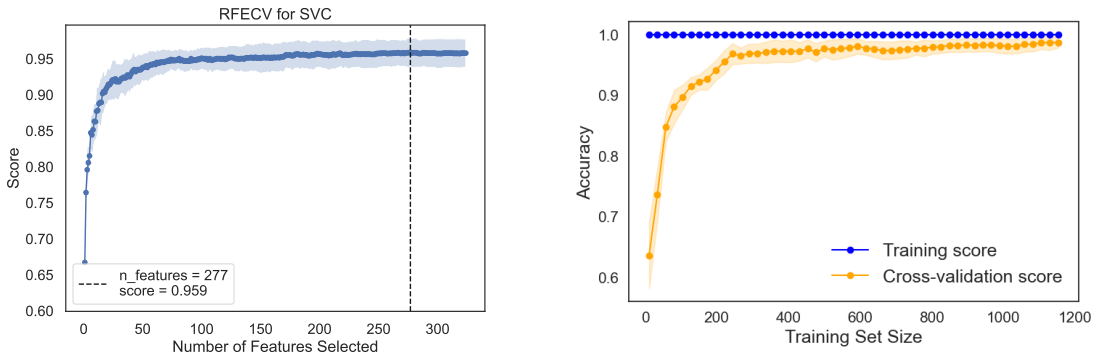

(a) RFECV (b) Learning curve

FIG. 6. RFECV (a) and the learning curve (b) of the SVM model. In (a), it can be seen that optimal performance is achieved with 277 features. In (b), the learning curves considering the training data set (1282 connectivity matrices) are shown for the training accuracy (blue) and the validation accuracy (orange), and it can be seen that the maximum performance was obtained using the entire training set.

TABLE V. Results obtained from SVM classifier using the 277 features selected by the RFECV.

ML method	Subset	AUC	Accuracy	Recall	Precision
SVM	Train	0.999 ± 0.001	0.988 ± 0.004	0.988 ± 0.004	0.988 ± 0.004
	Test	1.000	0.995	0.995	0.995

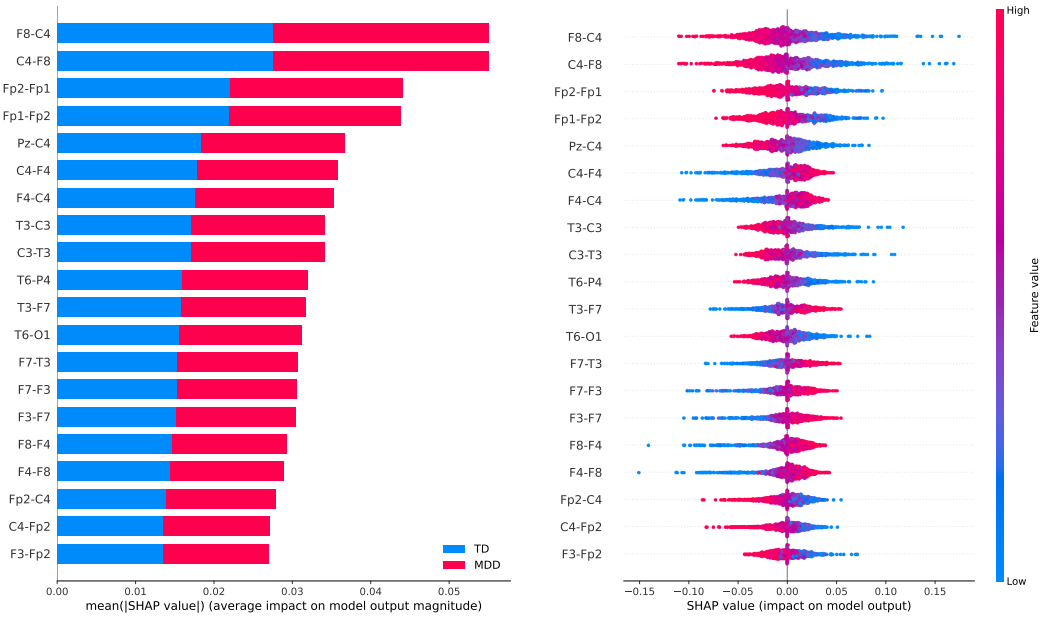

(a) (b)

FIG. 7. Feature importance ranking for the SVM classifier, with the brain regions ranked in descending order of importance for MDD. Figure 7(a) illustrates the average impact of each feature for the TD class and MDD class. Figure 7(b) shows the effect of each feature for the classification related to MDD class.

essential for identifying TD patients.

B. Complex network measures

We reconstructed the brain topology of MDD and TD subjects based on the connectivity matrices that resulted in the best classification performance. These matrices were derived using the Spearman correlation coefficient applied to segmented time series with a 10-second window size. By reconstructing the brain networks, we aimed to understand the network differences between MDD and TD subjects. Additionally, we investigated whether using only the complex network metrics derived from these reconstructed topologies could achieve good classification performance. The extracted network measures were stored in a matrix, which was then used as input to the SVM classifier, as this machine learning algorithm demonstrated the best performance, as discussed in the previous subsection. The results for the SVM algorithm using the complex network measures are shown in table VI.

According to the results in Table VI, the AUC and accuracy values on the test set were 0.875 and 0.804, respectively. Using network metrics for the classification problem did not lead to superior performance compared to using connectivity matrices (see Table IV). However, it did lead to an acceptable performance. The confusion matrix, ROC curve and learning curve were used to evaluate the performance and the results are shown in Figure 8.

The influence of the complex network measures on the model's performance was then assessed using the SHAP summary plot.

The complex network measures crucial to discriminating MDD patients from TD patients are ranked according to their global importance in Figure 9. All features are shown in order of global importance, with the first being the most important and the last being the least important.

According to Figure 9, the most critical network measures for discriminating between MDD and TD subjects were assortativity, entropy of the degree distribution (ED) and density, in that order. High values (red dots) of assortativity have a high positive contribution to the detection of MDD patients. In contrast, low values of these variables (blue dots) have a high negative contribution to the detection of MDD patients. Low values (blue dots)

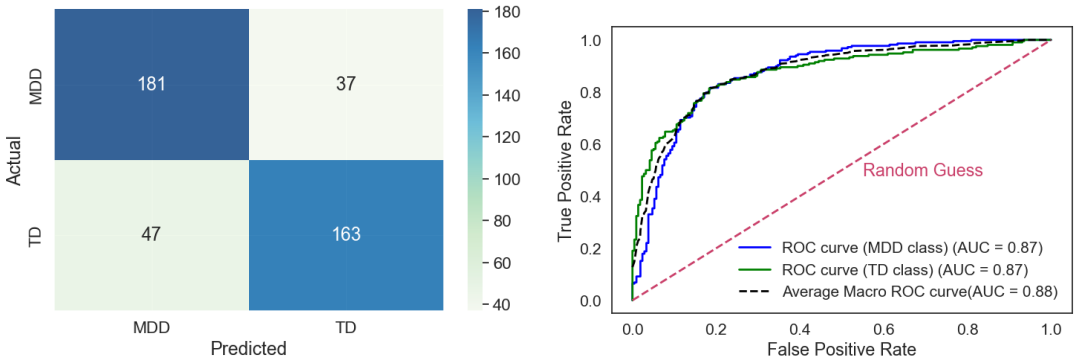

(a) Confusion matrix (b) ROC curve

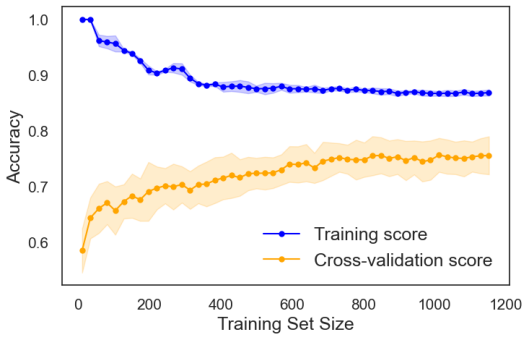

(c) Learning curve

FIG. 8. Results obtained from SVM classifier using the complex network measures that were calculated by connectivity matrices constructed through Spearman correlation coefficient with sliding window of 10s.

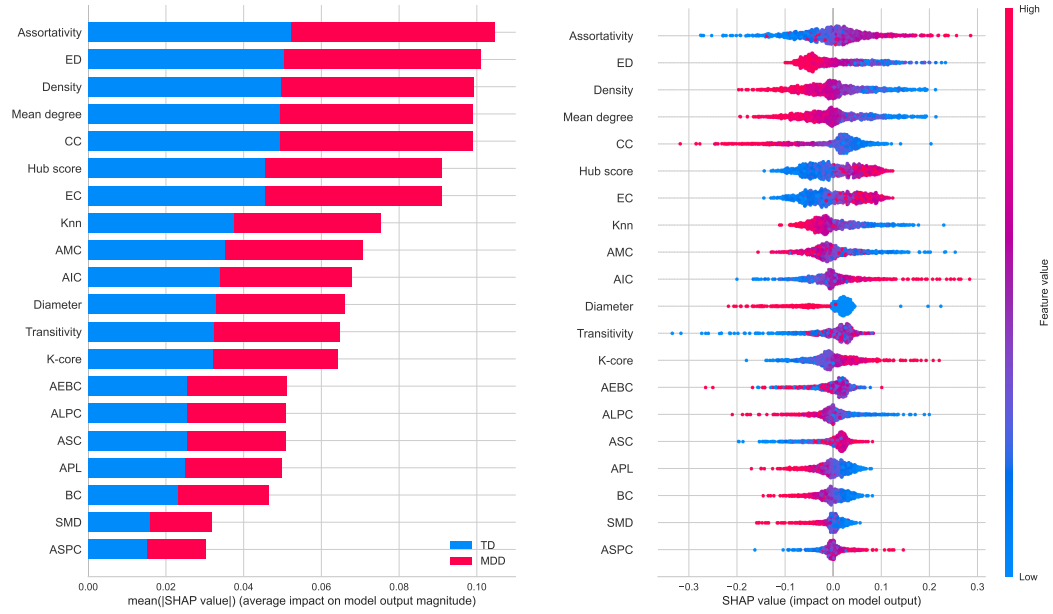

(a) (b)

FIG. 9. Feature importance ranking for the SVM classifier with the complex network measures ranked in descending order of importance for Major Depressive Disorder (MDD). Figure 9(a) shows the average influence of each metric for the TD class and the MDD class. Figure 9(b) shows the effect of each metric for classification in relation to the MDD class.

TABLE VI. Results obtained by the SVM classifier using the complex network measures computed using the connectivity matrices constructed by the Spearman correlation coefficient with a window size of 10s.

ML method	Subset	AUC	Accuracy	Recall	Precision
SVM	Train	0.843 ± 0.033	0.766 ± 0.047	0.766 ± 0.047	0.770 ± 0.047
	Test	0.875	0.804	0.804	0.804

of ED and Density have a high positive contribution to the detection of MDD patients. In addition, high values (red dots) of these variables have a high negative contribution to the detection of MDD patients. The same interpretation can be applied to the other variables.

V. DISCUSSION

A. Connectivity matrices

Among all applied connectivity methods, SC exhibited the best performance for the test set, with AUC and accuracy values of 1.000 and 0.995, respectively (see Table III). To the best of our knowledge, these results exceed those reported in the literature (see Table I). Even when compared to more complex and computationally expensive deep learning methods, our method stands out. For instance, the results from two deep learning-based approaches reported in Table III show that even though the models achieve high performance, they do so at a significant computational cost. In the work by [31], the ex-1DCNN model achieved an AUC of 98.73% and accuracy of 98.63%, while the DL model in [35] attained an AUC of 0.96 and accuracy of 98.45%. While these values are impressive, our method demonstrates superior performance with a perfect AUC of 1.000 and an accuracy of 0.995, all achieved with a less complex approach. This underscores the efficiency and effectiveness of our methodology in MDD classification using EEG time series.

The SC metric is a nonparametric measure of rank correlation [71], widely employed as a tool in neuroscience and brain research, with consistently favourable results [72–75]. It plays a crucial role in the study of brain disorders by assessing the monotonic relationship [76] between brain regions, that is, as the signal of one region increases, so does the signal of the other region, or as the signal of one region increases, the signal of the other region decreases.

In addition, SC assesses the strength and direction of a monotonic association, allowing complex, non-linear dependencies between brain regions to be captured [77]. This suggests that the relationship between brain activities associated with depression may tend to become monotonic, not necessarily linear.

The confusion matrix (Fig. 4(a)) clearly shows that the SVM model achieves a 99% of probability in distinguishing the TD class from the MDD class and also indicates a 100% of probability that the SVM model can distinguish the MDD class from the TD class. This indicates that sensitivity (true positives) slightly exceeds specificity (true negatives), suggesting that the SVM model using connectivity matrices as input is marginally better at identifying patients with MDD than those with TD. The area under the ROC curve (Fig. 4(b)) is equal to 1.00 for both classes, indicating that the SVM model can discriminate perfectly between the TD and MDD classes.

The learning curve analysis presented in Figure 4(c) reveals some key insights. The training score remains high regardless of the size of the training set. Conversely, the test score increases with the size of the training data set, indicating that performance improves with more data until it reaches a plateau. This indicates that it is not useful to acquire new data, as the generalisation performance of the model will not increase further. There is also a relatively small gap between the training and cross-validation scores when considering the entire dataset, indicating that the model generalises well and has a good bias-variance trade-off.

Alternative machine learning methods were explored to assess whether there was an improvement in performance. As shown in table IV, both SVM and MLP gave satisfactory results. However, SVM produced slightly better results. Considering this analysis, SVM was selected as the ML method for the subsequent steps.

Although the classification performance achieved high values, the results from the insertion of random noise (Figure 5) suggest that the model can identify patterns even in the presence of noise. In other words, the model generalises to noisy data and learns the underlying patterns.

Based on the SHAP summary plot (Figure 7), the critical discriminator between MDD and TD patients was the connection between region C4 and F8, which was ranked as the most significant. This connection was followed by the connection between regions Fp1-Fp2. The SHAP plot showed that the most critical connections were located in both the right and left hemispheres of the brain, particularly in the frontal lobe. These results were consistent with previous findings in the literature, such as in [16, 78, 79].

In particular, low SC values in C4-F8 and Fp1-Fp2 connections contributed to the identification of the MDD group. The schematic brain plot in Figure 10 illustrates the key connections associated with altered connectivity in the neural network structure of individuals with MDD.

The C4 electrode is positioned in a brain region that is associated with the motor cortex and voluntary movement control [82, 83], which is involved in the planning,

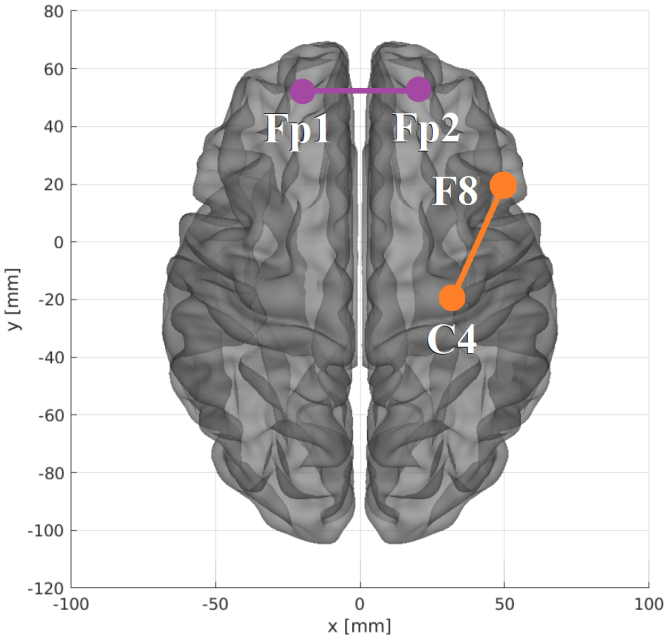

FIG. 10. The most relevant connections, in terms of correlations, are found in the two-dimensional schematic (ventral axis), highlighted in descending order of importance in orange and purple. The brain plot was developed using the Braph tool [80], based on the coordinates in [81].

control, and execution of voluntary movements [84]. The F8 electrode is positioned in the right frontal area of the brain. This region involves various cognitive functions, such as attention, decision-making, social skills, emotional processing, and social cognition [85–88]. Results from the literature suggest that the frontal lobe plays a vital role in depression [78, 87].

Disruption in C4-F8 brain connectivity in individuals with depression may suggest deficits in attention, working memory, decision-making, and problem-solving. This observation is in accordance with the findings of the literature [89, 90], where the frontoparietal was shown to exhibit lower functional connectivity in patients with MDD than in healthy participants.

Frontal lobe dysfunction has been reported in patients with MDD [73, 87, 91]. In [73], the authors identified that, in addition to the frontal lobe, the central lobes are also involved in the impairment associated with MDD. This suggests that the fronto-central regions could serve as reliable indicators of attention deficits in MDD patients, which appears to be linked to the severity of subjective depressive symptoms. Our results are consistent with these previous findings in the literature. Additionally, a recent study on mental disorders with suicide [92] found impairment in the fronto-central regions of the suicidal group, suggesting that the brain's electrical activity in these regions may be damaged, leading to an increased risk of suicide in mental disorders.

The Fp1 electrode is located over the left frontopolar lobe and is involved in cognition, working memory and perception [93]. The Fp2 electrode is placed over the right frontopolar cortical area and is related to affective processing and social cognition [93]. A disruption in connectivity between FP1 and FP2 could lead to cognitive dysfunction, including difficulties with concentration, memory and decision-making, which are often seen in people with MDD. It may also contribute to difficulties in regulating emotions, leading to symptoms such as persistent sadness, irritability and mood swings, which are common in MDD. These findings are consistent with the literature [94].

Figure 7 illustrates the impact of MDD on both hemispheres of the brain, in line with findings in the literature [22, 78, 95–97]. In addition, Mohan et al. [98] highlighted the central brain region, particularly C3 and C4, as highly effective in detecting depression. Furthermore, Yang et al. [99] highlighted the importance of analysing the MDD brain by considering a combination of frontal, temporal and central lobe regions, confirming some of the critical regions identified in our study.

B. Complex network measures

As can be seen from the results presented in Table VI, using network metrics for the classification problem did not yield comparable or better performance than using connectivity matrices. The AUC and accuracy results for the test set were 0.875 and 0.804, respectively (see table IV).

The confusion matrix (Fig. 8(a)) shows that the SVM model achieved an accuracy of 77.6% in discriminating the TD class from the MDD class and 83.0% in the differentiation of the MDD class from the TD class. This means that the sensitivity exceeds the specificity, suggesting that the SVM model, when using the attribute matrix as input, is also better at identifying patients with MDD than those with TD. The ROC curve (Fig. 8(b)) shows an 87% of probability that the SVM model can discriminate between the TD and MDD classes.

Regarding the learning curve (Fig. 8(c)), we can see that the training score is very high when using few samples for training, and it decreases as the number of samples increases until a certain amount of data, after which it stabilizes. In contrast, the test score is initially low and increases with the addition of more samples. Besides, there is a significant difference between training and validation accuracy.

The results indicate that complex network measures did not provide accurate results compared to connectivity matrices. This finding suggests that the differences between the brains of healthy people and those with MDD are very subtle and not captured by the measures we used. Subtle differences between the brains of controls and people with mental disorders have been observed before [100].

Despite that, the investigation regarding complex network measures offers valuable insight to uncover significant characteristics of the topology of the MDD brain and how it is discerned from the TD brain. These measures provide an understanding of the intricate connectivity patterns within the brain network, allowing for the identification of key features that contribute to the manifestation of MDD. Hence, we examined the impact of complex network measures on the model's performance using the SHAP summary plot.

As shown in the SHAP summary plot (Figure 9), assortativity emerges as the primary discriminator between MDD and TD patients, ranking as the most significant complex network measure. ED and density are also relevant features for the diagnosis of MDD. The assortativity coefficient is a topological measure that refers to the tendency of nodes to connect to others with similar characteristics [55, 101]. Specifically, it measures the correlation between the degrees of neighbouring nodes in the network. From the SHAP summary plot, high values of assortativity are associated with the MDD group. This result contrasts with the literature, which found no difference in assortativity values between MDD and TD [102] or lower assortativity in MDD patients [103]. Higher assortativity tends to show a higher degree of modularity and leads to more robust networks, which has already been reported in the literature [42, 47].

The entropy of the degree distribution (ED) is an average measure of the heterogeneity of the network and can be used to quantify network complexity [104]. A high entropy means that there is a wide range of node degrees in the network, indicating a more heterogeneous structure. Our results suggest that MDD brains present smaller values of ED, indicating a less structured topology. Our results are also consistent with [41–43, 47].

We also observed a lower density value in MDD brains, as indicated by the SHAP summary plot. Density quantifies the extent to which nodes in the network are connected to each other [105]. A density of 0 indicates a completely disconnected network, while a density of 1 represents a completely connected network. Networks with higher densities often have more robust connectivity, while networks with lower densities may be more sparse, with fewer connections as seen in functional MDD brain network.

VI. CONCLUSIONS AND FUTURE WORK

Our research helps to understand the characteristics of MDD brains. The analysis of different approaches to construct the connectivity matrix showed that the Spearman correlation coefficient, especially with a sliding window of 10 seconds, had the highest accuracy in discriminating between MDD and TD subjects. The SVM model was the best classifier. Our results showed an AUC of 1.00 and an accuracy of 0.993 for the test set. This performance exceeds the results documented in the literature.

From the SHAP summary plot, the right fronto-central connection, specifically F8-C4, are the regions most associated with MDD. Low PC scores for this connection are also associated with the MDD group, suggesting a disruption in the connectivity of brain networks that affect emotional regulation, cognitive processing and social cognition.

The second most important connection (Fp1-Fp2) associated with MDD is located in the frontopolar region of the brain, in both the right and left hemispheres. These regions are associated with affective processing, social cognition, working memory and perception. Low SC scores for this connection are associated with MDD patients and may be related to poor concentration, memory and decision-making difficulties. It may also contribute to problems in regulating emotions, leading to mood swings. These features are often observed in people with MDD.

Abnormal EEG patterns were found to be prevalent in both hemispheres of the MDD brain, which is consistent with existing literature. Interestingly, the application of complex network measures showed inferior classification performance compared to connectivity matrices. The test set yielded an AUC of 0.875 and an accuracy of 0.804. However, the network approach highlighted the importance of some measures such as assortativity, entropy of the degree distribution and density of connections. The functional MDD brain network has a more homogeneous degree distribution, resulting in a less structured topology, which could reduce the efficiency of information flow.

Our future study could include comparing local and

global data to identify the most effective approach for patient differentiation and topology interpretation. In addition, exploring the different frequencies of EEG signals may provide insights into potential improvements in predictive accuracy and a deeper understanding of the intricate dynamics of MDD-related brain changes.

VII. ACKNOWLEDGEMENTS

L.F.S. is indebted to Capes (grant 88887.645667/2021-00) for the financial provided to this research. F.A.R acknowledges CNPq (grant 308162/2023-4) and FAPESP (grants 24/02322-0, 20/09835-1 and 13/07375-0) for the financial support given for his research.

[1] G. . Collaborators, Global burden of disease study 2020 (gbd 2020) results, Institute for Health Metrics and Evaluation (IHME) (2021).

[2] T. Vos, R. M. Barber, B. Bell, A. Bertozzi-Villa, S. Biryukov, I. Bolliger, F. Charlson, A. Davis, L. Degenhardt, D. Dicker, *et al.*, Global, regional, and national incidence, prevalence, and years lived with disability for 301 acute and chronic diseases and injuries in 188 countries, 1990–2013: a systematic analysis for the global burden of disease study 2013, The lancet **386**, 743 (2015).

[3] C. Otte, S. M. Gold, B. W. Penninx, C. M. Pariante, A. Etkin, M. Fava, D. C. Mohr, and A. F. Schatzberg, Major depressive disorder, Nature reviews Disease primers **2**, 1 (2016).

[4] R. H. Belmaker and G. Agam, Major depressive disorder, New England Journal of Medicine **358**, 55 (2008).

[5] W. Marx, B. W. Penninx, M. Solmi, T. A. Furukawa, J. Firth, A. F. Carvalho, and M. Berk, Major depressive disorder, Nature Reviews Disease Primers **9**, 44 (2023).

[6] V. Krishnan and E. J. Nestler, The molecular neurobiology of depression, Nature **455**, 894 (2008).

[7] M. aan het Rot, S. J. Mathew, and D. S. Charney, Neurobiological mechanisms in major depressive disorder, Cmaj **180**, 305 (2009).

[8] M. Pallagrosi, L. Fonzi, A. Picardi, and M. Biondi, Association between clinician's subjective experience during patient evaluation and psychiatric diagnosis, Psychopathology **49**, 83 (2016).

[9] X. Li, X. Zhang, J. Zhu, W. Mao, S. Sun, Z. Wang, C. Xia, and B. Hu, Depression recognition using machine learning methods with different feature generation strategies, Artificial intelligence in medicine **99**, 101696 (2019).

[10] A. M. Milne, G. M. MacQueen, and G. B. Hall, Abnormal hippocampal activation in patients with extensive history of major depression: an fmri study, Journal of Psychiatry and Neuroscience **37**, 28 (2012).

[11] D. A. Pizzagalli, Frontocingulate dysfunction in depression: toward biomarkers of treatment response, Neuropsychopharmacology **36**, 183 (2011).

[12] M. J. Rosa, L. Portugal, T. Hahn, A. J. Fallgatter, M. I. Garrido, J. Shawe-Taylor, and J. Mourao-Miranda, Sparse network-based models for patient classification using fmri, Neuroimage **105**, 493 (2015).

[13] E. Bondi, E. Maggioni, P. Brambilla, and G. Delvecchio, A systematic review on the potential use of machine learning to classify major depressive disorder from healthy controls using resting state fmri measures, Neuroscience & Biobehavioral Reviews **144**, 104972 (2023).

[14] C. J. Bench, K. J. Friston, R. G. Brown, R. Frackowiak, and R. J. Dolan, Regional cerebral blood flow in depression measured by positron emission tomography: the relationship with clinical dimensions, Psychological medicine **23**, 579 (1993).

[15] H. S. Mayberg, Positron emission tomography imaging in depression: a neural systems perspective, Neuroimaging Clinics **13**, 805 (2003).

[16] A. A. Fingelkurts, A. A. Fingelkurts, H. Rytsälä, K. Suominen, E. Isometsä, and S. Kähkönen, Impaired functional connectivity at eeg alpha and theta frequency bands in major depression, Human brain mapping **28**, 247 (2007).

[17] A. Miljevic, N. W. Bailey, O. W. Murphy, M. P. N. Perera, and P. B. Fitzgerald, Alterations in eeg functional connectivity in individuals with depression: A systematic review, Journal of Affective Disorders (2023).

[18] S. Olbrich and M. Arns, Eeg biomarkers in major depressive disorder: discriminative power and prediction of treatment response, International Review of Psychiatry **25**, 604 (2013).

[19] F. S. de Aguiar Neto and J. L. G. Rosa, Depression biomarkers using non-invasive eeg: A review, Neuroscience & Biobehavioral Reviews **105**, 83 (2019).

[20] A. A. Fingelkurts and A. A. Fingelkurts, Altered structure of dynamic electroencephalogram oscillatory pattern in major depression, Biological Psychiatry **77**, 1050 (2015).

[21] R. A. Movahed, G. P. Jahromi, S. Shahyad, and G. H. Meftahi, A major depressive disorder classification framework based on eeg signals using statistical, spectral, wavelet, functional connectivity, and nonlinear analysis, Journal of Neuroscience Methods **358**, 109209 (2021).

[22] W. Mumtaz, L. Xia, S. S. A. Ali, M. A. M. Yasin, M. Hussain, and A. S. Malik, Electroencephalogram (eeg)-based computer-aided technique to diagnose major depressive disorder (mdd), Biomedical Signal Processing and Control **31**, 108 (2017).

[23] S. Mahato and S. Paul, Classification of depression patients and normal subjects based on electroencephalogram (eeg) signal using alpha power and theta asymmetry, Journal of medical systems **44**, 1 (2020).

[24] M. Saeedi, A. Saeedi, and A. Maghsoudi, Major depressive disorder assessment via enhanced k-nearest neighbor method and eeg signals, Physical and Engineering Sciences in Medicine **43**, 1007 (2020).

[25] C. L. Alves, T. G. d. O. Toutain, P. de Carvalho Aguiar, A. M. Pineda, K. Roster, C. Thielemann, J. A. M. Porto, and F. A. Rodrigues, Diagnosis of autism spectrum disorder based on functional brain networks and machine learning, Scientific Reports **13**, 8072 (2023).

[26] C. L. Alves, G. d. O. Thaise, J. A. M. Porto, P. M. de Carvalho Aguiar, E. P. de Sena, F. A. Rodrigues,

A. M. Pineda, and C. Thielemann, Analysis of functional connectivity using machine learning and deep learning in different data modalities from individuals with schizophrenia, Journal of Neural Engineering **20**, 056025 (2023).

[27] C. L. Alves, A. M. Pineda, K. Roster, C. Thielemann, and F. A. Rodrigues, Eeg functional connectivity and deep learning for automatic diagnosis of brain disorders: Alzheimer's disease and schizophrenia, Journal of Physics: complexity **3**, 025001 (2022).

[28] B. Hosseinifard, M. H. Moradi, and R. Rostami, Classifying depression patients and normal subjects using machine learning techniques and nonlinear features from eeg signal, Computer methods and programs in biomedicine **109**, 339 (2013).

[29] C.-T. Wu, H.-C. Huang, S. Huang, I.-M. Chen, S.-C. Liao, C.-K. Chen, C. Lin, S.-H. Lee, M.-H. Chen, C.-F. Tsai, *et al.*, Resting-state eeg signal for major depressive disorder detection: a systematic validation on a large and diverse dataset, Biosensors **11**, 499 (2021).

[30] A. Dev, N. Roy, M. K. Islam, C. Biswas, H. U. Ahmed, M. A. Amin, F. Sarker, R. Vaidyanathan, and K. A. Mamun, Exploration of eeg-based depression biomarkers identification techniques and their applications: a systematic review, IEEE Access **10**, 16756 (2022).

[31] I. A. Anik, A. Kamal, M. A. Kabir, S. Uddin, and M. A. Moni, A robust deep-learning model to detect major depressive disorder utilising eeg signals, IEEE Transactions on Artificial Intelligence (2024).

[32] C. Uyulan, T. T. Ergüzel, H. Unubol, M. Cebi, G. H. Sayar, M. Nezhad Asad, and N. Tarhan, Major depressive disorder classification based on different convolutional neural network models: Deep learning approach, Clinical EEG and neuroscience **52**, 38 (2021).

[33] P. P. Thoduparambil, A. Dominic, and S. M. Varghese, Eeg-based deep learning model for the automatic detection of clinical depression, Physical and Engineering Sciences in Medicine **43**, 1349 (2020).

[34] A. Safayari and H. Bolhasani, Depression diagnosis by deep learning using eeg signals: A systematic review, Medicine in Novel Technology and Devices **12**, 100102 (2021).

[35] M. Xia, Y. Zhang, Y. Wu, and X. Wang, An end-to-end deep learning model for eeg-based major depressive disorder classification, IEEE Access **11**, 41337 (2023).

[36] A. F. Alexander-Bloch, P. E. Vértes, R. Stidd, F. Lalonde, L. Clasen, J. Rapoport, J. Giedd, E. T. Bullmore, and N. Gogtay, The anatomical distance of functional connections predicts brain network topology in health and schizophrenia, Cerebral cortex **23**, 127 (2013).

[37] P. Barttfeld, B. Wicker, S. Cukier, S. Navarta, S. Lew, R. Leiguarda, and M. Sigman, State-dependent changes of connectivity patterns and functional brain network topology in autism spectrum disorder, Neuropsychologia **50**, 3653 (2012).

[38] A. Fathian, Y. Jamali, and M. R. Raoufy, The trend of disruption in the functional brain network topology of alzheimer's disease, Scientific reports **12**, 14998 (2022).

[39] W. Chen, Y. Cai, A. Li, K. Jiang, and Y. Su, Mdd brain network analysis based on eeg functional connectivity and graph theory, Heliyon **10** (2024).

[40] B. Nobakhsh, A. Shalbaf, R. Rostami, and R. Kazemi, Graph-based analysis to predict repetitive transcranial magnetic stimulation treatment response in patients with major depressive disorder using eeg signals, Basic and Clinical Neuroscience **15**, 199 (2024).

[41] B. Zhang, G. Yan, Z. Yang, Y. Su, J. Wang, and T. Lei, Brain functional networks based on resting-state eeg data for major depressive disorder analysis and classification, IEEE Transactions on Neural Systems and Rehabilitation Engineering **29**, 215 (2020).

[42] F. Hasanzadeh, M. Mohebbi, and R. Rostami, Graph theory analysis of directed functional brain networks in major depressive disorder based on eeg signal, Journal of neural engineering **17**, 026010 (2020).

[43] S. Sun, X. Li, J. Zhu, Y. Wang, R. La, X. Zhang, L. Wei, and B. Hu, Graph theory analysis of functional connectivity in major depression disorder with high-density resting state eeg data, IEEE Transactions on Neural Systems and Rehabilitation Engineering **27**, 429 (2019).

[44] M. Shim, C.-H. Im, Y.-W. Kim, and S.-H. Lee, Altered cortical functional network in major depressive disorder: A resting-state electroencephalogram study, NeuroImage: Clinical **19**, 1000 (2018).

[45] Z. Guo, X. Wu, J. Liu, L. Yao, and B. Hu, Altered electroencephalography functional connectivity in depression during the emotional face-word stroop task, Journal of neural engineering **15**, 056014 (2018).

[46] S. J. Leistedt, N. Coumans, M. Dumont, J.-P. Lanquart, C. J. Stam, and P. Linkowski, Altered sleep brain functional connectivity in acutely depressed patients, Human brain mapping **30**, 2207 (2009).

[47] M. Zhang, H. Zhou, L. Liu, L. Feng, J. Yang, G. Wang, and N. Zhong, Randomized eeg functional brain networks in major depressive disorders with greater resilience and lower rich-club coefficient, Clinical Neurophysiology **129**, 743 (2018).

[48] T. G. L. de O. Toutain, J. G. V. Miranda, R. S. do Rosário, and E. P. de Sena, Brain instability in dynamic functional connectivity in schizophrenia, Journal of Neural Transmission **130**, 171 (2023).

[49] G. Orru, W. Pettersson-Yeo, A. F. Marquand, G. Sartori, and A. Mechelli, Using support vector machine to identify imaging biomarkers of neurological and psychiatric disease: a critical review, Neuroscience & Biobehavioral Reviews **36**, 1140 (2012).

[50] R. Albert and A.-L. Barabási, Statistical mechanics of complex networks, Reviews of modern physics **74**, 47 (2002).

[51] L. C. Freeman, A set of measures of centrality based on betweenness, Sociometry , 35 (1977).

[52] L. C. Freeman, Centrality in social networks conceptual clarification, Social networks **1**, 215 (1978).

[53] R. Albert, H. Jeong, and A.-L. Barabási, Diameter of the world-wide web, nature **401**, 130 (1999).

[54] M. E. Newman, The structure and function of complex networks, SIAM review **45**, 167 (2003).

[55] M. E. Newman, Assortative mixing in networks, Physical review letters **89**, 208701 (2002).

[56] J. M. Kleinberg, Hubs, authorities, and communities, ACM computing surveys (CSUR) **31**, 5 (1999).

[57] P. Hage and F. Harary, Eccentricity and centrality in networks, Social networks **17**, 57 (1995).

[58] P. Bonacich, Power and centrality: A family of measures, American journal of sociology **92**, 1170 (1987).

[59] D. Eppstein, M. S. Paterson, and F. F. Yao, On nearest-neighbor graphs, Discrete & Computational Geometry

17, 263 (1997).
[60] J. Doyle and J. Graver, Mean distance in a graph, Discrete Mathematics **17**, 147 (1977).
[61] M. Dehmer and A. Mowshowitz, A history of graph entropy measures, Information Sciences **181**, 57 (2011).
[62] D. J. Watts and S. H. Strogatz, Collective dynamics of 'small-world'networks, Nature **393**, 440 (1998).
[63] M. E. Newman, D. J. Watts, and S. H. Strogatz, Random graph models of social networks, Proceedings of the National Academy of Sciences **99**, 2566 (2002).
[64] T. A. Snijders, The degree variance: an index of graph heterogeneity, Social networks **3**, 163 (1981).
[65] S. B. Seidman, Network structure and minimum degree, Social networks **5**, 269 (1983).
[66] M. Newman, *Networks: an introduction* (Oxford university press, 2010).
[67] B. S. Anderson, C. Butts, and K. Carley, The interaction of size and density with graph-level indices, Social networks **21**, 239 (1999).
[68] V. Latora and M. Marchiori, Economic small-world behavior in weighted networks, The European Physical Journal B-Condensed Matter and Complex Systems **32**, 249 (2003).
[69] C. Alves, L. Wissel, P. Capetian, and C. Thielemann, P 55 functional connectivity and convolutional neural networks for automatic classification of eeg data, Clinical Neurophysiology **137**, e47 (2022).
[70] C. L. Alves, R. G. Cury, K. Roster, A. M. Pineda, F. A. Rodrigues, C. Thielemann, and M. Ciba, Application of machine learning and complex network measures to an eeg dataset from ayahuasca experiments, Plos one **17**, e0277257 (2022).
[71] S. Siegel, Nonparametric statistics, The American Statistician **11**, 13 (1957).
[72] D. Watts, R. F. Pulice, J. Reilly, A. R. Brunoni, F. Kapczinski, and I. C. Passos, Predicting treatment response using eeg in major depressive disorder: A machine-learning meta-analysis, Translational psychiatry **12**, 332 (2022).
[73] S.-C. Roh, E.-J. Park, M. Shim, and S.-H. Lee, Eeg beta and low gamma power correlates with inattention in patients with major depressive disorder, Journal of affective disorders **204**, 124 (2016).
[74] A. Damborská, M. I. Tomescu, E. Honzírková, R. Barteček, J. Hořínková, S. Fedorová, Š. Ondruš, and C. M. Michel, Eeg resting-state large-scale brain network dynamics are related to depressive symptoms, Frontiers in psychiatry **10**, 548 (2019).
[75] D. A. Pizzagalli, T. R. Oakes, and R. J. Davidson, Coupling of theta activity and glucose metabolism in the human rostral anterior cingulate cortex: an eeg/pet study of normal and depressed subjects, Psychophysiology **40**, 939 (2003).
[76] L. Myers and M. J. Sirois, Spearman correlation coefficients, differences between, Encyclopedia of statistical sciences **12** (2004).
[77] J. Hauke and T. Kossowski, Comparison of values of pearson's and spearman's correlation coefficients on the same sets of data, Quaestiones geographicae **30**, 87 (2011).
[78] J. Ricardo-Garcell, J. J. González-Olvera, E. Miranda, T. Harmony, E. Reyes, L. Almeida, L. Galán, D. Díaz, L. Ramírez, A. Fernández-Bouzas, *et al.*, Eeg sources in a group of patients with major depressive disorders, International Journal of Psychophysiology **71**, 70 (2009).
[79] A. F. Leuchter, I. A. Cook, A. M. Hunter, C. Cai, and S. Horvath, Resting-state quantitative electroencephalography reveals increased neurophysiologic connectivity in depression, PloS one **7**, e32508 (2012).
[80] M. Mijalkov, E. Kakaei, J. B. Pereira, E. Westman, G. Volpe, and A. D. N. Initiative, Braph: a graph theory software for the analysis of brain connectivity, PloS one **12**, e0178798 (2017).
[81] K. Vigasina, E. Sharova, V. Bordyug, E. Masherov, G. Boldyreva, A. Smirnov, and P. Gotovtsev, Eeg functional connectivity in motor tasks: Experience of application of graph analysis, Human Physiology **49**, 453 (2023).
[82] T. Mima, J. Steger, A. E. Schulman, C. Gerloff, and M. Hallett, Electroencephalographic measurement of motor cortex control of muscle activity in humans, Clinical neurophysiology **111**, 326 (2000).
[83] Y. Wang, B. Hong, X. Gao, and S. Gao, Phase synchrony measurement in motor cortex for classifying single-trial eeg during motor imagery, in *2006 international conference of the IEEE engineering in medicine and biology society* (IEEE, 2006) pp. 75–78.
[84] K. Svoboda and N. Li, Neural mechanisms of movement planning: motor cortex and beyond, Current opinion in neurobiology **49**, 33 (2018).
[85] D. T. Stuss, Functions of the frontal lobes: relation to executive functions, Journal of the international neuropsychological Society **17**, 759 (2011).
[86] C. Chayer and M. Freedman, Frontal lobe functions, Current neurology and neuroscience reports **1**, 547 (2001).
[87] Y. Shi, Y. Zeng, L. Wu, W. Liu, Z. Liu, S. Zhang, J. Yang, and W. Wu, A study of the brain abnormalities of post-stroke depression in frontal lobe lesion, Scientific reports **7**, 13203 (2017).
[88] X. Shao, S. Sun, J. Li, W. Kong, J. Zhu, X. Li, and B. Hu, Analysis of functional brain network in mdd based on improved empirical mode decomposition with resting state eeg data, IEEE Transactions on Neural Systems and Rehabilitation Engineering **29**, 1546 (2021).
[89] N. Javaheripour, M. Li, T. Chand, A. Krug, T. Kircher, U. Dannlowski, I. Nenadić, J. P. Hamilton, M. D. Sacchet, I. H. Gotlib, *et al.*, Altered resting-state functional connectome in major depressive disorder: a mega-analysis from the psymri consortium, Translational psychiatry **11**, 511 (2021).
[90] F. Bermpohl, M. Walter, B. Sajonz, C. Lücke, C. Hägele, P. Sterzer, M. Adli, A. Heinz, and G. Northoff, Attentional modulation of emotional stimulus processing in patients with major depression—alterations in prefrontal cortical regions, Neuroscience letters **463**, 108 (2009).
[91] Y. Liao, X. Huang, Q. Wu, C. Yang, W. Kuang, M. Du, S. Lui, Q. Yue, R. C. Chan, G. J. Kemp, *et al.*, Is depression a disconnection syndrome? meta-analysis of diffusion tensor imaging studies in patients with mdd, Journal of Psychiatry and Neuroscience **38**, 49 (2013).
[92] M. Duan, L. Wang, X. Liu, F. Su, L. An, and S. Liu, Abnormal brain activity in fronto-central regions in mental disorders with suicide: An eeg study, in *2021 43rd Annual International Conference of the IEEE Engineering in Medicine & Biology Society (EMBC)* (IEEE, 2021)

pp. 1035–1038.
[93] S. Bludau, S. B. Eickhoff, H. Mohlberg, S. Caspers, A. R. Laird, P. T. Fox, A. Schleicher, K. Zilles, and K. Amunts, Cytoarchitecture, probability maps and functions of the human frontal pole, Neuroimage **93**, 260 (2014).
[94] P. W. Fettes, M. Moayedi, K. Dunlop, F. Mansouri, F. Vila-Rodriguez, P. Giacobbe, K. D. Davis, R. W. Lam, S. H. Kennedy, Z. J. Daskalakis, *et al.*, Abnormal functional connectivity of frontopolar subregions in treatment-nonresponsive major depressive disorder, Biological Psychiatry: Cognitive Neuroscience and Neuroimaging **3**, 337 (2018).
[95] T.-W. Lee, Y.-T. Wu, Y. W.-Y. Yu, M.-C. Chen, and T.-J. Chen, The implication of functional connectivity strength in predicting treatment response of major depressive disorder: a resting eeg study, Psychiatry Research: Neuroimaging **194**, 372 (2011).
[96] J. L. Stewart, J. A. Coan, D. N. Towers, and J. J. Allen, Resting and task-elicited prefrontal eeg alpha asymmetry in depression: Support for the capability model, Psychophysiology **51**, 446 (2014).
[97] C. Greco, O. Matarazzo, G. Cordasco, A. Vinciarelli, Z. Callejas, and A. Esposito, Discriminative power of eeg-based biomarkers in major depressive disorder: A systematic review, IEEE Access **9**, 112850 (2021).
[98] Y. Mohan, S. S. Chee, D. K. P. Xin, and L. P. Foong, Artificial neural network for classification of depressive and normal in eeg, in *2016 IEEE EMBS conference on biomedical engineering and sciences (IECBES)* (IEEE, 2016) pp. 286–290.
[99] J. Yang, Z. Zhang, P. Xiong, and X. Liu, Depression detection based on analysis of eeg signals in multi brain regions, Journal of Integrative Neuroscience **22**, 93 (2023).
[100] G. F. de Arruda, L. da Fontoura Costa, D. Schubert, and F. A. Rodrigues, Structure and dynamics of functional networks in child-onset schizophrenia, Clinical Neurophysiology **125**, 1589 (2014).
[101] M. Rubinov and O. Sporns, Complex network measures of brain connectivity: uses and interpretations, Neuroimage **52**, 1059 (2010).
[102] M. D. Sacchet, G. Prasad, L. C. Foland-Ross, P. M. Thompson, and I. H. Gotlib, Support vector machine classification of major depressive disorder using diffusion-weighted neuroimaging and graph theory, Frontiers in psychiatry **6**, 21 (2015).
[103] G. Wagner, F. de la Cruz, S. Köhler, F. Pereira, S. Richard-Devantoy, G. Turecki, K.-J. Bär, and F. Jollant, Connectomics-based functional network alterations in both depressed patients with suicidal behavior and healthy relatives of suicide victims, Scientific reports **9**, 14330 (2019).
[104] K. Anand, D. Krioukov, and G. Bianconi, Entropy distribution and condensation in random networks with a given degree distribution, Physical Review E **89**, 062807 (2014).
[105] A. Avena-Koenigsberger, B. Misic, and O. Sporns, Communication dynamics in complex brain networks, Nature reviews neuroscience **19**, 17 (2018).

Appendix A: Grid search hyperparameter tuning

Machine Learning Method	**Hyperparameters**
Random Forest (RF)	n_estimators: range(1, 50, 2)
Support Vector Machine (SVM)	C: range(1, 30, 1)
Naive Bayes (NB)	var_smoothing: np.logspace(0,-9, num=100)
Multi-layer Perceptron (MLP)	hidden_layer_sizes: [(50,50,50), (50,100,50), (100,)]
K-Nearest Neighbors (KNN)	n_neighbors: range(1, 30, 1)
Logistic Regression (LR)	C: np.logspace(-3,3,7), penalty: [“l1”, “l2”]
XGBoost (XGboost)	min_child_weight: [1, 5, 10], gamma: [0.5, 1, 1.5, 2, 5], subsample: [0.6, 0.8, 1.0], colsample_bytree: [0.6, 0.8, 1.0], max_depth: [3, 4, 5]

TABLE VII. Machine learning models used and their respective hyperparameters tested.

Appendix B: Differences of the connectivity matrices

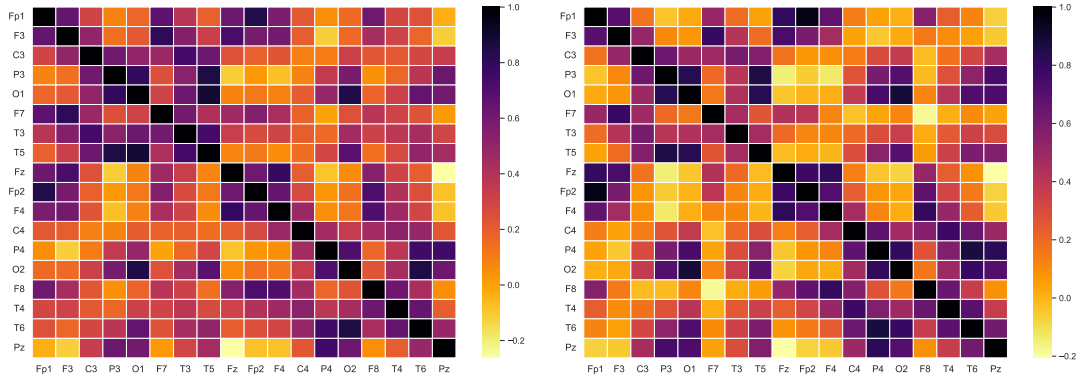

(a) PC matrix for MDD

(b) PC matrix for TD

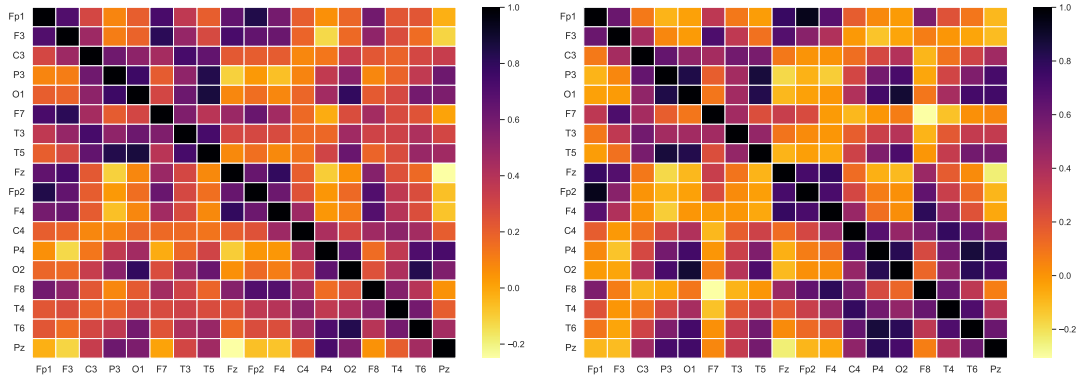

(c) SC matrix for MDD

(d) SC matrix for TD

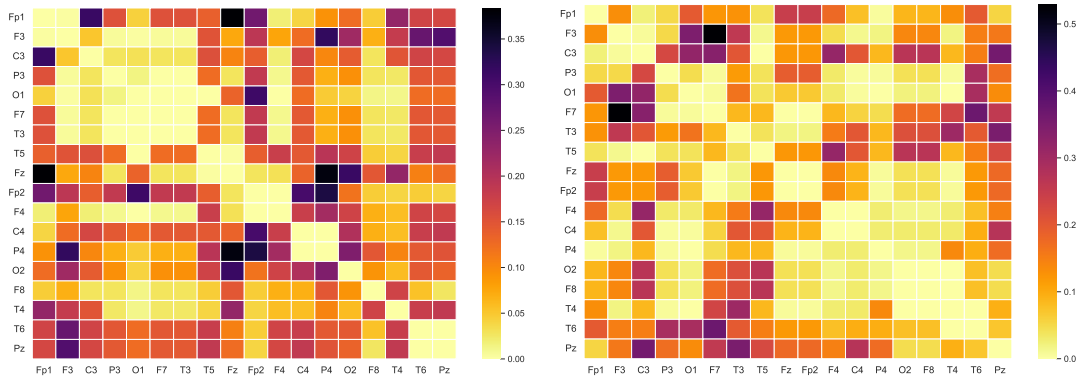

(e) TE matrix for MDD

(f) TE matrix for TD

FIG. 11. Connectivity matrices of MDD and TD patients constructed using PC, SC and TE.

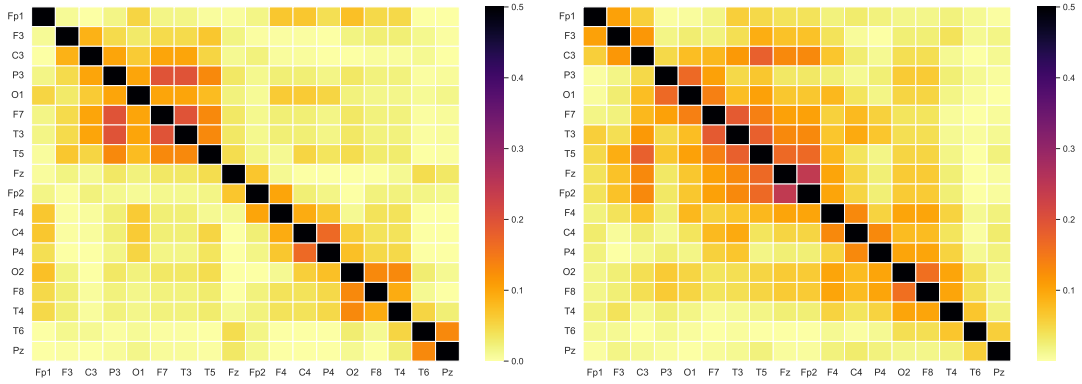

(a) MI matrix for MDD

(b) MI matrix for TD

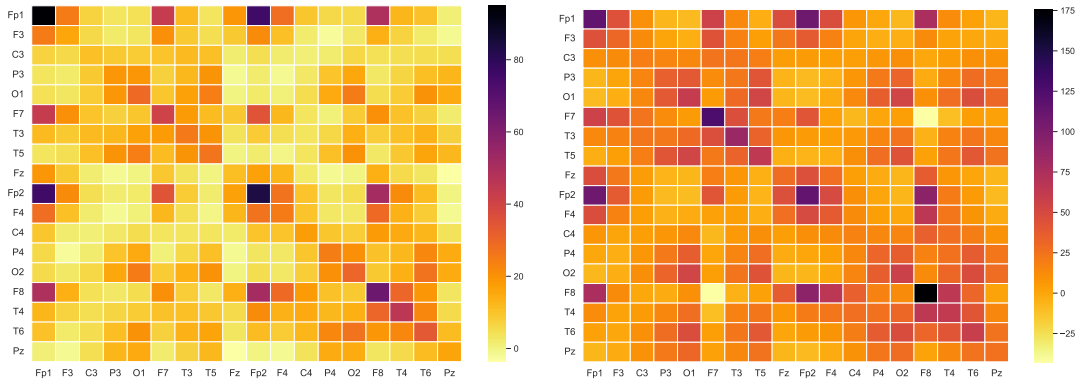

(c) LW matrix for MDD

(d) LW matrix for TD

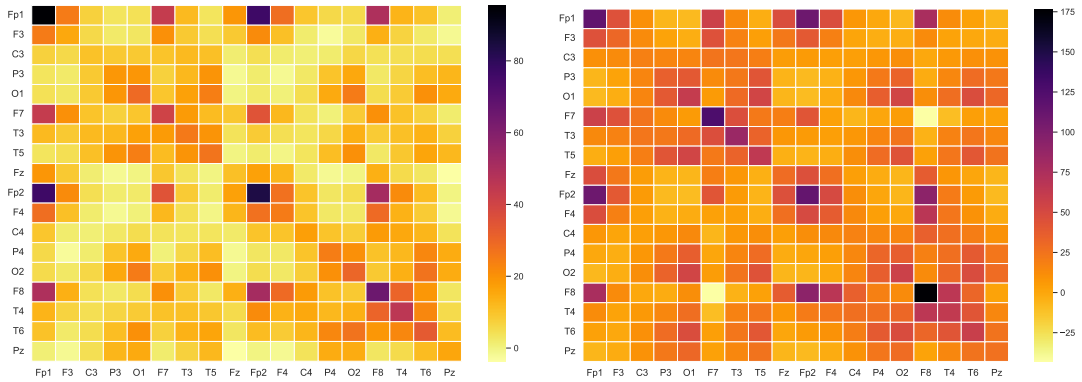

(e) SCC matrix for MDD

(f) SCC matrix for TD

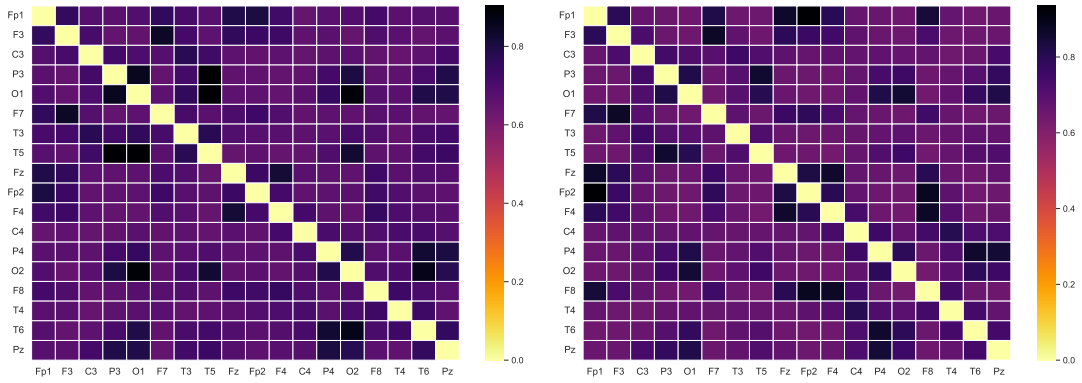

(g) Sync matrix for MDD

(h) Sync matrix for TD

FIG. 12. Connectivity matrices of MDD and TD patients constructed using MI, LW, SCC and Sync

CHAPTER

4

MULTICLASS CLASSIFICATION OF MENTAL DISORDERS

Multiclass classification of autism spectrum disorder, attention deficit hyperactivity disorder, and typically developed individuals using fMRI functional connectivity analysis. Caroline L. Alves, Tiago Martinelli, Loriz Francisco Sallum, Francisco Aparecido Rodrigues, Thaise G. L. de O. Toutain, Joel Augusto Moura Porto, Christiane Thielemann, Patrícia Maria de Carvalho Aguiar, Michael Moeckel. *Plos one 19(10)*, 2024.

4.1 Context

Neurodevelopmental disorders, such as autism spectrum disorder (ASD) and attention deficit hyperactivity disorder (ADHD), severely affect cognition, behavior and social interaction (LI *et al.*, 2019b; MAHONE; WARSCHAUSKY; ZABEL, 2018; THAPAR; COOPER; RUTTER, 2017). ASD is characterized by difficulties in social communication and repetitive behaviors (LORD *et al.*, 2018), while ADHD is marked by inattention, hyperactivity, and impulsivity (DU; FU; CALHOUN, 2018). Although they have different diagnostic criteria, the overlap in symptoms between ASD and ADHD (ROMMELSE *et al.*, 2011), and their frequent co-occurrence (SIMONOFF *et al.*, 2008), makes diagnosis and treatment planning more complicated.

Despite advances in clinical assessment, current diagnostic methods rely extensively on subjective evaluations of symptoms that contribute to frequent misdiagnosis or underdiagnosis. This challenge highlights the need for objective, data-driven approaches that integrate biological and behavioral insights. Recent studies have used machine learning (ML) techniques to address these diagnostic challenges (UDDIN; WANG; WOODBURY-SMITH, 2019; DUDA *et al.*, 2016; DUDA *et al.*, 2017). Although many have successfully implemented binary classifications to differentiate ASD or ADHD from typically developing (TD) individuals (DU; FU; CALHOUN, 2018; ARBABSHIRANI *et al.*, 2017; NOGAY; ADELI, 2020; RASHID; CALHOUN, 2020;

HARIKUMAR *et al.*, 2021; ESLAMI *et al.*, 2021; MORIDIAN *et al.*, 2022; WASHINGTON; WALL, 2023), relatively few have explored the simultaneous classification of multiple conditions. The majority of ML studies are based on survey data, which, although convenient, can introduce biases (WASHINGTON; WALL, 2023) and do not capture the complexity of the underlying neural mechanisms. Functional magnetic resonance imaging (fMRI), on the other hand, offers a direct view of brain activity and connectivity, providing a richer basis for distinguishing these conditions.

Furthermore, while some studies have explored complex network analysis to identify differences in brain connectivity, these efforts often lack the interpretability required for clinical adoption. This gap highlights the critical need for machine learning methods that not only achieve high classification accuracy but also provide insights that are consistent with clinical observations.

4.2 Contributions

This study presents a novel approach using functional magnetic resonance imaging (fMRI) data combined with machine learning techniques to distinguish between individuals with ASD, ADHD, and TD. Using multiclass classification algorithms, we achieve an accuracy that exceeds previous benchmarks, demonstrating the effectiveness of our approach in addressing the complexity of these neurodevelopmental disorders. In contrast to previous studies, that rely primarily on survey data, our work uses fMRI-derived connectivity matrices constructed using normalized transfer entropy. In addition, we incorporate three key measures - effective information, determinism and degeneracy coefficients - to analyse network segregation and integration, providing a deeper understanding of brain dynamics across ASD, ADHD and TD profiles. Furthermore, to the best of our knowledge, this is the first study to apply SHAP values to a multiclass classification of ASD and ADHD, thereby improving both the interpretability and robustness of our classification results.

Our findings reveal unique connectivity patterns for the ASD, ADHD and TD groups. In particular, connections involving the Left-ParsOrbitalis played a central role in the discrimination between TD and ASD, possibly reflecting deficits in decision-making and social cognition commonly associated with ASD. Similarly, unique neural patterns were identified in ADHD, particularly in connections to the cerebellum, Left-Visual Association cortex and Right Angular Gyrus, suggesting their involvement in cognitive functions and sensory processing differences. These neural signatures are aligned with established clinical observations, bridging the gap between model predictions and real-world diagnostic criteria.

In addition, our analysis of complex network measures reveals differences in the brain network properties of each group, revealing different patterns of integration and segregation. The ASD group had the lowest scores on several network metrics, indicating a fragmented

network structure. In contrast, the ADHD group showed intermediate values for the same metrics, reflecting a network that is more integrated than ASD but less cohesive than TD.

In conclusion, this study represents a significant improvement in the understanding of the neural mechanisms underlying ASD, ADHD and TD by using advanced analytical techniques and machine learning methods. Our results surpass existing benchmarks in distinguishing these conditions, providing a strong basis for the development of improved diagnostic tools and reliable clinical decision support systems, while paving the way for further research and advances in personalized care for neurodevelopmental disorders.

PLOS ONE

RESEARCH ARTICLE

Multiclass classification of Autism Spectrum Disorder, attention deficit hyperactivity disorder, and typically developed individuals using fMRI functional connectivity analysis

Caroline L. Alves[1]*, Tiago Martinelli[2], Loriz Francisco Sallum[2], Francisco Aparecido Rodrigues[2], Thaise G. L. de O. Toutain[3], Joel Augusto Moura Porto[4,5], Christiane Thielemann[6], Patrícia Maria de Carvalho Aguiar[7,8], Michael Moeckel[1]

1 Laboratory for Hybrid Modeling, Aschaffenburg University of Applied Sciences, Aschaffenburg, Bayern, Germany, **2** Institute of Mathematical and Computer Sciences, University of São Paulo, São Paulo, São Paulo, Brazil, **3** Health Sciences Institute, Federal University of Bahia, Salvador, Bahia, Brazil, **4** Institute of Physics of São Carlos (IFSC), University of São Paulo (USP), São Carlos, São Paulo, Brazil, **5** Institute of Biological Information Processing, Heinrich Heine University Düsseldorf, Düsseldorf, North Rhine–Westphalia Land, Germany, **6** BioMEMS Lab, Aschaffenburg University of Applied Sciences, Aschaffenburg, Bayern, Germany, **7** Hospital Israelita Albert Einstein, São Paulo, São Paulo, Brazil, **8** Department of Neurology and Neurosurgery, Federal University of São Paulo, São Paulo, São Paulo, Brazil

* CarolineLourencoAlves@th-ab.de

OPEN ACCESS

Citation: Alves CL, Martinelli T, Sallum LF, Rodrigues FA, Toutain TGLdO, Porto JAM, et al. (2024) Multiclass classification of Autism Spectrum Disorder, attention deficit hyperactivity disorder, and typically developed individuals using fMRI functional connectivity analysis. PLoS ONE 19(10): e0305630. https://doi.org/10.1371/journal.pone.0305630

Editor: Yangsong Zhang, Southwest University of Science and Technology, CHINA

Received: December 7, 2023

Accepted: June 3, 2024

Published: October 17, 2024

Peer Review History: PLOS recognizes the benefits of transparency in the peer review process; therefore, we enable the publication of all of the content of peer review and author responses alongside final, published articles. The editorial history of this article is available here: https://doi.org/10.1371/journal.pone.0305630

Data Availability Statement: All relevant data are within the article and its Supporting information

Abstract

Neurodevelopmental conditions, such as Autism Spectrum Disorder (ASD) and Attention Deficit Hyperactivity Disorder (ADHD), present unique challenges due to overlapping symptoms, making an accurate diagnosis and targeted intervention difficult. Our study employs advanced machine learning techniques to analyze functional magnetic resonance imaging (fMRI) data from individuals with ASD, ADHD, and typically developed (TD) controls, totaling 120 subjects in the study. Leveraging multiclass classification (ML) algorithms, we achieve superior accuracy in distinguishing between ASD, ADHD, and TD groups, surpassing existing benchmarks with an area under the ROC curve near 98%. Our analysis reveals distinct neural signatures associated with ASD and ADHD: individuals with ADHD exhibit altered connectivity patterns of regions involved in attention and impulse control, whereas those with ASD show disruptions in brain regions critical for social and cognitive functions. The observed connectivity patterns, on which the ML classification rests, agree with established diagnostic approaches based on clinical symptoms. Furthermore, complex network analyses highlight differences in brain network integration and segregation among the three groups. Our findings pave the way for refined, ML-enhanced diagnostics in accordance with established practices, offering a promising avenue for developing trustworthy clinical decision-support systems.

files. Neuroimaging data were obtained from two large, publicly available datasets: ADHD-200 (http://fcon_1000.projects.nitrc.org/indi/adhd200/) and ABIDE (Autism Brain Imaging Data Exchange; http://fcon_1000.projects.nitrc.org/indi/abide/).

Funding: ZeWiS is funded through public research projects by the Bavarian State Ministry for Sciences and the Arts. The funder provided support in the form of salaries for authors but did not have any additional role in the study design, data collection and analysis, decision to publish, or manuscript preparation. The specific roles of these authors are articulated in the 'author contributions' section.

Competing interests: EpilabKI is funded through the Bavarian stated Ministery for Sciences and the Arts research. This does not alter our adherence to PLOS ONE policies on sharing data and materials.

1 Introduction

1.1 Clinical background

Neurodevelopmental disorders encompass a spectrum of conditions that manifest early in life and have diverse impacts on brain development and function, often presenting with genetic and clinical heterogeneity [1]. These disorders profoundly affect neurological functioning, including cognition, communication, behavior, motor skills, and social interaction [2–4].

Two prominent examples of neurodevelopmental disorders are Autism Spectrum Disorder (ASD) and Attention Deficit Hyperactivity Disorder (ADHD). ASD is characterized by challenges in social interaction, communication, repetitive behaviors, and sensory sensitivities [5]. Globally, ASD affects approximately 1 in 36 children and is more prevalent in males than females [6]. ASD is a spectrum disorder, displaying a wide range of symptom severity and presentation, making diagnosis a challenging task [7–9]. Furthermore, ASD is marked by significant heterogeneity, with no discernible patterns consistently emerging among affected individuals [10].

ADHD, another prevalent neurodevelopmental disorder, is defined by inattention, hyperactivity, and impulsivity symptoms, which can substantially impact daily functioning [11]. It affects 5–8% of children, with a higher prevalence among boys [12]. Despite extensive research, the prevalence of ADHD remains elusive [13], and diagnosis primarily relies on the assessment of behavioral symptoms [11].

While ASD and ADHD are traditionally classified as distinct neurodevelopmental disorders, they exhibit a significant degree of symptom overlap [14]. This shared symptomatology often complicates the accurate diagnosis and treatment planning for affected individuals. Furthermore, it is noteworthy that ADHD frequently co-occurs with ASD, making it one of the most prevalent comorbidities among individuals with ASD [15]. This comorbidity adds another layer of complexity to the neurodevelopmental profile of affected individuals, contributing to the challenges in diagnosis and care. Consequently, these circumstances often lead to cases of misdiagnosis and underdiagnosis.

1.2 Previous ML approaches

Given the inherent complexity of diagnosing ASD and ADHD, many studies are using machine learning methods to improve the diagnosis [16]. In the study by [17], machine learning models were trained and tested on an imbalanced dataset from research records based on the Social Responsiveness Scale (SRS). The SRS is a parent-administered questionnaire frequently employed for measuring autism traits. Notably, the superior performance algorithms were Support Vector Machines (SVM), Ridge Regression, Least Absolute Shrinkage and Selection Operator (LASSO), and Linear Discriminant Analysis, achieving accuracies ranging from 0.962 to 0.965. These results underscore the effectiveness of machine learning techniques in accurately distinguishing individuals with ASD from those with ADHD. Moreover, in [18] it was incorporated a crowdsourced dataset comprising responses to 15 SRS-derived questions. In this subsequent analysis, Linear Discriminant Analysis (LDA) and Elastic Net (ENet) emerged as the top-performing methods, both achieving an Area Under the ROC Curve (AUC) of 0.89 when tested on survey data containing the 15 questions.

Machine methods have also been applied to neuroimaging data to develop more precise and reliable approaches for characterizing and predicting ASD and ADHD in a binary way to distinguish from TD [11, 13, 19–24]. Most studies in the literature are primarily focused on distinguishing individuals with a specific condition from typically developing (TD) individuals, resulting in a binary classification problem. However, a more desirable scenario would

Table 1. Studies with ML classification algorithms for distinguishing ASD and ADHD groups described in subsection 1.2.

Studies	Dataset type	ML algorithm	Classification type	Correlation metric	AUC	Accuracy	Recall	Precision
[17]	research records survey	SVM, Ridge Regression, LASSO, and LDA	Binary (ASD and ADHD)	-	-	0.962–0.965	-	-
[18]	research records survey	LDA and ENet	Binary (ASD and ADHD)	-	0.890	-	-	-
[25]	research records survey	SVM	Binary (ASD and ADHD)	-	0.910	-	0.680	-
[26]	MRI	GPC	Multiclass (ASD, ADHD and TD)	-	-	0.682	-	-
[30]	fMRI	SVM	Multiclass (ASD, ADHD and TD)	Pearson correlation	-	0.66	0.82	0.59

https://doi.org/10.1371/journal.pone.0305630.t001

involve the differentiation among multiple neurological conditions characterized by overlapping symptoms or co-occurrence, as seen in the case of ASD and ADHD. Preliminary efforts have been made in this direction, in which various machine learning techniques have been employed [17, 18, 25]. For instance, one of the pioneering studies to differentiate adolescents with ADHD from those with ASD or TD was published in 2013 [26]. The authors considered structural magnetic resonance imaging (MRI) data and a 3-class Gaussian Process Classification (GPC) approach to classify ADHD, ASD, and TD groups simultaneously [26]. Their model achieved a balanced accuracy of 0.682, with sensitivities of 0.759, 0.655, and 0.632 for the ADHD, TD, and ASD groups, respectively. The positive predictive values for the respective groups were also 0.629, 0.731, and 0.75.

In [27], centrality abnormalities in cortical and subcortical regions were discovered, some of them shared between ADHD and ASD. They observed increased centrality in the right striatum/pallidum for ADHD and bilateral temporolimbic areas for ASD. In [28], it was conducted a comparative analysis of the network topology patterns among ASD, ADHD, and neurotypical (NT) groups. They found substantial overlap at the global level of community structure among all groups. However, the overlap between the two clinical conditions was less than that between each condition and the control group.

Additionally, the ASD and ADHD groups exhibited a more pronounced reduction in correlation strength with increased distance compared to the NT group. Notably, the ADHD group displayed reduced wiring costs, thinner cortical regions, and lower hub degrees than the ASD group. Significant findings emerged in the study [29] regarding oscillatory patterns in children with ASD and ADHD during task conditions. Children with ASD exhibited significant hypoconnectivity in large-scale networks during these tasks, while those with ADHD showed hyperconnectivity in large-scale networks under similar conditions. In a recent study [30], an SVM algorithm with l2-regularization emerged as the top-performing method, achieving an accuracy of 0.66, an f1-score of 0.68, a precision of 0.59, and a recall of 0.82. Notably, their findings unveiled a substantial convergence in functional brain connectivity patterns between ADHD and ASD, particularly within the right ventral attention network, the salience network, and the default mode network (DMN) as observed in resting-state fMRI data.

Table 1 concisely overviews the primary research using machine learning classification methods and the ASD and ADHD groups outlined in this subsection.

1.3 Research gap

Previous ML models have yet to be constructed using explainable AI approaches. This limits their interpretability and, hence, the trustworthiness of their model predictions. In particular,

a clear connection between established clinical symptoms and model properties has yet to be drawn, raising doubts among medical professionals and hindering the use of ML modeling in actual clinical diagnosis [31].

Upon reviewing the landscape of studies within the domain of ASD and ADHD classification, a notable trend emerges, as illustrated in the summarized literature (Table 1): a predominant focus on binary comparisons between ASD and ADHD, often reliant on survey-based symptomatic datasets, which not alllows clear separation in the cases that have overlapping of symptoms. This emphasis on a binary framework potentially oversimplifies the nuanced complexities inherent in these neurodevelopmental disorders. Moreover, the reliance on survey data in many studies raises concerns regarding introducing biases [32], particularly when compared to more direct neuroimaging modalities such as EEG and fMRI. Our previous research [33, 34] highlights the critical role of correlation metrics in constructing connectivity matrices to effectively capture brain changes associated with these conditions. While studies such as [30] use fMRI and a multiclass approach, they predominantly utilize linear measures like Pearson correlation; the robustness of alternative metrics such as normalized transfer entropy still needs to be explored. In our prior works [34, 35], we demonstrated the robustness of normalized transfer entropy in distinguishing neurodevelopmental disorders from TD individuals, underscoring the need to explore these metrics further. Furthermore, the prevailing focus on ML methodologies overlooks the exploration of complex network topology changes and needs more medical interpretation. There is a clear need for a more holistic approach that integrates diverse methodologies and prioritizes nuanced understanding over simplistic binary classifications. Such an approach holds the potential to advance our comprehension of the underlying mechanisms of ASD and ADHD and inform more effective interventions and treatments.

1.4 Objective and hypothesis

Our study aims to bridge the existing research gap by advancing beyond simplistic binary comparisons in the classification of ASD, ADHD, and TD individuals using fMRI datasets. Building upon prior work that underscores the limitations of binary frameworks and the potential bias introduced by survey-based datasets, our hypothesis posits that distinct brain activity patterns underlie these neurodevelopmental disorders and can facilitate their reliable separation. We seek to investigate whether these patterns align with existing clinical knowledge of ASD and ADHD, thereby providing deeper insights into these conditions' underlying mechanisms and proving our methodology's trustworthiness.

Additionally, we aim to explore the utility of complex network measures in achieving a clean separation of the groups, surpassing the conventional focus on machine learning methodologies, through the integration of diverse methodologies alongside advanced analytical techniques such as normalized transfer entropy, our study endeavors to enhance prediction accuracy while ensuring an explainable and trustworthy machine learning approach.

2 Materials and methods

2.1 Innovations in the methodology

The current paper endeavors to investigate the feasibility of automatically detecting brain changes associated with ASD and ADHD while simultaneously providing a biological rationale for these observations. We leverage the blood oxygenation level-dependent (BOLD) time series data to achieve this objective and develop a classification method to distinguish individuals with ASD, ADHD, and TD profiles. Following dataset preprocessing (described in subsection 2.2), we employed two levels of data abstraction: (A) the calculation of correlations, determined by the normalized transfer entropy between specific fMRI regions of interest (described

in subsection 2.3), and (B) the extraction of complex network measures from the correlations (A) (described in subsection 2.4). It is important to note that while our methodology bears similarity to our previous work [33–37], where binary classification was primarily explored, the present study aims to establish a multiclass classifier. Moreover, departing from existing literature, which often focuses on utilizing only one of these abstraction levels, our study pioneers the simultaneous use of both levels in a multiclass context, marking a novel contribution to the field.

To enhance the interpretability of our machine learning results, we incorporated cutting-edge techniques that have emerged in recent years. One such technique is the application of SHapley Additive ExPlanations (SHAP) values [38]. These values help identify the most critical features within our model, shedding light on essential brain areas and connections between regions. Notably, SHAP values have demonstrated superior performance compared to prior research efforts [33, 36, 39] in pinpointing significant brain areas and connectivity patterns and have been an integral part of our previous work.

Differently from [33–37], we added three measures to analyze the segregation and integration concepts: Effective Information, determinism, and degeneracy coefficients. These measures provide a comprehensive understanding of the dynamics of brain networks in individuals with ASD, ADHD, and TD profiles. Furthermore, to the best of our knowledge, this is the first study that employed the SHAP values methodology for a multiclass classification of ASD and ADHD, enhancing the interpretability and robustness of our classification results.

The Python code with the methodology used in this work and described in this section is available at: https://github.com/Carol180619/Multiclass-ADHD-ASD.git.

2.2 Data and data preprocessing

The ADHD dataset used in this study was sourced from the Neuro Bureau ADHD-200 Preprocessed repository, as detailed in [40]. During a 6-minute resting-state fMRI scan, participants received instructions to relax, maintain closed eyes, avoid falling asleep, and refrain from engaging in specific thoughts. The resting-state fMRI data captures spontaneous fluctuations in BOLD signals, widely acknowledged as indicative of underlying brain activity. In this investigation, we utilized the ADHD-200 dataset via the Nilearn package. Nilearn is a Python package [41] tailored explicitly for analyzing neuroimaging data. Our selection of Nilearn seamlessly integrated with our existing workflow, as we had already incorporated Nilearn into our analysis pipeline. Nilearn provides a comprehensive set of tools for preprocessing, feature extraction, and statistical analysis of neuroimaging data. It was used in numerous studies [42–44], making it a suitable and convenient choice for our research. Within the Nilearn package, the dataset comprises 40 child and adolescent participants aged 7 to 27, equally divided between individuals diagnosed with ADHD and healthy control subjects.

As in our previous work [34], we considered the preprocessed version of the Autism Brain Imaging Data Exchange (ABIDE) (Avaiable in https://fcon_1000.projects.nitrc.org/indi/abide/) which consists of 1112 datasets comprised of 539 ASD and 573 TD with 300s BOLD time series (7–64 years, median 14.7 years across groups). Further, it is also available for use in Nilearn's Python package. We used the same amount of 40 subjects from the ADHD dataset. For TD groups, we randomly selected 20 subjects for the ABIDE dataset and 20 for the Neuro Bureau ADHD-200 Preprocessed repository.

In our study, rather than utilizing the entire BOLD time series obtained from each voxel in brain images, we focused on specific Brain Regions of Interest (ROIs). These ROIs are defined based on a brain atlas; only the BOLD time series from these ROIs are considered. The choice

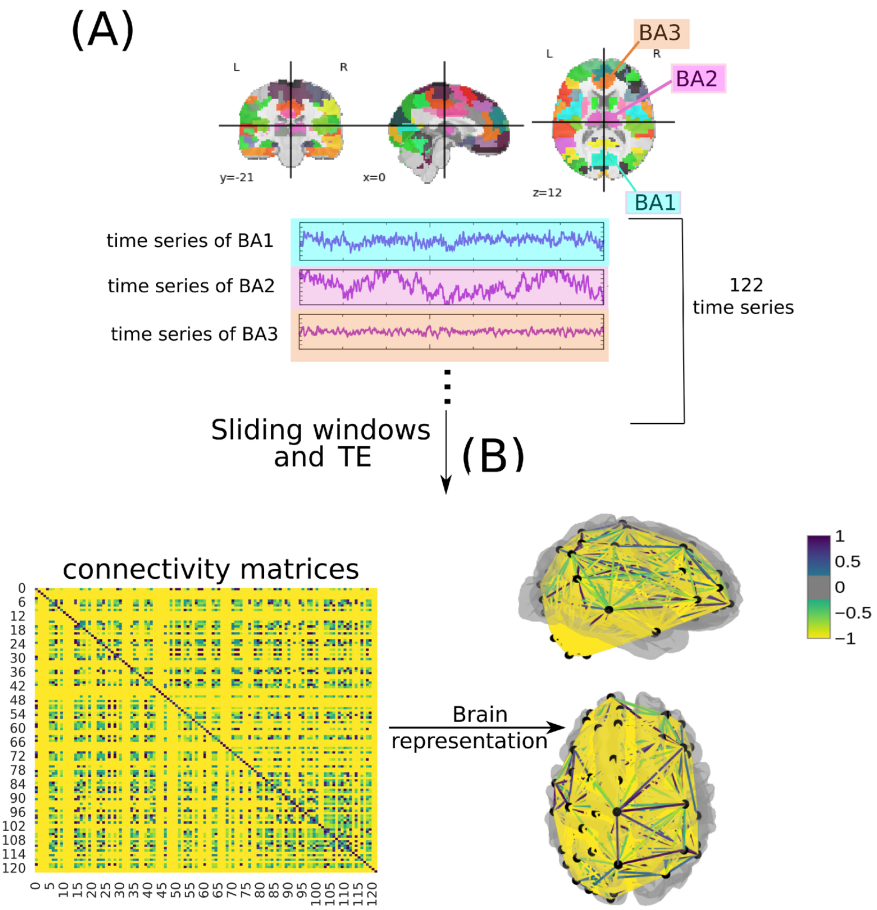

Fig 1. Methodology to obtain the connectivity matrices based on [34]. In (A), a time series of 122 ROI is extracted from fMRI data using the BASC BOLD atlas (highlighted in blue, purple, and orange). A sliding window was performed as a data augmentation. Then, they are correlated (B) to form the connectivity matrices, where each row and column corresponds to one of the Brodmann areas for a patient with ASD, TD, and ADHD (the figure illustrates an example of a connectivity matrix with a normalized TE of a subject presenting ADHD). The same highlighted matrices represent the brain in a three-dimensional (in a top and left perspective) schematic.

https://doi.org/10.1371/journal.pone.0305630.g001

of Brain Atlas is crucial, and in our work, we employed the Bootstrap Analysis of Stable Clusters (BASC) atlas, selected for its exceptional performance in discriminating Autism Spectrum Disorder (ASD) patients using deep learning models, as reported in [45]. The BASC atlas, introduced initially in [46], is derived from group-level brain parcellation through the BASC method, an algorithm utilizing k-means clustering to identify brain networks with coherent activity in resting-state fMRI, as described in [47]. BASC map with a cluster number of 122 ROIs is used here (see Fig 1A). From our previous work [34], a manual use of Yale BioImage Suite Package web application (Avaiable in https://bioimagesuiteweb.github.io/webapp/mni2tal.html) labeled the coordinates of each ROI for the identification of their names (see Fig 1A).

After extracting the BOLD time series, a sliding time window of 20 seconds was employed for data augmentation. This duration was selected based on our previous study [34], where it demonstrated optimal performance for the ASD dataset. Additionally, to ensure comparability between the ASD and ADHD datasets, the same window size was

utilized for the ADHD dataset. By employing consistent time windows across both datasets, we aimed to mitigate potential biases arising from variations in data acquisition protocols between different sites and enhance the robustness of our analyses. Through the data augmentation process, 600 matrices were randomly selected, ensuring an equal representation of each class.

Once the time series for each of the 122 regions had been extracted for each time window, they were correlated according to normalized transfer entropy (TE)(see Fig 1B). The TE is described in [48] and given by the Eq 1. The normalized TE metric was selected as our study's primary analytical tool, building upon prior research findings [34, 35]. TE has demonstrated its efficacy in capturing changes in brain dynamics associated with neurodevelopmental disorders. This choice was motivated by several advantages it offers. Firstly, normalized TE is adept at capturing directional dependencies [49], providing a nuanced understanding of information flow within neural systems [50, 51]. Unlike linear measures, such as Spearman and Pearson correlation, TE is non-linear and model-free, making it particularly suitable for analyzing complex, non-stationary, and non-Gaussian datasets [52–54]. Moreover, TE stands apart from traditional correlation measures like the Pearson correlation. While the latter is confined to assessing linear or monotonic relationships between variables, regardless of their direction of influence, TE excels in identifying and quantifying the directional dependencies between time series [55], thereby facilitating a more comprehensive assessment of neural interactions. Noteworthy, as in our previous work [34, 35], for computing TE, a Min-max normalization and then a thresholding process was performed, with a value of 0.5, since this measures deal best with binary values.

$$TE_{Y\to X}(\tau) = \sum_{i=1}^{N} P(x_{t+\tau}^{i}, x_{t}^{i}, y_{t}^{i}) \log \frac{P(x_{t+\tau}^{i} | x_{t}^{i}, y_{t}^{i})}{P(x_{t+\tau}^{i} | x_{t}^{i})} \quad (1)$$

where:

- $TE_{Y\to X}(\tau)$ denotes the transfer entropy from Y to X at time lag τ.
- x_t^i and y_t^i represent samples from time series X and Y respectively.
- N is the total number of samples.
- $P(x_{t+\tau}^{i}, x_{t}^{i}, y_{t}^{i})$ is the joint probability distribution of $x_{t+\tau}^{i}$, x_t^i, and y_t^i.
- $P(x_{t+\tau}^{i} | x_{t}^{i}, y_{t}^{i})$ is the conditional probability distribution of $x_{t+\tau}^{i}$ given x_t^i and y_t^i.
- $P(x_{t+\tau}^{i} | x_{t}^{i})$ is the conditional probability distribution of $x_{t+\tau}^{i}$ given x_t^i.

In addition to the aforementioned preprocessing steps, we employed the NeuroImaging Analysis Kit (NIAK) [56] to further standardize and enhance the quality of our neuroimaging data for both datasets. NIAK offers a comprehensive set of tools for preprocessing fMRI data, including motion correction, slice timing correction, spatial normalization, and nuisance signal regression [40, 57]. These preprocessing procedures are crucial for mitigating potential confounding factors introduced by differences in data acquisition protocols across multiple sites. By implementing the same preprocessing pipeline in both datasets, we aimed to minimize site-related variations and ensure the consistency and reliability of our data across different acquisition sites. This standardized approach facilitated the integration of neuroimaging data from disparate sources, enhancing the validity and generalizability of our findings.

2.3 Connectivity matrices

Similar to our prior research endeavors [33–37], we leveraged Machine Learning (ML) algorithms to analyze fMRI data at different levels of abstraction the connectivity matrix (A) and the attribute matrix (B), which comprises complex network metrics derived from (A). To conduct our analysis, we employed a diverse set of ML classifiers, including the Support Vector Machine (SVM) [58], Naive Bayes (NB) [59], Multilayer Perceptron (MLP) [60], a fine-tuned Convolutional Neural Network (CNN), and Long Short-Term Memory neural networks (LSTM) [61].

Subsequently, the SHAP values method was employed for the biological interpretation, as it provides a comprehensive explanation of the predictive contribution of each feature. To ensure robustness and unbiased assessment of the machine learning models, we adopted a consistent evaluation approach: 10-fold stratified cross-validation with shuffling. This cross-validation technique partitions the dataset into ten equal stratified folds, ensuring that each fold, denoted as *k*, maintains a balanced distribution of samples from each class. This approach guarantees that all classes are equally represented across the folds, thus enhancing the reliability of our model evaluations. The algorithm then trains on nine of these folds and validates on the remaining fold, repeating this process ten times, each serving as the validation set once. We used k = 10, which is a common value for this method [62–66]. However, to show the stability of the model's performance, we also tested different values of k. Moreover, the shuffle strategy ensures the data is randomized before being split into folds to prevent ordering effects; this randomization helps prevent any potential bias stemming from data ordering, ensuring the robustness of the model training process.

Furthermore, as a crucial step in our experimental methodology, we performed an initial partition of 30% of the original dataset (comprising a total of 600 matrices) for final testing, constituting an exclusive reserve of 180 matrices. This separation is done before the model's training using a 10-fold cross-validation. Adopting such a practice is commonplace in machine learning, and it serves the dual purpose of assessing model performance while mitigating overfitting and ensuring its ability to generalize to new, unseen data [67, 68].

This procedure was applied for model selection and hyperparameter optimization. It was also considered the grid search method, commonly used in the literature [69–73], used for all ML algorithms except the CNN and LSMT models. In the deep learning models, we used random search optimization because it offers a more computationally efficient alternative for hyperparameter tuning compared to grid search, which is particularly advantageous, given the high computational demands of deep learning tasks. The hyper-parameter optimization values for each classifier model can be seen in more detail in [33–36]. In Tables 2 and 3, we present the architectural details and hyperparameter configurations for CNN and LSTM models, respectively. Notably, dropout regularization, as indicated in Tables 2 and 3, is a widely-used technique in neural network training to combat overfitting [74]. Dropout operates by randomly deactivating neurons during training, compelling the network to learn more resilient and generalizable features [75]. Empirically, dropout has effectively enhanced the generalization capabilities of deep learning architectures and medical data [76, 77].

Additionally, in our training set, we applied a process known as standardization. Standardization in machine learning typically involves rescaling features to have a mean of zero and a standard deviation of one [78]. This step is pivotal as it transforms the data, facilitating more straightforward comparisons and analyses [79]. This practice is essential because it ensures that all model attributes are equally important and share a consistent scale [80]. Moreover, standardization safeguards against the undue influence of outliers and features with substantial variability on the model's performance [81].

Table 2. Hyperparameters and layer configurations for the CNN model.

Type of Layer	Tuning hyperparameter	Value
Convolutional	—	—
Convolutional	dropout	[0.00, 0.05, 0.10, 0.15, 0.20, 0.25, 0.30, 0.35, 0.40, 0.45, 0.50]
Convolutional	—	—
Convolutional	number of filters	[32, 64]
Max Pooling	dropout	[0.00, 0.50, 0.10, 0.15, 0.20]
Flatten	—	—
Dense	- units	[32, 64, 96. . ..512]
	-activation	[relu, tanh, sigmoid]
Dropout	rate	[0.00, 0.50, 0.10, 0.15, 0.20]
Adam optimization compile	learning rate	$min - value = 1e^{-4}$
		$max - value = 1e^{-2}$
		sampling = LOG

https://doi.org/10.1371/journal.pone.0305630.t002

First and foremost, we considered the widely-used accuracy metric, which provides an overall assessment of our classification model's correctness [82–86]. We expanded our evaluation to incorporate additional standard metrics such as precision and recall [87–90]. Precision, also known as a positive predictive value, measures our model's ability to classify instances belonging to a specific class correctly. In our case, precision helps gauge our model's accuracy in identifying the TD group. On the other hand, recall, also known as sensitivity, assesses how effectively our classifier predicts positive examples, which now encompass ASD and ADHD individuals. To visualize the performance of our classification model, we continued to utilize the Receiver Operating Characteristic (ROC) curve, a standard method for illustrating the trade-off between true and false positive rates. The Area Under the ROC Curve (AUC) remained a key evaluation metric, with values ranging from 0 to 1. An AUC of 1 signifies a flawless classification, while 0.5 suggests a random choice where the classifier cannot distinguish between classes effectively [72, 82, 91, 92].

In this three-class classification context, we calculated the micro-average AUC independently for each class (TD, ASD, or ADHD) to provide insights into individual class performance. This micro-average computation treats each class equally, allowing us to assess how well our model performs for each group. Furthermore, we introduced the concept of macro average in our evaluation, which considers the classes individually and aggregates their contributions before calculating the average. Unlike the micro average, the macro average does not

Table 3. Hyperparameters and layer configurations for the LSTM model.

Type of Layer	Tuning hyperparameter	Value
LSTM	—	—
LSTM	dropout	[0.00, 0.05, 0.10, 0.15, 0.20, 0.25, 0.30, 0.35, 0.40, 0.45, 0.50]
LSTM	—	—
LSTM	units	[70, 60, 50, 40]
Dense	- units	3
	-activation	softmax
Adam optimization compile	learning rate	$min - value = 1e^{-10}$
		$max - value = 1e^{-1}$
		sampling = LOG

https://doi.org/10.1371/journal.pone.0305630.t003

treat all classes equally, providing a different perspective on the overall performance of our classification model. Subsequently, the SHAP values method was used for the biological interpretation, as it explains the predictive power of each attribute. The SHAP values method was subsequently employed for the biological interpretation, as it explains the predictive potential of each attribute. The results regarding the connectivity matrix of the first level of abstraction (A) can be found in subsection 3.1.

2.4 Complex network measures

Considering the performance and computational cost, the best ML algorithm was used to evaluate the complex network measure's level of abstraction. To characterize the structure of the brain's network, the following complex network measurements were computed as used in the previous work [33–37]: average shortest path length (APL) [93], betweenness centrality (BC) [94], closeness centrality (CC) [95], diameter [96], assortativity coefficient [97, 98], hub score [99], eccentricity [100], eigenvector centrality (EC) [101], average degree of nearest neighbors [102] (Knn), mean degree [103], entropy of the degree distribution [104], transitivity [105, 106], second moment of the degree distribution (SMD) [107], complexity, k-core [108, 109], density [110], and efficiency [111].

In this study, we employed recently developed metrics, as comprehensively detailed in [36], to quantify the number of communities within a complex network. Our investigation also incorporated various community detection algorithms [112–114]. The outcomes of community detection measures were consolidated into a single scalar value. Specifically, we focused on identifying the largest community within each network, followed by the computation of the average path length within that community, resulting in a singular metric. The suite of community detection algorithms encompassed fast greedy (FC) [115], infomap (IC) [116], leading eigenvector (LC) [117], label propagation (LPC) [118], edge betweenness (EBC) [119], spin-glass (SPC) [120], and multilevel community identification (MC) [121]. For clarity and coherence, we extended the abbreviations by appending the letter 'A' (indicating average path length) to denote the corresponding approach, resulting in AFC, AIC, ALC, ALPC, AEBC, ASPC, and AMC.

Further, we used three measures to analyze the segregation and integration concepts: Effective Information (*EI*) and determinism and degeneracy coefficients. Measures of integrated information promise general applicability to questions in neuroscience, in which part-whole relations play a role, and are our interest here [122]. In this paradigm, a system can show a balance between two competing tendencies [123]:

- integration, i.e., the system behaves as one;
- segregation, i.e., the parts of the system behave independently.

In other words, integration in network analysis refers to how well nodes in a network are interconnected, facilitating efficient information flow, and highly integrated networks allow for smooth information exchange between nodes [124, 125]. Segregation, on the other hand, pertains to distinct subgroups or communities within a network; segregated networks have subsets of nodes that are more tightly connected within their subgroups, often forming distinct clusters or communities [126, 127].

The *EI* was first introduced to capture the causal influence between two subsets of neurons as a step in calculating integrated information in the brain [128]. Later, a system-wide version of *EI* was shown to capture fundamental causal properties such as determinism and redundancy [129, 130]. To expand the *EI* framework to networks, in [131], the intervention operation in the *EI* calculation is relaxed by assuming that W^{out} has modulus one and interpreted as

leaving a random walker on the network. This allows us to investigate the dynamics by inspecting the graph topology. Quantitatively, the *EI* is based on two uncertainties: the first is the Shannon entropy of the average out-weight vector in the network, $H(W_i^{\text{out}})$, which captures how distributed out-weights of the network are; the second is the average entropy of each node's $H(W_i^{\text{out}})$, giving:

$$EI = H(W_i^{\text{out}}) - H(W_i^{\text{out}}).$$

Further, two fundamental components of *EI* are the determinism and degeneracy coefficients. They are based on a network's connectivity, specifically the degree of overlapping weight in the networks. The determinism is based on the average of how much information is not lost in a walker's uncertainty, $H(W_i^{\text{out}})$. Since $\log_2(n)$ represents maximal determinism, i.e., when all walkers have the output $w_{ij} = 1$. Then, the determinism is given by $\log_2(n) - H(W_i^{\text{out}})$. Meanwhile, the degeneracy describes how non-uniform the weight distribution is of the network. If all nodes lead only to one node, that network is perfectly degenerate. The degeneracy can be captured by $\log_2(n) - H(W_i^{\text{out}})$. Together, determinism and degeneracy can be used to re-define *EI*:

$$EI = \text{determinism} - \text{degeneracy}.$$

However, this study considers three classes, differently from the previous ones [33–37] that only consider two classes. Therefore, it was not possible to classify ADHD from TD using the complex network measures. To address this challenge and gain insights into the underlying patterns within the data, we performed a Principal Components Analysis (PCA). PCA is a dimensionality reduction technique that transforms the original high-dimensional data into a lower-dimensional representation while preserving as much of the variance in the data as possible [132, 133]. By extracting the main components, we aimed to uncover hidden structures and reduce the dimensionality of the dataset, which can be beneficial for subsequent analysis and visualization. This approach allowed us to explore the relationships between the variables and potentially reveal patterns that may not be apparent in the raw data, ultimately contributing to a deeper understanding of the complex network measures in the context of ADHD and TD classification.

After PCA, we conducted a statistical analysis using the Wilcoxon test with Bonferroni correction to compare the three classes: ASD, ADHD, and TD. The Bonferroni correction controls the family-wise error rate in multiple hypothesis testing scenarios, such as when performing multiple pairwise comparisons [134]. In our context, it helps address the issue of inflated Type I error rates that can occur when conducting multiple statistical tests simultaneously. The Wilcoxon test, also known as the Mann-Whitney U test in the case of two groups or the Kruskal-Wallis test for more than two groups [135–137], is a non-parametric test used to assess whether there are statistically significant differences between groups when the assumptions of normality and equal variances are not met. In this specific analysis, the Wilcoxon test allowed us to determine if there were significant differences in some measure or variable among the ASD, ADHD, and TD groups. To apply the Bonferroni correction, the significance level (alpha) for each comparison is adjusted to reduce the overall probability of making a Type I error (Type I error, also known as a false positive, occurs when a true null hypothesis is rejected in a statistical test [138]. In the context of multiple comparisons, it refers to the increased likelihood of mistakenly concluding that there is a significant difference when there is not due to the increased number of tests being performed simultaneously. The Bonferroni correction helps to reduce this risk) across all comparisons [139]. This adjustment is achieved by dividing the original alpha level by the number of comparisons being made. The

adjusted alpha becomes more stringent, making it harder to declare a result as statistically significant. Consequently, the Bonferroni correction helps to mitigate the risk of false positives when conducting multiple comparisons. These results can be seen in subsection 3.2, and the following symbols represent the statistical significance:

- ns: $5.00e-02 < p <= 1.00e+00$;
- *: $1.00e-02 < p <= 5.00e-02$;
- **: $1.00e-03 < p <= 1.00e-02$;
- ***: $1.00e-04 < p <= 1.00e-03$;
- ****: $p <= 1.00e-04$.

3 Results

3.1 Connectivity matrices

According to Table 4, the best classifiers were LSTM and SVM. LSTM performance for the test set was equal to 0.983 for the mean AUC, 0.978 for precision, 0.978 for recall, and 0.978 for accuracy. SVM performance for the test set was equal to 0.946 for the AUC, 0.928 for the precision, 0.928 for the recall, and 0.928 for the accuracy. Each classifier's confusion matrices and ROC curves are depicted in Figs 2 and 3, respectively.

Further, we investigated potential biases arising from variations in data acquisition protocols between different sites to enhance the robustness of our analysis; we compared the TD group for the ADHD dataset and the ASD dataset using the SVM. The results in Fig 4 show that all metric performance stands around 0.50 in a random classifier. Therefore, it is impossible to distinguish between the TD groups of the different datasets, proving that we could mitigate potential biases from variations in data acquisition protocols.

Since SVM has a lower computational cost, it was chosen for the following subsequent analyses. To determine the optimal number of features required for peak performance, we conducted a Recursive Feature Elimination (RFE) analysis, as illustrated in Fig 5A. RFE, often used in the literature in prediction models in medical data [140–142], iteratively removes less

Table 4. Results from different ML algorithms. The best ML algorithms were LSTM and SVM, whose performances are highlighted in bold.

Model	Subset	AUC	Accuracy	Recall	Precision
LSTM	**Train**	0.987±0.022	0.968±0.051	0.951±0.082	0.954±0.074
	Test	**0.983**	**0.978**	**0.978**	**0.978**
SVM	**Train**	0.951±0.020	0.936±0.026	0.936±0.026	0.940±0.025
	Test	**0.946**	**0.928**	**0.928**	**0.928**
LR	**Train**	0.948±0.022	0.931±0.029	0.931±0.029	0.934±0.028
	Test	0.946	0.928	0.928	0.927
CNN	**Train**	0.956±0.042	0.904±0.048	0.852±0.072	0.860±0.073
	Test	0.938	0.920	0.913	0.913
MLP	**Train**	0.932±0.025	0.910±0.033	0.910±0.033	0.913±0.035
	Test	0.929	0.905	0.905	0.905
NB	**Train**	0.834±0.028	0.779±0.037	0.779±0.037	0.800±0.042
	Test	0.854	0.805	0.805	0.812

https://doi.org/10.1371/journal.pone.0305630.t004

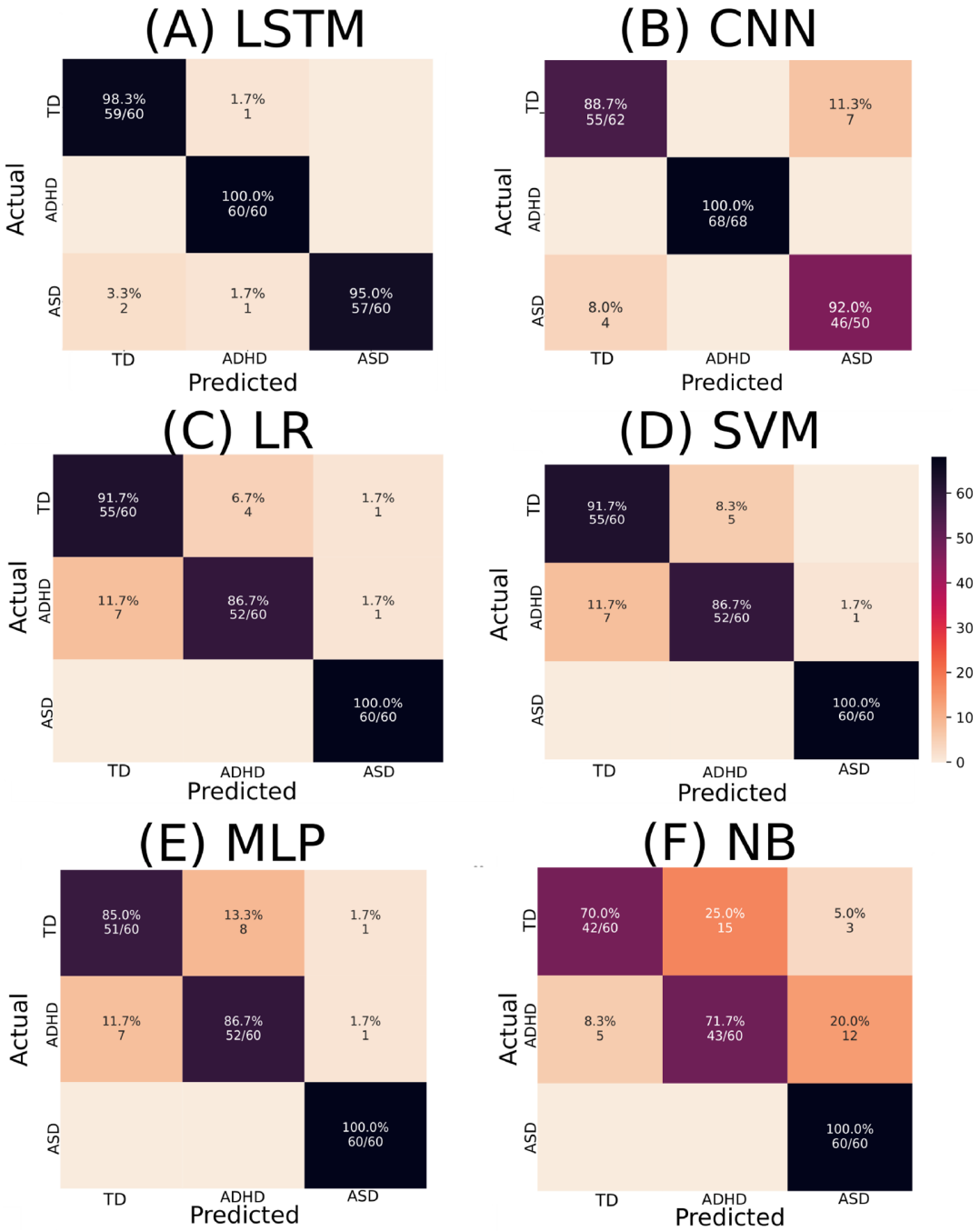

Fig 2. Confusion matrices depict the performance of various ML algorithms. The elements in the figure labeled A to F correspond to LSTM, CNN, LR, SVM, MLP, and NB, respectively. The diagonal elements represent TP values, showcasing each algorithm's accuracy in correctly identifying positive instances. This is noteworthy on a test sample containing 180 instances.

https://doi.org/10.1371/journal.pone.0305630.g002

critical features to gauge their impact on model performance, allowing us to pinpoint the most relevant features. Fig 5A demonstrates that greater accuracy is attained while using 310 characteristics. Thus, including a complete feature set was not necessary to achieve maximum effectiveness.

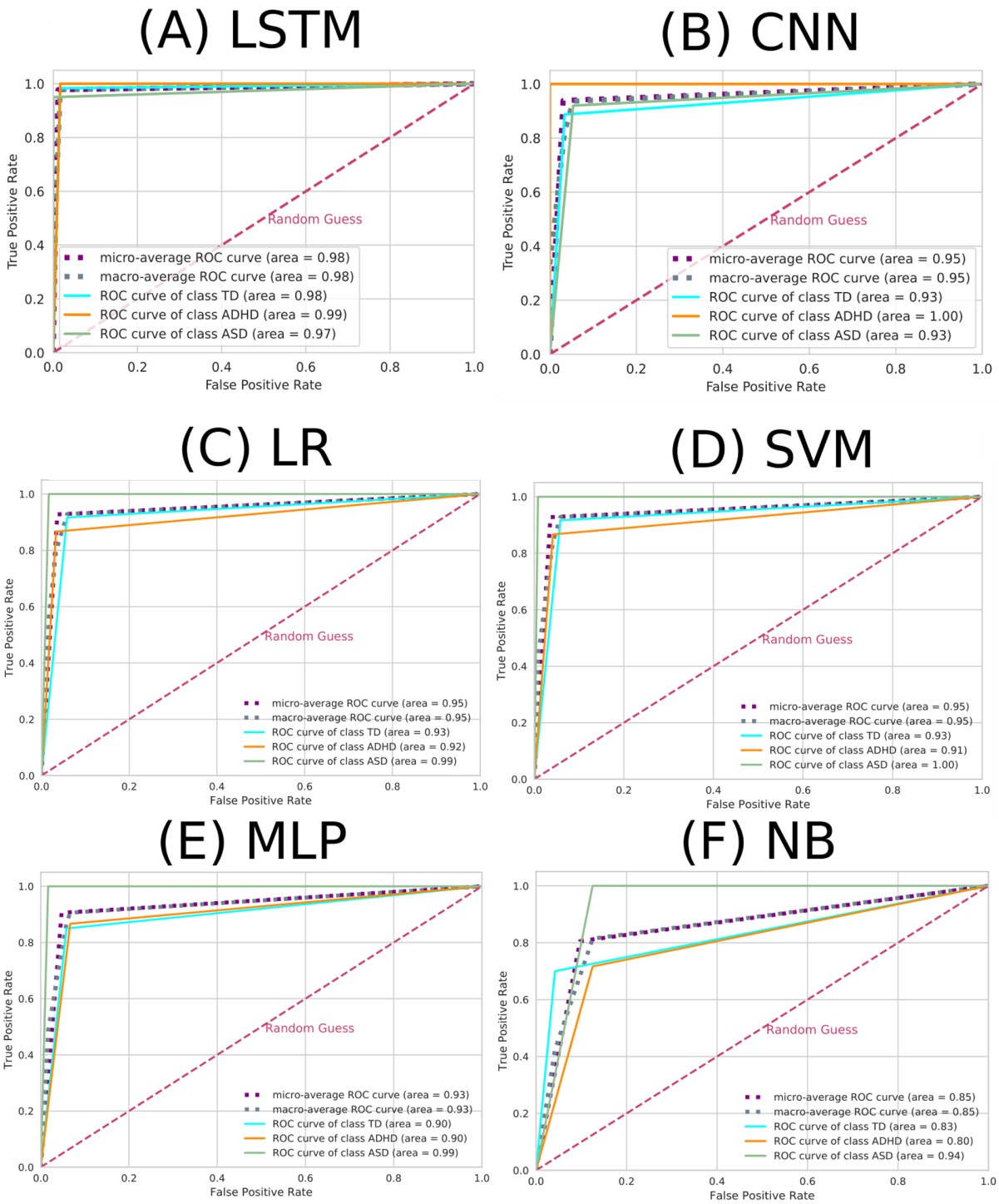

Fig 3. ROC curve for each ML algorithm. The elements in the figure labeled A to F correspond to LSTM, CNN, LR, SVM, MLP, and NB, respectively. The dashed pink line represents the random choice classifier, the purple line the micro-average ROC curve, the gray line the macro-average ROC curve, the turquoise line the ROC curve referring to the TD class, the orange line the ROC curve referring to the ADHD class, and the green line the ROC curve referring to the ASD class.

https://doi.org/10.1371/journal.pone.0305630.g003

Fig 4. Investigation of potential biases arising from variations in data acquisition protocols. Comparing the TD groups from different datasets results in all metric performance standing around 0.50 in a random classifier, proving that we could mitigate potential biases from variations in data acquisition protocols with our preprocessing.

https://doi.org/10.1371/journal.pone.0305630.g004

In addition to RFE, we generated a learning curve, as illustrated in Fig 5B, to gain insights into the influence of dataset size on our model's performance. This curve visually represents how the number of training instances affects the model's predictive accuracy. Therefore, RFE and the learning curve enable us to fine-tune our SVM model, ensuring it achieves the optimal equilibrium between feature selection and data volume. From Fig 5B, it can be seen that the maximum performance occurred with 450 subjects without the need for the complete dataset.

Then, we used the 310 features obtained from RFE analysis to perform the SHAP values methodology. The results can be seen in Fig 6.

As in Fig 6, it can be seen that for all classes, mainly for distinguishing TD and ASD (in Fig 6A, dark blue and green, respectively), the two primary connections were Left-ParsOrbitalis-Left-PrimMotor and Left-ParsOrbitalis-Left-Thalamus. Regarding the ASD class, the primary connections found were Left-ParsOrbitalis-Left-Thalamus and Left-ParsOrbitalis-Left-PrimMotor, with a low correlation value for this class (in Fig 6B). Regarding the ADHD class, the primary connections found were Left-VisualAssoc-Outside defined BAS1 and Right-AngGyrus-Outside defined BAS1, with a low correlation value for this class (in Fig 6C). From our previous work, the Outside defined BAS1 was identified as the cerebellum. Fig 7 contains the two-dimensional schematic (ventral-axis) with the man regions found regarding ASD and ADHD.

Furthermore, we introduced noise generated by a normal distribution, with different means (level of the noise) while keeping the standard deviation constant at 0.1. This resulted in a range of noisy matrices that we used to evaluate our SVM model's performance. We assessed the SVM model's performance using AUC and accuracy depicted in Fig 8, which indicates that our SVM model exhibits robustness to noise in the input data matrices. Even when noise levels vary from 0.0 to 1.5, the model maintains a relatively high AUC and accuracy, indicating its ability to accurately classify patients with ASD, ADHD, and TD individuals. The model's performance gradually decreases as the noise level increases, which is expected. However, it is noteworthy that even at noise levels as high as 1.0 (where the data is significantly distorted), the model still achieves a reasonable AUC of 0.70 and an accuracy of 0.60 (see Fig 8).

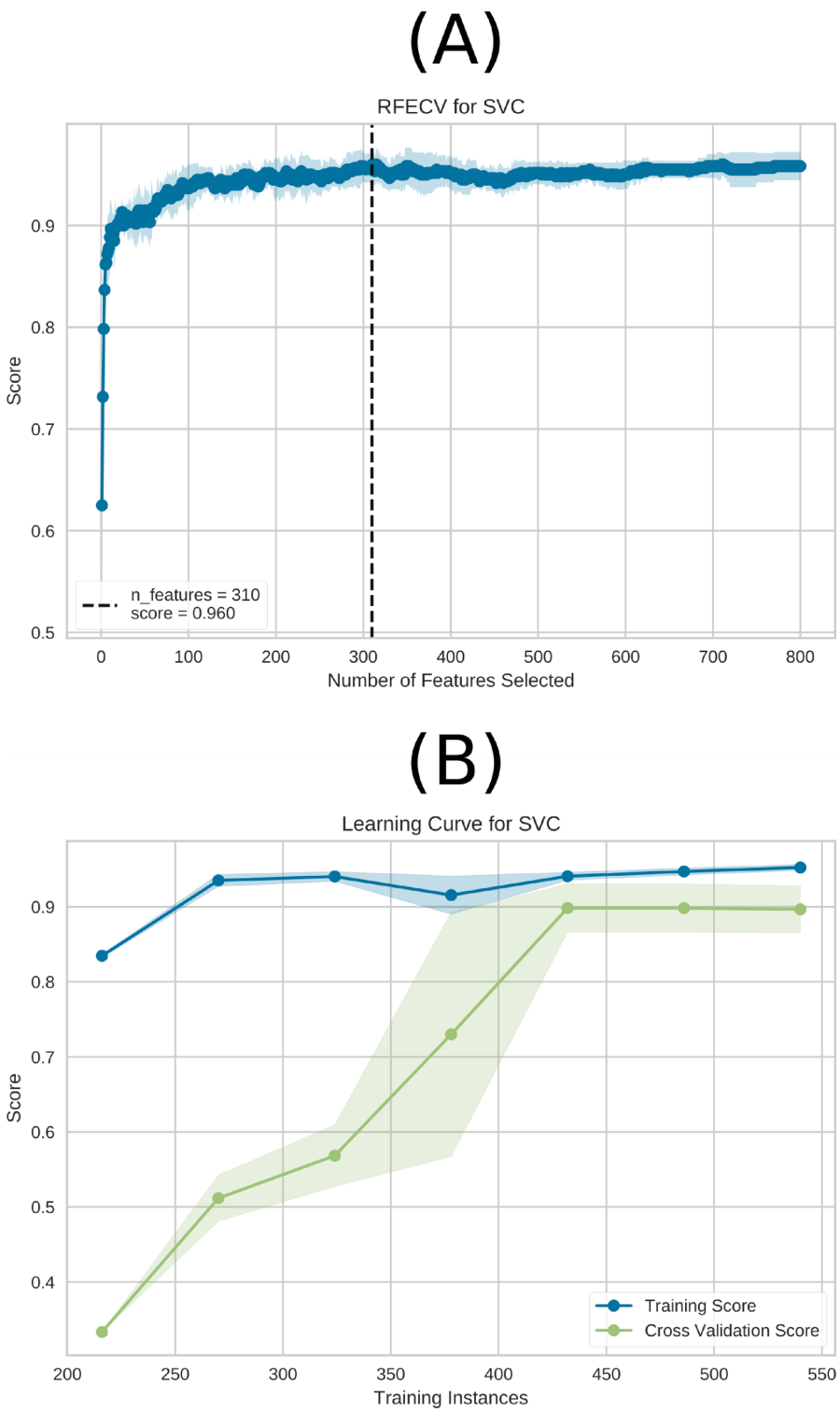

Fig 5. RFE and the learning curve for the SVM model are depicted in (A) and (B), respectively. The best performance is achieved with a total of 310 characteristics, as shown by (A). In (B), the learning curve is presented for the training Accuracy (blue) and test Accuracy (green) using the entire dataset (600 connectivity matrices subjects). The highest performance was achieved with 450 connectivity matrices subjects without requiring the entire dataset. Notably, the connectivity matrices were generated using the data augmentation technique sliding window, and 600 connectivity matrices were used in total in the ML approach before the sampling technique.

https://doi.org/10.1371/journal.pone.0305630.g005

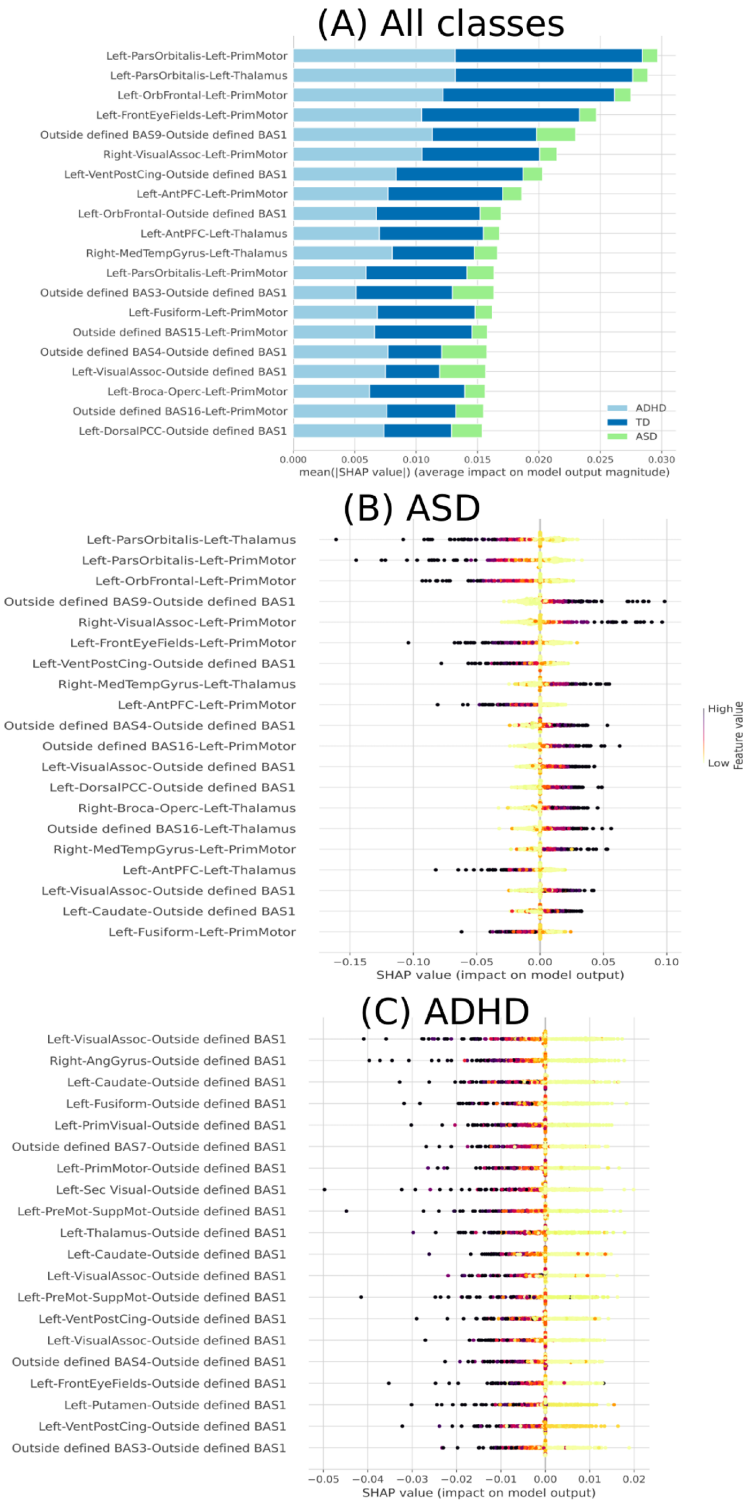

Fig 6. Feature importance ranking using the SHAP values methodology for the SVM classifier with brain regions in descending order. (A) Feature ranking based on the average of absolute SHAP values over all subjects considered. (B) Feature importance ranking regarding ASD class. (C) Feature importance ranking regarding ADHD class.

https://doi.org/10.1371/journal.pone.0305630.g006

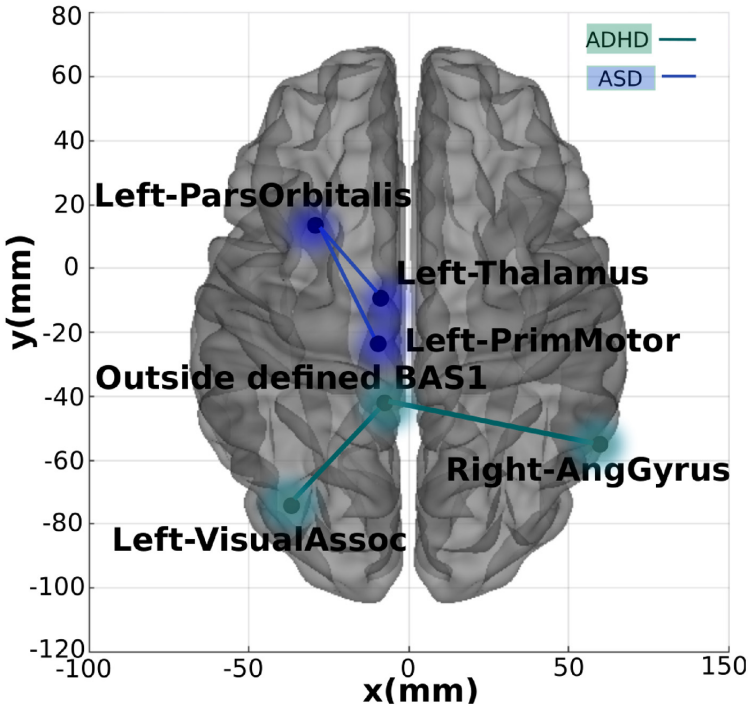

Fig 7. The most important connections found. Two-dimensional schematic (ventral-axis), where the most important connection for ADHD and ASD are highlighted in green and blue, respectively. The brain plot was developed by the Braph tool [143], and each region was plotted using a Brodmann map from the Yale BioImage Suite Package.

https://doi.org/10.1371/journal.pone.0305630.g007

This suggests that the SVM model is resilient to noise and can provide valuable diagnostic information in real-world scenarios where data may be imperfect.

Further, we conducted stratified k-fold cross-validation with values beyond k = 10, namely 2, 3, 5, and 15. The resulting plot in Fig 9 reveals trends in the SVM model's performance on

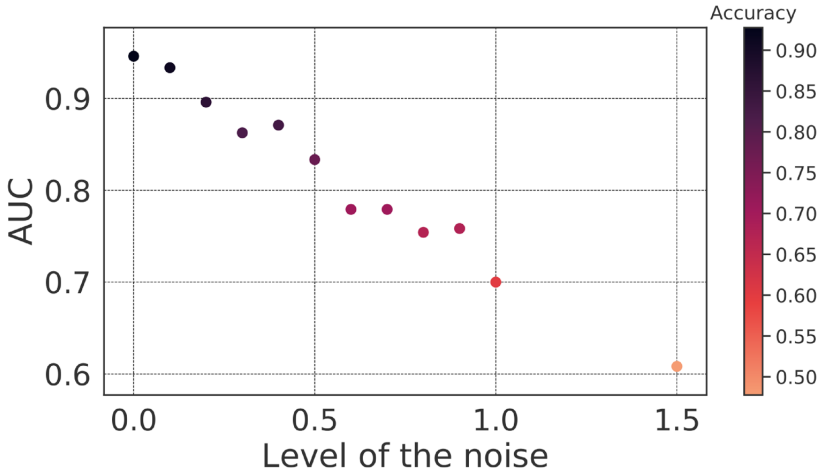

Fig 8. SVM behavior after insertion of noise. The mean AUC of the test was obtained with the insertion of noise generated by a normal distribution with 0.1 standard deviation and a 0–1.5 mean range.

https://doi.org/10.1371/journal.pone.0305630.g008

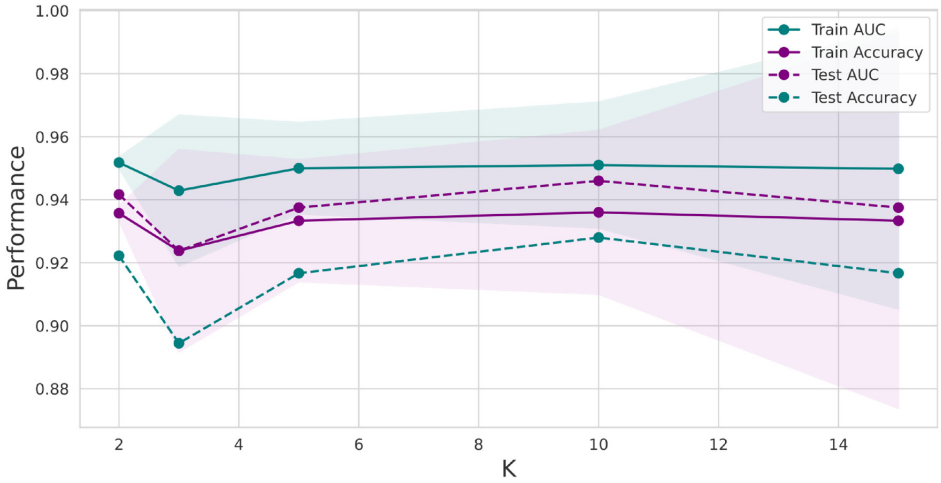

Fig 9. Plot for the SVM model with performance measures. The AUC and Accuracy, in the y-axis, in blue and purple, respectively, were obtained by varying the number of k in the stratified k-fold-cross-validation (x-axis))—the dashed lines corresponding to the test sample and the complete lines to the training sample. Furthermore, the shaded represents the standard deviation in the training sample.

https://doi.org/10.1371/journal.pone.0305630.g009

the training dataset. As the value of k increases, the AUC remains relatively stable, with values ranging from approximately 0.94 to 0.95. This suggests that the SVM model consistently discriminates between the three groups—ASD, ADHD, and TD. The corresponding accuracy values remain steady, ranging from approximately 0.93 to 0.94. We observed similar stability in AUC values for the test dataset, which ranges from about 0.92 to 0.95 as k varies. This indicates that the SVM model's ability to distinguish between groups holds when applied to unseen data. The accuracy on the test dataset also remains steady, with values ranging from approximately 0.89 to 0.93. This robustness is particularly valuable when dealing with real-world data where k can impact model stability.

3.2 Complex network

The performance of the test sample considering the complex network yielded the confusion matrix and the ROC curve depicted in Fig 10.

The performance of the test sample considering the complex network yielded the confusion matrix, and the ROC curve depicted in Fig 10 indicates that the model did not perform well for the ADHD class (with an accurate positive accuracy of 0.53 and an AUC of 0.72). This suboptimal performance can be attributed to several factors. Firstly, when we performed PCA with two and three components, as shown in Fig 11, it became evident that the ADHD and TD instances formed two overlapping groups, differently from the ASD instance class. This lack of clear separation in the PCA space suggests that the initial feature set does not easily capture the inherent characteristics distinguishing ADHD from TD cases. This inherent overlap in feature distributions can significantly hinder the performance of a classifier like SVM, which relies on well-defined class boundaries.

Additionally, we observed in Fig 11 that none of the features displayed strong correlations with the principal components. This lack of feature-component solid correlations suggests that the initial feature set may need to contain clear discriminatory information, making it challenging for the SVM to distinguish between classes effectively.

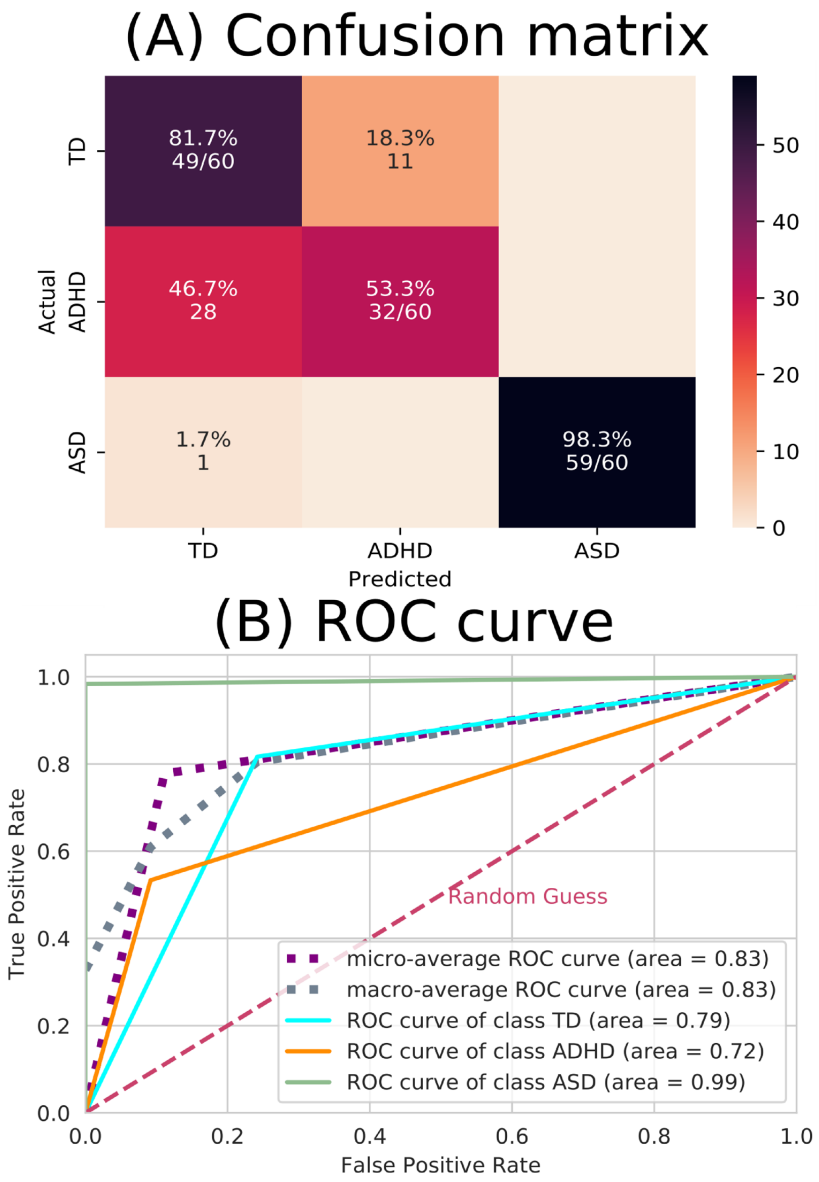

Fig 10. ML results from complex network measures. (A) The confusion matrix indicates that there were a lot of incorrect predictions between the TD and ADHD groups. (B) The ROC curve, where the dashed pink line represents the random choice classifier, the purple line is the micro-average ROC curve, the gray line is the macro-average ROC curve, the turquoise line the ROC curve referring to the TD class, the orange line the ROC curve referring to the ADHD class (which can be seen the ADHD has the lowest-distinguished curve) and the green line the ROC curve referring to the ASD class (which can be seen the ASD has the best-distinguished curve).

https://doi.org/10.1371/journal.pone.0305630.g010

Therefore, to improve the model performance, it may be necessary to consider additional domain-specific features that could better capture the nuances of ADHD and TD differentiation within the dataset.

Then, we performed a statistical t-test with Bonferroni correction. This choice was driven by our need to rigorously assess the significance of differences in the means of individual features between the ADHD and TD groups. By conducting this test, we could identify which

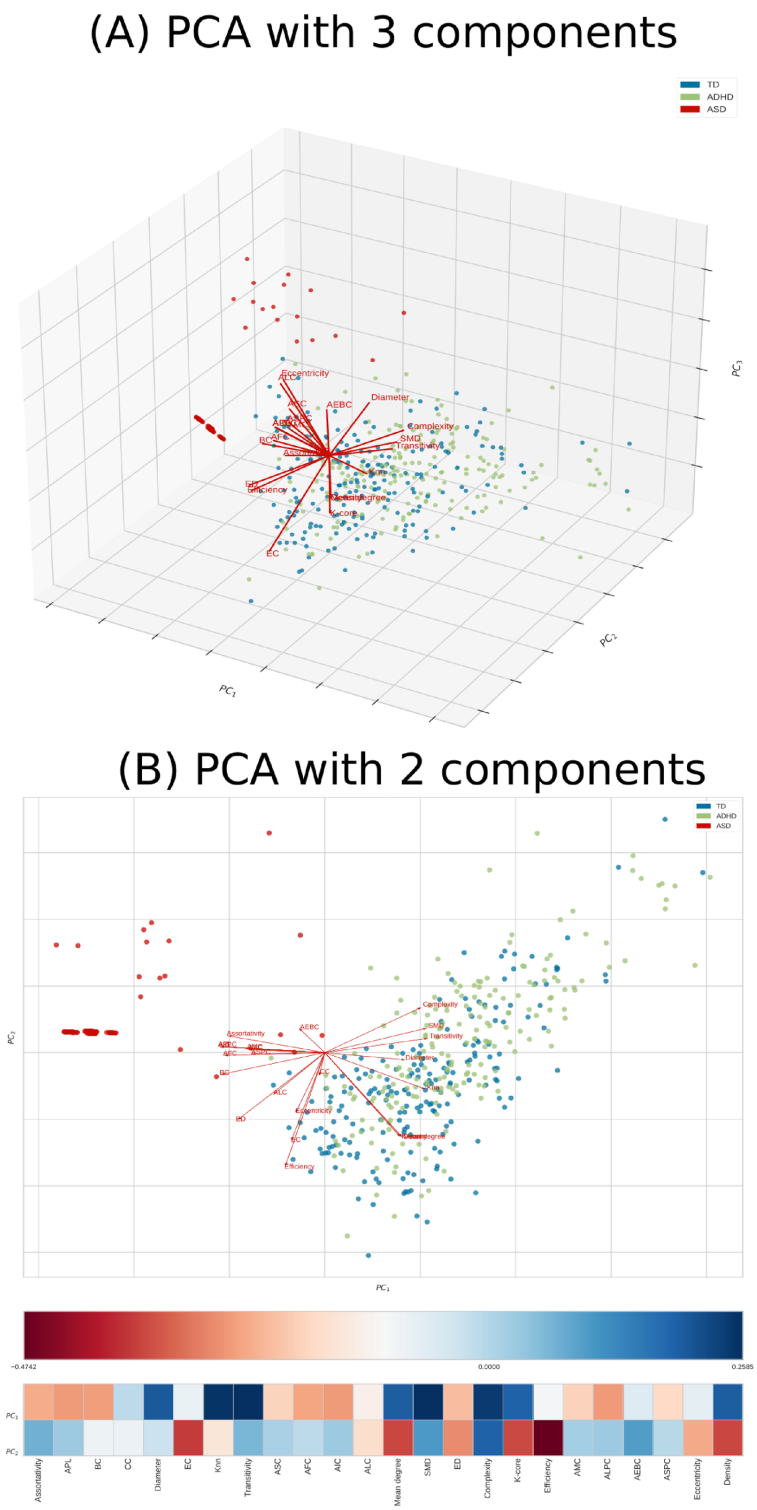

Fig 11. PCA using the complex network measures. The features for ASD, ADHD, and TD are depicted in red, green, and blue, respectively. In (A), PCA with three components, namely PC1, PC2, and PC3, is illustrated in the plot axis. In (B), PCA with two components, namely PC1 and PC2, is presented in the plot axis; further, the heatmap shows that any of the features were highly correlated with the two components.

https://doi.org/10.1371/journal.pone.0305630.g011

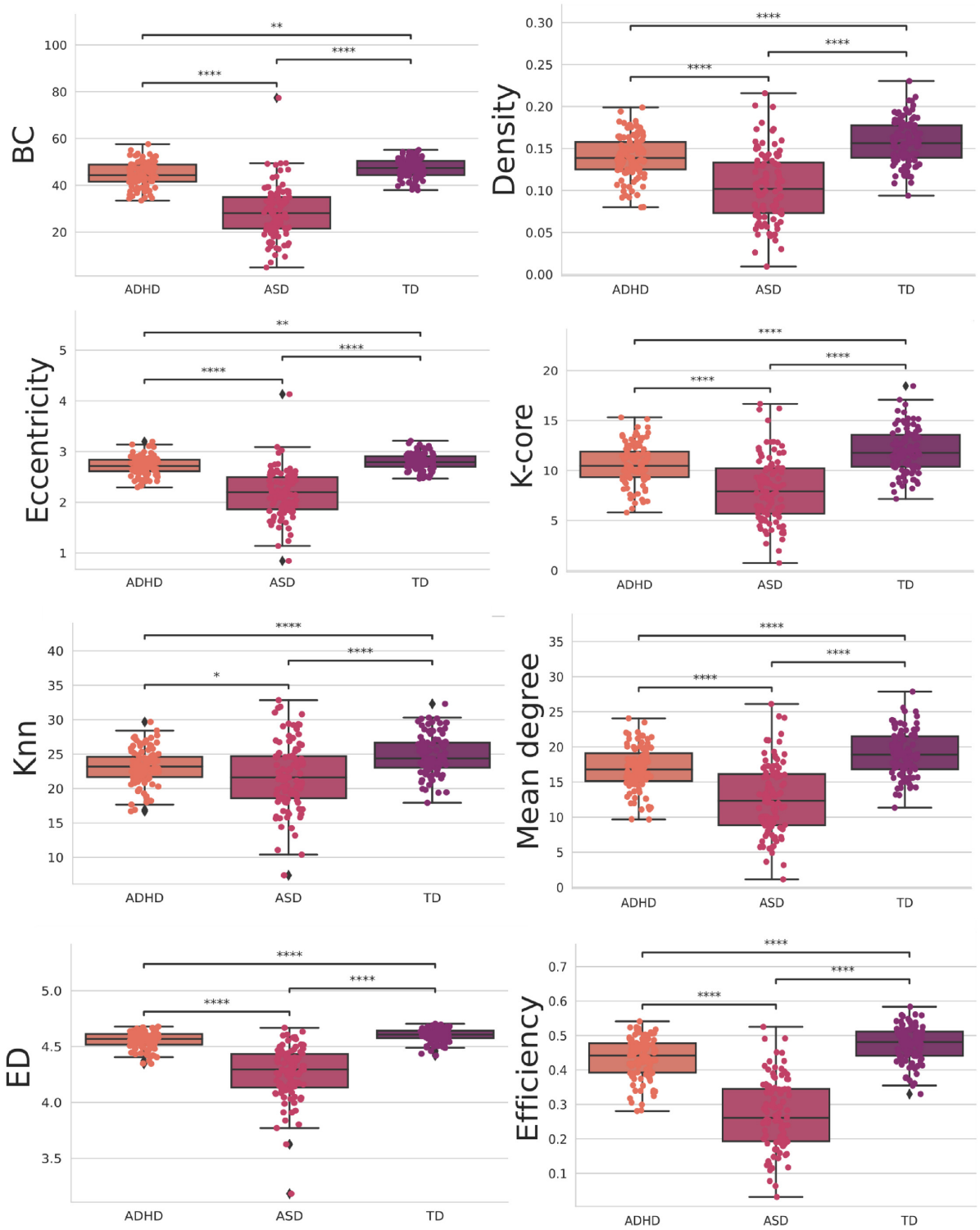

Fig 12. Features were statistically significant between all groups when using the t-test with Bonferroni correction. The orange, pink, and purple boxplots show the features that obtained the most statistically significant differences regarding the classes ADH, ASD, and TD, respectively.

https://doi.org/10.1371/journal.pone.0305630.g012

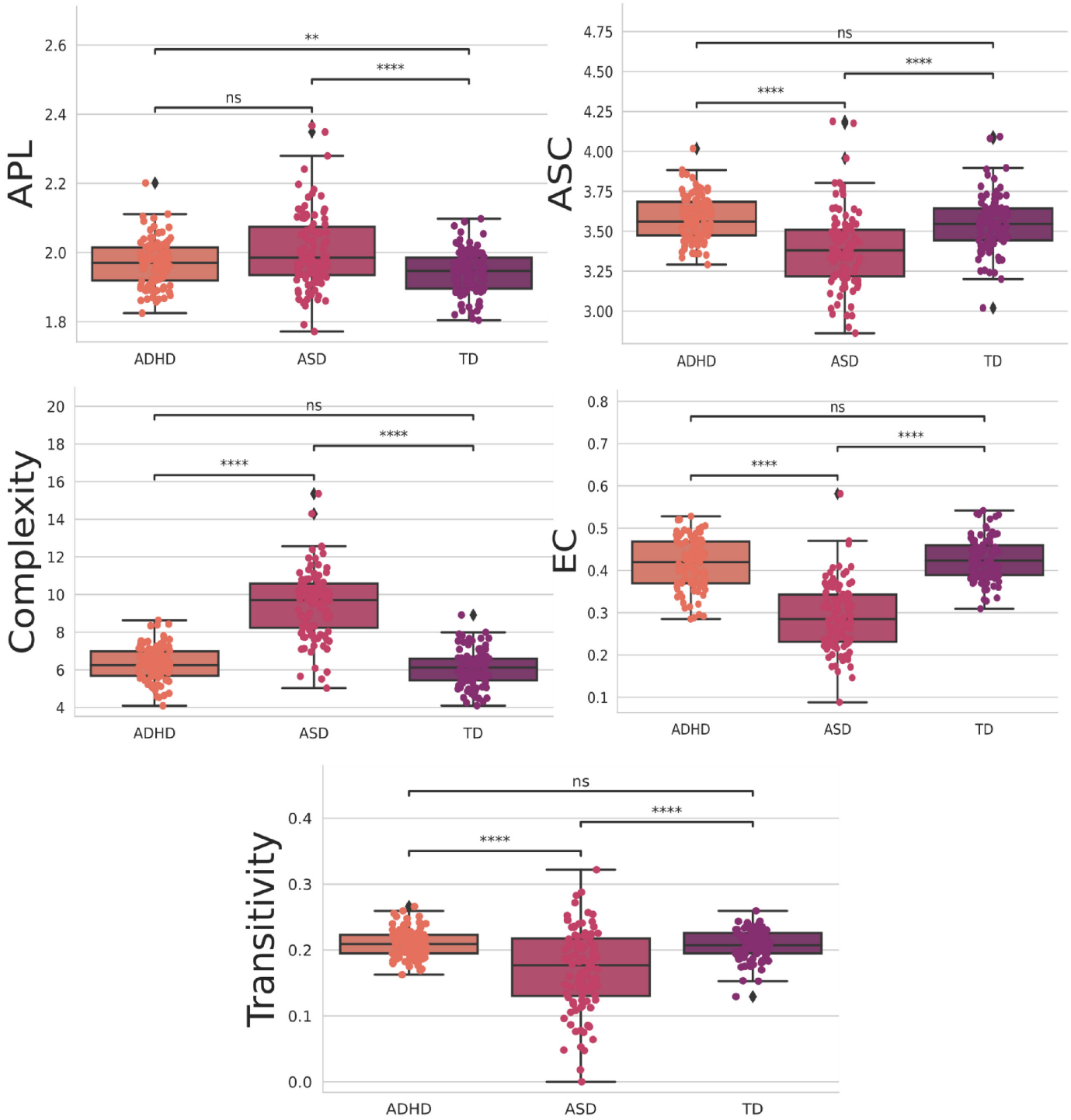

Fig 13. Features were four stars statistically significant, at least between one of the groups, when using the t-test with Bonferroni correction. The orange, pink, and purple boxplots show the features that obtained the most statistically significant differences regarding the classes ADH, ASD, and TD, respectively.

https://doi.org/10.1371/journal.pone.0305630.g013

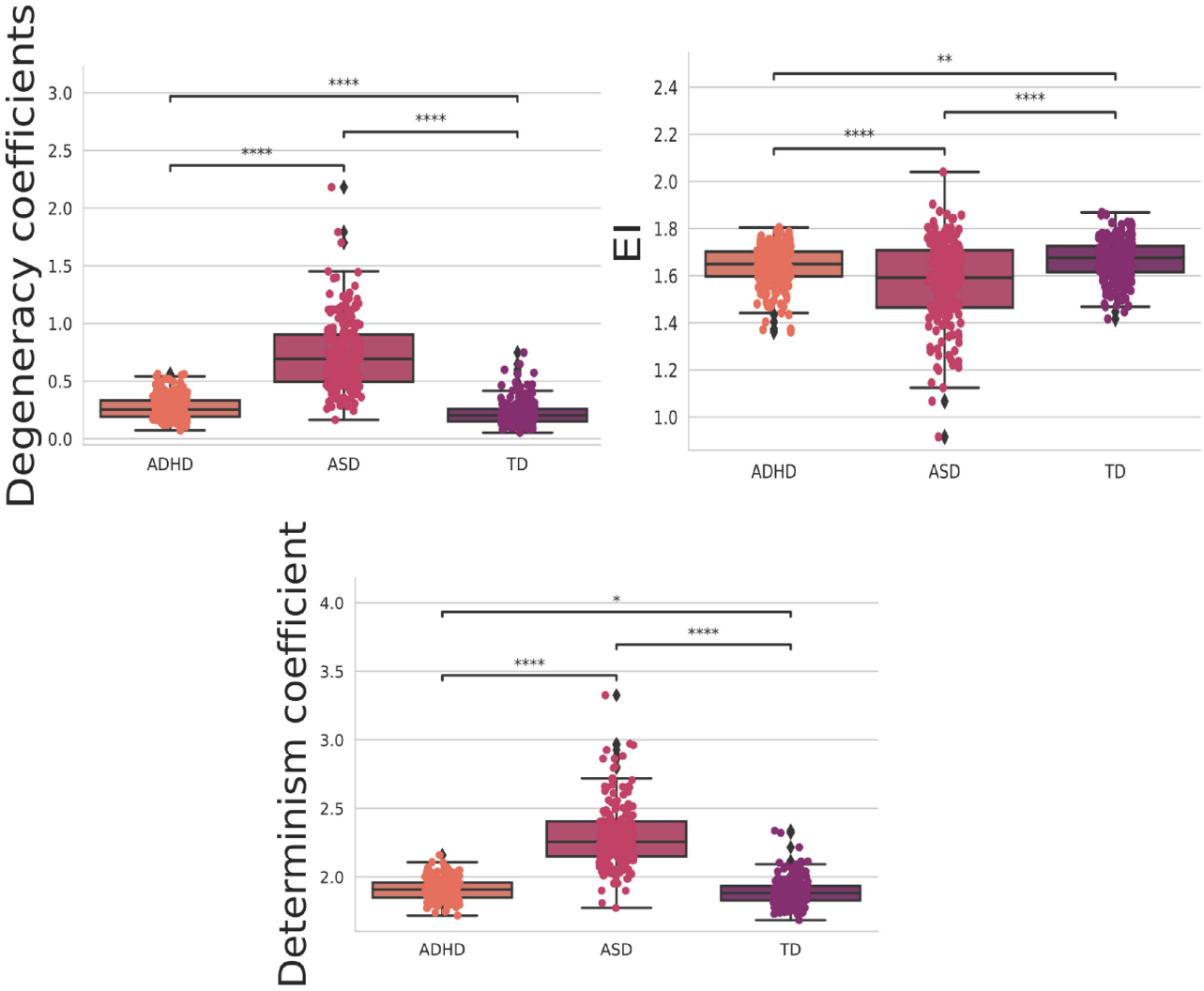

Fig 14. The t-test with Bonferroni correction for the integrated measures. The orange, pink, and purple boxplots show the features that obtained the most statistically significant differences regarding the classes ADH, ASD, and TD, respectively.

https://doi.org/10.1371/journal.pone.0305630.g014

specific features exhibit statistically significant distinctions between these two classes. The Bonferroni correction is applied to mitigate the issue of multiple comparisons, ensuring that we maintained a low family-wise error rate. In other words, it helps control the higher probability of obtaining false positives when examining numerous features simultaneously. The statistically significant ones between all groups are depicted in Fig 12, and the ones with four stars at least between one of the groups are in Fig 13. Further, the statistical test with the integrated measures can be found in Fig 14.

4 Discussion

4.1 Connectivity matrices

Overall, we obtained the best performance compared to the multiclass machine learning algorithm comparing ASD, ADHD, and TD in the literature, as described in section 1. Analysis

from Table 1 reveals that our methodology outperforms existing multiclass approaches. In our prior research [33] focusing on EEG time series, we demonstrated the superior accuracy of constructing connectivity matrices compared to conventional methods employing raw EEG data. This underscores the significance of network topology in characterizing brain data.

Furthermore, in subsequent investigations [34, 35], we found that employing a distinct correlation metric yielded improved detection of brain changes associated with ASD and schizophrenia, respectively. Interestingly, TE proved effective in capturing such changes in the fMRI dataset. Thus, one of our hypotheses for achieving optimal performance revolves around selecting an appropriate correlation metric.

Furthermore, our findings, as illustrated in Fig 6, provide valuable insights into the functional roles of specific brain regions in distinguishing between individuals with ASD, ADHD, and TD based on fMRI matrices. These results shed light on the neural circuitry implicated in these neurodevelopmental conditions.

In Fig 6A, where TD and ASD are distinguished, the two primary connections of interest are Left-ParsOrbitalis-Left-PrimMotor and Left-ParsOrbitalis-Left-Thalamus. This observation suggests that these connections play a significant role in discriminating between TD and ASD individuals. The Left-ParsOrbitalis is associated with decision-making and social cognition [144], areas commonly affected in individuals with ASD [145]. The connections to the PrimMotor and Thalamus imply that motor control and sensory processing also contribute to distinguishing between these groups and are also found in our previous work [34]. Further, Fig 6B highlights the primary connections for the ASD class, with a focus on Left-ParsOrbitalis-Left-Thalamus and Left-ParsOrbitalis-Left-PrimMotor. These connections are consistent with the findings in Fig 6A, emphasizing the importance of the Left-ParsOrbitalis in distinguishing individuals with ASD. This region's involvement in social cognition, decision-making, and language processing may reflect the cognitive and behavioral characteristics associated with ASD.

In Fig 6C, which pertains to the ADHD class, the primary connections identified are Left-VisualAssoc-Outside defined BAS1 and Right-AngGyrus-Outside defined BAS1, both with low correlation values. Our previous work has identified the "Outside defined BAS1" as the cerebellum. The cerebellum is traditionally linked to motor control [146]. However, emerging research suggests its involvement in cognitive functions, including attention and executive control [147] and in several studies associated with ADHD [146, 148, 149]. The Left-VisualAssoc connection might signify differences in visual processing [150], while the Right-AngGyrus could be related to higher-order cognitive functions [151]. Both areas play a significant role in visuospatial attention processes [152, 153]. The low correlation values may imply that these connections are less distinctive for distinguishing ADHD from the other groups, suggesting a more complex neural signature for this condition.

4.2 Complex network measures

The results in Fig 12 offer valuable insights into the network properties of three distinct groups: ASD, ADHD, and TD. We employed a range of complex network measures to assess valuable insights into the network properties of three distinct groups. Further, with these metrics, we can observe distinct patterns in integration and segregation, which are fundamental concepts in network analysis, across the three groups [154, 155].

The ASD group exhibits the lowest values across various network metrics, such as BC, Density, Eccentricity, K-core, KNN, Mean Degree, ED, and Efficiency. This suggests that individuals with ASD have a more fragmented and segregated network structure, indicating challenges in information integration within the network. In other words, their networks may have more

isolated clusters of nodes that do not communicate effectively with each other, according to the literature [34, 156, 157].

On the other hand, the ADHD group demonstrates higher values in these metrics compared to ASD; however, it falls short of the performance observed in the TD group, indicating that individuals with ADHD have a network structure that is more integrated than ASD but still not as optimal as the control group. This implies that individuals with ADHD have a network structure that is more cohesive than ASD but not as cohesive as typical development.

Furthermore, as shown in Fig 13, the ASD group exhibits the lowest values for both the ASC measure, gauging the size of community networks, EC, network influence, and transitivity. In contrast, the ADHD group displays higher values in these metrics than the ASD group but still lags behind the TD group. These findings suggest that individuals with ASD may have smaller and less influential networks within their communities, while those with ADHD fall in between ASD and TD individuals regarding these network characteristics.

By computing the *EI* in the TD, ASD, and ADHD groups, there is a lower average value of *EI* in the ASD group than the others, showing a tendency to have a more segregated than integrated structure in this group (see Fig 14). Interestingly, there is an analysis of determinism and degeneracy coefficients in the groups. The greater value of determinism and degeneracy coefficients in the ASD than the others shows that the graph structure in this group resembles a star (sparse connections) instead of a complete (well-connected) network [131] strengthening the *EI* interpretation in the last paragraph.

In [158], functional segregation was characterized as the capacity for specialized processing within tightly interconnected brain regions. In other words, neuronal processing is distributed across functionally related regions organized into modules. These modules are described as communities exhibiting dense internal connectivity among their constituent nodes and limited communication with nodes from other communities. This network analysis can be linked to the long-observed fact by clinicians that those with ASD are impaired in their ability to generalize—that is, to relate new stimuli to past experiences. Instead, these groups are good at specializing in learned habits [159, 160].

5 Conclusion

Our study used fMRI datasets and explainable IA methods to generate an interpretable classifier for ASD, ADHD, and TD. We have found distinct brain activity patterns underlying these neurodevelopmental disorders by advancing beyond binary comparisons and integrating complex network measures alongside machine learning methodologies.

Our findings confirm the existence of unique neural signatures for ASD, ADHD, and TD groups. Notably, connections involving Left-ParsOrbitalis emerged as crucial in distinguishing between TD and ASD, possibly indicating underlying deficits in decision-making and social cognition observed in ASD. Similarly, distinct neural signatures were observed for ADHD, with connections to the cerebellum, Left-VisualAssoc, and Right-AngGyrus, highlighting potential involvement in cognitive functions and sensory processing differences. The observed connectivity patterns on which the ML classification rests agree with established diagnostic approaches based on clinical symptoms, proving the trustworthiness and efficiency of our multiclass ML approach's interpretability technique. Moreover, we demonstrate the superior performance of our multiclass machine learning approach compared to existing literature. This heightened performance is essential for reliable discrimination between neurodevelopmental conditions, promising prospects for more precise diagnostic tools.

Furthermore, our analysis of complex network measures elucidated the network properties of each group, unveiling differences in integration and segregation patterns. The ASD group

exhibited the lowest values across various network metrics, suggesting a fragmented network structure. In contrast, the ADHD group demonstrated intermediate values, indicative of a network that is more integrated than ASD but less cohesive than typical development.

Despite these significant contributions, limitations such as data quantity constrain the generalizability of our findings. Future studies should aim to overcome these limitations by incorporating larger datasets encompassing a broader range of mental health conditions. Further investigations focusing on specific brain regions could provide deeper insights into group differences in brain connectivity. Further, we propose integrating our methodology with federated learning techniques as a promising avenue for advancing diagnostics and drug trials in neurodevelopmental conditions [161–163]. Federated learning offers a solution to data privacy and scalability challenges, allowing for collaborative model training across multiple datasets while preserving data decentralization [164–166]. This approach holds immense potential for improving diagnostic accuracy and guiding personalized treatment strategies tailored to specific demographics or clinical settings [167].

In summary, our study represents a significant step forward in understanding the neural underpinnings of neurodevelopmental conditions. By leveraging advanced analytical techniques and machine learning methodologies, we have surpassed performance in discrimination between ASD, ADHD, and TD individuals, paving the way for refined diagnostics and promising avenues for developing trustworthy clinical decision-support systems.

Supporting information

S1 File. Connectivity matrices attached in a zip file used to generate the results. This section contains the normalized transfer entropy connectivity matrices derived from the authors' preprocessed BOLD time series of 122 fMRI regions. These matrices served as inputs for the algorithms employed in this study and for extracting complex network measures.
(ZIP)

S2 File.
(ZIP)

Author Contributions

Conceptualization: Caroline L. Alves.

Formal analysis: Caroline L. Alves, Tiago Martinelli.

Funding acquisition: Michael Moeckel.

Investigation: Caroline L. Alves, Tiago Martinelli.

Methodology: Caroline L. Alves.

Project administration: Michael Moeckel.

Resources: Michael Moeckel.

Software: Caroline L. Alves, Tiago Martinelli.

Supervision: Michael Moeckel.

Validation: Caroline L. Alves, Tiago Martinelli, Loriz Francisco Sallum, Francisco Aparecido Rodrigues, Thaise G. L. de O. Toutain, Joel Augusto Moura Porto, Christiane Thielemann, Patrícia Maria de Carvalho Aguiar, Michael Moeckel.

Visualization: Caroline L. Alves.

Writing – original draft: Caroline L. Alves, Tiago Martinelli, Loriz Francisco Sallum.

Writing – review & editing: Caroline L. Alves, Francisco Aparecido Rodrigues, Thaise G. L. de O. Toutain, Joel Augusto Moura Porto, Christiane Thielemann, Patrícia Maria de Carvalho Aguiar, Michael Moeckel.

References

1. Parenti I, Rabaneda LG, Schoen H, Novarino G. Neurodevelopmental disorders: from genetics to functional pathways. Trends in Neurosciences. 2020; 43(8):608–621. https://doi.org/10.1016/j.tins.2020.05.004 PMID: 32507511
2. Li Y, Shen M, Stockton ME, Zhao X. Hippocampal deficits in neurodevelopmental disorders. Neurobiology of learning and memory. 2019; 165:106945. https://doi.org/10.1016/j.nlm.2018.10.001 PMID: 30321651
3. Mahone EM, Warschausky S, Zabel TA. Introduction to the JINS special issue: Neurodevelopmental disorders. Journal of the International Neuropsychological Society. 2018; 24(9):893–895. https://doi.org/10.1017/S1355617718000905
4. Thapar A, Cooper M, Rutter M. Neurodevelopmental disorders. The Lancet Psychiatry. 2017; 4 (4):339–346. https://doi.org/10.1016/S2215-0366(16)30376-5 PMID: 27979720
5. Lord C, Elsabbagh M, Baird G, Veenstra-Vanderweele J. Autism spectrum disorder. The lancet. 2018; 392(10146):508–520. https://doi.org/10.1016/S0140-6736(18)31129-2
6. Posar A, Visconti P. Autism Spectrum Disorder in 2023: A Challenge Still Open. Turkish Archives of Pediatrics. 2023;. https://doi.org/10.5152/TurkArchPediatr.2023.23194 PMID: 37850666
7. Masi A, DeMayo MM, Glozier N, Guastella AJ. An overview of autism spectrum disorder, heterogeneity and treatment options. Neuroscience bulletin. 2017; 33:183–193. https://doi.org/10.1007/s12264-017-0100-y PMID: 28213805
8. Constantino JN, Charman T. Diagnosis of autism spectrum disorder: reconciling the syndrome, its diverse origins, and variation in expression. The Lancet Neurology. 2016; 15(3):279–291. https://doi.org/10.1016/S1474-4422(15)00151-9 PMID: 26497771
9. Lord C, Charman T, Havdahl A, Carbone P, Anagnostou E, Boyd B, et al. The Lancet Commission on the future of care and clinical research in autism. The Lancet. 2022; 399(10321):271–334. https://doi.org/10.1016/S0140-6736(21)01541-5 PMID: 34883054
10. Lord C, Cook EH, Leventhal BL, Amaral DG. Autism spectrum disorders. Neuron. 2000; 28(2):355–363. https://doi.org/10.1016/S0896-6273(00)00115-X PMID: 11144346
11. Du Y, Fu Z, Calhoun VD. Classification and prediction of brain disorders using functional connectivity: promising but challenging. Frontiers in neuroscience. 2018; 12:525. https://doi.org/10.3389/fnins.2018.00525 PMID: 30127711
12. Salari N, Ghasemi H, Abdoli N, Rahmani A, Shiri MH, Hashemian AH, et al. The global prevalence of ADHD in children and adolescents: a systematic review and meta-analysis. Italian Journal of Pediatrics. 2023; 49(1):48. https://doi.org/10.1186/s13052-023-01456-1 PMID: 37081447
13. Arbabshirani MR, Plis S, Sui J, Calhoun VD. Single subject prediction of brain disorders in neuroimaging: Promises and pitfalls. Neuroimage. 2017; 145:137–165. https://doi.org/10.1016/j.neuroimage.2016.02.079 PMID: 27012503
14. Rommelse NN, Geurts HM, Franke B, Buitelaar JK, Hartman CA. A review on cognitive and brain endophenotypes that may be common in autism spectrum disorder and attention-deficit/hyperactivity disorder and facilitate the search for pleiotropic genes. Neuroscience & Biobehavioral Reviews. 2011; 35(6):1363–1396. https://doi.org/10.1016/j.neubiorev.2011.02.015 PMID: 21382410
15. Simonoff E, Pickles A, Charman T, Chandler S, Loucas T, Baird G. Psychiatric disorders in children with autism spectrum disorders: prevalence, comorbidity, and associated factors in a population-derived sample. Journal of the American Academy of Child & Adolescent Psychiatry. 2008; 47(8):921–929. https://doi.org/10.1097/CHI.0b013e318179964f
16. Uddin M, Wang Y, Woodbury-Smith M. Artificial intelligence for precision medicine in neurodevelopmental disorders. NPJ digital medicine. 2019; 2(1):112. https://doi.org/10.1038/s41746-019-0191-0 PMID: 31799421
17. Duda M, Ma R, Haber N, Wall D. Use of machine learning for behavioral distinction of autism and ADHD. Translational psychiatry. 2016; 6(2):e732–e732. https://doi.org/10.1038/tp.2015.221 PMID: 26859815

18. Duda M, Haber N, Daniels J, Wall D. Crowdsourced validation of a machine-learning classification system for autism and ADHD. Translational psychiatry. 2017; 7(5):e1133–e1133. https://doi.org/10.1038/tp.2017.86 PMID: 28509905

19. Nogay HS, Adeli H. Machine learning (ML) for the diagnosis of autism spectrum disorder (ASD) using brain imaging. Reviews in the Neurosciences. 2020; 31(8):825–841. https://doi.org/10.1515/revneuro-2020-0043

20. Rashid B, Calhoun V. Towards a brain-based predictome of mental illness. Human brain mapping. 2020; 41(12):3468–3535. https://doi.org/10.1002/hbm.25013 PMID: 32374075

21. Harikumar A, Evans DW, Dougherty CC, Carpenter KL, Michael AM. A review of the default mode network in autism spectrum disorders and attention deficit hyperactivity disorder. Brain connectivity. 2021; 11(4):253–263. https://doi.org/10.1089/brain.2020.0865 PMID: 33403915

22. Eslami T, Almuqhim F, Raiker JS, Saeed F. Machine learning methods for diagnosing autism spectrum disorder and attention-deficit/hyperactivity disorder using functional and structural MRI: A survey. Frontiers in neuroinformatics. 2021; p. 62. https://doi.org/10.3389/fninf.2020.575999 PMID: 33551784

23. Moridian P, Ghassemi N, Jafari M, Salloum-Asfar S, Sadeghi D, Khodatars M, et al. Automatic autism spectrum disorder detection using artificial intelligence methods with MRI neuroimaging: A review. Frontiers in Molecular Neuroscience. 2022; 15:999605. https://doi.org/10.3389/fnmol.2022.999605 PMID: 36267703

24. Washington P, Wall DP. A Review of and Roadmap for Data Science and Machine Learning for the Neuropsychiatric Phenotype of Autism. Annual Review of Biomedical Data Science. 2023; 6. https://doi.org/10.1146/annurev-biodatasci-020722-125454 PMID: 37137169

25. Wolff N, Kohls G, Mack JT, Vahid A, Elster EM, Stroth S, et al. A data driven machine learning approach to differentiate between autism spectrum disorder and attention-deficit/hyperactivity disorder based on the best-practice diagnostic instruments for autism. Scientific Reports. 2022; 12(1):18744. https://doi.org/10.1038/s41598-022-21719-x PMID: 36335178

26. Lim L, Marquand A, Cubillo AA, Smith AB, Chantiluke K, Simmons A, et al. Disorder-specific predictive classification of adolescents with attention deficit hyperactivity disorder (ADHD) relative to autism using structural magnetic resonance imaging. PloS one. 2013; 8(5):e63660. https://doi.org/10.1371/journal.pone.0063660 PMID: 23696841

27. Di Martino A, Zuo XN, Kelly C, Grzadzinski R, Mennes M, Schvarcz A, et al. Shared and distinct intrinsic functional network centrality in autism and attention-deficit/hyperactivity disorder. Biological psychiatry. 2013; 74(8):623–632. https://doi.org/10.1016/j.biopsych.2013.02.011 PMID: 23541632

28. Bethlehem RA, Romero-Garcia R, Mak E, Bullmore E, Baron-Cohen S. Structural covariance networks in children with autism or ADHD. Cerebral Cortex. 2017; 27(8):4267–4276. https://doi.org/10.1093/cercor/bhx135 PMID: 28633299

29. Shephard E, Tye C, Ashwood KL, Azadi B, Johnson MH, Charman T, et al. Oscillatory neural networks underlying resting-state, attentional control and social cognition task conditions in children with ASD, ADHD and ASD+ ADHD. Cortex. 2019; 117:96–110. https://doi.org/10.1016/j.cortex.2019.03.005 PMID: 30954695

30. Bathelt J, Caan M, Geurts H. More similarities than differences between ADHD and ASD in functional brain connectivity. 2020;.

31. Rudin C. Stop explaining black box machine learning models for high stakes decisions and use interpretable models instead. Nature machine intelligence. 2019; 1(5):206–215. https://doi.org/10.1038/s42256-019-0048-x PMID: 35603010

32. Althubaiti A. Information bias in health research: definition, pitfalls, and adjustment methods. Journal of multidisciplinary healthcare. 2016; p. 211–217. https://doi.org/10.2147/JMDH.S104807 PMID: 27217764

33. Alves CL, Pineda AM, Roster K, Thielemann C, Rodrigues FA. EEG functional connectivity and deep learning for automatic diagnosis of brain disorders: Alzheimer's disease and schizophrenia. Journal of Physics: Complexity. 2022; 3(2):025001.

34. Alves CL, Toutain TGdO, de Carvalho Aguiar P, Pineda AM, Roster K, Thielemann C, et al. Diagnosis of autism spectrum disorder based on functional brain networks and machine learning. Scientific Reports. 2023; 13(1):8072. https://doi.org/10.1038/s41598-023-34650-6 PMID: 37202411

35. Alves CL, Toutain TGdO, Porto JAM, Aguiar PMdC, Pineda A, Rodrigues FA, et al. Analysis of functional connectivity using machine learning and deep learning in different data modalities from individuals with schizophrenia. Journal of Neural Engineering. 2023;. https://doi.org/10.1088/1741-2552/acf734 PMID: 37673060

36. Alves CL, Cury RG, Roster K, Pineda AM, Rodrigues FA, Thielemann C, et al. Application of machine learning and complex network measures to an EEG dataset from ayahuasca experiments. Plos one. 2022; 17(12):e0277257. https://doi.org/10.1371/journal.pone.0277257 PMID: 36525422

37. Alves C, Wissel L, Capetian P, Thielemann C. P 55 Functional connectivity and convolutional neural networks for automatic classification of EEG data. Clinical Neurophysiology. 2022; 137:e47. https://doi.org/10.1016/j.clinph.2022.01.086

38. Lundberg SM, Lee SI. A unified approach to interpreting model predictions. In: Proceedings of the 31st international conference on neural information processing systems; 2017. p. 4768–4777.

39. Al-Beltagi M. Autism medical comorbidities. World journal of clinical pediatrics. 2021; 10(3):15. https://doi.org/10.5409/wjcp.v10.i3.15 PMID: 33972922

40. Bellec P, Chu C, Chouinard-Decorte F, Benhajali Y, Margulies DS, Craddock RC. The neuro bureau ADHD-200 preprocessed repository. Neuroimage. 2017; 144:275–286. https://doi.org/10.1016/j.neuroimage.2016.06.034 PMID: 27423255

41. Abraham A, Pedregosa F, Eickenberg M, Gervais P, Mueller A, Kossaifi J, et al. Machine learning for neuroimaging with scikit-learn. Frontiers in neuroinformatics. 2014; 8:14. https://doi.org/10.3389/fninf.2014.00014 PMID: 24600388

42. Lawrence RM, Bridgeford EW, Myers PE, Arvapalli GC, Ramachandran SC, Pisner DA, et al. Standardizing human brain parcellations. Scientific data. 2021; 8(1):78. https://doi.org/10.1038/s41597-021-00849-3 PMID: 33686079

43. Rubin TN, Koyejo O, Gorgolewski KJ, Jones MN, Poldrack RA, Yarkoni T. Decoding brain activity using a large-scale probabilistic functional-anatomical atlas of human cognition. PLoS computational biology. 2017; 13(10):e1005649. https://doi.org/10.1371/journal.pcbi.1005649 PMID: 29059185

44. Walsh J, Othmani A, Jain M, Dev S. Using U-Net network for efficient brain tumor segmentation in MRI images. Healthcare Analytics. 2022; 2:100098. https://doi.org/10.1016/j.health.2022.100098

45. Subah FZ, Deb K, Dhar PK, Koshiba T. A deep learning approach to predict autism spectrum disorder using multisite resting-state fMRI. Applied Sciences. 2021; 11(8):3636. https://doi.org/10.3390/app11083636

46. Bellec P, Rosa-Neto P, Lyttelton OC, Benali H, Evans AC. Multi-level bootstrap analysis of stable clusters in resting-state fMRI. Neuroimage. 2010; 51(3):1126–1139. https://doi.org/10.1016/j.neuroimage.2010.02.082 PMID: 20226257

47. Yang X, Zhang N, Schrader P. A study of brain networks for autism spectrum disorder classification using resting-state functional connectivity. Machine Learning with Applications. 2022; 8:100290. https://doi.org/10.1016/j.mlwa.2022.100290

48. Schreiber T. Measuring information transfer. Physical review letters. 2000; 85(2):461. https://doi.org/10.1103/PhysRevLett.85.461 PMID: 10991308

49. Lungarella M, Pitti A, Kuniyoshi Y. Information transfer at multiple scales. Physical Review E. 2007; 76(5):056117. https://doi.org/10.1103/PhysRevE.76.056117 PMID: 18233728

50. Shovon MHI, Nandagopal N, Vijayalakshmi R, Du JT, Cocks B. Directed connectivity analysis of functional brain networks during cognitive activity using transfer entropy. Neural Processing Letters. 2017; 45:807–824. https://doi.org/10.1007/s11063-016-9506-1

51. Wibral M, Rahm B, Rieder M, Lindner M, Vicente R, Kaiser J. Transfer entropy in magnetoencephalographic data: quantifying information flow in cortical and cerebellar networks. Progress in biophysics and molecular biology. 2011; 105(1-2):80–97. https://doi.org/10.1016/j.pbiomolbio.2010.11.006 PMID: 21115029

52. Mao X, Shang P. Transfer entropy between multivariate time series. Communications in Nonlinear Science and Numerical Simulation. 2017; 47:338–347. https://doi.org/10.1016/j.cnsns.2016.12.008

53. Orlandi JG, Stetter O, Soriano J, Geisel T, Battaglia D. Transfer entropy reconstruction and labeling of neuronal connections from simulated calcium imaging. PloS one. 2014; 9(6):e98842. https://doi.org/10.1371/journal.pone.0098842 PMID: 24905689

54. Gunaratne C, Ray SK, Lourenço Alves C, Waldl M. Exogenous Shocks Lead to Increased Responsiveness and Shifts in Sentimental Resilience in Online Discussions. In: Proceedings of the 2019 International Conference of The Computational Social Science Society of the Americas. Springer; 2021. p. 57–71.

55. Goetze F, Lai PY, Chan C. Identifying excitatory and inhibitory synapses in neuronal networks from dynamics using Transfer Entropy. BMC Neuroscience. 2015; 16:1–1. https://doi.org/10.1186/1471-2202-16-S1-P30

56. Bellec P, Carbonnell F, Perlbarg V, Lepage C, Lyttelton O, Fonov V, et al. A neuroimaging analyses kit for Matlab and octave. In: Human Brain Mapping HBM 2011 17th Annual Meeting of the Organization on Human Brain Mapping, Quebec City, Canada, June 26-30, 2011. Organization on Human Brain Mapping; 2011. p. 1–5.

57. Khodatars M, Shoeibi A, Sadeghi D, Ghaasemi N, Jafari M, Moridian P, et al. Deep learning for neuroimaging-based diagnosis and rehabilitation of autism spectrum disorder: a review. Computers in

biology and medicine. 2021; 139:104949. https://doi.org/10.1016/j.compbiomed.2021.104949 PMID: 34737139

58. Bottou L, Lin CJ. Support vector machine solvers. Large scale kernel machines. 2007; 3(1):301–320.
59. Friedman N, Geiger D, Goldszmidt M. Bayesian network classifiers. Machine learning. 1997; 29 (2):131–163. https://doi.org/10.1023/A:1007465528199
60. Hinton G, Rumelhart D, Williams R. Learning internal representations by error propagation. Parallel distributed processing. 1986; 1:318–362.
61. Hochreiter S, Schmidhuber J. Long short-term memory. Neural computation. 1997; 9(8):1735–1780. https://doi.org/10.1162/neco.1997.9.8.1735 PMID: 9377276
62. Berrar D. Cross-Validation.; 2019.
63. Bengio Y, Grandvalet Y. No unbiased estimator of the variance of k-fold cross-validation. Journal of machine learning research. 2004; 5(Sep):1089–1105.
64. Shah AA, Khan YD. Identification of 4-carboxyglutamate residue sites based on position based statistical feature and multiple classification. Scientific Reports. 2020; 10(1):1–10. https://doi.org/10.1038/s41598-020-73107-y PMID: 33037248
65. Kawamoto T, Kabashima Y. Cross-validation estimate of the number of clusters in a network. Scientific reports. 2017; 7(1):1–17. https://doi.org/10.1038/s41598-017-03623-x PMID: 28607441
66. Chan J, Rea T, Gollakota S, Sunshine JE. Contactless cardiac arrest detection using smart devices. NPJ digital medicine. 2019; 2(1):1–8. https://doi.org/10.1038/s41746-019-0128-7 PMID: 31304398
67. Kuhn M, Johnson K, et al. Applied predictive modeling. vol. 26. Springer; 2013.
68. Brownlee J. How to choose a feature selection method for machine learning. Machine Learning Mastery. 2019;10.
69. Sato M, Morimoto K, Kajihara S, Tateishi R, Shiina S, Koike K, et al. Machine-learning approach for the development of a novel predictive model for the diagnosis of hepatocellular carcinoma. Scientific reports. 2019; 9(1):1–7. https://doi.org/10.1038/s41598-019-44022-8 PMID: 31147560
70. Zhong Z, Yuan X, Liu S, Yang Y, Liu F. Machine learning prediction models for prognosis of critically ill patients after open-heart surgery. Scientific Reports. 2021; 11(1):1–10. https://doi.org/10.1038/s41598-021-83020-7 PMID: 33564090
71. Arcadu F, Benmansour F, Maunz A, Willis J, Haskova Z, Prunotto M. Author Correction: Deep learning algorithm predicts diabetic retinopathy progression in individual patients. NPJ digital medicine. 2020; 3 (1):1–6. https://doi.org/10.1038/s41746-020-00365-5 PMID: 33293570
72. Krittanawong C, Virk HUH, Kumar A, Aydar M, Wang Z, Stewart MP, et al. Machine learning and deep learning to predict mortality in patients with spontaneous coronary artery dissection. Scientific reports. 2021; 11(1):1–10. https://doi.org/10.1038/s41598-021-88172-0 PMID: 33903608
73. Rashidi HH, Sen S, Palmieri TL, Blackmon T, Wajda J, Tran NK. Early recognition of burn-and trauma-related acute kidney injury: a pilot comparison of machine learning techniques. Scientific reports. 2020; 10(1):1–9. https://doi.org/10.1038/s41598-019-57083-6 PMID: 31937795
74. Srivastava N, Hinton G, Krizhevsky A, Sutskever I, Salakhutdinov R. Dropout: a simple way to prevent neural networks from overfitting. The journal of machine learning research. 2014; 15(1):1929–1958.
75. Poernomo A, Kang DK. Biased dropout and crossmap dropout: learning towards effective dropout regularization in convolutional neural network. Neural networks. 2018; 104:60–67. https://doi.org/10.1016/j.neunet.2018.03.016 PMID: 29715684
76. Lemay A, Hoebel K, Bridge CP, Befano B, De Sanjosé S, Egemen D, et al. Improving the repeatability of deep learning models with Monte Carlo dropout. npj Digital Medicine. 2022; 5(1):174. https://doi.org/10.1038/s41746-022-00709-3 PMID: 36400939
77. Li X, Dou Q, Chen H, Fu CW, Qi X, Belav'y DL, et al. 3D multi-scale FCN with random modality voxel dropout learning for intervertebral disc localization and segmentation from multi-modality MR images. Medical image analysis. 2018; 45:41–54. https://doi.org/10.1016/j.media.2018.01.004 PMID: 29414435
78. Bisong E, Bisong E. Introduction to Scikit-learn. Building Machine Learning and Deep Learning Models on Google Cloud Platform: A Comprehensive Guide for Beginners. 2019; p. 215–229.
79. Raschka S. Python machine learning. Packt publishing ltd; 2015.
80. Raschka S, Mirjalili V. Python machine learning: Machine learning and deep learning with Python, scikit-learn, and TensorFlow 2. Packt Publishing Ltd; 2019.
81. Géron A. Hands-on machine learning with Scikit-Learn, Keras, and TensorFlow. " O'Reilly Media, Inc."; 2022.

82. Mincholé A, Rodriguez B. Artificial intelligence for the electrocardiogram. Nature medicine. 2019; 25 (1):22–23. https://doi.org/10.1038/s41591-018-0306-1 PMID: 30617324

83. Tolkach Y, Dohmgörgen T, Toma M, Kristiansen G. High-accuracy prostate cancer pathology using deep learning. Nature Machine Intelligence. 2020; 2(7):411–418. https://doi.org/10.1038/s42256-020-0200-7

84. Dukart J, Weis S, Genon S, Eickhoff SB. Towards increasing the clinical applicability of machine learning biomarkers in psychiatry. Nature Human Behaviour. 2021; 5(4):431–432. https://doi.org/10.1038/s41562-021-01085-w PMID: 33820977

85. Li RC, Asch SM, Shah NH. Developing a delivery science for artificial intelligence in healthcare. NPJ digital medicine. 2020; 3(1):1–3. https://doi.org/10.1038/s41746-020-00318-y PMID: 32885053

86. Park Y, Kellis M. Deep learning for regulatory genomics. Nature biotechnology. 2015; 33(8):825–826. https://doi.org/10.1038/nbt.3313 PMID: 26252139

87. Ito Y, Unagami M, Yamabe F, Mitsui Y, Nakajima K, Nagao K, et al. A method for utilizing automated machine learning for histopathological classification of testis based on Johnsen scores. Scientific reports. 2021; 11(1):1–11. https://doi.org/10.1038/s41598-021-89369-z PMID: 33967273

88. Kim J, Lee J, Park E, Han J. A deep learning model for detecting mental illness from user content on social media. Scientific reports. 2020; 10(1):1–6. https://doi.org/10.1038/s41598-020-68764-y PMID: 32678250

89. Li Y, Nowak CM, Pham U, Nguyen K, Bleris L. Cell morphology-based machine learning models for human cell state classification. NPJ systems biology and applications. 2021; 7(1):1–9. https://doi.org/10.1038/s41540-021-00180-y PMID: 34039992

90. Yu X, Pang W, Xu Q, Liang M. Mammographic image classification with deep fusion learning. Scientific Reports. 2020; 10(1):1–11. https://doi.org/10.1038/s41598-020-71431-x PMID: 32873872

91. Bracher-Smith M, Crawford K, Escott-Price V. Machine learning for genetic prediction of psychiatric disorders: a systematic review. Molecular Psychiatry. 2021; 26(1):70–79. https://doi.org/10.1038/s41380-020-0825-2 PMID: 32591634

92. Patel D, Kher V, Desai B, Lei X, Cen S, Nanda N, et al. Machine learning based predictors for COVID-19 disease severity. Scientific Reports. 2021; 11(1):1–7. https://doi.org/10.1038/s41598-021-83967-7 PMID: 33633145

93. Albert R, Barabási AL. Statistical mechanics of complex networks. Reviews of modern physics. 2002; 74(1):47. https://doi.org/10.1103/RevModPhys.74.47

94. Freeman LC. A set of measures of centrality based on betweenness. Sociometry. 1977; p. 35–41. https://doi.org/10.2307/3033543

95. Freeman LC. Centrality in social networks conceptual clarification. Social networks. 1978; 1(3):215–239. https://doi.org/10.1016/0378-8733(78)90021-7

96. Albert R, Jeong H, Barabási AL. Diameter of the world-wide web. nature. 1999; 401(6749):130–131. https://doi.org/10.1038/43601

97. Newman ME. The structure and function of complex networks. SIAM review. 2003; 45(2):167–256. https://doi.org/10.1137/S003614450342480

98. Newman ME. Assortative mixing in networks. Physical review letters. 2002; 89(20):208701. https://doi.org/10.1103/PhysRevLett.89.208701 PMID: 12443515

99. Kleinberg JM. Hubs, authorities, and communities. ACM computing surveys (CSUR). 1999; 31 (4es):5–es. https://doi.org/10.1145/345966.345982

100. Hage P, Harary F. Eccentricity and centrality in networks. Social networks. 1995; 17(1):57–63. https://doi.org/10.1016/0378-8733(94)00248-9

101. Bonacich P. Power and centrality: A family of measures. American journal of sociology. 1987; 92 (5):1170–1182. https://doi.org/10.1086/228631

102. Eppstein D, Paterson MS, Yao FF. On nearest-neighbor graphs. Discrete & Computational Geometry. 1997; 17(3):263–282. https://doi.org/10.1007/PL00009293

103. Doyle J, Graver J. Mean distance in a graph. Discrete Mathematics. 1977; 17(2):147–154. https://doi.org/10.1016/0012-365X(77)90144-3

104. Dehmer M, Mowshowitz A. A history of graph entropy measures. Information Sciences. 2011; 181 (1):57–78. https://doi.org/10.1016/j.ins.2010.08.041

105. Watts DJ, Strogatz SH. Collective dynamics of 'small-world' networks. Nature. 1998; 393(6684):440–442. https://doi.org/10.1038/30918 PMID: 9623998

106. Newman ME, Watts DJ, Strogatz SH. Random graph models of social networks. Proceedings of the National Academy of Sciences. 2002; 99(suppl 1):2566–2572. https://doi.org/10.1073/pnas.012582999 PMID: 11875211

107. Snijders TA. The degree variance: an index of graph heterogeneity. Social networks. 1981; 3(3):163–174. https://doi.org/10.1016/0378-8733(81)90014-9

108. Seidman SB. Network structure and minimum degree. Social networks. 1983; 5(3):269–287. https://doi.org/10.1016/0378-8733(83)90028-X

109. Newman M. Networks: an introduction. Oxford university press; 2010.

110. Anderson BS, Butts C, Carley K. The interaction of size and density with graph-level indices. Social networks. 1999; 21(3):239–267. https://doi.org/10.1016/S0378-8733(99)00011-8

111. Latora V, Marchiori M. Economic small-world behavior in weighted networks. The European Physical Journal B-Condensed Matter and Complex Systems. 2003; 32(2):249–263. https://doi.org/10.1140/epjb/e2003-00095-5

112. Newman ME. Communities, modules and large-scale structure in networks. Nature physics. 2012; 8 (1):25–31. https://doi.org/10.1038/nphys2162

113. Kim J, Lee JG. Community detection in multi-layer graphs: A survey. ACM SIGMOD Record. 2015; 44 (3):37–48. https://doi.org/10.1145/2854006.2854013

114. Zhao X, Liang J, Wang J. A community detection algorithm based on graph compression for large-scale social networks. Information Sciences. 2021; 551:358–372. https://doi.org/10.1016/j.ins.2020.10.057

115. Clauset A, Newman ME, Moore C. Finding community structure in very large networks. Physical review E. 2004; 70(6):066111. https://doi.org/10.1103/PhysRevE.70.066111 PMID: 15697438

116. Rosvall M, Axelsson D, Bergstrom CT. The map equation. The European Physical Journal Special Topics. 2009; 178(1):13–23. https://doi.org/10.1140/epjst/e2010-01179-1

117. Newman ME. Finding community structure in networks using the eigenvectors of matrices. Physical review E. 2006; 74(3):036104. https://doi.org/10.1103/PhysRevE.74.036104 PMID: 17025705

118. Raghavan UN, Albert R, Kumara S. Near linear time algorithm to detect community structures in large-scale networks. Physical review E. 2007; 76(3):036106. https://doi.org/10.1103/PhysRevE.76.036106 PMID: 17930305

119. Girvan M, Newman ME. Community structure in social and biological networks. Proceedings of the national academy of sciences. 2002; 99(12):7821–7826. https://doi.org/10.1073/pnas.122653799 PMID: 12060727

120. Reichardt J, Bornholdt S. Statistical mechanics of community detection. Physical review E. 2006; 74 (1):016110. https://doi.org/10.1103/PhysRevE.74.016110 PMID: 16907154

121. Blondel VD, Guillaume JL, Lambiotte R, Lefebvre E. Fast unfolding of communities in large networks. Journal of statistical mechanics: theory and experiment. 2008; 2008(10):P10008. https://doi.org/10.1088/1742-5468/2008/10/P10008

122. Barrett AB, Seth AK. Practical Measures of Integrated Information for Time-Series Data. PLOS Computational Biology. 2011; 7(1):1–18. https://doi.org/10.1371/journal.pcbi.1001052 PMID: 21283779

123. Mediano PAM, Seth AK, Barrett AB. Measuring Integrated Information: Comparison of Candidate Measures in Theory and Simulation. Entropy (Basel). 2018; 21(1):17. https://doi.org/10.3390/e21010017 PMID: 33266733

124. Park HJ, Friston K. Structural and functional brain networks: from connections to cognition. Science. 2013; 342(6158):1238411. https://doi.org/10.1126/science.1238411 PMID: 24179229

125. Sporns O. The non-random brain: efficiency, economy, and complex dynamics. Frontiers in computational neuroscience. 2011; 5:5. https://doi.org/10.3389/fncom.2011.00005 PMID: 21369354

126. Sporns O. Structure and function of complex brain networks. Dialogues in clinical neuroscience. 2022;.

127. Avena-Koenigsberger A, Misic B, Sporns O. Communication dynamics in complex brain networks. Nature reviews neuroscience. 2018; 19(1):17–33. https://doi.org/10.1038/nrn.2017.149

128. Tononi G, Sporns O, Edelman G. Measures of degeneracy and redundancy in biological networks. Proceedings of the National Academy of Sciences of the United States of America. 1999; 96:3257–62. https://doi.org/10.1073/pnas.96.6.3257 PMID: 10077671

129. Hoel EP, Albantakis L, Tononi G. Quantifying causal emergence shows that macro can beat micro. Proceedings of the National Academy of Sciences. 2013; 110(49):19790–19795. https://doi.org/10.1073/pnas.1314922110 PMID: 24248356

130. Hoel EP. When the Map Is Better Than the Territory. Entropy. 2017; 19(5). https://doi.org/10.3390/e19050188

131. Klein B, Hoel E. The Emergence of Informative Higher Scales in Complex Networks. Complexity. 2020; 2020:1–12. https://doi.org/10.1155/2020/8932526

132. Pearson K. LIII. On lines and planes of closest fit to systems of points in space. The London, Edinburgh, and Dublin philosophical magazine and journal of science. 1901; 2(11):559–572. https://doi.org/10.1080/14786440109462720

133. Ayesha S, Hanif MK, Talib R. Overview and comparative study of dimensionality reduction techniques for high dimensional data. Information Fusion. 2020; 59:44–58. https://doi.org/10.1016/j.inffus.2020.01.005

134. Dunn OJ. Multiple comparisons among means. Journal of the American statistical association. 1961; 56(293):52–64. https://doi.org/10.1080/01621459.1961.10482090

135. Kruskal WH, Wallis WA. Use of ranks in one-criterion variance analysis. Journal of the American statistical Association. 1952; 47(260):583–621. https://doi.org/10.1080/01621459.1952.10483441

136. Mann HB, Whitney DR. On a test of whether one of two random variables is stochastically larger than the other. The annals of mathematical statistics. 1947; p. 50–60. https://doi.org/10.1214/aoms/1177730491

137. Wilcoxon F. Probability tables for individual comparisons by ranking methods. Biometrics. 1947; 3 (3):119–122. https://doi.org/10.2307/3001946

138. Andrade C. Multiple testing and protection against a type 1 (false positive) error using the Bonferroni and Hochberg corrections. Indian journal of psychological medicine. 2019; 41(1):99–100. https://doi.org/10.4103/IJPSYM.IJPSYM_499_18 PMID: 30783320

139. Armstrong RA. When to use the Bonferroni correction. Ophthalmic and Physiological Optics. 2014; 34 (5):502–508. https://doi.org/10.1111/opo.12131 PMID: 24697967

140. Tan L, Guo X, Ren S, Epstein JN, Lu LJ. A computational model for the automatic diagnosis of attention deficit hyperactivity disorder based on functional brain volume. Frontiers in computational neuroscience. 2017; 11:75. https://doi.org/10.3389/fncom.2017.00075 PMID: 28943846

141. Mashrur FR, Rahman KM, Miya MTI, Vaidyanathan R, Anwar SF, Sarker F, et al. BCI-Based Consumers' Choice Prediction From EEG Signals: An Intelligent Neuromarketing Framework. Frontiers in human neuroscience. 2022; 16:861270. https://doi.org/10.3389/fnhum.2022.861270 PMID: 35693537

142. Richhariya B, Tanveer M, Rashid AH, Initiative ADN, et al. Diagnosis of Alzheimer's disease using universum support vector machine based recursive feature elimination (USVM-RFE). Biomedical Signal Processing and Control. 2020; 59:101903. https://doi.org/10.1016/j.bspc.2020.101903

143. Mijalkov M, Kakaei E, Pereira JB, Westman E, Volpe G, Initiative ADN. BRAPH: a graph theory software for the analysis of brain connectivity. PloS one. 2017; 12(8):e0178798. https://doi.org/10.1371/journal.pone.0178798 PMID: 28763447

144. Lehne M, Rohrmeier M, Koelsch S. Tension-related activity in the orbitofrontal cortex and amygdala: an fMRI study with music. Social cognitive and affective neuroscience. 2014; 9(10):1515–1523. https://doi.org/10.1093/scan/nst141 PMID: 23974947

145. Nickel K, Tebartz van Elst L, Manko J, Unterrainer J, Rauh R, Klein C, et al. Inferior frontal gyrus volume loss distinguishes between autism and (comorbid) attention-deficit/hyperactivity disorder—a FreeSurfer analysis in children. Frontiers in psychiatry. 2018; 9:521. https://doi.org/10.3389/fpsyt.2018.00521 PMID: 30405459

146. Murdoch BE. The cerebellum and language: historical perspective and review. Cortex. 2010; 46 (7):858–868. https://doi.org/10.1016/j.cortex.2009.07.018 PMID: 19828143

147. Timmann D, Daum I. Cerebellar contributions to cognitive functions: a progress report after two decades of research. The cerebellum. 2007; 6:159–162. https://doi.org/10.1080/14734220701496448 PMID: 17786810

148. Krain AL, Castellanos FX. Brain development and ADHD. Clinical psychology review. 2006; 26 (4):433–444. https://doi.org/10.1016/j.cpr.2006.01.005 PMID: 16480802

149. Curatolo P, D'Agati E, Moavero R. The neurobiological basis of ADHD. Italian journal of pediatrics. 2010; 36(1):1–7. https://doi.org/10.1186/1824-7288-36-79 PMID: 21176172

150. Ardila A, Bernal B, Rosselli M, et al. Language and visual perception associations: meta-analytic connectivity modeling of Brodmann area 37. Behavioural neurology. 2015; 2015. https://doi.org/10.1155/2015/565871 PMID: 25648869

151. Bernard F, Lemée JM, Ter Minassian A, Menei P. Right hemisphere cognitive functions: from clinical and anatomic bases to brain mapping during awake craniotomy part I: clinical and functional anatomy. World neurosurgery. 2018; 118:348–359. https://doi.org/10.1016/j.wneu.2018.05.024 PMID: 29763748

152. Seghier ML. The angular gyrus: multiple functions and multiple subdivisions. The Neuroscientist. 2013; 19(1):43–61. https://doi.org/10.1177/1073858412440596 PMID: 22547530

153. Tamm L, Menon V, Reiss AL. Parietal attentional system aberrations during target detection in adolescents with attention deficit hyperactivity disorder: event-related fMRI evidence. American Journal of Psychiatry. 2006; 163(6):1033–1043. https://doi.org/10.1176/ajp.2006.163.6.1033 PMID: 16741204

154. Fornito A, Zalesky A, Bullmore E. Fundamentals of brain network analysis. Academic press; 2016.

155. Sporns O. The human connectome: a complex network. Annals of the new York Academy of Sciences. 2011; 1224(1):109–125. https://doi.org/10.1111/j.1749-6632.2010.05888.x PMID: 21251014

156. Rudie JD, Brown J, Beck-Pancer D, Hernandez L, Dennis E, Thompson P, et al. Altered functional and structural brain network organization in autism. NeuroImage: clinical. 2013; 2:79–94. https://doi.org/10.1016/j.nicl.2012.11.006

157. Keown CL, Datko MC, Chen CP, Maximo JO, Jahedi A, Müller RA. Network organization is globally atypical in autism: a graph theory study of intrinsic functional connectivity. Biological Psychiatry: Cognitive Neuroscience and Neuroimaging. 2017; 2(1):66–75. https://doi.org/10.1016/j.bpsc.2016.07.008 PMID: 28944305

158. Rubinov M, Sporns O. Complex network measures of brain connectivity: Uses and interpretations. NeuroImage. 2010; 52(3):1059–1069. https://doi.org/10.1016/j.neuroimage.2009.10.003 PMID: 19819337

159. Rimland B. Infantile Autism. East Norwalk, CT, US: Appleton-Century-Crofts; 1964.

160. de Marchena AB, Eigsti IM, Yerys BE. Brief Report: Generalization Weaknesses in Verbally Fluent Children and Adolescents with Autism Spectrum Disorder. J Autism Dev Disord. 2015; 45(10):3370–3376. https://doi.org/10.1007/s10803-015-2478-6 PMID: 26031922

161. Nguyen DC, Pham QV, Pathirana PN, Ding M, Seneviratne A, Lin Z, et al. Federated learning for smart healthcare: A survey. ACM Computing Surveys (Csur). 2022; 55(3):1–37. https://doi.org/10.1145/3501296

162. Guan H, Yap PT, Bozoki A, Liu M. Federated learning for medical image analysis: A survey. Pattern Recognition. 2024; p. 110424. https://doi.org/10.1016/j.patcog.2024.110424 PMID: 38559674

163. Teo ZL, Jin L, Li S, Miao D, Zhang X, Ng WY, et al. Federated machine learning in healthcare: A systematic review on clinical applications and technical architecture. Cell Reports Medicine. 2024;. https://doi.org/10.1016/j.xcrm.2024.101481

164. Soltan AA, Thakur A, Yang J, Chauhan A, D'Cruz LG, Dickson P, et al. A scalable federated learning solution for secondary care using low-cost microcomputing: privacy-preserving development and evaluation of a COVID-19 screening test in UK hospitals. The Lancet Digital Health. 2024; 6(2):e93–e104. https://doi.org/10.1016/S2589-7500(23)00226-1 PMID: 38278619

165. Crowson MG, Moukheiber D, Arévalo AR, Lam BD, Mantena S, Rana A, et al. A systematic review of federated learning applications for biomedical data. PLOS Digital Health. 2022; 1(5):e0000033. https://doi.org/10.1371/journal.pdig.0000033 PMID: 36812504

166. Sadilek A, Liu L, Nguyen D, Kamruzzaman M, Serghiou S, Rader B, et al. Privacy-first health research with federated learning. NPJ digital medicine. 2021; 4(1):132. https://doi.org/10.1038/s41746-021-00489-2 PMID: 34493770

167. Zhang C, Meng X, Liu Q, Wu S, Wang L, Ning H. FedBrain: A robust multi-site brain network analysis framework based on federated learning for brain disease diagnosis. Neurocomputing. 2023; 559:126791. https://doi.org/10.1016/j.neucom.2023.126791

CHAPTER

5

REDEFINING AUTISM SUBTYPES

Redefining autism subtypes: A machine learning approach leveraging topological data analysis, network measures and hemispheric lateralization. Caroline L. Alves, Loriz Francisco Sallum, Francisco Aparecido Rodrigues, Thaise G. L. de O. Toutain, Joel Augusto Moura Porto, Patricia Maria de Carvalho Aguiar, Michael Moeckel. *NPJ Digital Medicine*. Current status: Submitted.

5.1 Context

Autism Spectrum Disorder (ASD) is a neurodevelopmental condition characterized by difficulties in social communication, restricted interests, and repetitive behaviors (TOWBIN, 2005). Historically, the Diagnostic and Statistical Manual of Mental Disorders, Fourth Edition (DSM-IV) recognized subtypes such as Pervasive Developmental Disorder-Not Otherwise Specified (PDD-NOS) and Asperger Syndrome (AS) (TOWBIN, 2005; KLIN; MCPARTLAND; VOLKMAR, 2005). However, with the introduction of the DSM-5, these subtypes were removed, and ASD was redefined as a single diagnostic category (NUCKOLS; NUCKOLS, 2013; WING; GOULD; GILLBERG, 2011), leading to ongoing debates about the neurobiological distinctiveness of these conditions.

For example, PDD-NOS is characterized by challenges in social interaction, communication, and motor skills (FOMBONNE, 2009; KOK *et al.*, 2016), while AS has distinct features such as restricted interests, repetitive behaviors and the absence of significant language delays, often leading to its classification as a 'high-functioning' form of ASD (KLIN; MCPARTLAND; VOLKMAR, 2005; CONSTANTINO; CHARMAN, 2016). These differences raise a question about whether the DSM-5's unified approach is adequate or if there should indeed be a distinction of subtypes to provide a more precise framework for understanding and treating these conditions.

While a considerable amount of work has explored the binary classification between ASD

and typically developing (TD) individuals (AHMADLOU; ADELI; ADELI, 2012; ELDRIDGE *et al.*, 2014; UDDIN *et al.*, 2013), there is a notable gap in research that has focused on the identification of distinct ASD subtypes using advanced methodologies. In addition, few studies have investigated subtype classification using machine learning (ML) (AL-HIYALI *et al.*, 2021; USTA *et al.*, 2019; THAPA *et al.*, 2024).

This study aims to determine whether the distinctions between AS, PDD-NOS and ASD are biologically justified or whether the unified approach of DSM-5 better captures the complexity of these disorders by systematically comparing global and regional connectivity patterns across subtypes. To this end, we present the first comprehensive framework that integrates topological data analysis (TDA), complex network measures and ML to assess ASD subtypes.

5.2 Contributions

This study provides a comprehensive analysis of neural connectivity patterns in ASD subtypes. By integrating advanced methodologies such as TDA, complex network measures, and machine learning, the research offers new insights into brain lateralization and connectivity in these conditions. The results highlight the left primary motor cortex as a key feature in subgroup differentiation, with most of the significant regions identified by the SHAP value methodology located in the left hemisphere.

The complex network approach clearly separates the AS group in the confusion matrix, highlighting its potential as a unique subtype within ASD. Statistical analysis reveals significant differences in network measures between the ASD, AS and TD groups. The AS group had the lowest mean scores for most measures, while showing higher transitivity compared to TD and ASD.

TDA measures were used to assess higher-order brain network connectivity in the ASD, AS and TD groups. Notably, the most significant TDA differences distinguished AS from TD, while fractal dimension effectively separated AS from ASD. These findings highlight AS as a distinct ASD subtype and demonstrate the value of these measures in capturing these differences.

The findings suggest that AS may merit recognition as a distinct subgroup within the ASD due to its unique neurobiological characteristics. These advances have important implications for future research and clinical applications, including the development of targeted interventions and a deeper exploration of the relationship between cognitive function and brain network organization in ASD.

Redefining Autism Subtypes: a machine learning approach leveraging topological data analysis, network measures and hemispheric lateralization

Caroline L. Alves[1,*], Loriz Francisco Sallum[2], Patrícia Maria de Carvalho Aguiar[5,6], Joel Augusto Moura Porto[3,4], Francisco Aparecido Rodrigues[2], Thaise G. L. de O. Toutain[2], Michael Moeckel[1]

[1]Laboratory for Hybrid Modeling, Aschaffenburg University of Applied Sciences, Aschaffenburg, Germany.
[2]Institute of Mathematical and Computer Sciences, University of São Paulo, São Paulo, Brazil.
[3]Institute of Physics of São Carlos, University of São Paulo (USP), São Paulo, Brazil.
[4]Institute of Biological Information Processing 1 (IBI-1), Forschungszentrum Jülich, Jülich, Germany.
[5]Hospital Israelita Albert Einstein, São Paulo, Brazil.
[6]Department of Neurology and Neurosurgery, Federal University of São Paulo, São Paulo, Brazil.
[*]Caroline.LourencoAlves@th-ab.de.

Abstract

Autism subtypes, including general Autism Spectrum Disorder (ASD) and Asperger Syndrome (AS), exhibit distinct neural connectivity patterns. This study is the first to systematically integrate Topological Data Analysis (TDA) with complex network measures and machine learning (ML) to investigate brain lateralization and connectivity differences among these subtypes. Using fMRI-derived connectivity matrices, TDA metrics—such as persistence entropy and fractal dimension—revealed that AS networks are highly integrated and hierarchically complex, distinguishing them from both ASD and typically developing (TD) groups. Shapley Additive Explanations (SHAP) analysis identified the left primary motor cortex as a key feature across all subtypes, and highlighted its

subtype-specific correlations with other brain regions. ML models trained on these features achieved high classification accuracy, with an AUC of 0.983. This fMRI-based analysis supports the classification of AS as a distinct group alongside ASD due to its unique neurobiological characteristics.

1 Introduction

Autism Spectrum Disorder (ASD) is a neurodevelopmental condition with complex genetic underpinnings and significant heterogeneity, as highlighted by extensive research in the field [1, 2]. ASD typically manifests within the first three years of life and is characterized by challenges in social communication as well as restricted and repetitive behaviors [3]. Historically, subtypes like Pervasive Developmental Disorder-Not Otherwise Specified (PDD-NOS) and Asperger Syndrome (AS) were recognized under the Diagnostic and Statistical Manual of Mental Disorders, Fourth Edition (DSM-IV) [4, 5]. However, the updated DSM-V framework unified these subtypes under a single ASD diagnosis, emphasizing a spectrum of symptom presentations rather than distinct categories [6, 7].

The DSM-V's shift toward a unified ASD diagnosis has sparked debate. Proponents argue that it simplifies diagnostic criteria, reflecting the overlapping features among subtypes, such as shared deficits in visuospatial and executive functions [8]. Critics, however, highlight that significant differences exist in the neural underpinnings, cognitive profiles, and developmental trajectories of subtypes like AS and PDD-NOS [9]. For instance, PDD-NOS is associated with difficulties in social relationships, communication, and motor skills [10, 11], whereas AS presents distinct characteristics, including narrow interests, repetitive activities, and the absence of significant language delays, often classifying it as a "high-functioning" form of ASD [5, 12]. These differences raise the question: Does the DSM-V's unified approach sufficiently capture the nuanced neurobiological and behavioral distinctions, or does the DSM-IV's separation of subtypes provide a more precise framework for understanding and treating these conditions?

While substantial work has explored binary classification between ASD and typically developing (TD) individuals [13–15], there is a notable gap in research focused on identifying distinct ASD subtypes using advanced methodologies. Few studies have investigated subtype classification using machine learning (ML). For instance, convolutional neural networks (CNNs) have been applied to resting-state fMRI data, achieving accuracy of 0.821 for DSM-IV-defined subtypes [16], while other ML models yielded similar performance using behavioral checklists [17, 18]. However, these efforts often lack detailed biological interpretability and do not leverage advanced tools like topological data analysis (TDA) or community detection metrics to elucidate the structural and functional distinctions among subtypes.

In this study, we aim to address these gaps. We evaluate whether evidence based on biological data supports the distinctions proposed by the DSM-IV and whether they still hold clinical and scientific relevance. Specifically, we investigate brain connectivity differences across ASD, AS, PDD-NOS, and TD groups using functional Magnetic Resonance Imaging (fMRI) data from the Autism Brain Imaging Data Exchange (ABIDE)

[19] , which leverages blood oxygenation level-dependent (BOLD) time series data. Our methodology introduces novel aspects, including the application of TDA to explore higher-order connectivity, using a systematic set of 26 complex network measures, and integrating ML techniques with Shapley Additive Explanations (SHAP) values for interpretability. TDA metrics, such as persistence entropy and fractal dimension, provide insights into the hierarchical and multi-scale topology of brain networks [20, 21]. Additionally, we analyze hemispheric differences to investigate lateralization patterns, motivated by evidence of atypical hemispheric specialization in ASD [22, 23].

By systematically comparing global and regional connectivity patterns across subtypes, we seek to determine whether the distinctions between AS, PDD-NOS, and ASD are biologically justified or whether the DSM-V's unified approach better captures the complexity of these conditions. Our findings may have significant implications for refining diagnostic criteria, improving targeted interventions, and advancing our understanding of the neurobiological basis of ASD subtypes.

In summary, this study presents the first comprehensive framework integrating TDA, complex network measures, and ML to evaluate ASD subtypes. By uncovering nuanced distinctions in brain network topology, we aim to revisit the ongoing debate about whether separating subtypes, as in the DSM-IV, offers greater insight into the neural mechanisms of ASD than the unified approach of the DSM-V.

2 Results

2.1 Summary of the main results

This study provides novel insights into the neurobiological underpinnings of ASD subtypes, focusing on distinct connectivity patterns across TD (N=518), ASD (N=282), AS (N=80), and PDD-NOS (N=48). The data from the ABIDE dataset included BOLD time series from 122 brain regions, with preprocessing details described in subsection 4.1. Our methodology employed ML classifiers together with advanced metrics such as complex network and TDA measures.

Our analysis highlighted the left primary motor cortex (Left-PrimMotor) as central to all subtypes, with additional group-specific connections identified, such as those involving the left orbitofrontal cortex (Left-OrbFrontal) in ASD and the left temporal pole (Left-Temporalpole) in AS. Cluster analysis revealed that PDD-NOS is closely related to ASD, while AS emerged as more distinct, suggesting nuanced differences within the spectrum (results detailed in Subsection 2.3).

Key novel findings include:

- **Benchmarking ML models for subtype classification:** ML results show clear separation of AS, while ASD exhibits less distinct patterns with other subtypes, indicating heterogeneity within ASD classifications (results detailed in Subsection 2.2);
- **Spatiotemporal correlation patterns:** Identification of the most relevant inter-regional brain correlations for each group, revealing unique functional connectivity signatures that differentiate AS, ASD, and TD (results detailed in Subsection 2.3);

- **Complex network measures highlight topological alterations in AS:** AS networks exhibit enhanced long-range connectivity and stronger local clustering, traits often associated with high-functioning autism (results detailed in Subsection 2.4).
- **Unique topological features in AS:** TDA metrics, including the fractal dimension and persistence entropy, revealed greater network complexity and hierarchical organization in AS. The elevated fractal dimension and topological feature variability underscore this subtype's distinct neural connectivity patterns (results detailed in Subsection 2.5).
- **Hemispheric and regional insights:** AS networks demonstrated pronounced hemispheric asymmetries, with reduced right-hemisphere efficiency and larger left-hemisphere diameter compared to ASD and TD. These findings highlight the interplay between localized inefficiencies and global robustness in AS (results detailed in Subsection 2.6).

2.2 Benchmarking ML models for subtype classification

In order to conduct our study, a diverse set of machine learning classifiers was used, including the support vector machine (SVM) [24], logistic regression (LR) [25] employing the limited-memory Broyden Fletcher Goldfarb Shanno (L-BFGS) solver, random forest (RF) [26], multilayer perceptron (MLP) [27], and convolutional neural network (CNN) [28, 29]. For evaluation, we used accuracy as the primary metric to assess the overall correctness of the classification model [30–34], along with precision and recall to evaluate class-specific performance [35–38]. Precision quantifies the model's ability to correctly classify instances within specific categories like TD, while recall (sensitivity) assesses its effectiveness in identifying positive examples across ASD, AS, and PDD-NOS. To visualize performance, we used receiver operating characteristic (ROC) curves, with the area under the ROC curve (AUC) serving as a key metric, ranging from 0.5 (random performance) to 1 (perfect classification) [30, 39–41]. We calculated the micro-average AUC, which treats all classes equally, and the macro-average AUC, which aggregates the contributions of each class individually, to assess both individual and overall classification performance [42].

According to Figure 1, the best classifiers were CNN and SVM. For the test set, CNN achieved a mean AUC of 0.983, precision of 0.962, recall of 0.962, and accuracy of 0.981. On the other hand, SVM achieved an AUC of 0.962, precision of 0.989, recall of 0.928, and accuracy of 0.986.

Since SVM has a lower computational cost, it was chosen for the subsequent steps. Figure 2 displays the confusion matrix (Figure 2-(a)), the learning curve (Figure 2-(b)), the ROC curve (2-(c)), and the precision-recall curve ((2-(c))), respectively. From Figures 2-(a) and (b), the confusion matrix and ROC curve, respectively, show that the group most difficult to distinguish was PDD-NOS (in the confusion matrix, PDD-NOS group has some mistaken classification with ASD group). A possible explanation for this is that PDD-NOS is indeed a subclass of ASD, leading to overlapping features between the groups. Additionally, this group has the least amount of data, which could potentially contribute to higher misclassification rates. In contrast, AS, ASD, and TD groups were clearly separated, suggesting that AS could be distinguished from

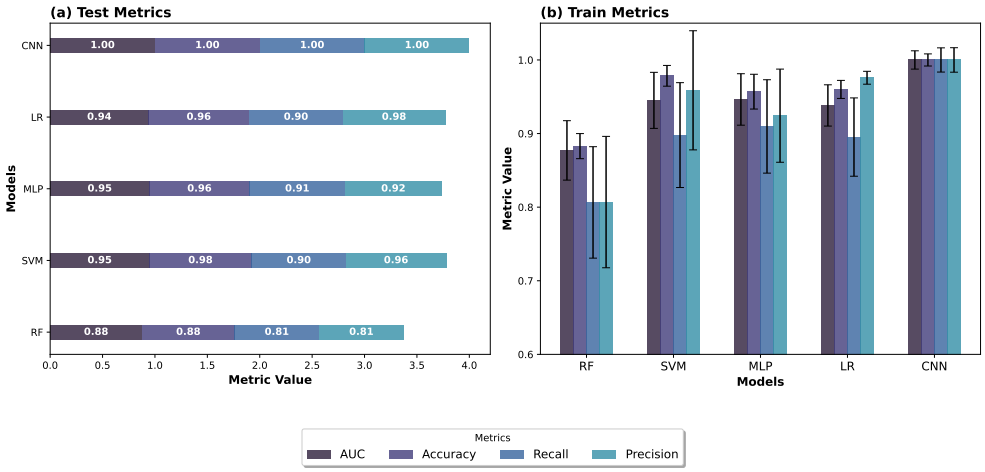

Fig. 1 Results of all ML classifiers: (a) the results for the test set and (b) the results for the training set, with error bars corresponding to the 10-fold stratified cross-validation. The best performance was achieved by CNN and SVM.

ASD group, further supporting its classification as a distinct subtype within the ASD spectrum.

The visual representation of the learning curve illustrates the impact of varying the number of training instances on the model's predictive accuracy [43]. Figure 2-(c) shows that the model requires the full dataset to achieve convergence. To address class imbalance due to differing numbers of patients in each diagnostic group, we computed Precision-Recall (PR) curves. These curves provide a comprehensive assessment of the model's performance by depicting the trade-off between precision (the proportion of true positive predictions among all positive predictions) and recall (the proportion of true positives correctly identified) [44]. As shown in Figure 2-(d), the macro-average PR curve summarizes the overall performance across all classes, while individual curves capture class-specific behavior. Despite the class imbalance, particularly the smaller sample size of PDD-NOS group, the PR curves indicate that the model maintains robust classification performance across all groups. The results reveal high Average Precision (AP) for the TD (1.00), ASD (0.99), and AS (1.00) classes, underscoring the model's ability to accurately distinguish these groups. Although PDD-NOS class exhibited a slightly lower AP (0.93), likely due to its limited sample size and feature overlap with the other groups, the overall macro-average performance highlights the model's effectiveness in handling the imbalanced dataset and maintaining high classification accuracy.

2.3 Spatiotemporal correlation patterns

The methodology used for SHAP value analysis produced the results shown in Figure 12 in Appendix A, which highlights the primary region involved in all connections across different autism subtypes. Notably, the Left-PrimMotor region consistently

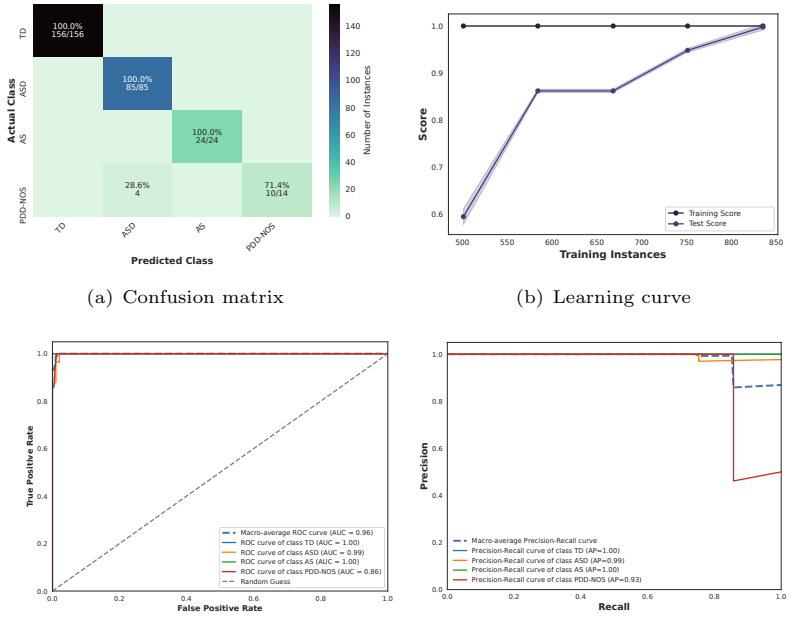

(a) Confusion matrix (b) Learning curve

(c) ROC curve (d) Precision-recall curve

Fig. 2 ML results on test sample from connectivity matrices. (a) Confusion Matrix depicting the performance of various ML algorithms on a test sample. The diagonal elements represent true positives (TP) values, indicating each algorithm's accuracy in correctly identifying positive instances. (b) Learning curve showing the training accuracy (purple) and test accuracy (blue) across different training sizes. (c) ROC curve for each class. The dashed grey line represents the random choice classifier, while the dashed blue line denotes the macro-average ROC curve. The solid blue, orange, green, and red lines correspond to the ROC curves for the TD, ASD, AS, and PDD-NOS classes, respectively. (d) Precision-Recall (PR) curve for each class. The blue dashed line represents the macro-average PR curve, while the solid blue, orange, green, and red lines correspond to the PR curves for the TD, ASD, AS, and PDD-NOS classes, respectively.

emerged as the central region for all subtypes. Specifically, for the ASD group, the predominant connections included Left-PrimMotor and Left-OrbFrontal, followed by Outside Brodmann Area 5 (Outside BAS5) and Left-PrimMotor. In the AS group, the primary connections were Left-PrimMotor and Left-Temporalpole, followed by Outside Brodmann Area 1 (Outside BAS1) and Left-PrimMotor. Similarly, for the PDD-NOS group, the key connections comprised Left-PrimMotor and Left Thalamus (Left-Thalamus), as well as Left Secondary Visual Cortex (Left-SecVisual) and Left-PrimMotor. To identify in more detail the Outside BAS regions that played a key role in these correlations, we used the Yale BioImage Suite Package web application to visualize these areas, as shown in Figure 3. Based on [45, 46], we identified Outside BAS5 (Figure 3-(b)) as the posterior cerebellum, and Outside BAS1 (Figure 3-(a)) as the anterior cerebellum.

Figure 4 summarizes the primary connections identified for each group. Additionally, Table 2.3 provides a structured overview of these connections, where the color

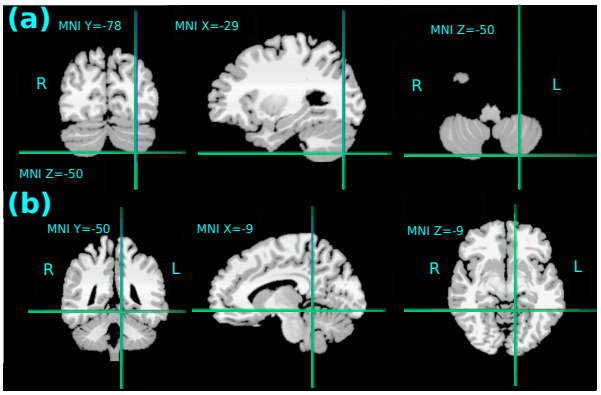

Fig. 3 Outside BAS regions involved in the most important correlation, plotted using the Yale BioImage Suite Package web. In (a), the Outside BAS 1 is identified as the anterior cerebellum, while in (b), the Outside BAS 5 is identified as the posterior cerebellum.

Table 1 Summary of the most important connections identified for each group using the SHAP value methodology. The connections are categorized by group (ASD, AS, and PDD), with color intensity in each cell representing the importance ranking, with darker shades indicating higher-ranked connections within each group.

Connections	ASD	AS	PDD
Left-OrbFrontal - Left-PrimMotor			
Left-PrimMotor -Left-PrimMotor			
Posterior Cerebellum - Left-PrimMotor			
Left-Temporalpole - Left-PrimMotor			
Anterior Cerebellum - Left-PrimMotor			
Left-Thalamus - Left-PrimMotor			
Left-SecVisual - Left-PrimMotor			

intensity reflects their importance ranking, with darker shades indicating a higher significance. In both Figure 4 and Table 2.3, the most relevant connections for ASD, AS, and PDD are highlighted in pink, purple, and green, respectively, ensuring a clear visual distinction between groups.

We employed the SHAP values methodology to derive a feature importance vector for each group. To evaluate the similarity between these vectors, we used cosine similarity—a metric that quantifies the directional similarity between two vectors and is widely applied in in the medical literature [48–50]. The cosine similarity scores for each group are visualized in the clustering map presented in Figure 5, which graphically represents the relationships between groups based on their feature importance profiles, facilitating a comprehensive understanding of the clustering patterns.

The resulting connectivity matrix illustrates the pairwise cosine similarity between the SHAP values of different subtypes. The values range from -1 to 1, where 1 indicates identical patterns, 0 implies no similarity, and -1 suggests completely opposite patterns. The off-diagonal elements reveal the degree of similarity between different subtypes. Notably, the TD group exhibits strong negative similarities with ASD,

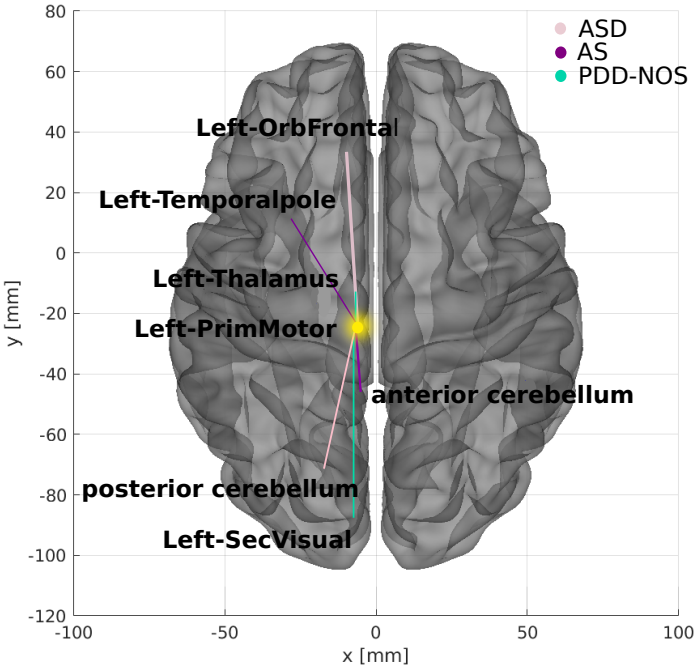

Fig. 4 The most important connections identified. A two-dimensional schematic (ventral-axis) highlights the most critical connection for ASD, AS, and PDD-NOS in pink, purple, and green, respectively. The region that most contributed to the primary connection across all groups is highlighted in yellow. The brain plot was generated using the Braph tool [47], with each region mapped according to the Brodmann map from the Yale BioImage Suite Package.

AS, and PDD-NOS, indicating distinct patterns in the identified important connection features. Meanwhile, ASD, Asperger, and PDD-NOS show positive similarities among themselves, suggesting shared connection patterns and potential underlying commonalities. This clustering pattern provides insights into the neural connectivity differences that distinguish individuals with ASD from TD and highlights potential nuances among the ASD subtypes, particularly AS.

Interestingly, the clustering map shows that PDD-NOS shares a 98% similarity with ASD, supporting the hypothesis that PDD-NOS may be a subtype within the broader autism spectrum. Additionally, the AS group shows a comparable level of similarity (approximately 80%) with both PDD-NOS and ASD, suggesting shared features with these groups while still maintaining distinct connection patterns. These clustering patterns provide valuable insights into the neural connectivity profiles identified as important for classification, highlighting the nuanced distinctions among ASD subtypes, particularly in the case of AS, which exhibits both shared and unique connection patterns.

A notable observation from our analysis is that most of the primary regions identified as important by the SHAP values methodology were located in the left hemisphere.

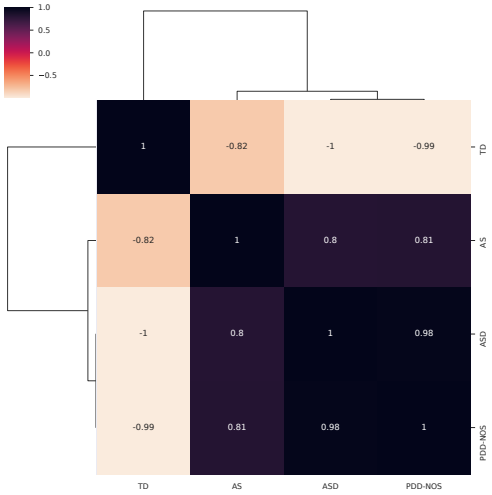

Fig. 5 The clustermap visualizes the similarity matrix, with each cell representing the cosine similarity between the SHAP values of two subtypes. The values range from -1 to 1, where 1 indicates identical patterns, 0 implies no similarity, and -1 suggests completely opposite patterns. The off-diagonal elements reveal the degree of similarity between different subtypes.

To further explore this hemispheric dominance, we isolated regions corresponding to the left hemisphere (86 regions), right hemisphere (13 regions), and cortex (12 regions). Connectivity matrices were generated separately for each of these subsets and used to train the ML algorithm. However, the classification performance for all subsets remained close to 50%, suggesting that analyzing isolated hemispheres or the cortex independently is insufficient for a robust classification. This limitation likely arises because, in the AS, ASD, and PDD-NOS groups, the most important connections involve cross-hemispheric or more global network patterns. These findings highlight the necessity of incorporating connections across all regions to fully capture the complexity of the neural connectivity patterns that distinguish these groups.

2.4 Complex network measures highlight topological alterations in AS

To characterize the network structure of the brain, we computed 26 complex network measurements, as used in our previous publications [51–55]. These measurements include average shortest path length (APL) [56], eccentricity [57], closeness centrality (CC) [58], diameter [59], density [60], betweenness centrality (BC) [61], hub score [62], eigenvector centrality (EC) [63], assortativity coefficient [64, 65], average degree of nearest neighbors [66] (Knn), second moment of the degree distribution (SMD) [67],

mean degree [68], entropy of the degree distribution (ED) [69], transitivity [70, 71], complexity, k-core [72], and efficiency [73].

In this study, we employed recently developed metrics (detailed in [52]) that quantify the number of communities within a complex network. Our investigation also incorporated community detection algorithms, as referenced in [74–76]. To integrate these community detection measures into the matrix, which requires a singular scalar value, we applied algorithms designed to identify the largest community. Subsequently, we computed the average path length within each community, resulting in a singular value. The community detection algorithms used in this study included fastgreedy (FC) [77], Infomap (IC) [78], leading eigenvector (LC) [79], label propagation (LPC) [80], edge betweenness (EBC) [81], spinglass (SPC) [82], and multilevel community identification (MC) [83]. o indicate the approach used for calculating the average path length, we extended the respective abbreviations with the letter "A" (AFC, AIC, ALC, ALPC, AEBC, ASPC, and AMC). Further details of these methodologies can be found in [52].

Within the context of brain networks, two fundamental concepts emerge: integration and segregation. Integration refers to the degree of interconnectedness among nodes in a network, enabling efficient information flow [84, 85]. Highly integrated networks facilitate seamless communication between brain regions [86, 87]. In contrast, segregation reflects the brain's ability to support specialized processing within tightly interconnected clusters or communities of brain regions [88, 89]. Following our previous research, we employed three measures to analyze these concepts: effective information (EI) and determinism and degeneracy coefficients (as elaborated in Alves). Lower EI values indicate a more segregated network structure, while higher values of determinism and degeneracy coefficients indicate that the graph structure is characterized by sparse connections rather than a highly interconnected network, further signifying increased segregation.

The performance of the test sample using the complex network approach resulted in a mean AUC of 0.829, precision of 0.938, recall of 0.715, and accuracy of 0.888. However, since the overall model accuracy did not exceed 90%, we opted to prioritize statistical tests over SHAP values for further analysis. Nonetheless, the clear separation of the AS group in the confusion matrix highlights its potential as a distinct subtype within ASD.

The statistical analysis, illustrated in Figure 6, reveals significant differences in network measures among the ASD, AS, and TD groups. Specifically, the AS group consistently exhibited the lowest average values across most metrics, including AFC, ALC, AMC, ASPC, and efficiency, while displaying higher transitivity values compared to TD and ASD. These findings underscore the unique network characteristics of the AS group, as shown in the boxplots, further supporting its distinctiveness within the ASD spectrum.

2.5 Unique topological features in AS

In this study, we employed TDA measures, including the number of simplices, fractal dimension, and persistence entropy, to explore the higher-order connectivity of brain networks across ASD, AS, and TD groups. These metrics are further detailed in

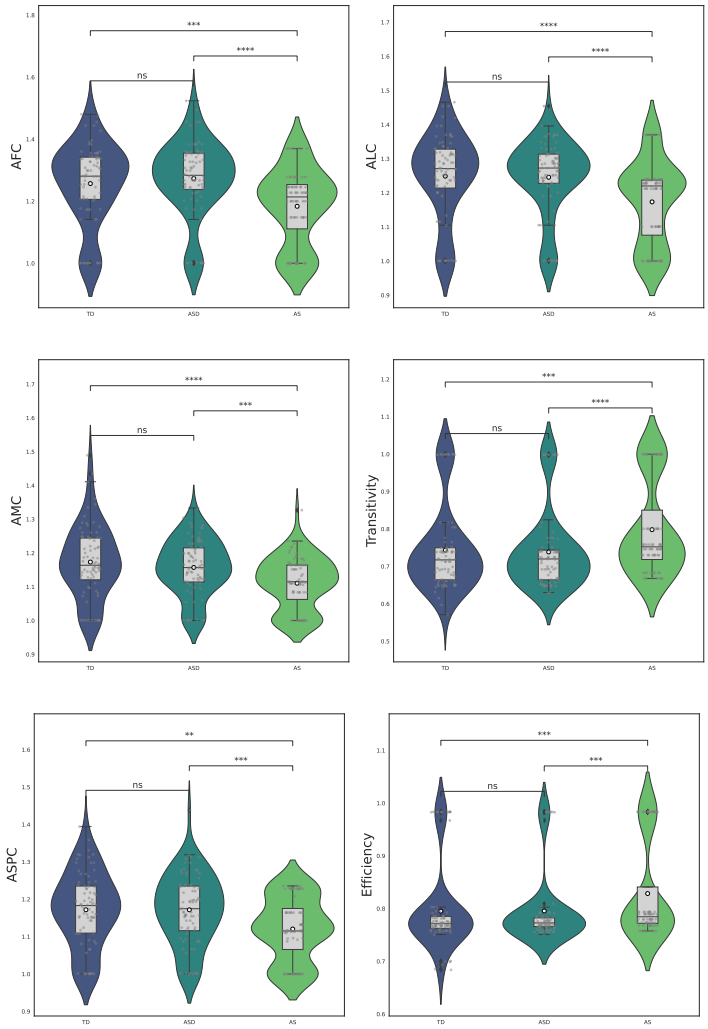

Fig. 6 Complex network measures obtained four and three stars in the t-test with Bonferroni correction compared to TD, ASD, and AS classes, represented in dark blue, blue, and green, respectively. Statistical significance is indicated as follows: ns for $5.00 \times 10^{-2} < p \leq 1.00$, * for $1.00 \times 10^{-2} < p \leq 5.00 \times 10^{-2}$, ** for $1.00 \times 10^{-3} < p \leq 1.00 \times 10^{-2}$, *** for $1.00 \times 10^{-4} < p \leq 1.00 \times 10^{-3}$, and **** for $p \leq 1.00 \times 10^{-4}$.

Subsection 4.1.3. The statistical analysis, illustrated in Figure 7, reveals significant differences in TDA measures among the three groups. The statistical analysis, visualized in Figure 7, highlights the significant differences in TDA measures among the ASD, AS, and TD groups. The number of simplices was higher in AS compared to TD and ASD, while the fractal dimension followed a similar trend, with AS exhibiting higher values than the other two groups. Persistence entropy, however, exhibited a different pattern, with AS showing the highest values, followed by TD, and ASD exhibiting the

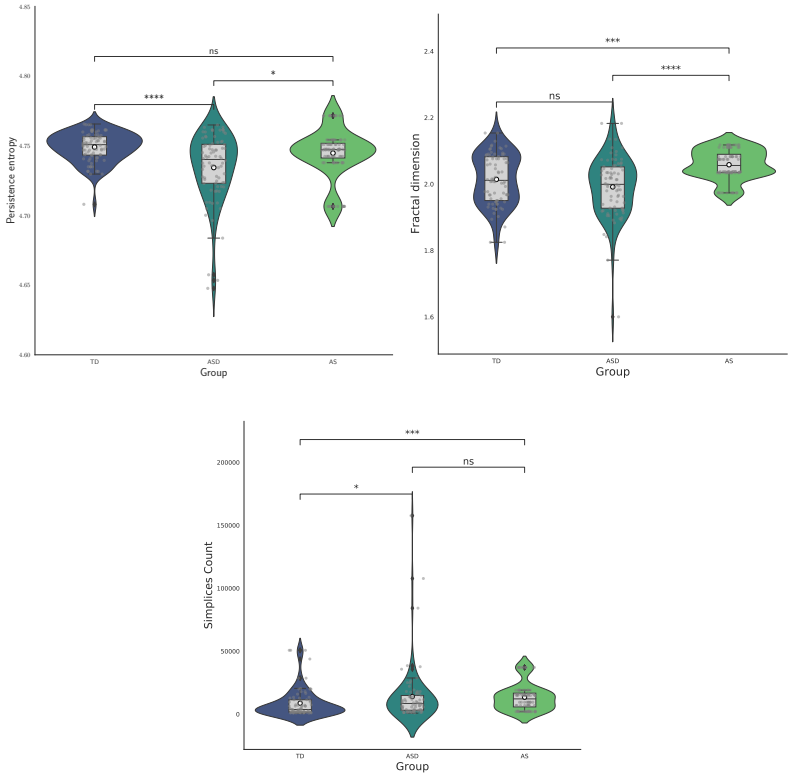

Fig. 7 TDA measures obtained four and three stars in the t-test with Bonferroni correction compared to TD, ASD, and AS groups, represented in dark blue, blue, and green, respectively. Statistical significance is defined as follows: ns for $5.00\times10^{-2} < p \leq 1.00$, * for $1.00\times10^{-2} < p \leq 5.00\times10^{-2}$, ** for $1.00\times10^{-3} < p \leq 1.00\times10^{-2}$, *** for $1.00\times10^{-4} < p \leq 1.00\times10^{-3}$, and **** for $p \leq 1.00\times10^{-4}$.

lowest. Notably, the most significant differences in TDA metrics were observed when distinguishing AS from TD, with the fractal dimension effectively distinguishing AS from ASD. These findings underscore the distinctiveness of AS as a subtype within the ASD and highlight the value of TDA measures in capturing these differences.

2.6 Hemispheric and regional insights

To gain a deeper understanding of the neural connectivity patterns distinguishing ASD and AS groups, we computed complex network measures for each brain region, focusing on the cortex, left hemisphere, and right hemisphere. While previous analysis showed that isolated connectivity matrices for individual hemispheres or regions were insufficient for robust classification, they underscored the importance of evaluating region-specific topological changes using statistical tests. The results, summarized in Table 2 and visualized in the boxplot in Appendix B, reveal significant differences in several complex network measures across the cortex, left, and right hemispheres. In particular, the cortex's diameter, CC, AEBC, AIC, ALPC, and efficiency consistently exhibited highly significant differences (****) between ASD and AS groups.

Table 2 Summary of significant differences in complex network measures between ASD and AS groups across the cortex, left, and right hemispheres. Measures include diameter, CC, AEBC, AIC, ALPC, and efficiency. Statistically significant (SS) differences are marked with stars (****), with the most notable distinctions observed in the cortex. Non-significant differences are indicated as "ns."

Measures	Cortex			Left Hemisphere			Right Hemisphere		
	ASD	AS	SS	ASD	AS	SS	ASD	AS	SS
Diameter	1.184	1.347	****	2.694	2.755	****	3.448	3.551	ns
CC	0.989	0.939	****	0.715	0.688	ns	0.565	0.488	ns
AEBC	1.009	1.015	****	1.114	1.113	ns	1.145	1.168	ns
AIC	1.015	1.049	****	1.447	1.488	ns	1.471	1.489	ns
ALPC	1.023	1.034	****	1.439	1.460	ns	1.449	1.485	ns
Efficiency	0.396	0.381	****	0.775	0.754	ns	0.662	0.667	ns

Notably, the diameter measure was higher in AS than ASD across all regions, with the most significant differences observed in the cortex and left hemisphere. CC and efficiency values were generally lower in AS compared to ASD, with significant differences primarily found to the cortex.

The boxplot in Figure 8 provides a detailed comparison of inter- and intra-regional differences between the right and left hemispheres, highlighting the distinct network characteristics of ASD and AS groups. To enhance clarity and focus on the differences between ASD and AS, the TD baseline has been removed from the analysis.

Among the evaluated metrics, diameter and efficiency showed statistical significance. Inter-regional analysis revealed that the AS group's left hemisphere had a significantly higher diameter (**) compared to the left hemisphere of the ASD group. Additionally, intra-regional differences were also detected within the AS group, where the left hemisphere's diameter significantly differed from the right hemisphere. In the ASD group, efficiency showed a notable intra-regional difference, with higher values in the right hemisphere compared to the left. These results highlight both inter-group and hemispheric asymmetries, providing deeper insights into the distinct structural properties of the ASD and AS groups.

3 Discussion

3.1 Benchmarking ML models for class separation and spatiotemporal correlation patterns

Overall, our approach outperformed existing multiclass ML algorithms for distinguishing ASD, AS, PDD-NOS, and TD, as discussed in Section 1.

The SHAP value analysis provided critical insights into the neural underpinnings of various autism subtypes. Notably, the Left-PrimMotor region consistently emerged as the central hub across all connections, highlighting its crucial role in the neurobiological mechanisms underlying ASD.

In the ASD subtype, the primary connections were identified between the Left-PrimMotor and Left-OrbFrontal regions. Additionally, significant connections

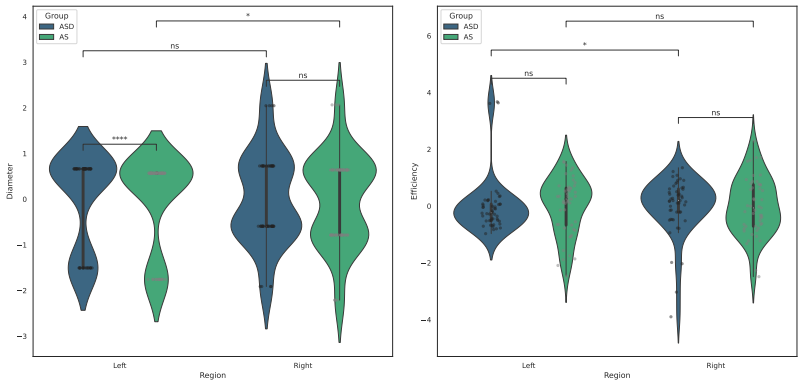

Fig. 8 Boxplots illustrating inter- and intra-regional differences in complex network measures (diameter and efficiency) between ASD and AS groups across the left and right hemispheres. Statistical significance is indicated as follows: ns for $5.00 \times 10^{-2} < p \leq 1.00$, * for $1.00 \times 10^{-2} < p \leq 5.00 \times 10^{-2}$, ** for $1.00 \times 10^{-3} < p \leq 1.00 \times 10^{-2}$, *** for $1.00 \times 10^{-4} < p \leq 1.00 \times 10^{-3}$, and **** for $p \leq 1.00 \times 10^{-4}$.

involving the posterior cerebellum and Left-PrimMotor. This finding aligns with existing literature emphasizing the role of the frontal lobe, particularly the orbital frontal cortex, in social cognition and executive functions, which are often affected in individuals with ASD [53, 90, 91]. The involvement of the cerebellum is also consistent with studies highlighting its contribution to motor control and cognitive processes, both of which are frequently altered in ASD [92, 93].

For the AS subtype, the principal connections were observed between the Left-PrimMotor and Left-Temporalpole regions. This finding is aligns with existing literature emphasizing the importance of the temporal lobe in processing social information and emotions—functions often impaired in individuals with AS [94, 95]. The involvement of the anterior cerebellum is particularly noteworthy, as research suggests its contribution to higher-order cognitive functions and language processing [93]. In the PDD-NOS subtype, critical connections were identified between the Left-PrimMotor and Left-Thalamus regions, as well as between the Left-SecVisual and Left-PrimMotor. The thalamus plays a well-documented role in sensory processing and integration, and its involvement in PDD-NOS further underscores the heterogeneity within the autism spectrum [96, 97]. Additionally, the involvement of the secondary visual cortex may indicate variations in visual processing, an aspect frequently reported in individuals with PDD-NOS [98].

Notably, the cluster map derived from the SHAP value methodology suggests that PDD-NOS is closely related to ASD, with a cosine similarity of 0.98. In contrast, the similarity between ASD and AS is 0.81. Since this value is lower than 0.90, it indicates that AS exhibits more distinct characteristics compared to ASD. This finding suggests that AS patients should be analyzed separately from the ASD group rather than being grouped within the broader ASD category.

3.2 Complex network measures highlight topological alterations in AS

The statistical analysis reveals significant differences in network measures among ASD, AS, and TD groups, with AS group uniquely exhibiting higher values for both global average efficiency and global transitivity. In contrast, TD and ASD groups showed no distinguishable differences in these metrics, underscoring the distinctiveness of AS group within the ASD spectrum. Furthermore, the AS group consistently displayed the lowest average values across most metrics, including AFC, ALC, AMC, and ASPC, while maintaining higher values for efficiency and transitivity.

Global average efficiency, which quantifies the ease and speed of information transfer across the entire network [99, 100], was notably higher in the AS group. This suggests that individuals with AS may exhibit enhanced global integration, facilitating more effective communication between distant brain regions. Similarly, global transitivity, defined as the ratio of triangles to connected triples in the network [101, 102], was also higher in the AS group, indicating strong local clustering and a well-defined modular organization. These findings highlight a unique balance between global and local network properties in the AS group, differentiating it from both ASD and TD groups.

In contrast, the consistently lower values of metrics such as AFC, ALC, AMC, and ASPC in AS group suggest a more compact and efficient internal structure within communities. This pattern may indicate that the AS group prioritizes tightly connected local modules while simultaneously maintaining effective global integration. Such a network configuration could facilitate enhanced cognitive abilities and localized processing capabilities, characteristics often associated with AS, which is frequently described as a high-functioning form of ASD [103–105].

The higher efficiency and transitivity values in the AS group align with characteristics traditionally associated with this syndrome, including stronger cognitive abilities and better social functioning compared to others on the ASD spectrum [106–108]. The combination of enhanced global integration and robust local clustering may contribute to the cognitive flexibility and social abilities observed in individuals with AS, despite challenges in other areas. Our findings are consistent with those of[109], which also reported increased global efficiency in AS compared to ASD and TD. Moreover, the absence of significant differences in efficiency and transitivity between TD and ASD groups further underscores the distinctiveness of AS group.

3.3 Unique topological features in AS

The TDA results further complement the complex network findings, highlighting the distinctiveness of AS group within ASD. Statistical analysis of TDA metrics revealed significant differences among ASD, AS, and TD groups, with AS group displaying unique topological characteristics. Specifically, AS group exhibited higher values for the number of simplices and fractal dimension, indicating greater network complexity and hierarchical organization. The high value of fractal dimension is consistent with the increased global efficiency and transitivity observed in the complex network analysis, suggesting a more intricate and hierarchically organized network with robust local

clustering. The high value of fractal dimension in AS may also correlate with the cognitive and behavioral traits associated with high-functioning ASD, implying that such intricate network structure could underlie their superior verbal skills and cognitive flexibility compared to other ASD subtypes.

Persistence entropy provided an additional dimension of analysis by quantifying the variability and prominence of topological features, such as connected components and loops, across multiple thresholds. Interestingly, persistence entropy exhibited the highest values in AS group, followed by TD, with ASD showing the lowest values. These findings suggest that AS networks possess a more complex and variable topology, potentially reflecting a combination of flexibility and intricate neural connectivity that may underlie the group's distinct cognitive and behavioral traits. The higher persistence entropy in AS may indicate an improved ability to integrate and process different information streams. In contrast, the lower persistence entropy in ASD suggests a more constrained and less adaptable network organization, potentially contributing to the group's characteristic difficulties in information processing and social interaction. The intermediate persistence entropy observed in TD reflects a balanced and flexible network structure, supporting a diverse range of neural functions.

The distinctive combination of higher fractal dimension and lower persistence entropy in AS group underscores a balance between network complexity and specialization. These findings provide valuable insights into how hierarchical organization and topological variability differentiate AS from other groups within the ASD spectrum. Moreover, the ability of persistence entropy to capture subtle differences between ASD and AS subtypes highlights its potential as a powerful metric for understanding neurodevelopmental disorders.

To the best of our knowledge, this is the first study to apply TDA metrics, including persistence entropy, to investigate brain network topology in AS and ASD. These findings highlight the potential of TDA to uncover novel insights into the neurobiological underpinnings of ASD subtypes, particularly AS, and pave the way for future research on targeted interventions and diagnostic tools.

3.4 Hemispheric and regional insights

The results reveal significant differences in network topology between ASD and AS groups, particularly in global efficiency, CC, and community detection metrics, as summarized in Table 2. Moreover, these differences highlight distinct patterns of integration and modularity at both regional and global levels ((discussed in Subsections 2.4 and 2.6, respectively). The AS group exhibits pronounced hemispheric asymmetries and localized inefficiencies, especially in the right hemisphere, while also displaying higher global network efficiency and transitivity compared to the ASD group. At the regional level, AS networks show pronounced hemispheric asymmetries, with the right hemisphere characterized by a larger diameter, lower CC, and reduced efficiency compared to the left hemisphere. his suggests fragmented integration in localized networks. These findings align with previous research indicating reduced right-hemisphere function in AS, which may contribute to difficulties in social communication and spatial processing [110, 111].

In contrast, the ASD group exhibits less pronounced hemispheric differences, with both hemispheres maintaining relatively high efficiency and similar CC values. This aligns with reports of reduced lateralization in ASD [112–114]. However, at the global level, AS networks exhibit higher global average efficiency and global transitivity compared to ASD, reflecting greater global integration and modularity. These findings are consistent with previous research suggesting increased global efficiency in AS, which may reflect improved long-range connectivity and more effective information transfer across the brain [108, 115]. This unique combination of regional inefficiencies and global robustness could explain some of the clinical characteristics traditionally associated with AS as a high-functioning form of autism. The higher global efficiency and transitivity in AS, also supported by the literature [109] could contribute to advanced cognitive functions, such as problem-solving, language processing, and analytical reasoning. Meanwhile, localized disruptions in the right hemisphere may be related to interpersonal difficulties [116, 117]. These network properties could underpin the superior verbal skills and intellectual capabilities often observed in individuals with AS, despite challenges in social interactions and emotional processing [118, 119].

The pronounced hemispheric asymmetries in AS, particularly the reduced integration in the right hemisphere, may reflect functional differences associated with cognitive and behavioral traits. The right hemisphere, often associated with spatial and emotional processing, shows reduced integration in AS, which could contribute to the interpersonal difficulties commonly reported in this group [120, 121]. Conversely, the relatively preserved integration and efficiency in the left hemisphere may support the advanced language and reasoning abilities characteristic of high-functioning ASD [122].

3.5 Summary of distinct neural profiles of ASD subtypes: insights, implications, and limitations

This study provides new insights into the neurobiological differences between ASD and AS, highlighting distinct patterns of intra-brain correlations and network topology across different scales. Notably, the AS group exhibits pronounced hemispheric asymmetries, with reduced integration and efficiency in the right hemisphere compared to the lef, while also demonstrating higher global efficiency and transitivity than ASD. These findings suggest a unique balance between global robustness and regional fragmentation in AS, which may contribute to its classification as high-functioning autism. The application of TDA metrics, including fractal dimension and Betti numbers, further enhances this understanding, as AS networks display a higher fractal dimension and fewer Betti numbers, indicating greater complexity and stronger integration. This study is the first to systematically compare the right, left, and cortical hemispheres of ASD and AS while integrating TDA, providing a novel framework for investigating brain connectivity. These findings support the broader perspective of AS as an distinct subtype within ASD spectrum.

While this study provides valuable insights into the neurobiological differences between ASD and AS, several limitations should be acknowledged. First, small sample size, particularly for certain subtypes such as PDD-NOS, restricts the statistical power and generalization of the findings. Additionally, although hemispheric and

cortical analysis revealed important distinctions, the study does not account for potential confounding factors such as age, sex, or comorbidity, which may also influence brain network properties. Future research with larger longitudinal datasets and more detailed assessments of clinical phenotypes is necessary to validate and further develop these findings.

4 Methods

4.1 Data and data preprocessing

The dataset used for this analysis, as in our previous work [53], originates from the ABIDE consortium, which comprises 1,112 datasets, including 539 individuals with ASD and 573 TD controls. The preprocessed data was obtained from the Preprocessed Connectomes Project (PCP) dataset, where a rigorous preprocessing pipeline was applied. This pipeline included slice-time correction, motion correction, intensity normalization, and removal of various artifacts such as breathing, heartbeat, and head motion. For each subject, a 300-second BOLD time series was used.

All data were strictly anonymous in compliance with HIPAA requirements, and analyses were conducted following the pre-approved protocols of the University of Utah Institutional Review Board. Informed consent was obtained from all participants according to the established procedures of human subjects research committees at each participating institution. Notably, the preprocessed data underwent a 0.5 Hz band-pass filter, consistent with recent fMRI literature findings indicating the relevance of fluctuations within this frequency range. Detailed information on data acquisition, informed consent procedures, and site-specific protocols can be accessed at http://fcon1000.projects.nitrc.org/indi/abide/. Moreover, the dataset is available for analysis using the Nilearn python package [19], a widely used tool for neuroimaging data processing and exploration, cited in numerous studies [123–127].

In this study, we extend our previous work [53] by providing a more detailed perspective on ASD through the inclusion of four distinct diagnostic groups: AS (N=80), PDD-NOS (N=48), ASD (N=282), and TD (N=518). Further, this work focuses on specific brain regions rather than analyzing the entire BOLD time series from each voxel in the brain image. Among various predefined atlases, we selected the Bootstrap Analysis of Stable Clusters (BASC) due to its superior performance in distinguishing individuals with ASD using a deep learning model, as reported in [53, 128]. Originally introduced by [129], the BASC atlas is derived from group-level brain parcellation using the BASC method, a k-means clustering algorithm that identifies brain networks with coherent activity during resting-state functional Magnetic Resonance Imaging (fMRI) [130, 131]. The BASC atlas used in this study consists of 122 regions of interest (ROIs) (see Figure 9-A). In our previous research [53], we used the Yale BioImage Suite Package web application[1] to manually assign coordinates to each ROI and determine their anatomical labels (see Figure 9-A).

After extracting time series data for each patient across 122 regions, we performed correlation analysis using Spearman's correlation coefficient [132] (see Figure 9-B).

[1] Accessible at https://bioimagesuiteweb.github.io/webapp/mni2tal.html

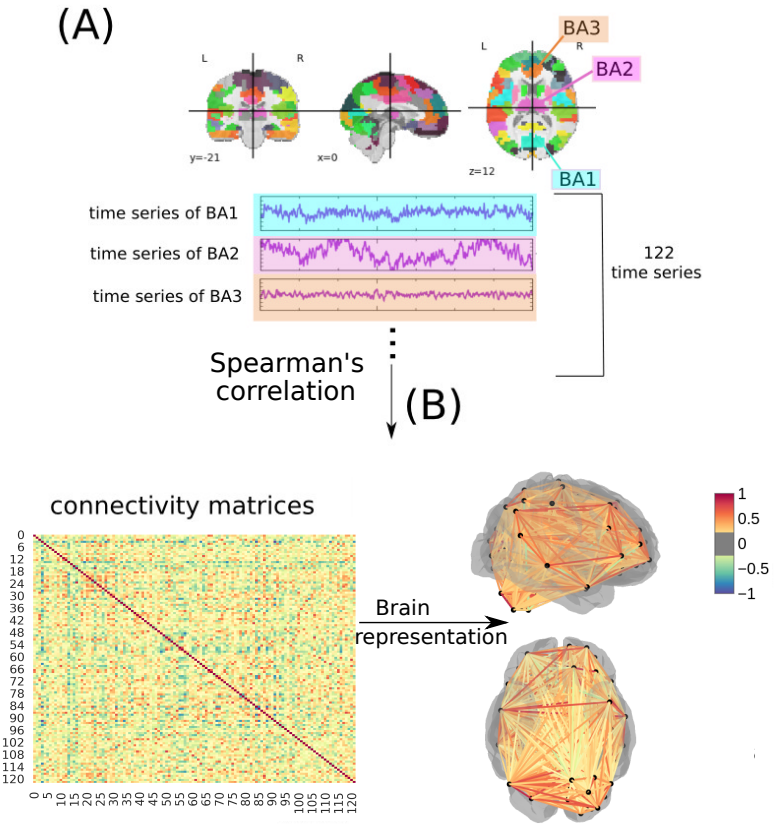

Fig. 9 Approach for generating connectivity matrices as described in [53]. In (A), a time series is extracted from 122 ROIs in the fMRI data using the BASC BOLD atlas (highlighted in blue, purple, and orange). These time series are then correlated (B) to generate the connectivity matrices, where each row and column corresponds to one of the Brodmann areas for a patient with AS, ASD, PDD-NOS, or TD (the figure illustrates an example for a subject with AS). The highlighted matrices represent the brain, as shown in a three-dimensional scheme (from bottom and right perspectives) .

This method was selected based on its superior performance in our previous study [53], where it effectively differentiated ASD patients from TD controls. Spearman's correlation measures the monotonic relationship between variables, making it a robust metric for assessing associations, particularly in the presence of nonlinear dependencies within brain data [133–135].

4.1.1 ML models pipeline

First, we applied standardization, a widely used ML technique to normalize features setting the mean to zero and the standard deviation to one [136]. This transformation is crucial for simplifying data analysis, ensuring consistent scaling, equal weighting of features, and increasing resilience to outliers and highly variable features within the

model. Subsequently, we split the data into training and test sets, with 30% of the data comprising the test set, a common practice in the literature [137–140].

To ensure robustness and unbiased evaluation of machine learning models in the training set, we consistently applied 10-fold stratified cross-validation with shuffling [141, 142]. This technique separates the dataset into ten equally stratified folds, ensuring that each fold (denoted as k) maintains a balanced distribution of samples across all classes. This approach guarantees equal representation of each class in every fold, enhancing the reliability of model evaluations. The algorithm trains on nine folds and validates on the remaining one, repeating this process ten times, with each fold serving as the validation set once. We used the common value of $k = 10$, as recommended in the literature [143–146]. Furthermore, to assess the stability of the model's performance, we also explored other values of k. The shuffling strategy ensures tthat the data is randomized before splitting into folds, mitigating potential ordering effects and biases, thereby strengthening the robustness of the model training process [147].

We employed hyperparameter optimization techniques to achieve optimal performance of the ML algorithm. The grid search method, widely adopted in the literature [41, 148–151], was used for fine-tuning hyperparameters in all ML algorithms, except for CNN. This method involves systematically searching through a predefined set of hyperparameter values to find the combination that yields the best model performance [152]. For deep learning models, specifically CNNs, we opted for random search optimization due to its superior computational efficiency in hyperparameter tuning compared to grid search. This choice was motivated by its superior computational efficiency in hyperparameter tuning compared to grid search. This is especially advantageous considering the substantial computational resources required for deep learning tasks. Detailed information on the hyperparameter optimization values for each classifier model can be found in [51–54].

In evaluating the stability of the model across different values of k in stratified cross-validation combined with SVM, as shown in Figure 10, we observed variations in both training and test performance metrics. The training AUC consistently increased with higher values of k, reaching a peak at $k = 10$ before slightly decreasing. Similarly, the training accuracy steadily improved with k, stabilizing around $k = 7$ and maintaining a high level thereafter. The overall stability of the model is supported by the relatively small fluctuations in test metrics and the convergence of training metrics, particularly after $k = 7$. Despite some variability, the model consistently achieves high performance, indicating that the chosen configuration provides robust results for the dataset and classification task at hand.

To identify the optimal number of features required to achieve peak performance, we conducted a Recursive Feature Elimination (RFE) analysis, as shown in Figure 11. This method, widely used in predictive modeling, particularly in medical data applications [153–156], systematically removes less influential features in a stepwise manner to evaluate their impact on model performance. Through this iterative process, we identified the most relevant features. As shown in Figure 11, the highest accuracy is achieved with a set of 176 features. This finding indicates that using the entire feature set is unnecessary for optimal performance.

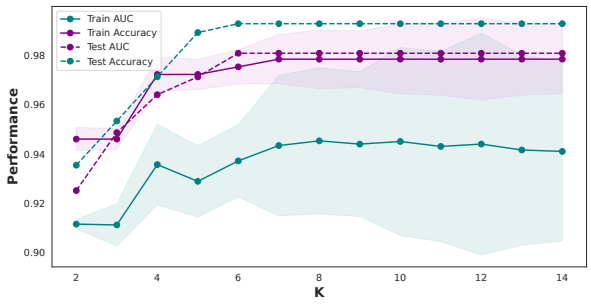

Fig. 10 SVM model performance varying the number of K in stratified cross-validation. The figure illustrates the performance metrics of the SVM model, specifically AUC and accuracy, represented in blue and purple on the y-axis. These metrics were obtained by varying the number of K in the stratified k-fold cross-validation, shown on the x-axis. Dashed lines represent the results from the test set, while solid lines represent the outcomes from the training set. The shaded region indicates the standard deviation within the training set.

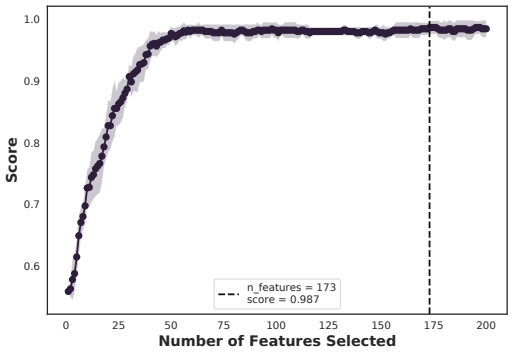

Fig. 11 RFE. Optimal performance is achieved with 176 features, indicating that the full set of features is unnecessary for achieving peak efficacy.

Subsequently, we applied the SHAP value approach to provide a biological interpretation, highlighting the predictive significance of individual attributes.

4.1.2 Statistical test

Finally, a statistical analysis was conducted to compare the four distinct groups: ASD, AS, PDD-NOS, and TD. Due to the varying group sizes, random selection was employed, with the minimum number of individuals in any group set at 48, consistent with the PDD-NOS group.

The Wilcoxon test, also known as the Mann-Whitney U test for two groups or the Kruskal-Wallis test for more than two groups [157–159], is a non-parametric test used in this study to compare two groups. Specifically, the Wilcoxon test was employed to identify significant differences in measures or variables among the ASD, AS, PDD-NOS, and TD groups.

Furthermore, we applied the Bonferroni correction to address the potential issue of inflated Type I error rates (false positives), which occur when a null hypothesis that is actually true is incorrectly rejected in a statistical test [160]. This correction was used in our study to control for the increased risk of Type I errors arising from conducting multiple simultaneous statistical tests [161].

The following symbols represent the statistical significance:

- ns: $5.00e-02 < p <= 1.00e+00$
- *: $1.00e-02 < p <= 5.00e-02$
- **: $1.00e-03 < p <= 1.00e-02$
- ***: $1.00e-04 < p <= 1.00e-03$
- ****: $p <= 1.00e-04$

4.1.3 TDA metrics

In this study, we employed Vietoris–Rips complex, also known as the Rips complex, a fundamental tool in TDA, to investigate the higher-order connectivity of brain networks across ASD, AS, and TD groups [162, 163]. Rips complexes represent the connectivity of data points as simplices (points, edges, triangles, and higher-dimensional structures) based on a specified distance threshold, capturing the underlying topological features of a dataset [164, 165]. Using the Gudhi library [166], we computed the number of simplices up to a fixed maximum dimension ($d_{\max} = 2$), capturing points, edges, and triangular structures [167]. For each group, correlation matrices were used to construct Rips complexes, applying a distance threshold of 0.5 to retain only the strongest connections, thereby emphasizing the core connectivity structure of the networks [168]. This metric reflects the density of higher-order connectivity in the networks and provides insights into the underlying neural architecture [169].

We employed the fractal dimension to quantify the complexity and hierarchical organization of brain networks by analyzing the growth of simplices in Rips complexes across multiple thresholds (0.1 to 1.0) and dimensions ($d_{\max} = 1$ to 4) [170]. This method captures the scaling behavior of brain connectivity, revealing how topological features emerge at varying connectivity thresholds [171]. The fractal dimension was calculated as the slope of the log-log relationship between the number of simplices and the thresholds, providing a quantitative measure of the network's self-similarity and multi-scale organization [172]. Lower dimensions ($d_{\max} = 1$) capture basic connectivity patterns, while higher dimensions ($d_{\max} = 2, 3, 4$) represent more intricate features such as loops and voids, indicative of complex network interactions.

In this study, persistence entropy, derived from persistent homology, quantifies the variability of topological features, such as connected components and loops, as they persist across multiple thresholds in Rips complexes. [20]. Using the Gudhi library, we calculated persistence entropy from Rips complexes and persistence diagrams, capturing the variability of these topological features across thresholds ranging from 0.1 to 1.0. This measure effectively captures the distribution and lifespan of topological features [20, 173–175].

Acknowledgements. We thank Marius Oechsner for his insightful suggestions on brain lateralization analysis, particularly the distinctions between left and right hemispheres, and his invaluable support throughout this work.

References

[1] Lord, C., Brugha, T.S., Charman, T., Cusack, J., Dumas, G., Frazier, T., Jones, E.J., Jones, R.M., Pickles, A., State, M.W., *et al.*: Autism spectrum disorder. Nature reviews Disease primers **6**(1), 1–23 (2020)

[2] Al-Beltagi, M.: Autism medical comorbidities. World journal of clinical pediatrics **10**(3), 15 (2021)

[3] Bertelsen, N., Landi, I., Bethlehem, R.A., Seidlitz, J., Busuoli, E.M., Mandelli, V., Satta, E., Trakoshis, S., Auyeung, B., Kundu, P., *et al.*: Imbalanced social-communicative and restricted repetitive behavior subtypes of autism spectrum disorder exhibit different neural circuitry. Communications biology **4**(1), 574 (2021)

[4] Towbin, K.E.: Pervasive developmental disorder not otherwise specified. Handbook of autism and pervasive developmental disorders **1**, 165–200 (2005)

[5] Klin, A., McPartland, J., Volkmar, F.R.: Asperger syndrome. Handbook of autism and pervasive developmental disorders **1**, 88–125 (2005)

[6] Nuckols, C.C., Nuckols, C.C.: The diagnostic and statistical manual of mental disorders,(dsm-5). Philadelphia: American Psychiatric Association (2013)

[7] Wing, L., Gould, J., Gillberg, C.: Autism spectrum disorders in the dsm-v: better or worse than the dsm-iv? Research in developmental disabilities **32**(2), 768–773 (2011)

[8] Aronowitz, B.R., Decaria, C., Allen, A., Weiss, N., Saunders, A., Margolin, L., Mosovich, S., Baum, M., Hollander, E.: The neuropsychiatry of autism and asperger's disorder: review of the literature and case reports. CNS spectrums **2**(5), 43–60 (1997)

[9] Enticott, P.G., Rinehart, N.J., Tonge, B.J., Bradshaw, J.L., Fitzgerald, P.B.: A preliminary transcranial magnetic stimulation study of cortical inhibition and excitability in high-functioning autism and asperger disorder. Developmental Medicine & Child Neurology **52**(8), 179–183 (2010)

[10] Fombonne, E.: Epidemiology of pervasive developmental disorders. Pediatric research **65**(6), 591–598 (2009)

[11] Kok, F.M., Groen, Y., Becke, M., Fuermaier, A.B., Tucha, O.: Self-reported empathy in adult women with autism spectrum disorders–a systematic mini

review. PloS one **11**(3), 0151568 (2016)

[12] Constantino, J.N., Charman, T.: Diagnosis of autism spectrum disorder: reconciling the syndrome, its diverse origins, and variation in expression. The Lancet Neurology **15**(3), 279–291 (2016)

[13] Ahmadlou, M., Adeli, H., Adeli, A.: Fuzzy synchronization likelihood-wavelet methodology for diagnosis of autism spectrum disorder. Journal of neuroscience methods **211**(2), 203–209 (2012)

[14] Eldridge, J., Lane, A.E., Belkin, M., Dennis, S.: Robust features for the automatic identification of autism spectrum disorder in children. Journal of neurodevelopmental disorders **6**(1), 1–12 (2014)

[15] Uddin, L.Q., Supekar, K., Lynch, C.J., Khouzam, A., Phillips, J., Feinstein, C., Ryali, S., Menon, V.: Salience network–based classification and prediction of symptom severity in children with autism. JAMA psychiatry **70**(8), 869–879 (2013)

[16] Al-Hiyali, M.I., Yahya, N., Faye, I., Hussein, A.F.: Identification of autism subtypes based on wavelet coherence of bold fmri signals using convolutional neural network. Sensors **21**(16), 5256 (2021)

[17] Usta, M.B., Karabekiroglu, K., Sahin, B., Aydin, M., Bozkurt, A., Karaosman, T., Aral, A., Cobanoglu, C., Kurt, A.D., Kesim, N., *et al.*: Use of machine learning methods in prediction of short-term outcome in autism spectrum disorders. Psychiatry and Clinical Psychopharmacology **29**(3), 320–325 (2019)

[18] Thapa, R., Garikipati, A., Ciobanu, M., Singh, N., Browning, E., DeCurzio, J., Barnes, G., Dinenno, F., Mao, Q., Das, R.: Machine learning differentiation of autism spectrum sub-classifications. Journal of Autism and Developmental Disorders, 1–16 (2023)

[19] Abraham, A., Pedregosa, F., Eickenberg, M., Gervais, P., Mueller, A., Kossaifi, J., Gramfort, A., Thirion, B., Varoquaux, G.: Machine learning for neuroimaging with scikit-learn. Frontiers in neuroinformatics **8**, 14 (2014)

[20] Benigni, B., Ghavasieh, A., Corso, A., d'Andrea, V., De Domenico, M.: Persistence of information flow: A multiscale characterization of human brain. Network Neuroscience **5**(3), 831–850 (2021)

[21] Li, Z., Li, X., Li, M., Zhang, K., Zhang, X., Zhou, X.: Evaluation of human epileptic brain networks by constructing simplicial complexes. Chaos, Solitons & Fractals **189**, 115699 (2024)

[22] Keehn, B., Vogel-Farley, V., Tager-Flusberg, H., Nelson, C.A.: Atypical hemispheric specialization for faces in infants at risk for autism spectrum disorder.

Autism Research **8**(2), 187–198 (2015)

[23] Peterson, M., Prigge, M.B., Floris, D.L., Bigler, E.D., Zielinski, B.A., King, J.B., Lange, N., Alexander, A.L., Lainhart, J.E., Nielsen, J.A.: Reduced lateralization of multiple functional brain networks in autistic males. Journal of Neurodevelopmental Disorders **16**(1), 23 (2024)

[24] Bottou, L., Lin, C.-J.: Support vector machine solvers. Large scale kernel machines **3**(1), 301–320 (2007)

[25] Tolles, J., Meurer, W.J.: Logistic regression: relating patient characteristics to outcomes. Jama **316**(5), 533–534 (2016)

[26] Breiman, L.: Random forests. Machine learning **45**(1), 5–32 (2001)

[27] Hinton, G., Rumelhart, D., Williams, R.: Learning internal representations by error propagation. Parallel distributed processing **1**, 318–362 (1986)

[28] Schmidhuber, J.: Deep learning in neural networks: An overview. Neural networks **61**, 85–117 (2015)

[29] LeCun, Y., Bengio, Y., Hinton, G.: Deep learning. nature **521**(7553), 436–444 (2015)

[30] Mincholé, A., Rodriguez, B.: Artificial intelligence for the electrocardiogram. Nature medicine **25**(1), 22–23 (2019)

[31] Tolkach, Y., Dohmgörgen, T., Toma, M., Kristiansen, G.: High-accuracy prostate cancer pathology using deep learning. Nature Machine Intelligence **2**(7), 411–418 (2020)

[32] Dukart, J., Weis, S., Genon, S., Eickhoff, S.B.: Towards increasing the clinical applicability of machine learning biomarkers in psychiatry. Nature Human Behaviour **5**(4), 431–432 (2021)

[33] Li, R.C., Asch, S.M., Shah, N.H.: Developing a delivery science for artificial intelligence in healthcare. NPJ digital medicine **3**(1), 1–3 (2020)

[34] Park, Y., Kellis, M.: Deep learning for regulatory genomics. Nature biotechnology **33**(8), 825–826 (2015)

[35] Ito, Y., Unagami, M., Yamabe, F., Mitsui, Y., Nakajima, K., Nagao, K., Kobayashi, H.: A method for utilizing automated machine learning for histopathological classification of testis based on johnsen scores. Scientific reports **11**(1), 1–11 (2021)

[36] Kim, J., Lee, J., Park, E., Han, J.: A deep learning model for detecting mental illness from user content on social media. Scientific reports **10**(1), 1–6 (2020)

[37] Li, Y., Nowak, C.M., Pham, U., Nguyen, K., Bleris, L.: Cell morphology-based machine learning models for human cell state classification. NPJ systems biology and applications **7**(1), 1–9 (2021)

[38] Yu, X., Pang, W., Xu, Q., Liang, M.: Mammographic image classification with deep fusion learning. Scientific Reports **10**(1), 1–11 (2020)

[39] Bracher-Smith, M., Crawford, K., Escott-Price, V.: Machine learning for genetic prediction of psychiatric disorders: a systematic review. Molecular Psychiatry **26**(1), 70–79 (2021)

[40] Patel, D., Kher, V., Desai, B., Lei, X., Cen, S., Nanda, N., Gholamrezanezhad, A., Duddalwar, V., Varghese, B., Oberai, A.A.: Machine learning based predictors for covid-19 disease severity. Scientific Reports **11**(1), 1–7 (2021)

[41] Krittanawong, C., Virk, H.U.H., Kumar, A., Aydar, M., Wang, Z., Stewart, M.P., Halperin, J.L.: Machine learning and deep learning to predict mortality in patients with spontaneous coronary artery dissection. Scientific reports **11**(1), 1–10 (2021)

[42] Ferri, C., Hernández-Orallo, J., Salido, M.A.: Volume under the roc surface for multi-class problems. In: European Conference on Machine Learning, pp. 108–120 (2003). Springer

[43] Prottasha, N.J., Murad, S.A., Muzahid, A.J.M., Rana, M., Kowsher, M., Adhikary, A., Biswas, S., Bairagi, A.K.: Impact learning: A learning method from feature's impact and competition. Journal of Computational Science **69**, 102011 (2023)

[44] Megahed, F.M., Chen, Y.-J., Megahed, A., Ong, Y., Altman, N., Krzywinski, M.: The class imbalance problem. Nat Methods **18**(11), 1270–2 (2021)

[45] Gao, Z., Liu, X., Zhang, D., Liu, M., Hao, N.: The indispensable role of the cerebellum in visual divergent thinking. Scientific reports **10**(1), 16552 (2020)

[46] Lehman, V.T., Black, D.F., DeLone, D.R., Blezek, D.J., Kaufmann, T.J., Brinjikji, W., Welker, K.M.: Current concepts of cross-sectional and functional anatomy of the cerebellum: a pictorial review and atlas. The British Journal of Radiology **93**(1106), 20190467 (2020)

[47] Mijalkov, M., Kakaei, E., Pereira, J.B., Westman, E., Volpe, G., Initiative, A.D.N.: Braph: a graph theory software for the analysis of brain connectivity. PloS one **12**(8), 0178798 (2017)

[48] Memarzadeh, H., Ghadiri, N., Samwald, M., Lotfi Shahreza, M.: A study into patient similarity through representation learning from medical records. Knowledge and Information Systems **64**(12), 3293–3324 (2022)

[49] Zheng, T., Gao, Y., Wang, F., Fan, C., Fu, X., Li, M., Zhang, Y., Zhang, S., Ma, H.: Detection of medical text semantic similarity based on convolutional neural network. BMC medical informatics and decision making **19**, 1–11 (2019)

[50] Sebenius, I., Seidlitz, J., Warrier, V., Bethlehem, R.A., Alexander-Bloch, A., Mallard, T.T., Garcia, R.R., Bullmore, E.T., Morgan, S.E.: Robust estimation of cortical similarity networks from brain mri. Nature Neuroscience **26**(8), 1461–1471 (2023)

[51] Alves, C.L., Pineda, A.M., Roster, K., Thielemann, C., Rodrigues, F.A.: Eeg functional connectivity and deep learning for automatic diagnosis of brain disorders: Alzheimer's disease and schizophrenia. Journal of Physics: complexity **3**(2), 025001 (2022)

[52] Alves, C.L., Cury, R.G., Roster, K., Pineda, A.M., Rodrigues, F.A., Thielemann, C., Ciba, M.: Application of machine learning and complex network measures to an eeg dataset from ayahuasca experiments. Plos one **17**(12), 0277257 (2022)

[53] Alves, C.L., Toutain, T.G.d.O., Carvalho Aguiar, P., Pineda, A.M., Roster, K., Thielemann, C., Porto, J.A.M., Rodrigues, F.A.: Diagnosis of autism spectrum disorder based on functional brain networks and machine learning. Scientific Reports **13**(1), 8072 (2023)

[54] Alves, C.L., Toutain, T.G.d.O., Porto, J.A.M., Aguiar, P.M.d.C., Pineda, A., Rodrigues, F.A., Sena, E.P., Thielemann, C.: Analysis of functional connectivity using machine learning and deep learning in different data modalities from individuals with schizophrenia. Journal of Neural Engineering (2023)

[55] Alves, C., Wissel, L., Capetian, P., Thielemann, C.: P 55 functional connectivity and convolutional neural networks for automatic classification of eeg data. Clinical Neurophysiology **137**, 47 (2022)

[56] Albert, R., Barabási, A.-L.: Statistical mechanics of complex networks. Reviews of modern physics **74**(1), 47 (2002)

[57] Hage, P., Harary, F.: Eccentricity and centrality in networks. Social networks **17**(1), 57–63 (1995)

[58] Freeman, L.C.: Centrality in social networks conceptual clarification. Social networks **1**(3), 215–239 (1978)

[59] Albert, R., Jeong, H., Barabási, A.-L.: Diameter of the world-wide web. nature **401**(6749), 130–131 (1999)

[60] Anderson, B.S., Butts, C., Carley, K.: The interaction of size and density with graph-level indices. Social networks **21**(3), 239–267 (1999)

[61] Freeman, L.C.: A set of measures of centrality based on betweenness. Sociometry, 35–41 (1977)

[62] Kleinberg, J.M.: Hubs, authorities, and communities. ACM computing surveys (CSUR) **31**(4es), 5 (1999)

[63] Bonacich, P.: Power and centrality: A family of measures. American journal of sociology **92**(5), 1170–1182 (1987)

[64] Newman, M.E.: The structure and function of complex networks. SIAM review **45**(2), 167–256 (2003)

[65] Newman, M.E.: Assortative mixing in networks. Physical review letters **89**(20), 208701 (2002)

[66] Eppstein, D., Paterson, M.S., Yao, F.F.: On nearest-neighbor graphs. Discrete & Computational Geometry **17**(3), 263–282 (1997)

[67] Snijders, T.A.: The degree variance: an index of graph heterogeneity. Social networks **3**(3), 163–174 (1981)

[68] Doyle, J., Graver, J.: Mean distance in a graph. Discrete Mathematics **17**(2), 147–154 (1977)

[69] Dehmer, M., Mowshowitz, A.: A history of graph entropy measures. Information Sciences **181**(1), 57–78 (2011)

[70] Watts, D.J., Strogatz, S.H.: Collective dynamics of 'small-world'networks. Nature **393**(6684), 440–442 (1998)

[71] Newman, M.E., Watts, D.J., Strogatz, S.H.: Random graph models of social networks. Proceedings of the National Academy of Sciences **99**(suppl 1), 2566–2572 (2002)

[72] Seidman, S.B.: Network structure and minimum degree. Social networks **5**(3), 269–287 (1983)

[73] Latora, V., Marchiori, M.: Economic small-world behavior in weighted networks. The European Physical Journal B-Condensed Matter and Complex Systems **32**(2), 249–263 (2003)

[74] Newman, M.E.: Communities, modules and large-scale structure in networks. Nature physics **8**(1), 25–31 (2012)

[75] Kim, J., Lee, J.-G.: Community detection in multi-layer graphs: A survey. ACM SIGMOD Record **44**(3), 37–48 (2015)

[76] Zhao, X., Liang, J., Wang, J.: A community detection algorithm based on graph

compression for large-scale social networks. Information Sciences **551**, 358–372 (2021)

[77] Clauset, A., Newman, M.E., Moore, C.: Finding community structure in very large networks. Physical review E **70**(6), 066111 (2004)

[78] Rosvall, M., Axelsson, D., Bergstrom, C.T.: The map equation. The European Physical Journal Special Topics **178**(1), 13–23 (2009)

[79] Newman, M.E.: Finding community structure in networks using the eigenvectors of matrices. Physical review E **74**(3), 036104 (2006)

[80] Raghavan, U.N., Albert, R., Kumara, S.: Near linear time algorithm to detect community structures in large-scale networks. Physical review E **76**(3), 036106 (2007)

[81] Girvan, M., Newman, M.E.: Community structure in social and biological networks. Proceedings of the national academy of sciences **99**(12), 7821–7826 (2002)

[82] Reichardt, J., Bornholdt, S.: Statistical mechanics of community detection. Physical review E **74**(1), 016110 (2006)

[83] Blondel, V.D., Guillaume, J.-L., Lambiotte, R., Lefebvre, E.: Fast unfolding of communities in large networks. Journal of statistical mechanics: theory and experiment **2008**(10), 10008 (2008)

[84] Sporns, O.: Network attributes for segregation and integration in the human brain. Current opinion in neurobiology **23**(2), 162–171 (2013)

[85] Tononi, G., Sporns, O., Edelman, G.M.: A measure for brain complexity: relating functional segregation and integration in the nervous system. Proceedings of the National Academy of Sciences **91**(11), 5033–5037 (1994)

[86] Park, H.-J., Friston, K.: Structural and functional brain networks: from connections to cognition. Science **342**(6158), 1238411 (2013)

[87] Sporns, O.: The non-random brain: efficiency, economy, and complex dynamics. Frontiers in computational neuroscience **5**, 5 (2011)

[88] Sporns, O.: Structure and function of complex brain networks. Dialogues in clinical neuroscience (2022)

[89] Avena-Koenigsberger, A., Misic, B., Sporns, O.: Communication dynamics in complex brain networks. Nature reviews neuroscience **19**(1), 17–33 (2018)

[90] Dapretto, M., Davies, M.S., Pfeifer, J.H., Scott, A.A., Sigman, M., Bookheimer, S.Y., Iacoboni, M.: Understanding emotions in others: mirror neuron dysfunction

in children with autism spectrum disorders. Nature neuroscience **9**(1), 28–30 (2006)

[91] Kana, R.K., Keller, T.A., Minshew, N.J., Just, M.A.: Inhibitory control in high-functioning autism: decreased activation and underconnectivity in inhibition networks. Biological psychiatry **62**(3), 198–206 (2007)

[92] Fatemi, S.H., Aldinger, K.A., Ashwood, P., Bauman, M.L., Blaha, C.D., Blatt, G.J., Chauhan, A., Chauhan, V., Dager, S.R., Dickson, P.E., *et al.*: Consensus paper: pathological role of the cerebellum in autism. The Cerebellum **11**, 777–807 (2012)

[93] Stoodley, C.J.: Distinct regions of the cerebellum show gray matter decreases in autism, adhd, and developmental dyslexia. Frontiers in systems neuroscience **8**, 92 (2014)

[94] Baron-Cohen, S., Ring, H.A., Bullmore, E.T., Wheelwright, S., Ashwin, C., Williams, S.: The amygdala theory of autism. Neuroscience & Biobehavioral Reviews **24**(3), 355–364 (2000)

[95] Schultz, R.T.: Developmental deficits in social perception in autism: the role of the amygdala and fusiform face area. International Journal of Developmental Neuroscience **23**(2-3), 125–141 (2005)

[96] Di Cristo, G.: Development of cortical gabaergic circuits and its implications for neurodevelopmental disorders. Clinical genetics **72**(1), 1–8 (2007)

[97] Marco, E.J., Hinkley, L.B., Hill, S.S., Nagarajan, S.S.: Sensory processing in autism: a review of neurophysiologic findings. Pediatric research **69**(8), 48–54 (2011)

[98] Simmons, D.R., Robertson, A.E., McKay, L.S., Toal, E., McAleer, P., Pollick, F.E.: Vision in autism spectrum disorders. Vision research **49**(22), 2705–2739 (2009)

[99] Latora, V., Marchiori, M.: Efficient behavior of small-world networks. Physical review letters **87**(19), 198701 (2001)

[100] Vragović, I., Louis, E., Díaz-Guilera, A.: Efficiency of informational transfer in regular and complex networks. Physical Review E—Statistical, Nonlinear, and Soft Matter Physics **71**(3), 036122 (2005)

[101] Wasserman, S.: Social network analysis: Methods and applications. The Press Syndicate of the University of Cambridge (1994)

[102] Barrat, A., Barthelemy, M., Pastor-Satorras, R., Vespignani, A.: The architecture of complex weighted networks. Proceedings of the national academy of

sciences **101**(11), 3747–3752 (2004)

[103] Jolliffe, T., Baron-Cohen, S.: A test of central coherence theory: linguistic processing in high-functioning adults with autism or asperger syndrome: is local coherence impaired? Cognition **71**(2), 149–185 (1999)

[104] Rinehart, N.J., Bradshaw, J.L., Moss, S.A., Brereton, A.V., Tonge, B.J.: Atypical interference of local detail on global processing in high-functioning autism and asperger's disorder. The Journal of Child Psychology and Psychiatry and Allied Disciplines **41**(6), 769–778 (2000)

[105] Loukusa, S., Moilanen, I.: Pragmatic inference abilities in individuals with asperger syndrome or high-functioning autism. a review. Research in Autism Spectrum Disorders **3**(4), 890–904 (2009)

[106] Szatmari, P., Archer, L., Fisman, S., Streiner, D.L., Wilson, F.: Asperger's syndrome and autism: Differences in behavior, cognition, and adaptive functioning. Journal of the American Academy of Child & Adolescent Psychiatry **34**(12), 1662–1671 (1995)

[107] Iwanaga, R., Kawasaki, C., Tsuchida, R.: Brief report: Comparison of sensory-motor and cognitive function between autism and asperger syndrome in preschool children. Journal of Autism and Developmental Disorders **30**(2), 169 (2000)

[108] Whitby, P.J.S., Mancil, G.R.: Academic achievement profiles of children with high functioning autism and asperger syndrome: A review of the literature. Education and Training in Developmental Disabilities, 551–560 (2009)

[109] Javaheripour, N., Wagner, G., Cruz, F., Walter, M., Szycik, G.R., Tietze, F.-A.: Altered brain network organization in adults with asperger's syndrome: decreased connectome transitivity and assortativity with increased global efficiency. Frontiers in Psychiatry **14**, 1223147 (2023)

[110] Bhat, A., McDonald, N., Eilbott, J., Pelphrey, K.: Exploring cortical activation and connectivity in infants with and without familial risk for autism during naturalistic social interactions: a preliminary study. Infant Behavior and Development **57**, 101337 (2019)

[111] Gunter, H.L., Ghaziuddin, M., Ellis, H.D.: Asperger syndrome: Tests of right hemisphere functioning and interhemispheric communication. Journal of autism and developmental disorders **32**, 263–281 (2002)

[112] Kevin, K.Y., Cheung, C., Chua, S.E., McAlonan, G.M.: Can asperger syndrome be distinguished from autism? an anatomic likelihood meta-analysis of mri studies. Journal of Psychiatry and Neuroscience **36**(6), 412–421 (2011)

[113] Ellis, H.D., Ellis, D.M., Fraser, W., Deb, S.: A preliminary study of right hemisphere cognitive deficits and impaired social judgments among young people with asperger syndrome. European child & adolescent psychiatry **3**, 255–266 (1994)

[114] McKelvey, J.R., Lambert, R., Mottron, L., Shevell, M.I.: Right-hemisphere dysfunction in asperger's syndrome. Journal of Child Neurology **10**(4), 310–314 (1995)

[115] Kunce, L., Mesibov, G.B.: Educational approaches to high-functioning autism and asperger syndrome. Asperger syndrome or high-functioning autism?, 227–261 (1998)

[116] Minshew, N.J., Goldstein, G., Siegel, D.J.: Neuropsychologic functioning in autism: Profile of a complex information processing disorder. Journal of the International Neuropsychological society **3**(4), 303–316 (1997)

[117] Laurent, A.C., Rubin, E.: Challenges in emotional regulation in asperger syndrome and high-functioning autism. Topics in Language Disorders **24**(4), 286–297 (2004)

[118] Meilleur, A.-A.S., Jelenic, P., Mottron, L.: Prevalence of clinically and empirically defined talents and strengths in autism. Journal of autism and developmental disorders **45**, 1354–1367 (2015)

[119] Vickerstaff, S., Heriot, S., Wong, M., Lopes, A., Dossetor, D.: Intellectual ability, self-perceived social competence, and depressive symptomatology in children with high-functioning autistic spectrum disorders. Journal of autism and developmental disorders **37**, 1647–1664 (2007)

[120] Gainotti, G.: Emotions and the right hemisphere: can new data clarify old models? The Neuroscientist **25**(3), 258–270 (2019)

[121] Heilman, K.M., Bowers, D., Valenstein, E., Watson, R.T.: The right hemisphere: neuropsychological functions. Journal of neurosurgery **64**(5), 693–704 (1986)

[122] Minshew, N.J., Goldstein, G., Siegel, D.J.: Speech and language in high-functioning autistic individuals. Neuropsychology **9**(2), 255 (1995)

[123] Orfanos, D.P., Michel, V., Schwartz, Y., Pinel, P., Moreno, A., Le Bihan, D., Frouin, V.: The brainomics/localizer database. NeuroImage **144**, 309–314 (2017)

[124] Rubin, T.N., Koyejo, O., Gorgolewski, K.J., Jones, M.N., Poldrack, R.A., Yarkoni, T.: Decoding brain activity using a large-scale probabilistic functional-anatomical atlas of human cognition. PLoS computational biology **13**(10), 1005649 (2017)

[125] Kumar, M., Ellis, C.T., Lu, Q., Zhang, H., Capotă, M., Willke, T.L., Ramadge, P.J., Turk-Browne, N.B., Norman, K.A.: Brainiak tutorials: User-friendly learning materials for advanced fmri analysis. PLoS computational biology **16**(1), 1007549 (2020)

[126] Lawrence, R.M., Bridgeford, E.W., Myers, P.E., Arvapalli, G.C., Ramachandran, S.C., Pisner, D.A., Frank, P.F., Lemmer, A.D., Nikolaidis, A., Vogelstein, J.T.: Standardizing human brain parcellations. Scientific data **8**(1), 78 (2021)

[127] Walsh, J., Othmani, A., Jain, M., Dev, S.: Using u-net network for efficient brain tumor segmentation in mri images. Healthcare Analytics **2**, 100098 (2022)

[128] Subah, F.Z., Deb, K., Dhar, P.K., Koshiba, T.: A deep learning approach to predict autism spectrum disorder using multisite resting-state fmri. Applied Sciences **11**(8), 3636 (2021)

[129] Bellec, P., Rosa-Neto, P., Lyttelton, O.C., Benali, H., Evans, A.C.: Multi-level bootstrap analysis of stable clusters in resting-state fmri. Neuroimage **51**(3), 1126–1139 (2010)

[130] Dadi, K., Rahim, M., Abraham, A., Chyzhyk, D., Milham, M., Thirion, B., Varoquaux, G., Initiative, A.D.N., *et al.*: Benchmarking functional connectome-based predictive models for resting-state fmri. NeuroImage **192**, 115–134 (2019)

[131] Yang, X., Zhang, N., Schrader, P.: A study of brain networks for autism spectrum disorder classification using resting-state functional connectivity. Machine Learning with Applications **8**, 100290 (2022)

[132] Lubinski, D.: Introduction to the special section on cognitive abilities: 100 years after spearman's (1904)"'general intelligence,'objectively determined and measured". Journal of personality and social psychology **86**(1), 96 (2004)

[133] Bazyar, S., Ramalho, J., Eldeniz, C., An, H., Lee, Y.Z.: Comparison of cerebral blood volume and plasma volume in untreated intracranial tumors. Plos one **11**(9), 0161807 (2016)

[134] Widman, G., Schreiber, T., Rehberg, B., Hoeft, A., Elger, C.: Quantification of depth of anesthesia by nonlinear time series analysis of brain electrical activity. Physical Review E **62**(4), 4898 (2000)

[135] Murphy, M.C., Jones, D.T., Jack Jr, C.R., Glaser, K.J., Senjem, M.L., Manduca, A., Felmlee, J.P., Carter, R.E., Ehman, R.L., Huston III, J.: Regional brain stiffness changes across the alzheimer's disease spectrum. NeuroImage: Clinical **10**, 283–290 (2016)

[136] Bisong, E., Bisong, E.: Introduction to scikit-learn. Building Machine Learning and Deep Learning Models on Google Cloud Platform: A Comprehensive Guide

for Beginners, 215–229 (2019)

[137] Kim, D.W., Lee, S., Kwon, S., Nam, W., Cha, I.-H., Kim, H.J.: Deep learning-based survival prediction of oral cancer patients. Scientific reports **9**(1), 6994 (2019)

[138] Su, Q., Liu, Q., Lau, R.I., Zhang, J., Xu, Z., Yeoh, Y.K., Leung, T.W., Tang, W., Zhang, L., Liang, J.Q., *et al.*: Faecal microbiome-based machine learning for multi-class disease diagnosis. Nature Communications **13**(1), 6818 (2022)

[139] Singh, V., Pencina, M., Einstein, A.J., Liang, J.X., Berman, D.S., Slomka, P.: Impact of train/test sample regimen on performance estimate stability of machine learning in cardiovascular imaging. Scientific reports **11**(1), 14490 (2021)

[140] Avuçlu, E., Elen, A.: Evaluation of train and test performance of machine learning algorithms and parkinson diagnosis with statistical measurements. Medical & Biological Engineering & Computing **58**, 2775–2788 (2020)

[141] Brownlee, J.: How to choose a feature selection method for machine learning. Machine Learning Mastery **10** (2019)

[142] Mahesh, T., Geman, O., Margala, M., Guduri, M., *et al.*: The stratified k-folds cross-validation and class-balancing methods with high-performance ensemble classifiers for breast cancer classification. Healthcare Analytics **4**, 100247 (2023)

[143] Shah, A.A., Khan, Y.D.: Identification of 4-carboxyglutamate residue sites based on position based statistical feature and multiple classification. Scientific Reports **10**(1), 1–10 (2020)

[144] Bengio, Y., Grandvalet, Y.: No unbiased estimator of the variance of k-fold cross-validation. Journal of machine learning research **5**(Sep), 1089–1105 (2004)

[145] Chan, J., Rea, T., Gollakota, S., Sunshine, J.E.: Contactless cardiac arrest detection using smart devices. NPJ digital medicine **2**(1), 1–8 (2019)

[146] Kawamoto, T., Kabashima, Y.: Cross-validation estimate of the number of clusters in a network. Scientific reports **7**(1), 1–17 (2017)

[147] Lopez-Martin, M., Nevado, A., Carro, B.: Detection of early stages of alzheimer's disease based on meg activity with a randomized convolutional neural network. Artificial Intelligence in Medicine **107**, 101924 (2020)

[148] Zhong, Z., Yuan, X., Liu, S., Yang, Y., Liu, F.: Machine learning prediction models for prognosis of critically ill patients after open-heart surgery. Scientific Reports **11**(1), 1–10 (2021)

[149] Sato, M., Morimoto, K., Kajihara, S., Tateishi, R., Shiina, S., Koike, K., Yatomi,

Y.: Machine-learning approach for the development of a novel predictive model for the diagnosis of hepatocellular carcinoma. Scientific reports **9**(1), 1–7 (2019)

[150] Arcadu, F., Benmansour, F., Maunz, A., Willis, J., Haskova, Z., Prunotto, M.: Author correction: Deep learning algorithm predicts diabetic retinopathy progression in individual patients. NPJ digital medicine **3**(1), 1–6 (2020)

[151] Rashidi, H.H., Sen, S., Palmieri, T.L., Blackmon, T., Wajda, J., Tran, N.K.: Early recognition of burn-and trauma-related acute kidney injury: a pilot comparison of machine learning techniques. Scientific reports **10**(1), 1–9 (2020)

[152] Bischl, B., Binder, M., Lang, M., Pielok, T., Richter, J., Coors, S., Thomas, J., Ullmann, T., Becker, M., Boulesteix, A.-L., *et al.*: Hyperparameter optimization: Foundations, algorithms, best practices, and open challenges. Wiley Interdisciplinary Reviews: Data Mining and Knowledge Discovery **13**(2), 1484 (2023)

[153] Richhariya, B., Tanveer, M., Rashid, A.H., Initiative, A.D.N., *et al.*: Diagnosis of alzheimer's disease using universum support vector machine based recursive feature elimination (usvm-rfe). Biomedical Signal Processing and Control **59**, 101903 (2020)

[154] Yang, M., Wu, Y., Yang, X.-b., Liu, T., Zhang, Y., Zhuo, Y., Luo, Y., Zhang, N.: Establishing a prediction model of severe acute mountain sickness using machine learning of support vector machine recursive feature elimination. Scientific Reports **13**(1), 4633 (2023)

[155] Wu, Z., Chen, H., Ke, S., Mo, L., Qiu, M., Zhu, G., Zhu, W., Liu, L.: Identifying potential biomarkers of idiopathic pulmonary fibrosis through machine learning analysis. Scientific Reports **13**(1), 16559 (2023)

[156] Gadalla, A.A., Friberg, I.M., Kift-Morgan, A., Zhang, J., Eberl, M., Topley, N., Weeks, I., Cuff, S., Wootton, M., Gal, M., *et al.*: Identification of clinical and urine biomarkers for uncomplicated urinary tract infection using machine learning algorithms. Scientific reports **9**(1), 19694 (2019)

[157] Kruskal, W.H., Wallis, W.A.: Use of ranks in one-criterion variance analysis. Journal of the American statistical Association **47**(260), 583–621 (1952)

[158] Mann, H.B., Whitney, D.R.: On a test of whether one of two random variables is stochastically larger than the other. The annals of mathematical statistics, 50–60 (1947)

[159] Wilcoxon, F.: Probability tables for individual comparisons by ranking methods. Biometrics **3**(3), 119–122 (1947)

[160] Andrade, C.: Multiple testing and protection against a type 1 (false positive) error using the bonferroni and hochberg corrections. Indian journal of psychological medicine **41**(1), 99–100 (2019)

[161] Dunn, O.J.: Multiple comparisons among means. Journal of the American statistical association **56**(293), 52–64 (1961)

[162] Das, S., Anand, D.V., Chung, M.K.: Topological data analysis of human brain networks through order statistics. Plos one **18**(3), 0276419 (2023)

[163] Khan, M.S.: An approach to extract topological information from intuitionistic fuzzy sets and their application in obtaining a natural hierarchical clustering algorithm. Applied Soft Computing **160**, 111691 (2024)

[164] Carlsson, G.: Topological methods for data modelling. Nature Reviews Physics **2**(12), 697–708 (2020)

[165] El-Yaagoubi, A.B., Chung, M.K., Ombao, H.: Dynamic topological data analysis: a novel fractal dimension-based testing framework with application to brain signals. Frontiers in Neuroinformatics **18**, 1387400 (2024)

[166] Maria, C., Boissonnat, J.-D., Glisse, M., Yvinec, M.: The gudhi library: Simplicial complexes and persistent homology. In: Mathematical Software–ICMS 2014: 4th International Congress, Seoul, South Korea, August 5-9, 2014. Proceedings 4, pp. 167–174 (2014). Springer

[167] Estrada, E., Ross, G.J.: Centralities in simplicial complexes. applications to protein interaction networks. Journal of theoretical biology **438**, 46–60 (2018)

[168] Xia, K., Feng, X., Tong, Y., Wei, G.W.: Persistent homology for the quantitative prediction of fullerene stability. Journal of computational chemistry **36**(6), 408–422 (2015)

[169] Baccini, F., Geraci, F., Bianconi, G.: Weighted simplicial complexes and their representation power of higher-order network data and topology. Physical Review E **106**(3), 034319 (2022)

[170] Datseris, G., Kottlarz, I., Braun, A.P., Parlitz, U.: Estimating fractal dimensions: A comparative review and open source implementations. Chaos: An Interdisciplinary Journal of Nonlinear Science **33**(10) (2023)

[171] Hahn, K., Massopust, P.R., Prigarin, S.: A new method to measure complexity in binary or weighted networks and applications to functional connectivity in the human brain. BMC bioinformatics **17**, 1–18 (2016)

[172] De, S., Mitra, D., Pandit, R.: Dynamic multiscaling in stochastically forced burgers turbulence. Scientific Reports **13**(1), 7151 (2023)

[173] Xia, K., Li, Z., Mu, L.: Multiscale persistent functions for biomolecular structure characterization. Bulletin of mathematical biology **80**, 1–31 (2018)

[174] Aktas, M.E., Akbas, E., Fatmaoui, A.E.: Persistence homology of networks: methods and applications. Applied Network Science **4**(1), 1–28 (2019)

[175] Arfi, B.: The promises of persistent homology, machine learning, and deep neural networks in topological data analysis of democracy survival. Quality & Quantity **58**(2), 1685–1727 (2024)

A SHAP values plot

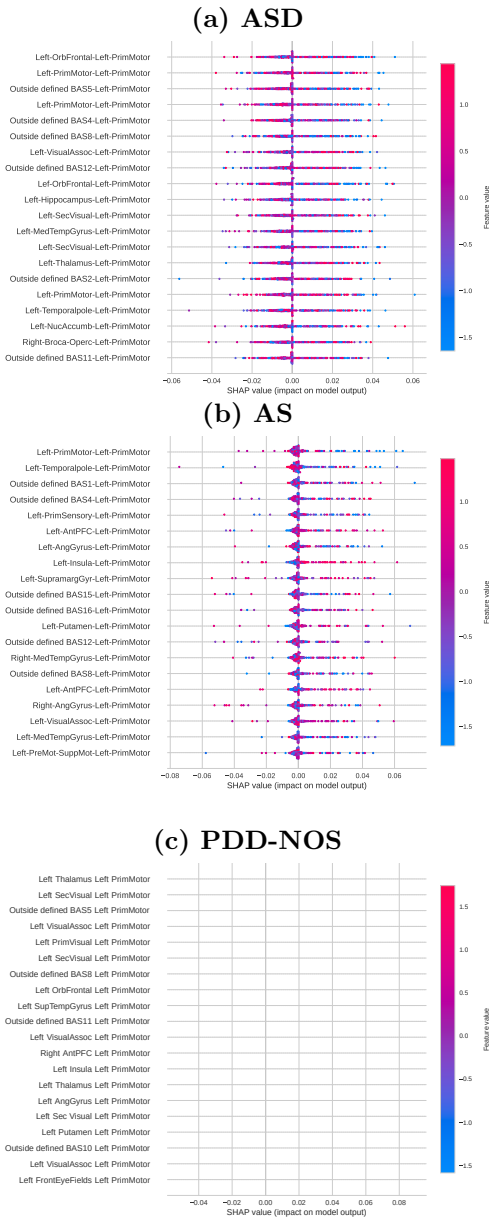

Fig. 12 Feature importance ranking using the SHAP values methodology for the SVM classifier, with brain regions in descending order: (a) Feature importance ranking for the ASD class. (b) Feature importance ranking for the AS class. (c) Feature importance ranking for the PDD-NOS class.

B Complex Network Measures Across Regions

The boxplot figures in 13 illustrate the statistical differences in complex network measures between ASD and AS groups across the cortex, left, and right hemispheres. To facilitate comparisons and emphasize distinctions between ASD and AS, the TD baseline has been excluded from these figures. This adjustment enables a more focused analysis of the specific differences between ASD and AS groups. The figures visually support the summarized results in Table 2, highlighting regional differences in measures such as diameter, CC, AEBC, AIC, ALPC, and efficiency. Specifically, the figures show higher diameter values for AS compared to ASD across all regions, as well as lower CC and efficiency values for AS compared to ASD in the cortex. Non-significant differences (ns) in measures such as CC and efficiency in the left and right hemispheres further emphasize the localized nature of these distinctions in the cortex.

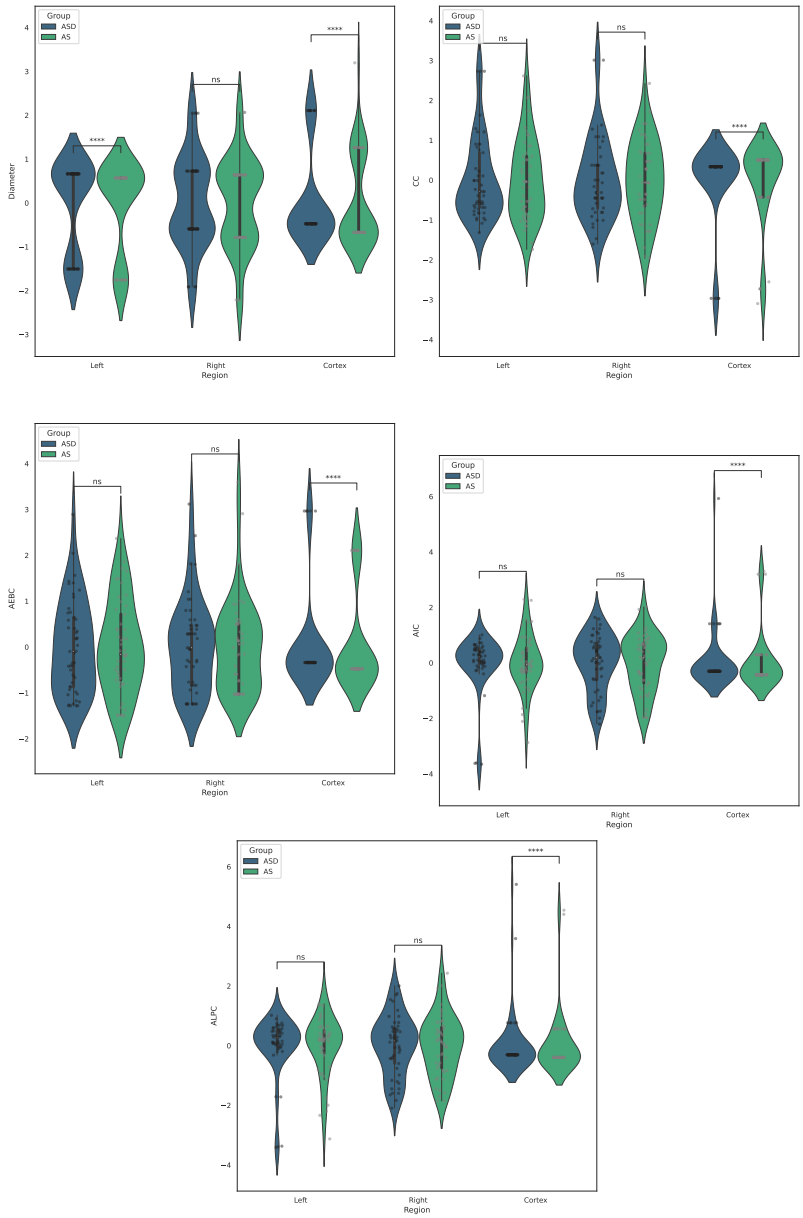

Fig. 13 Complex network measures that achieved four and three stars in the t-test with Bonferroni correction are compared across the TD, ASD, and AS classes, represented by dark blue, blue, and green, respectively. Statistical significance is indicated as follows: ns for $5.00 \times 10^{-2} < p \leq 1.00$, * for $1.00 \times 10^{-2} < p \leq 5.00 \times 10^{-2}$, ** for $1.00 \times 10^{-3} < p \leq 1.00 \times 10^{-2}$, *** for $1.00 \times 10^{-4} < p \leq 1.00 \times 10^{-3}$, and **** for $p \leq 1.00 \times 10^{-4}$.

CHAPTER

6

TEMPORAL PATTERNS OF EEG CONNECTIVITY UNVEIL PARKINSON'S DISEASE PROGRESSION

Temporal Patterns of EEG Connectivity Unveil Parkinson's Disease Progression: Insights from Machine Learning Analysis. Caroline L. Alves, Loriz Francisco Sallum, Francisco Aparecido Rodrigues, Thaise G. L. de O. Toutain, Patricia Maria de Carvalho Aguiar, Michael Moeckel. *Journal of Physics: Complexity*. Current status: Accepted.

6.1 Context

Parkinson's disease (PD) is a progressive neurodegenerative disorder characterized primarily by the loss of dopaminergic neurons in the substantia nigra pars compacta (POEWE *et al.*, 2017; BALESTRINO; SCHAPIRA, 2020; RAZA; ANJUM *et al.*, 2019). This neuronal degeneration leads to characteristic motor symptoms, including bradykinesia, tremor, rigidity, and postural instability (POEWE *et al.*, 2017; BALESTRINO; SCHAPIRA, 2020; RAZA; ANJUM *et al.*, 2019), as well as non-motor manifestations such as cognitive impairment and depression (TSUBOI *et al.*, 2022; SCHAPIRA; CHAUDHURI; JENNER, 2017). Despite extensive research into the causes and progression of PD, the complex interplay between genetic predisposition, environmental factors and aging remains a challenge to fully understand (MÜLLER-NEDEBOCK *et al.*, 2023; KAIDERY; TARANNUM; THOMAS, 2013). While numerous studies have applied machine learning (ML) to distinguish PD patients from healthy controls (QIU *et al.*, 2024; KHARE; BAJAJ; ACHARYA, 2021; LOH *et al.*, 2021; ALJALAL *et al.*, 2022; RIZVI *et al.*, 2023), a critical gap remains in understanding how disease duration affects neural connectivity patterns (KILZHEIMER *et al.*, 2019; POSTUMA; BERG, 2019; SUBRAMANIAN *et al.*, 2022; AMOROSO *et al.*, 2018). Addressing this gap is particularly important given the dynamic and multifaceted nature of PD progression.

To investigate this, we analyzed electroencephalography (EEG) signals using innovative methodologies. Unlike traditional approaches that focus on medication effects, we stratified PD patients into two groups based on disease duration (1–3 years and 6–12 years) to capture subtle neural variations over time. By applying advanced connectivity metrics and machine learning (ML) algorithms, we aimed to identify distinct connectivity patterns and improve classification accuracy. To improve model interpretability (LUNDBERG, 2017), we used Shapley Additive Explanations (SHAP) values to identify key brain regions and connectivity patterns.

6.2 Contributions

Our study provide valuable perspectives into the progression of PD. By categorizing patients based on disease duration, we identified a continuum of neural connectivity patterns, showing that early-stage PD shares similarities with healthy brain function, while advanced PD exhibits distinct features of disease progression. Notably, coherence emerged as a key metric, effectively capturing synchronized signal behavior and distinguishing PD patients from controls with high accuracy. Further analysis revealed a reversal of synchronization trends between specific brain regions, including FP1, FC5, FP2, and FC6, suggesting potential physiological adaptations or the long-term effects of treatment.

The incorporation of SHAP values improved the interpretability of machine learning models, providing insights into the neural connections most relevant to PD pathophysiology. This methodological transparency strengthens the reliability and clinical applicability of our results, facilitating the integration of computational analysis into clinical practice. Furthermore, our binary classification tasks achieved higher accuracy than previously reported studies, highlighting the robustness of our approach.

Although the small dataset size remains a limitation, our findings offer valuable insights into the complex interactions between neural dynamics, disease progression, and age-related changes in PD, suggesting potential directions for further research and clinical applications.

Dynamical patterns of EEG connectivity unveil Parkinson's disease progression: Insights from Machine Learning analysis

Caroline L. Alves,[1,*] Loriz Francisco Sallum,[2] Francisco Aparecido Rodrigues,[2] Thaise G. L. de O. Toutain,[3] Patrícia Maria de Carvalho Aguiar,[4,5] and Michael Moeckel[1]

[1] *Laboratory for Hybrid Modeling, Aschaffenburg University of Applied Sciences, Aschaffenburg, Germany*
[2] *Institute of Mathematical and Computer Sciences, University of São Paulo, São Paulo, Brazil*
[3] *Health Sciences Institute, Federal University of Bahia, Bahia, Brazil*
[4] *Hospital Israelita Albert Einstein, São Paulo, Brazil*
[5] *Department of Neurology and Neurosurgery, Federal University of São Paulo, São Paulo, Brazil*

Objective: Parkinson's disease (PD) is a multifactorial neurodegenerative disorder with complex progression. This study aims to analyze electroencephalography (EEG) connectivity patterns to better understand PD progression and stage of the disease using machine learning.

Methods: Resting-state, eyes-closed EEG recordings were acquired from 31 individuals: 16 healthy controls (HC) and 15 PD patients. The PD group was stratified by disease duration into early-stage (1–3 years, $n = 9$) and advanced-stage (6–12 years, $n = 6$). EEG was recorded using a 32-channel Biosemi Active-Two system (512 Hz), with signals segmented into non-overlapping 10-second windows. Functional connectivity matrices were constructed using multiple metrics, including coherence, Pearson, Spearman, canonical correlation, and Ledoit-Wolf shrinkage. Machine learning models were applied for both binary (PD vs HC) and multiclass (HC vs early vs advanced PD) classification. Interpretability was achieved using Shapley Additive Explanations (PD) methodology , and the most discriminative neural connections were statistically validated using the Wilcoxon test with Bonferroni correction.

Results: Our approach achieved high accuracy in classifying PD stages, with coherence emerging as the optimal metric for capturing synchronized neural activity. SHAP values revealed critical brain regions and connectivity patterns associated with disease progression. Statistical validation confirmed the significance of these connections across disease stages. Early-stage PD exhibited neural connectivity patterns similar to healthy controls, while advanced stages showed distinct connectivity changes. **Conclusions:** The findings highlight the utility of EEG connectivity and machine learning in staging PD, offering insights into PD pathogenesis and progression. SHAP-enhanced model interpretability ensures reliable identification of key neural connections, supporting personalized diagnostics and therapeutic strategies.

Highlights

- Novel EEG connectivity analysis reveals Parkinson's disease progression patterns.
- Machine learning achieves high accuracy in staging Parkinson's disease.
- SHAP values identify key brain regions and connectivity alterations.

INTRODUCTION

Parkinson's disease (PD) is a progressive neurodegenerative disorder marked by dopaminergic neuron loss in the *substantia nigra pars compacta*, leading to motor symptoms like bradykinesia, tremors, rigidity, and postural instability [15, 76, 82]. Non-motor symptoms, such as cognitive impairment, depression, and autonomic dysfunction, also significantly affect patients' quality of life [87, 101]. While PD's exact etiology remains elusive, evidence suggests a complex interaction of genetic susceptibility, environmental factors, and aging [46, 69].

On the other hand, EEG-based connectivity measures enable the characterization of functional brain network disruptions in neuropsychiatric and neurodegenerative conditions [2, 31, 107]. These approaches model the brain as a complex system by computing statistical or spectral associations between EEG signals from different regions, producing functional connectivity matrices that can reveal altered communication pathways [108]. For example, EEG-based connectivity characterizes altered network segregation in Alzheimer's disease [13] and atypical integration patterns in attention-deficit/hyperactivity disorder (ADHD) [14], highlighting its potential as a non-invasive diagnostic support tool.

Various studies employ machine learning (ML) and deep learning algorithms to differentiate between individuals with PD and healthy control (HC), as evidenced in Table 1. The predominant dataset utilized across these studies is the San Diego dataset, which we used in our analysis. PD presents significant challenges across its various duration and stage of the condition, highlighting a critical gap in current diagnostic methodologies [49, 77, 95]. Although considerable efforts have been made to discern patterns and markers indicative of PD,

* Caroline.Alves@th-ab.de

the complexities inherent in the disease's progression still need to be addressed [10].

Our methodology extends beyond conventional approaches by delving into the nuances of PD progression through a refined segmentation of the patient cohort. Unlike previous studies that commonly compare PD patients with medication, without medication, and controls, we adopt a novel stratification strategy based on disease duration. Specifically, we categorize individuals into two distinct groups: those with a disease duration of 1-3 years and those with a 6-12 years duration. This tailored segmentation offers a more nuanced perspective on PD progression by capturing potential variations in EEG signals that correspond to different durations and stages of the disease.

Importantly, functional brain connectivity patterns also change across the lifespan, even in healthy individuals [19, 27, 30]. For example, aging is associated reduced synchronization in resting-state EEG networks [26, 92]. Therefore, when comparing patient and control groups using EEG-based connectivity, it is crucial to control for age effects. In this study, we ensured that age ranges of the PD and healthy control cohorts were largely overlapping, with statistical confirmation of age comparability across groups (see Figure 2-b).

In addition to activity pattern analysis, we use pairwise statistical metrics to construct connectivity matrices, based on techniques proven effective for preprocessing EEG time series data [8]. In particular, we explore the efficacy of these metrics in binary classification tasks to distinguish PD patients from controls, along with their utility in multiclass classification to differentiate between subgroups within the PD cohort based on disease duration. Furthermore, similar to our previous work [4, 6–9], we enhance the interpretability of our machine learning models using Shapley Additive Explanations (SHAP) values [64]. The SHAP framework identifies which features—in this context, specific neural connections—contribute most to the model's decision-making process [64]. By elucidating the most influential connectivity patterns, this approach provides a deeper understanding of the underlying neural dynamics of PD. The integration of this explanatory framework with our high-performing classifier not only refines current diagnostic approaches, as proven in previous research [1, 6, 7], but also establishes a basis for developing personalized therapeutic interventions that account for PD patients with different durations and disease progression.

METHODS

Figure 1 summarizes the methodology used in the present work. The python code with the methodology used in this work is available at: `https://github.com/Carol180619/Paper-temporal-Parkinson.git`.

A. Data and EEG preprocessing

EEG signals were recorded with a 32-channel Biosemi Active-Two system at a sampling rate of 512 Hz, using the international 10–20 electrode placement re-referenced to the common average, and a high-pass filter at 0.5 Hz was applied during acquisition to suppress slow drifts to enhance signal clarity[85]. Furthermore, summary statistics of participants' age, MMSE scores, and gender distribution are provided in Figure 2.

Here, offline preprocessing was conducted using MNE-Python [38]. We applied a band-pass Finite Impulse Response (FIR) filter (0.5–50Hz, Hamming window) to retain neurophysiologically relevant delta to low-gamma activity while reducing noise [72, 91]. Independent Component Analysis (ICA) was employed to identify and remove ocular and other artifacts [103], with each component visually inspected and excluded for each participant (see Figure D-A).

To ensure methodological rigor and avoid information leakage during classification, the raw EEG recordings were first split split into training (75%) and test (25%). Further, data were segmented into non-overlapping 10-second epochs to enhance our dataset's size and facilitate comprehensive analysis of EEG signals. This technique involves partitioning EEG signals into smaller time windows [56], typically lasting 10 seconds [43, 66, 70], which effectively increases the number of instances available for analysis. We acknowledge that the small number of patients may impose limitations on the generalizability of our findings.

All processed segments were then used to compute connectivity matrices with Pearson Correlation (PC) [16], Spearman Correlation (SC) [63], Sparse Canonical Correlation Analysis (CCA) [42], and Ledoit-Wolf shrinkage (LW) [57]. We emphasize coherence (Sync) [23, 33] for its unique ability to measure synchronization in pairwise EEG signals, enhances the dataset analysis, providing a nuanced exploration of EEG signals that were previously unexplored in our prior work [4, 6–9].

The Sync. measure between signals i and j, denoted as $\text{Sync}[i, j]$, is computed using the average coherence across all frequency points, as defined by Equation 1:

$$\text{Sync}[i, j] = \frac{1}{N} \sum_{k=1}^{N} \frac{|P_{ij}(f_k)|^2}{P_{ii}(f_k) \cdot P_{jj}(f_k)} \tag{1}$$

where:

- $Sync[i, j]$ is the synchronization between signals i and j,
- N is the number of frequency points,
- $P_{ij}(f_k)$ is the cross-spectral density between signals i and j at frequency f_k,
- $P_{ii}(f_k)$ is the auto-spectral density of signal i at frequency f_k,

Authors	Correlation metric	ML method	AUC	Accuracy	Recall	Precision
[79]	Phase Locking Value	Deep learning (Multiscale CNN)	88.7	88.7	86.7	Not reported
[48]	Not reported	Least Squares SVM	Not reported	97.65	96.67	98.76
[61]	Not reported	Deep learning (2D-CNN)	Not reported	99.46	99.46	99.48
[3]	Not reported	KNN	Not reported	99.89	99.87	Not reported
[84]	Not reported	Deep learning (CNN)	98.96	97.90	97.87	98.0

TABLE I. Overview of PD binary classification research using the same publicly accessible PD dataset as this study. "Not reported" indicates that the corresponding information was not explicitly provided in the referenced study. Most of these studies rely on direct time-series input rather than on derived connectivity matrices, which explains the absence of correlation metric information.

- $P_{jj}(f_k)$ is the auto-spectral density of signal j at frequency f_k,
- f_k represents the set of sampled points with a constant sampling frequency, assumed to be 50 Hz.

B. Binary and multiclass classification

To prepare the data for model training and evaluation, we applied standardization and cross-validation procedures aimed at improving model generalizability and avoiding data leakage. Feature standardization was performed using the function StandScaler from the Scikit-learn library python package [75], which transforms features to have zero mean and unit variance [99]. This step ensures consistent scaling across all features and enhances the robustness of the classifiers to varying feature magnitudes and outliers [36, 80].

For model evaluation, we employed stratified 10-fold cross-validation with shuffling [25, 55, 65] in the training set. This approach preserves class proportions (PD and HC) across folds and provides a robust estimate of model performance by ensuring that each observation is used for both training and validation [18, 53]. The use of shuffling within each fold further mitigates the effects of temporal dependencies introduced by sliding window segmentation [22, 102].

By combining feature standardization, stratification, and data shuffling, we minimize the risk of information leakage and improve the fairness of evaluation [12, 21, 25, 36, 50, 55, 62, 65, 80, 89, 94]. This methodology enables the model to be tested on unseen data, thereby strengthening the validity and reproducibility of our findings [47, 88].

To classify PD patients and healthy controls (HC, with 16 individuals), we used a multiclass machine learning framework. The PD group was segmented based on disease duration into two subgroups: 1–3 years (PD 1–3, 9 individuals) and 6–12 years (PD 6–12, 6 individuals), as shown in Figure 3-(a). This division was chosen primarily to achieve a more balanced class distribution, given the limited sample size, and to allow meaningful training and evaluation of the classification models.

Furthermore, in order to assess not only the temporal changes attributable to PD but also its stage, we stratified the PD EEG dataset based on the Unified Parkinson's Disease Rating Scale (UPDRS). The UPDRS is a widely used clinical rating scale that evaluates the severity of PD symptoms and functional impairment. Detailed information on UPDRS and the present dataset can be found in [35]. We divided the dataset into two groups based on the UPDRS scores: 20-40 (UPDRS1), comprising eight individuals, and 43-75 (UPDRS2), comprising six individuals. This segmentation mirrors the distribution of UPDRS scores illustrated in Figure 3-(b). UPDRS1 typically represents milder stages of PD, while UPDRS2 indicates the more advanced stages, reflecting the progression of the disease severity between participants.

The current work builds upon our previous research, which have established a foundation for employing machine learning techniques in the classification of PD and HC groups [4–9]. Initially, we utilize the support vector machine (SVM) to select connectivity metrics, leveraging its lower computational cost and effectiveness in binary classification [8]. Afterwards, various machine learning algorithms, including Logistic Regression (LR), Random Forest (RF), Multilayer Perceptron (MLP), Long Short-Term Memory neural networks (LSTM), and Convolutional Neural Networks (CNN), are tested with the selected connectivity metric, as detailed in the subsection C. Noteworthy, leveraging 10 seconds slicing windows data augmentations, a total dataset of 400 connectivity matrices is used, comprised of 200 datapoints representing HC, 100 PD in an early stage, and 100 PD in an progressed stage.

Hyperparameter optimization techniques, such as grid search and random search, are further employed to fine-tune the machine learning algorithms for optimal performance, with evaluation metrics including accuracy, precision, recall, Receiver Operating Characteristic (ROC) curves, and Area Under the ROC Curve (AUC) [6–9, 11, 20, 24, 29, 32, 44, 51, 54, 58, 59, 67, 73, 74, 81, 86, 100, 106, 109]. Additionally, the SHAP value technique is employed for medical interpretation, providing insights into the predictive importance of specific traits in the multiclass classification setting, as discussed in subsection D.

Further, we conducted comprehensive statistical analyses on these connections to further validate the machine learning findings, particularly the most significant cortical connections identified through the SHAP values methodology. Specifically, we selected the connection

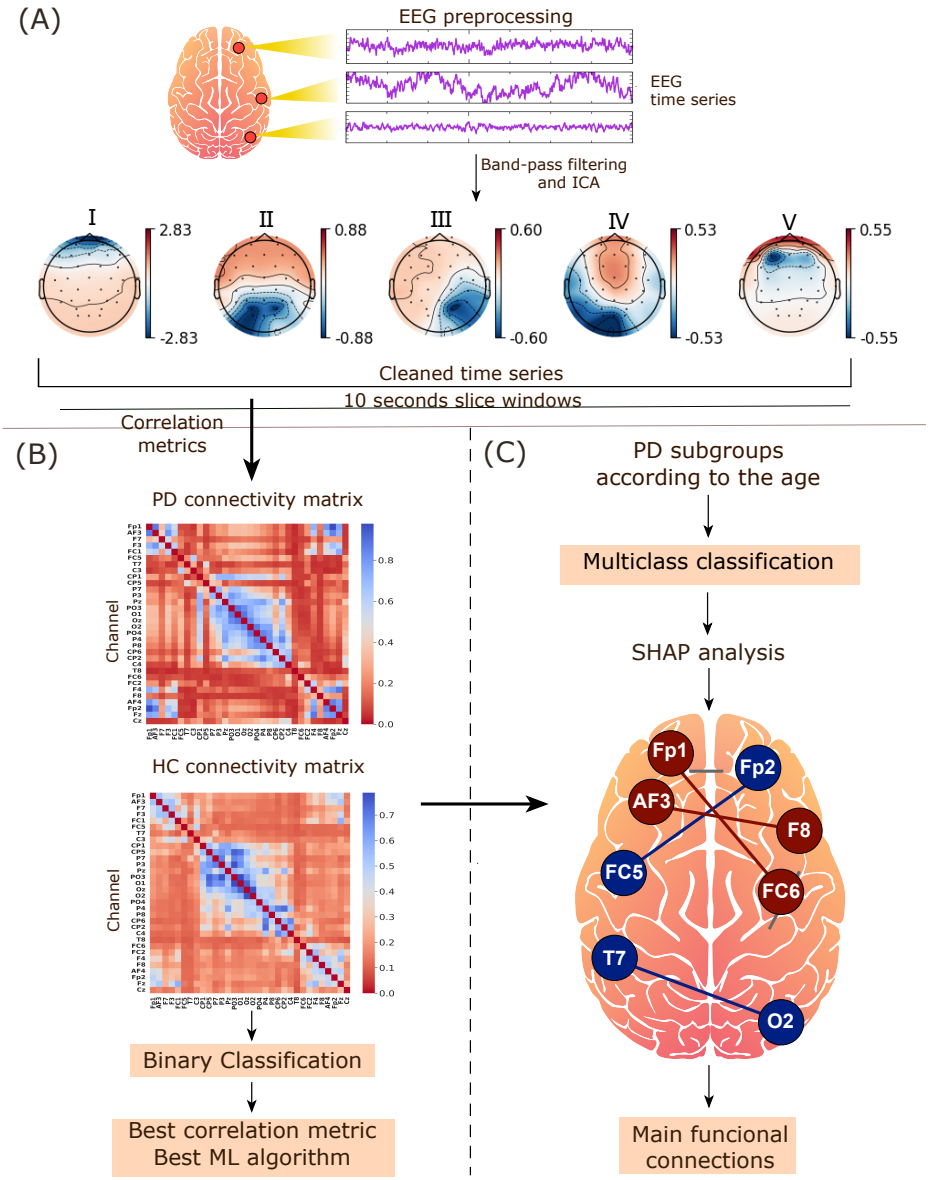

FIG. 1. **Summary of the methodology.** In (A), which corresponds to the EEG preprocessing described in subsection A, the EEG time series passed for a band-pass filter and to an independent component analysis. The Figure illustrates, as an example, a decomposition of the EEG signal of a PD patient into five components. In the Figure, as an example, the last component with higher frontal activity, indicating blink eye, was removed, and this process was made for all PD and control individuals. After preprocessing, we did 10 seconds of slicing windows as a data augmentation technique. In (B), which corresponds to the binary classification described in subsection B, the cleaned and sliced EEG time series were used to compute various connectivity matrices with different correlation metrics. Using a support vector machine (SVM), the best correlation metric to distinguish PD from HC was found. Also, in (B), many ML algorithms were tested, and the best was selected. The results for part (B) can be found in subsection C. With the best correlation metric's connectivity matrices and the best ML algorithm from part (B) used in a multiclass way to the connectivity matrices, the PD group was decomposed into two other groups according to the stage of the disease, depicted in part (C) and described in subsection B. Further, in (C), the SHAP values methodology was used to find the best connections. The results of the part (C) are in the subsection D.

strength values between pertinent cortical regions and evaluated them across three distinct groups: HC, PD 1-3, and PD 6-12.

We employed the Wilcoxon rank-sum test for each connection to compare the distributions between groups. The Bonferroni correction was applied to account for multiple comparisons and control the family-wise error rate. The following symbols denote the levels of statistical significance:

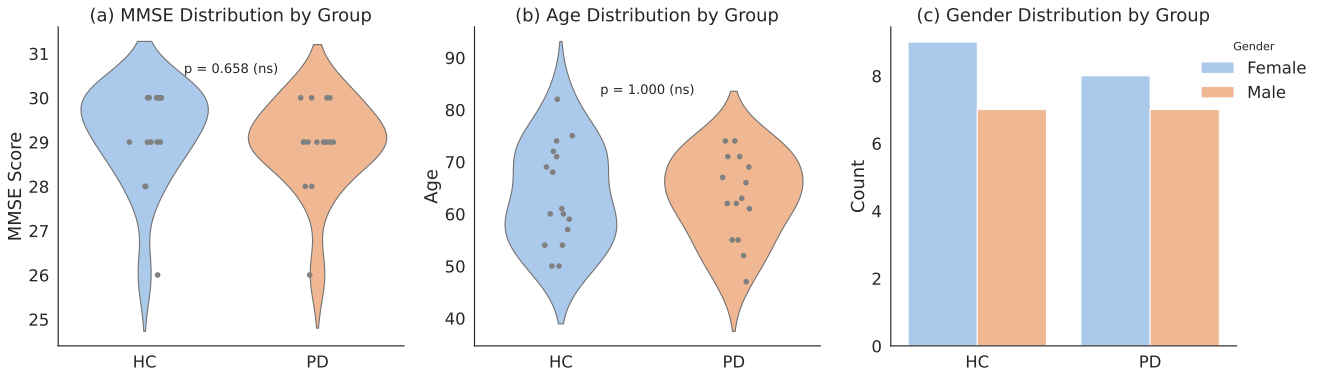

FIG. 2. Demographic characteristics of the dataset. (a) Violin and strip plot of MMSE scores showing cognitive performance distribution across groups. (b) Violin and strip plot of participant age by group. (c) Gender distribution per group. Statistical comparisons for panels (a) and (b) were performed using the two-sided Mann–Whitney U test with Bonferroni correction for multiple comparisons. No significant differences were found between groups in MMSE (p = 0.658, ns) or age (p = 1.000, ns). Note: PD = Parkinson's Disease, HC = Healthy Controls; ns = not significant.

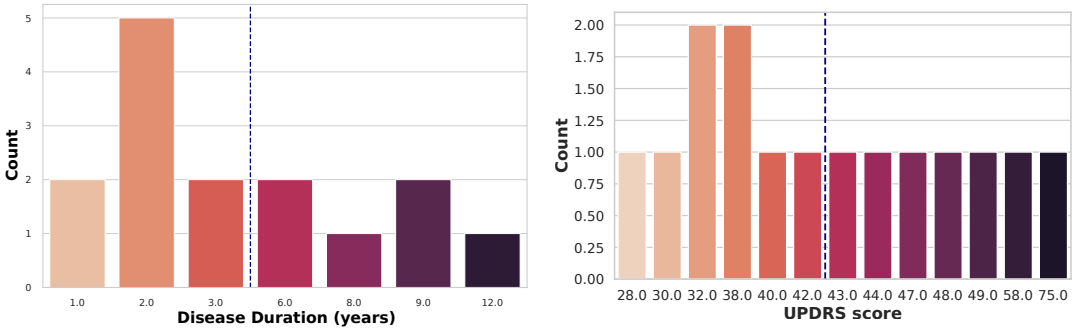

(a) Disease duration (years)

(b) UPDRS

FIG. 3. **Distribution of the disease duration and UPDRS in PD group.** In (a) The blue line is split according to the labels used for the multiclass classifier: those with a disease duration of 1-3 years (PD 1-3) and those with a disease duration of 6-12 years (PD 6-12). In (b) The blue line is split according to the labels used for the multiclass classifier: those with a disease stage of 20-40 (UPDRS1) and those with a disease stage of 43-75 (UPDRS2).

- ns: $5.00e-02 < p \leq 1.00e+00$
- *: $1.00e-02 < p \leq 5.00e-02$
- **: $1.00e-03 < p \leq 1.00e-02$
- ***: $1.00e-04 < p \leq 1.00e-03$
- ****: $p \leq 1.00e-04$

This rigorous statistical approach ensures that the observed differences in connection strengths are not attributed to random chance, thereby reinforcing the validity of the machine learning-derived insights.

RESULTS

C. Binary classification

Considering the AUC metric, the performance of each connectivity metric is illustrated in Figure 4. The Sync measure has the best performance for the test set, equal to 0.980 for the mean AUC, 0.981 for precision, 0.979 for recall, and 0.980 for accuracy.

Then, we tested all ML algorithms that resulted in Figure 5; the best classifiers were CNN and MLP. CNN performance for the test set was equal to 0.999 for the mean AUC, 0.990 for precision, 0.990 for recall, and 0.990 for accuracy. MLP performance for the test set was equal to 0.990 for the AUC, 0.989 for the precision, 0.991 for the recall, and 0.990 for the accuracy. Considering the performance and the computational cost, we selected the MLP classifier for use in the next section.

To optimize model performance, we performed feature

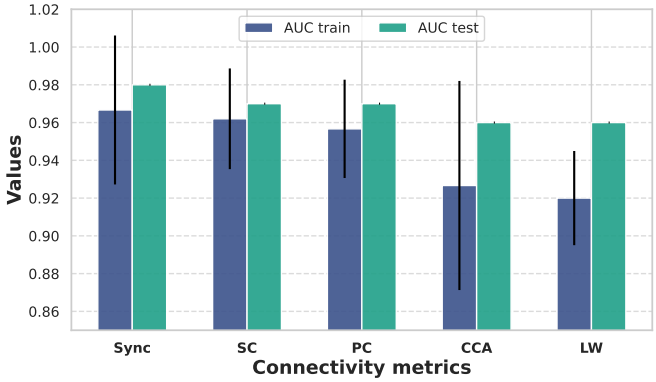

FIG. 4. **Selection of optimal correlation metrics with SVM**. In blue is the AUC of the train set; in green is the AUC of the test set. The best performance was the Sync.

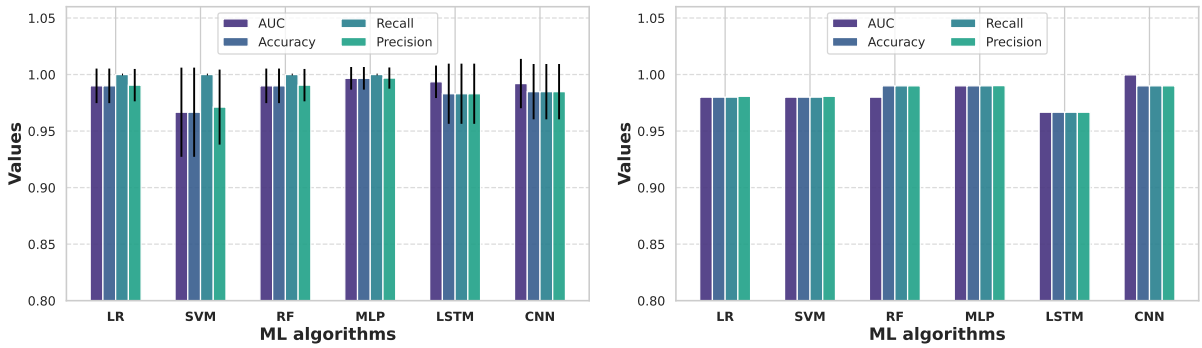

(a) Train set results

(b) Test set results

FIG. 5. **Results for method selection: best performance by MLP.** In (a) the results refer to the train set with the error bar due to the 10-fold stratified cross-validation and (b) the results of the test set.

selection using Recursive Feature Elimination (RFE), an iterative method designed to identify the subset of features that maximizes classification accuracy. RFE is well-established in medical data analysis [34, 83, 104, 105] and works by progressively removing the least important features and reevaluating the model. Here, the RFE analysis was implemented with the Yellowbrick library [17] and revealed that peak performance was achieved with a subset of 136 features (Figure 6). Consequently, this optimized feature set was used for all subsequent modeling, as the analysis confirmed that the complete feature set was unnecessary for achieving maximal efficacy.

D. Multiclass classification

Regarding the temporal changes due to PD, the general performance for the MLP in a multiclass classifier for the test set was equal to 0.983 for the mean AUC, 0.989 for precision, 0.977 for recall, and 0.983 for accuracy. Figure 7 displays the learning curve (Figure 7-(a)) and the confusion matrix (7-(c)), respectively. From Figures 7-(a), the confusion matrix showed that the group most difficult to distinguish was the PD 6-12 (in the confusion matrix, the PD 6-12 group has some mistaken classification with the group HC).

The visual representation of the learning curve illustrates the impact of varying the number of training instances on the model's predictive accuracy [78]. Figure 7-(c) shows that all the data was required to converge the model.

For the interpretability of the model and the decision-making process, we performed a SHAP analysis. Although RFE identified 136 features as optimal for predictive performance, we intentionally used a broader set of the top 300 features for the SHAP analysis. This expanded set, chosen despite its high computational cost, allows for a more comprehensive and robust investigation of the features ranked by their global contribution. The analysis identified distinct connectivity patterns driving the classification of early-stage versus late-stage PD (Figure 8). In these plots, the feature value represents the connectivity strength, where red indicates high synchronization and blue indicates low synchronization. For the PD 1-3 group, model predictions were most influenced by decreased synchronization between the FP2-FC5 and O2-

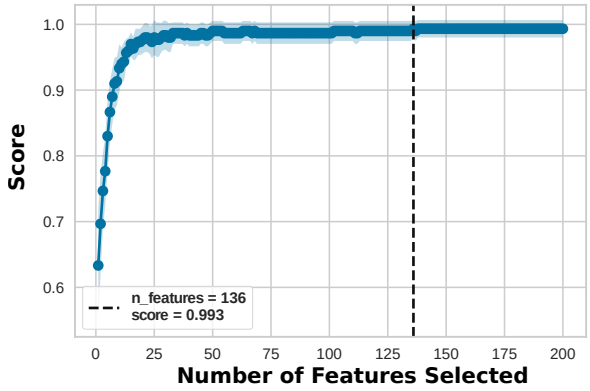

FIG. 6. **Recursive feature elimination (RFE)**. The optimal performance is attained with 136 features, so utilizing the entire comprehensive feature set is unnecessary.

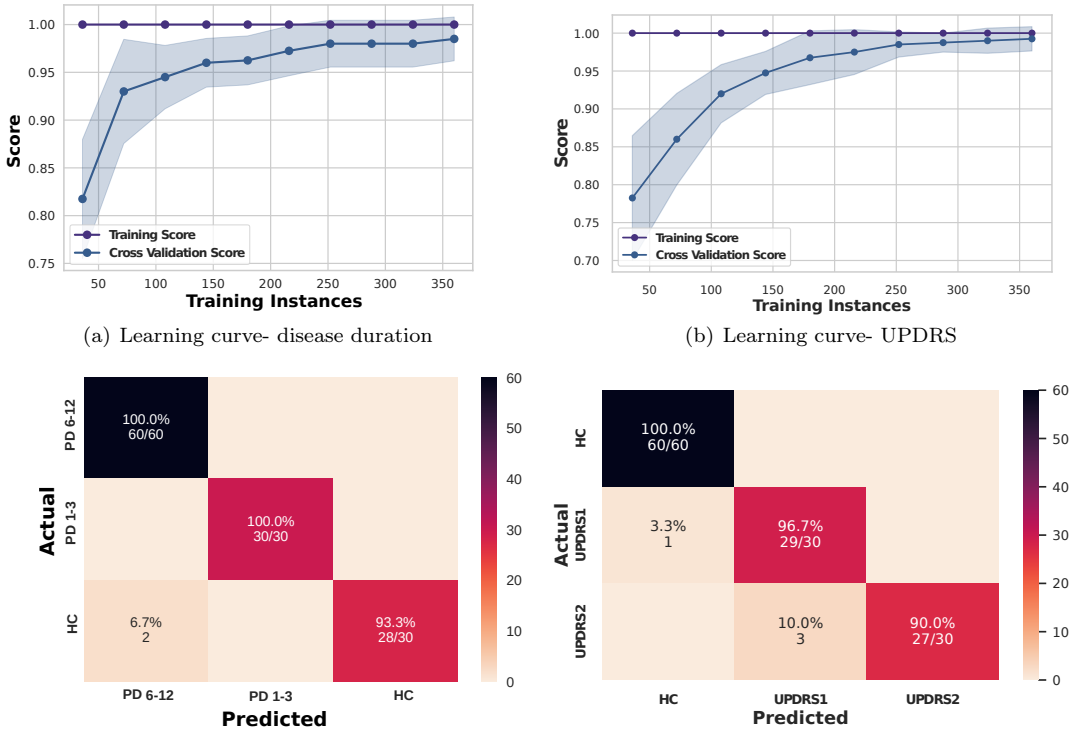

(a) Learning curve- disease duration

(b) Learning curve- UPDRS

(c) Confusion matrix- disease duration

(d) Confusion matrix- UPDRS

FIG. 7. **The test sample ML results from connectivity matrices using disease duration and UPDRS.** (a, b) Learning curves for disease duration and UPDRS, showing training (purple) and test (blue) accuracies. (c, d) Confusion matrices for disease duration and UPDRS, where diagonal elements represent true positives (TP), highlighting the classification performance for different classes.

T7 electrode pairs. Conversely, for the PD 6-12 group, the most decisive features were increased synchronization between F8-AF3 and FC6-Fp1.

SHAP value matrices for each class are concatenated into a single array, with rows representing samples and columns representing features. We averaged SHAP values across instances within each class for clarity. A cluster map, shown in Figure 9, was generated using hierarchical clustering with cosine similarity as the distance metric, which captures the orientation of feature importance patterns rather than their magnitude differences [93]. The resulting dendrogram groups rows and columns

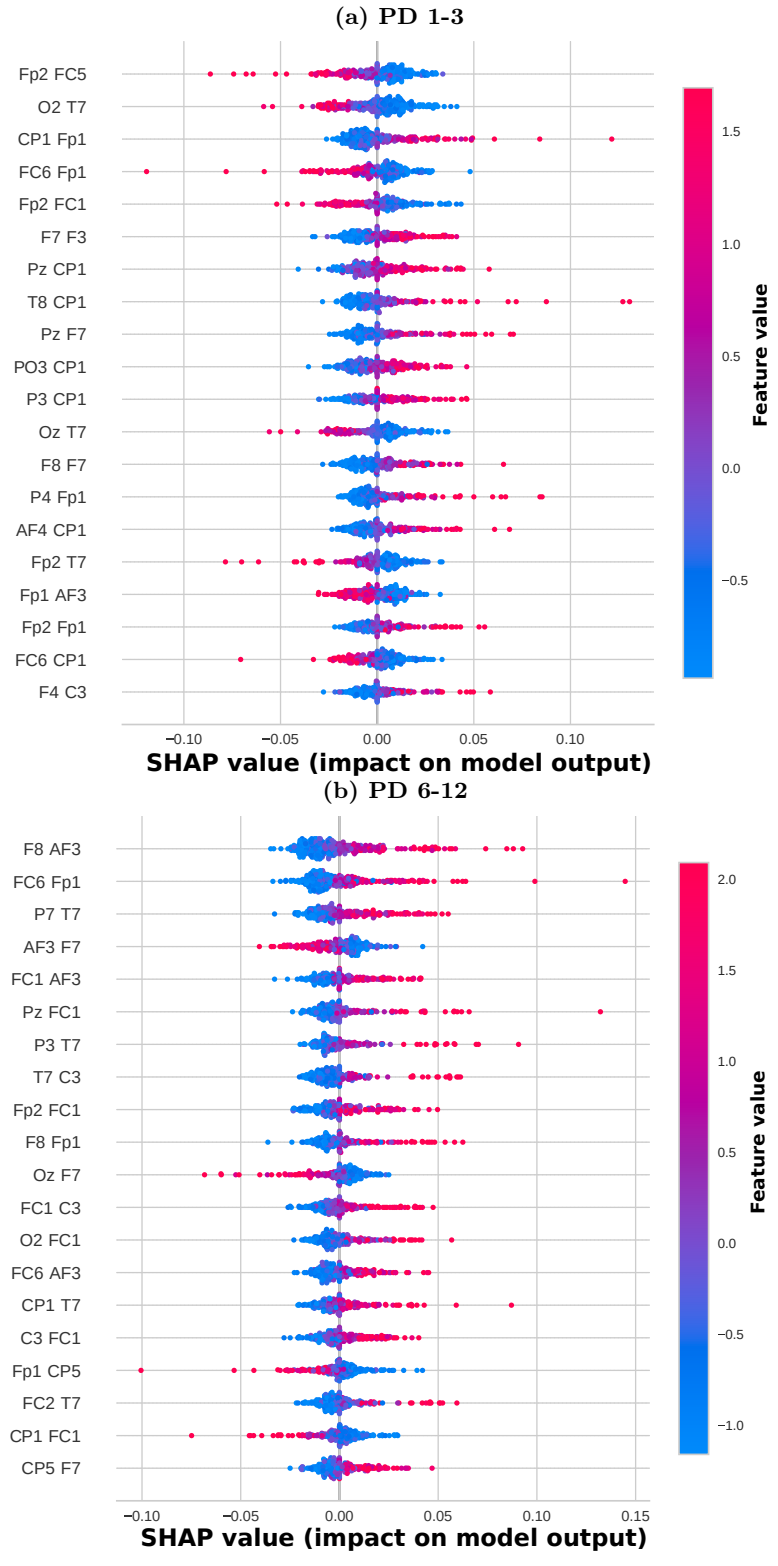

FIG. 8. Feature importance ranking using the SHAP values methodology for the MLP classifier with brain EEG channels in descending order. The y-axis represents the most important EEG connections, ranked by mean absolute SHAP value. The x-axis represents the SHAP value, indicating the magnitude and direction of a feature's impact on the model's prediction for that class. The feature value represents the connectivity strength (red = high synchronization, blue = low synchronization).(a) Feature importance ranking regarding PD 1-3 class. (b) Feature importance ranking regarding PD 6-12 class.

with similar SHAP patterns, with heatmap colors indicating SHAP value magnitudes (blue color scale for negative, red color scale for positive, and white for values near zero).

The dendogram clearly shows that the PD 1-3 group clusters most closely with the HC group. This proximity indicates that the model identifies significant similarities in the neural connectivity patterns of early-stage PD and healthy individuals. More importantly, this combined group is directly linked to the late-stage PD group based on their Shap values. This indicates a potential continuum or progression of the features, reflecting a gradual transition between the groups. In essence, the model has identified a measurable path of change as the disease progresses.

Further, as a complement to the temporal changes results due to PD, the differentiates changes were evaluated using the UPDRS scores; the general performance for the MLP in a multiclass classifier for the test set was equal to 0.969 for the mean AUC, 0.963 for precision, 0.955 for recall, and 0.967 for accuracy. Figure 7 displays the learning curve (Figure 7-(b)) and the confusion matrix (7-(d)), respectively. From Figure 7-(d), the confusion matrix, respectively, showed that the group most difficult to distinguish was the UPDRS1 (in the confusion matrix, the UPDRS1 group has some mistaken classification with the group HC). This difficulty likely stems from the lower UPDRS scores associated with the UPDRS1 group, implying an earlier stage of PD progression.

We employed the MLP along with SHAP values to identify the five most significant connections for each correlation metric in the PD 1-3 and PD 6-12 classes (Figures 11 and 10). This was done to assess the impact of the metrics, as their mathematical differences make them sensitive to distinct connectivity structures. For example, they capture different aspects of the signal, including linear (Pearson), rank-based (Spearman), frequency-domain (Synchronization), shrinkage-based (Ledoit-Wolf), and multivariate dependencies (CCA), which in turn leads to the identification of different sets of dominant connections.

Figure 12 illustrates the main EEG connectivity patterns identified for both PD 1-3 and PD 6-12 classes, based on the data from Tables 11 and 10. In both classes, there is a concentration of significant connections in the frontal and prefrontal regions across multiple correlation metrics (Sync, SC, and CCA). Further, Figure 12 shows that ongoing disease progression and the correlation of the frontal region (F7 and Fp2) with other areas is reduced.

In addition to the machine learning validation using SHAP values, we conducted rigorous statistical tests on the connectivity metrics, mainly focusing on the most significant connections identified through the SHAP values methodology. The results, depicted in Figures 13 and 14, confirm that all connections found were statistically significant in at least one of the group comparisons (HC vs. PD 1-3, HC vs. PD 6-12, or PD 1-3 vs. PD 6-12). These figures illustrate the strength of each connection across the groups, with significance levels indicated by the symbols described in the corresponding figure captions.

DISCUSSION

E. Binary classification

Among the evaluated connectivity metrics, coherence (Sync) yielded the best performance in the binary classification task. As defined by Bowyer [23], coherence captures both amplitude and phase coupling across a range of frequencies, providing a more comprehensive measure of signal synchronization. This makes it particularly suitable for analyzing brain connectivity in Parkinson's disease (PD), a condition known to alter both spectral power and synchrony in multiple brain regions. The emphasis on interregional signal coupling aligns with the underlying pathophysiology of PD, where disruptions in neural signaling and coordination are hallmark features [28, 96–98]. Therefore, coherence emerges not only as a theoretically appropriate metric but also as an empirically superior one, offering unique insights and enhanced discriminatory power within our machine learning framework to distinguish PD patients from healthy controls.

Further, the best machine learning algorithms were the MLP classifier and CNN, which tested the AUC metric of 0.990 and 0.999, respectively. These performances are higher compared to the literature, according to Table 1, which studies using the same dataset of this study also in a binary approach comparing PD patients from HC.

F. Multiclass classification

Regarding the temporal changes due to PD, using the MLP, the obtained accuracies of 0.933 for PD 6-12 and 1.000 for both PD 1-3 (depicted in Figure 7-(c)) and HC suggest a promising discrimination capability of the machine learning model in distinguishing between different groups based on connectivity matrices. The perfect classification for PD 1-3 and HC groups could indicate distinct patterns of brain connectivity in these cohorts, reflecting the early duration of PD progression and healthy brain function, respectively. The slightly lower accuracy for PD 6-12 implies greater heterogeneity or subtler differences in connectivity patterns that become more complex or less distinct as the disease progresses among patients with longer disease duration despite medication intake. Nonetheless, the model can still distinguish between the two groups with high metric performance.

After employing the SHAP value methodology, we identified the most influential connections for the PD 1-3 group. Notably, lower synchronization values in regions such as FP2 and FC5 were found. The frontopolar cortex (FP2) is implicated in various higher-order

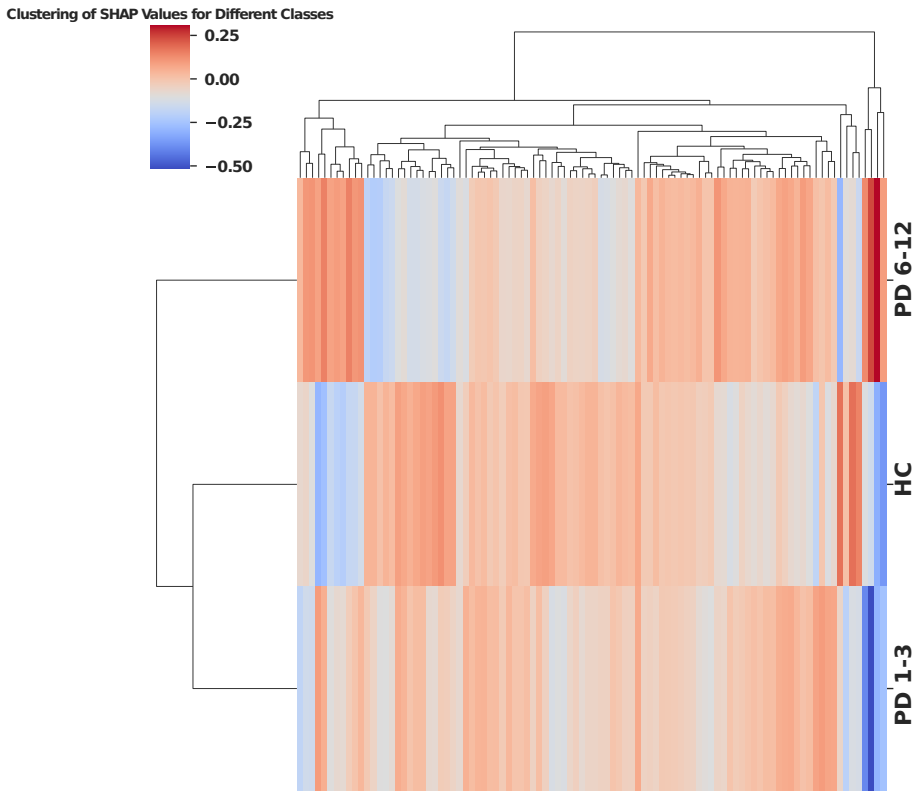

FIG. 9. **Cluster map generated through hierarchical clustering of SHAP values**. The dendrogram of the superior part corresponds to the hierarchy clustering for each of the 300 features used in the SHAP value methodology. The heatmap colors represent SHAP value magnitudes (blue color scale for negative, red color scale for positive, and white for values near zero). The left side of the plot corresponds to the resulting clustering regarding the dendrogram SHAP values features wherein the groups PD 1-3, PD 6-12, and HC.

Connections	Sync.	SC	PC	CCA	LW
Fp2-FC5					
O2-T7					
Cp1-Fp1					
Fc6-Fp1					
Fp2-Fc1					
T7-Af3					
Cp1-F7					
F3-Fp1					
F8-Fp1					
Fc1-Fp1					
Fc5-Fp1					
T7- F7					
Fp2-Fp1					
Pz-Af3					
Fp2-F7					
Fc2-Fp1					

FIG. 10. **Table depicting the most significant connections identified through the SHAP value methodology and MLP classifier for each correlation metric and the class PD 1-3.** Connection importance is denoted by the intensity of red shading. In bold are the main connections that appear in both classes, PD1-3 and PD6-12.

Connections	Sync.	SC	PC	CCA	LW
F8-Af3					
Fc6-Fp1					
P7-T7					
Af3-F7					
Fc1-Af3					
Cp5-Af3					
Cp5-Fp1					
Fp2-F7					
Cp2-Fp1					
Fp1-Af3					
Po3-Fp1					
P7-Af3					
Cp6-Fp1					

FIG. 11. **Table depicting the most significant connections identified through the SHAP value methodology and MLP classifier for each correlation metric and the class PD 6-12.** Connection importance is denoted by the intensity of red shading. In bold are the main connections that appear in both classes, PD1-3 and PD6-12.

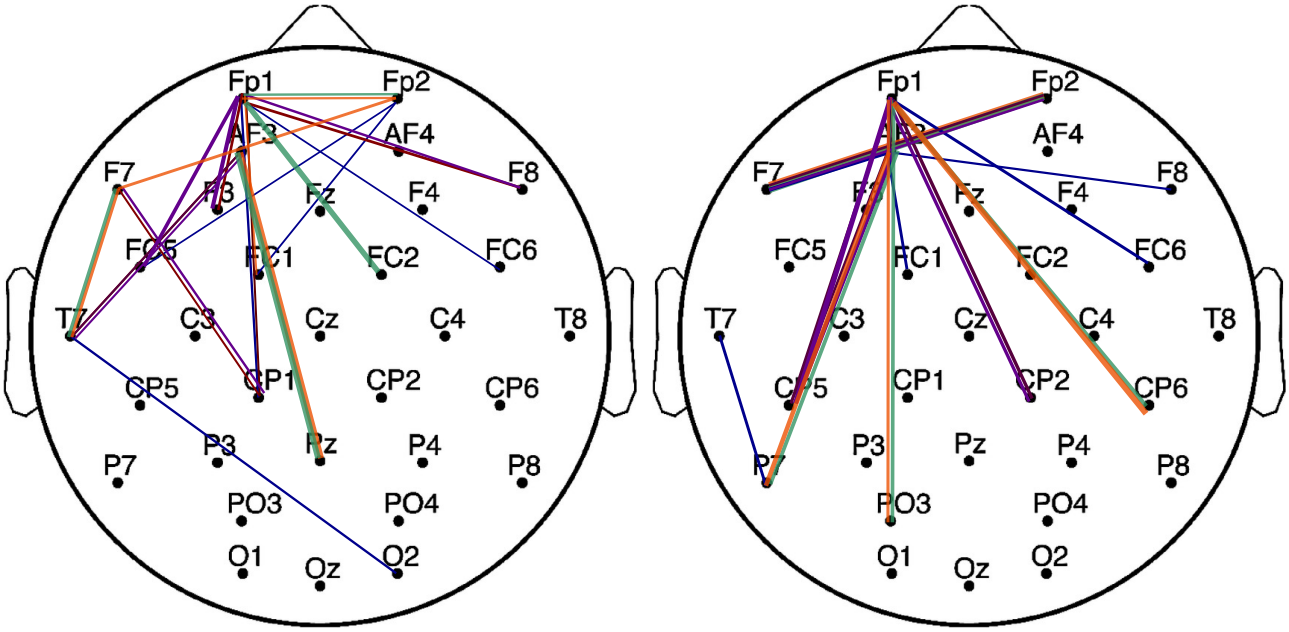

(a) Significant EEG connections in PD 1-3 class

(b) Significant EEG connections in PD 6-12 class

FIG. 12. **Main EEG connections identified through SHAP value methodology and MLP classifier for each correlation metric in PD 1-3 (a) and PD 6-12 (b) classes.** The color scheme denotes different metrics: Sync (blue), SC (red), PC (purple), CCA (orange), and LW (green).

cognitive processes, including decision-making, executive function, and social cognition [37, 52]. On the other hand, the left frontal cortex (FC5) plays a crucial role in motor planning and execution, as well as language processing [39, 60]. Thus, alterations in synchronization patterns within these regions may signify underlying deficits in both cognitive processing and motor coordination [45, 90]. Additionally, decreased synchronization in regions like O2 and T7 suggests possible impairment in sensory processing and attention, which are commonly affected in the early duration of PD [41]. Conversely, for the PD 6-12 group, heightened synchronization in regions like F8 and AF3 emerged as significant contributors, possibly reflecting potential compensatory mechanisms or adaptations occurring in response to disease progression and stage-related changes in neural circuitry

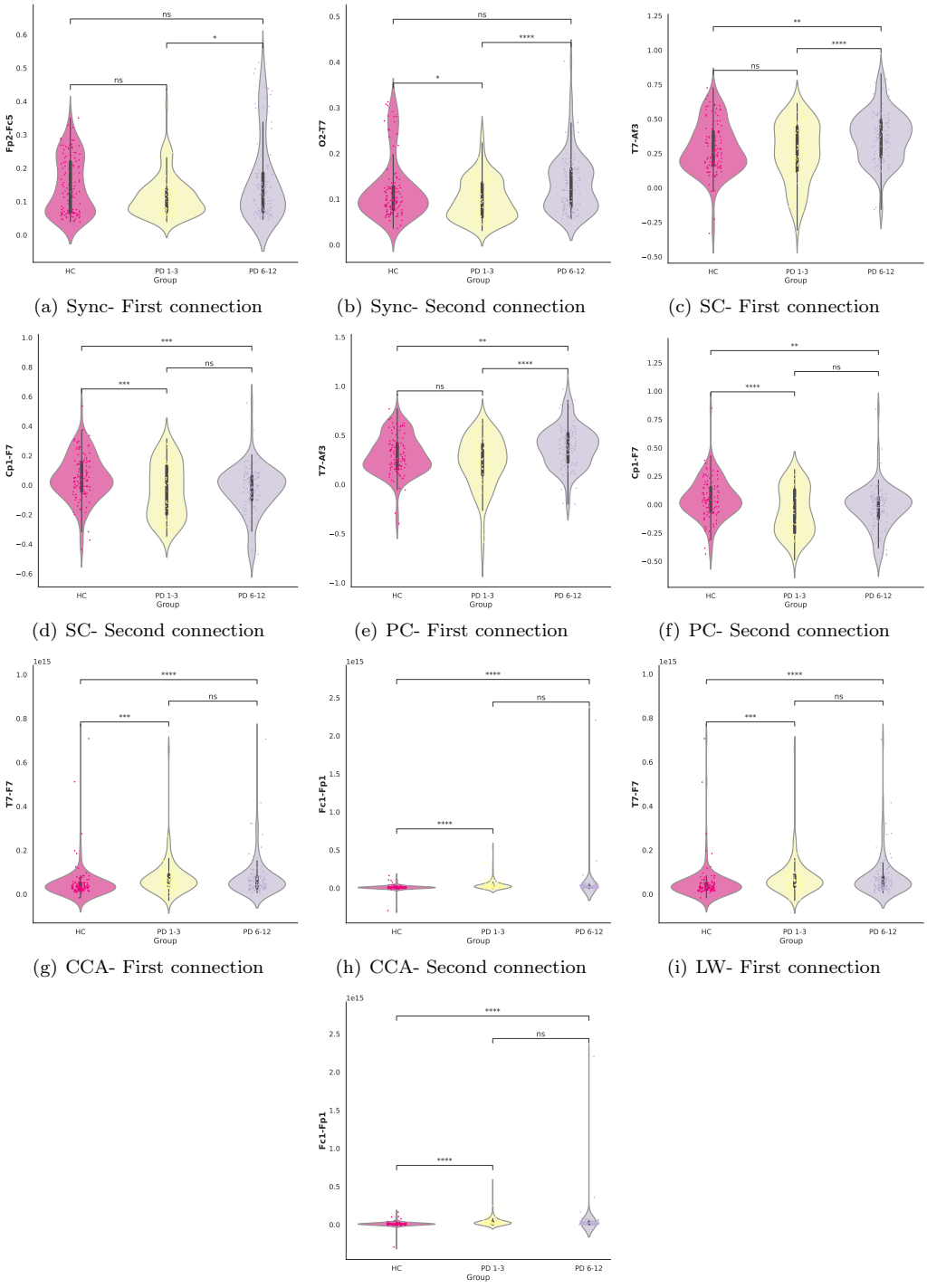

(a) Sync- First connection (b) Sync- Second connection (c) SC- First connection

(d) SC- Second connection (e) PC- First connection (f) PC- Second connection

(g) CCA- First connection (h) CCA- Second connection (i) LW- First connection

(j) LW- Second connection

FIG. 13. **Statitical test of Shap value methodology's main connection found for PD 1-3**. Statistical analysis of the most significant connections identified through the SHAP values methodology for the PD 1-3 group. Each subplot shows the distribution of connection strengths between specific cortical regions for HC, PD 1-3, and PD 6-12. The following symbols indicate the statistical significance between the groups: ns ($5.00e-02 < p \leq 1.00e+00$), * ($1.00e-02 < p \leq 5.00e-02$), ** ($1.00e-03 < p \leq 1.00e-02$), *** ($1.00e-04 < p \leq 1.00e-03$), and **** ($p \leq 1.00e-04$).

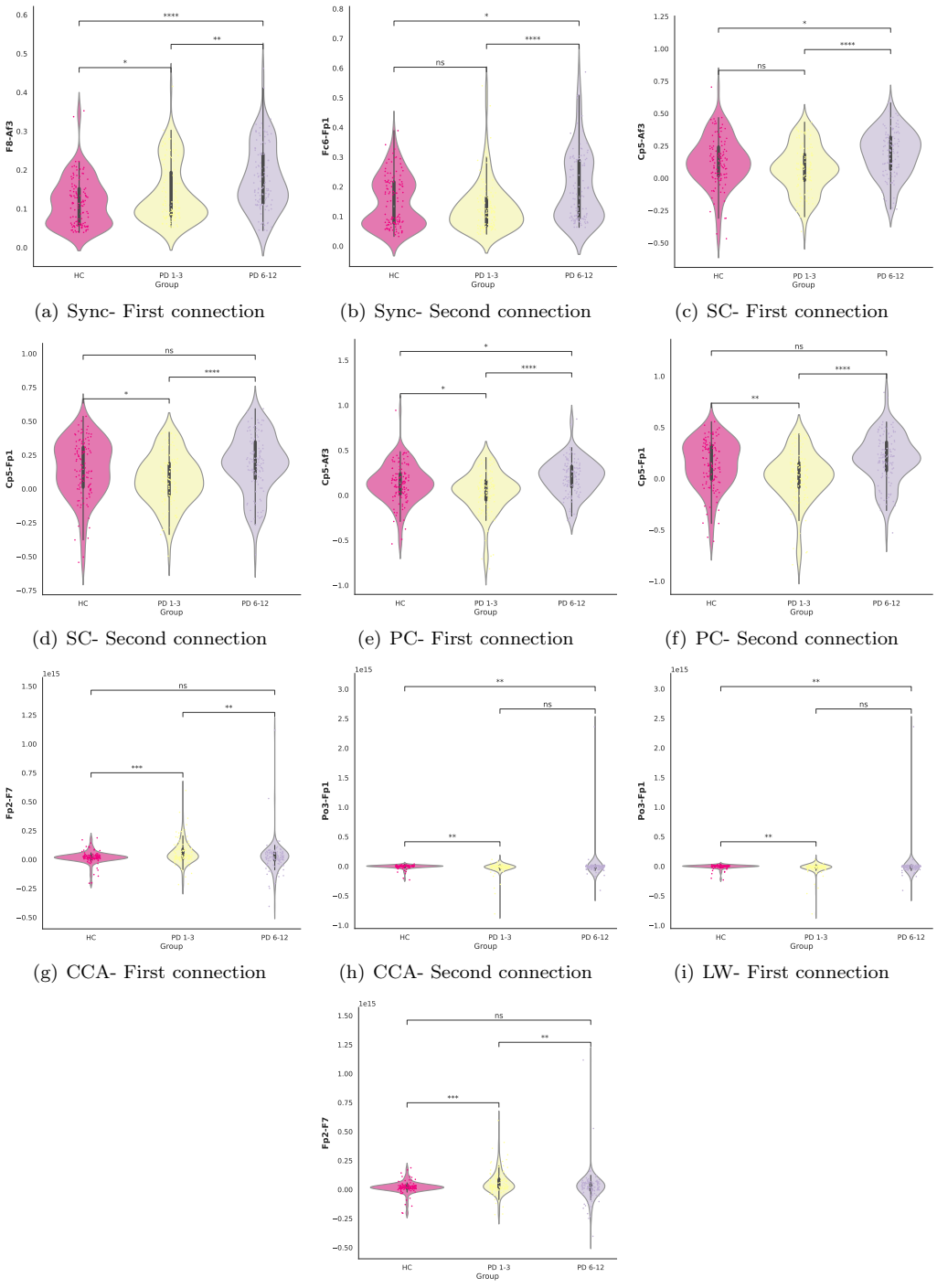

(a) Sync- First connection (b) Sync- Second connection (c) SC- First connection

(d) SC- Second connection (e) PC- First connection (f) PC- Second connection

(g) CCA- First connection (h) CCA- Second connection (i) LW- First connection

(j) LW- Second connection

FIG. 14. **Statitical test of Shap value methodology's main connection found for PD 6-12**. Statistical analysis of the most significant connections identified through the SHAP values methodology for the PD 6-12 group. Each subplot shows the distribution of connection strengths between specific cortical regions for the groups HC, PD 1-3, and PD 6-12. The statistical significance between the groups is indicated by the following symbols: ns ($5.00e-02 < p \leq 1.00e+00$), * ($1.00e-02 < p \leq 5.00e-02$), ** ($1.00e-03 < p \leq 1.00e-02$), *** ($1.00e-04 < p \leq 1.00e-03$), and **** ($p \leq 1.00e-04$).

[71].

Furthermore, our investigation unveiled a significant association between the FC6 and FP1 electrodes in both PD 1-3 and PD 6-12 cohorts, showcasing diminished synchrony in the former and amplified synchrony in the latter. This observed increase in synchronization within frontal brain areas regarding PD is consistent with findings from other studies [40, 68].

These findings underscore the complex interplay between neural connectivity patterns, disease progression, and stage-related changes in PD.

Our analysis revealed intriguing clustering behavior that sheds light on the underlying patterns of feature importance across different disease duration. Specifically, the SHAP values associated with PD 1-3 demonstrated a notable proximity to those of the HC class, forming a distinct cluster. This clustering suggests that the features contributing to the ML model's predictions for early-duration PD share similarities with those of healthy brain function. Moreover, we observed a connection between this cluster and the SHAP values corresponding to PD duration 6-12. This linkage implies a potential continuum or progression in the underlying neural connectivity patterns captured by the model, spanning from the early to later duration of PD. The hierarchical clustering highlights the distinctiveness of brain connectivity patterns in early-duration PD and healthy brains. It suggests a gradual shift towards features more characteristic of advanced PD as the disease progresses.

Regarding the results of PD stages, using the MLP in a multiclass classifier for the test set was equal to 0.969 for the mean AUC, 0.963 for precision, 0.955 for recall, and 0.967 for accuracy. Therefore, it was possible to distinguish PD patients from the temporal and stage degree of the disease. Further, Figure 7-(a) demonstrates that the model achieved convergence without necessitating the entirety of the dataset. This suggests that distinguishing between PD patients and HC subjects based on disease stage was relatively straightforward compared to predicting disease duration. Consequently, to accurately model disease duration, it was imperative to utilize the entire dataset for convergence

Our analysis regarding correlation metrics' influence on the SHAP values results, as illustrated in Figures 11 and 10, uncovered consistent patterns across various correlation metrics, notably in characteristic regions such as Fp1. However, distinct correlations emerged as significant within specific groups of metrics. Notably, linear correlation metrics like SC and PC clustered together, while CCA and LW formed another cohesive group. Additionally, Sync. stood out as an independent correlation metric. Importantly, these findings represent novel results that have not been evaluated in the existing literature to the best of our knowledge.

Further, the connections FC6-Fp1 and Fp2-F7 appear for both classes (highlighted in bold in Tables 11 and 10).

Finally, validation of the machine learning findings was conducted through rigorous statistical tests on the connectivity metrics, mainly focusing on the most significant connections identified using the SHAP values methodology. These analyses revealed that all identified connections were statistically significant in at least one of the group comparisons (HC vs. PD 1-3, HC vs. PD 6-12, or PD 1-3 vs. PD 6-12). This statistical significance across comparisons underscores the robustness of the connections identified by the machine learning model, further validating their importance in distinguishing between different stages of PD. This further validates the importance of these connections in distinguishing between different stages of PD.

I. CONCLUSIONS AND FUTURE WORK

In conclusion, our study presents a novel approach to understanding PD progression through refined segmentation and advanced analysis of EEG signals. By stratifying patients based on disease duration, we reveal distinct neural connectivity patterns corresponding to different disease trajectory duration. Our findings underscore the critical role of coherence in capturing the synchronized behavior of signals, which scontributes to distinguishing PD patients from controls. Moreover, employing machine learning algorithms such as the MLP classifier and CNN, we achieved high accuracy rates compared to those reported in the literature, particularly in binary classification tasks. This indicates the robustness of our methodology in identifying subtle differences in connectivity patterns associated with PD progression and stage.

Furthermore, leveraging SHAP values enhances the interpretability of our models, revealing relevant connectivity patterns implicated in PD pathophysiology. An intriguing finding was the reduction of synchronization between EEG channels and the progression of the disease.

To ensure the robustness of our findings, we further validated the most significant connections using statistical tests. This validation confirmed that all identified connections were statistically significant in at least one group comparison.

Our analysis suggests changes in neural connectivity patterns across different disease stages. Notably, early-duration PD exhibits similarities with healthy brain function, while later stages manifest distinctive features indicative of disease progression.

However, it is essential to acknowledge the limitations of our methodology, particularly its reliance on small data. Furthermore, the San Diego dataset lacks detail regarding UPDRS assessments, such as whether they were conducted in ON or OFF medication states and the use of non-specialist raters. These factors may affect the reliability of disease staging. Future research should ensure clinically rigorous evaluations by trained professionals and include a broader range of disease durations to understand the impact of these interventions better.

Overall, our study contributes valuable insights into

the complex interplay between neural dynamics, disease progression, and stage-related changes in PD, offering new avenues for further research and clinical application.

CONFLICT OF INTEREST

The authors have no conflicts of interest to declare.

AUTHOR CONTRIBUTIONS STATEMENT

C.L.A.: conceptualization, formal analysis, investigation, methodology, visualization, validation, software and writing – original draft. L.F.S.: validation, writing writing – original draft. F.A.R.: validation, writing – review editing. T.L.G.L.O.T.: validation, writing – review editing. P.M.C.A: validation, writing – review editing. M.M: funding acquisition, project administration, resources, supervision, validation, writing – review editing.

DATA AVAILABILITY

The authors have no conflicts of interest to declare. The study used the SanDiego dataset, openly available at `https://openneuro.org/datasets/ds002778/versions/1.0.5.`.

ETHICAL APPROVAL

This study utilized the San Diego Parkinson's dataset, which is publicly available and fully de-identified, ensuring participant privacy. All analyses were conducted in accordance with ethical standards and the dataset's usage policies.

[1] Al-Beltagi, M. (2021). Autism medical comorbidities. *World journal of clinical pediatrics*, 10(3):15.

[2] Al-Ezzi, A., Arechavala, R. J., Butler, R., Nolty, A., Kang, J. J., Shimojo, S., Wu, D.-A., Fonteh, A. N., Kleinman, M. T., Kloner, R. A., et al. (2024). Disrupted brain functional connectivity as early signature in cognitively healthy individuals with pathological csf amyloid/tau. *Communications Biology*, 7(1):1037.

[3] Aljalal, M., Aldosari, S. A., Molinas, M., AlSharabi, K., and Alturki, F. A. (2022). Detection of parkinson's disease from eeg signals using discrete wavelet transform, different entropy measures, and machine learning techniques. *Scientific Reports*, 12(1):22547.

[4] Alves, C., Wissel, L., Capetian, P., and Thielemann, C. (2022a). P 55 functional connectivity and convolutional neural networks for automatic classification of eeg data. *Clinical Neurophysiology*, 137:e47.

[5] Alves, C. L., Ciba, M., Toutain, T. G. d. O., Porto, J. A. M., de Sena, E. P., Thielemann, C., and Rodrigues, F. A. (2024). On the advances in machine learning and complex network measures to an eegdataset from dmt experiments. *Journal of Physics: Complexity*.

[6] Alves, C. L., Cury, R. G., Roster, K., Pineda, A. M., Rodrigues, F. A., Thielemann, C., and Ciba, M. (2022b). Application of machine learning and complex network measures to an eeg dataset from ayahuasca experiments. *Plos one*, 17(12):e0277257.

[7] Alves, C. L., Pineda, A. M., Roster, K., Thielemann, C., and Rodrigues, F. A. (2022c). Eeg functional connectivity and deep learning for automatic diagnosis of brain disorders: Alzheimer's disease and schizophrenia. *Journal of Physics: complexity*, 3(2):025001.

[8] Alves, C. L., Toutain, T. G. d. O., de Carvalho Aguiar, P., Pineda, A. M., Roster, K., Thielemann, C., Porto, J. A. M., and Rodrigues, F. A. (2023a). Diagnosis of autism spectrum disorder based on functional brain networks and machine learning. *Scientific Reports*, 13(1):8072.

[9] Alves, C. L., Toutain, T. G. d. O., Porto, J. A. M., Aguiar, P. M. d. C., Pineda, A., Rodrigues, F. A., de Sena, E. P., and Thielemann, C. (2023b). Analysis of functional connectivity using machine learning and deep learning in different data modalities from individuals with schizophrenia. *Journal of Neural Engineering*.

[10] Amoroso, N., La Rocca, M., Monaco, A., Bellotti, R., and Tangaro, S. (2018). Complex networks reveal early mri markers of parkinson's disease. *Medical image analysis*, 48:12–24.

[11] Arcadu, F., Benmansour, F., Maunz, A., Willis, J., Haskova, Z., and Prunotto, M. (2020). Author correction: Deep learning algorithm predicts diabetic retinopathy progression in individual patients. *NPJ digital medicine*, 3(1):1–6.

[12] Avuçlu, E. and Elen, A. (2020). Evaluation of train and test performance of machine learning algorithms and parkinson diagnosis with statistical measurements. *Medical & Biological Engineering & Computing*, 58:2775–2788.

[13] Aydın, S. (2024). Alzhemimer's disease is characterized by lower segregation in resting-state eyes-closed eeg. *Journal of Medical and Biological Engineering*, 44(6):894–902.

[14] Aydın, S., Cetin, F. H., Uytun, M. Ç., Babadagi, Z., Gueven, A. S., and Işık, Y. (2022). Comparison of domain specific connectivity metrics for estimation brain network indices in boys with adhd-c. *Biomedical Signal Processing and Control*, 76:103626.

[15] Balestrino, R. and Schapira, A. (2020). Parkinson disease. *European journal of neurology*, 27(1):27–42.

[16] Benesty, J., Chen, J., Huang, Y., and Cohen, I. (2009). Pearson correlation coefficient. In *Noise reduction in speech processing*, pages 1–4. Springer.

[17] Bengfort, B. and Bilbro, R. (2019). Yellowbrick: Visualizing the scikit-learn model selection process. *Journal of Open Source Software*, 4(35):1075.

[18] Bengio, Y. and Grandvalet, Y. (2003). No unbiased estimator of the variance of k-fold cross-validation. *Advances in Neural Information Processing Systems*, 16.

[19] Betzel, R. F., Byrge, L., He, Y., Goñi, J., Zuo, X.-N., and Sporns, O. (2014). Changes in structural and functional connectivity among resting-state networks across the human lifespan. *Neuroimage*, 102:345–357.

[20] Bischl, B., Binder, M., Lang, M., Pielok, T., Richter, J., Coors, S., Thomas, J., Ullmann, T., Becker, M., Boulesteix, A.-L., et al. (2023). Hyperparameter optimization: Foundations, algorithms, best practices, and open challenges. *Wiley Interdisciplinary Reviews: Data Mining and Knowledge Discovery*, 13(2):e1484.

[21] Bisong, E. and Bisong, E. (2019). Introduction to scikit-learn. *Building Machine Learning and Deep Learning Models on Google Cloud Platform: A Comprehensive Guide for Beginners*, pages 215–229.

[22] Blum, A., Kalai, A., and Langford, J. (1999). Beating the hold-out: Bounds for k-fold and progressive cross-validation. In *Proceedings of the twelfth annual conference on Computational learning theory*, pages 203–208.

[23] Bowyer, S. M. (2016). Coherence a measure of the brain networks: past and present. *Neuropsychiatric Electrophysiology*, 2:1–12.

[24] Bracher-Smith, M., Crawford, K., and Escott-Price, V. (2021). Machine learning for genetic prediction of psychiatric disorders: a systematic review. *Molecular Psychiatry*, 26(1):70–79.

[25] Brownlee, J. (2019). How to choose a feature selection method for machine learning. *Machine Learning Mastery*, 10.

[26] Chow, R., Rabi, R., Paracha, S., Hasher, L., Anderson, N. D., and Alain, C. (2022). Default mode network and neural phase synchronization in healthy aging: A resting state eeg study. *Neuroscience*, 485:116–128.

[27] Collin, G. and Van Den Heuvel, M. P. (2013). The ontogeny of the human connectome: development and dynamic changes of brain connectivity across the life span. *The Neuroscientist*, 19(6):616–628.

[28] Conte, A., Khan, N., Defazio, G., Rothwell, J. C., and Berardelli, A. (2013). Pathophysiology of somatosensory abnormalities in parkinson disease. *Nature Reviews Neurology*, 9(12):687–697.

[29] Dukart, J., Weis, S., Genon, S., and Eickhoff, S. B. (2021). Towards increasing the clinical applicability of machine learning biomarkers in psychiatry. *Nature Human Behaviour*, 5(4):431–432.

[30] Edde, M., Leroux, G., Altena, E., and Chanraud, S. (2021). Functional brain connectivity changes across the human life span: From fetal development to old age. *Journal of Neuroscience Research*, 99(1):236–262.

[31] Edlow, B. L., Claassen, J., Schiff, N. D., and Greer, D. M. (2021). Recovery from disorders of consciousness: mechanisms, prognosis and emerging therapies. *Nature Reviews Neurology*, 17(3):135–156.

[32] Ferri, C., Hernández-Orallo, J., and Salido, M. A. (2003). Volume under the roc surface for multi-class problems. In *European conference on machine learning*, pages 108–120. Springer.

[33] French, C. C. and Beaumont, J. G. (1984). A critical review of eeg coherence studies of hemisphere function. *International Journal of Psychophysiology*, 1(3):241–254.

[34] Gadalla, A. A., Friberg, I. M., Kift-Morgan, A., Zhang, J., Eberl, M., Topley, N., Weeks, I., Cuff, S., Wootton, M., Gal, M., et al. (2019). Identification of clinical and urine biomarkers for uncomplicated urinary tract infection using machine learning algorithms. *Scientific reports*, 9(1):19694.

[35] George, J. S., Strunk, J., Mak-McCully, R., Houser, M., Poizner, H., and Aron, A. R. (2013). Dopaminergic therapy in parkinson's disease decreases cortical beta band coherence in the resting state and increases cortical beta band power during executive control. *NeuroImage: Clinical*, 3:261–270.

[36] Géron, A. (2022). *Hands-on machine learning with Scikit-Learn, Keras, and TensorFlow*. " O'Reilly Media, Inc.".

[37] Gilbert, S. J., Spengler, S., Simons, J. S., Steele, J. D., Lawrie, S. M., Frith, C. D., and Burgess, P. W. (2006). Functional specialization within rostral prefrontal cortex (area 10): a meta-analysis. *Journal of cognitive neuroscience*, 18(6):932–948.

[38] Gramfort, A., Luessi, M., Larson, E., Engemann, D. A., Strohmeier, D., Brodbeck, C., Parkkonen, L., and Hämäläinen, M. S. (2014). Mne software for processing meg and eeg data. *neuroimage*, 86:446–460.

[39] Hagoort, P. (2014). Nodes and networks in the neural architecture for language: Broca's region and beyond. *Current opinion in Neurobiology*, 28:136–141.

[40] Hammond, C., Bergman, H., and Brown, P. (2007). Pathological synchronization in parkinson's disease: networks, models and treatments. *Trends in neurosciences*, 30(7):357–364.

[41] Hanganu, A., Bedetti, C., Degroot, C., Mejia-Constain, B., Lafontaine, A.-L., Soland, V., Chouinard, S., Bruneau, M.-A., Mellah, S., Belleville, S., et al. (2014). Mild cognitive impairment is linked with faster rate of cortical thinning in patients with parkinson's disease longitudinally. *Brain*, 137(4):1120–1129.

[42] Hardoon, D. R. and Shawe-Taylor, J. (2011). Sparse canonical correlation analysis. *Machine Learning*, 83(3):331–353.

[43] Hoffmann, A., Jäger, L., Werhahn, K., Jaschke, M., Noachtar, S., and Reiser, M. (2000). Electroencephalography during functional echo-planar imaging: detection of epileptic spikes using post-processing methods. *Magnetic Resonance in Medicine: An Official Journal of the International Society for Magnetic Resonance in Medicine*, 44(5):791–798.

[44] Ito, Y., Unagami, M., Yamabe, F., Mitsui, Y., Nakajima, K., Nagao, K., and Kobayashi, H. (2021). A method for utilizing automated machine learning for histopathological classification of testis based on johnsen scores. *Scientific reports*, 11(1):1–11.

[45] Jones, S. R., Pritchett, D. L., Stufflebeam, S. M., Hämäläinen, M., and Moore, C. I. (2007). Neural correlates of tactile detection: a combined magnetoencephalography and biophysically based computational modeling study. *Journal of Neuroscience*, 27(40):10751–10764.

[46] Kaidery, N. A., Tarannum, S., and Thomas, B. (2013). Epigenetic landscape of parkinson's disease: emerging role in disease mechanisms and therapeutic modalities. *Neurotherapeutics*, 10(4):698–708.

[47] Kapoor, S. and Narayanan, A. (2023). Leakage and the reproducibility crisis in machine-learning-based science. *Patterns*, 4(9).

[48] Khare, S. K., Bajaj, V., and Acharya, U. R. (2021). Detection of parkinson's disease using automated tunable q wavelet transform technique with eeg signals. *Biocybernetics and Biomedical Engineering*, 41(2):679–689.

[49] Kilzheimer, A., Hentrich, T., Burkhardt, S., and Schulze-Hentrich, J. M. (2019). The challenge and opportunity to diagnose parkinson's disease in midlife. *Frontiers in Neurology*, 10:1328.

[50] Kim, D. W., Lee, S., Kwon, S., Nam, W., Cha, I.-H., and Kim, H. J. (2019). Deep learning-based survival prediction of oral cancer patients. *Scientific reports*, 9(1):6994.

[51] Kim, J., Lee, J., Park, E., and Han, J. (2020). A deep learning model for detecting mental illness from user content on social media. *Scientific reports*, 10(1):1–6.

[52] Koechlin, E. and Summerfield, C. (2007). An information theoretical approach to prefrontal executive function. *Trends in cognitive sciences*, 11(6):229–235.

[53] Kohavi, R. et al. (1995). A study of cross-validation and bootstrap for accuracy estimation and model selection. In *Ijcai*, volume 14, pages 1137–1145. Montreal, Canada.

[54] Krittanawong, C., Virk, H. U. H., Kumar, A., Aydar, M., Wang, Z., Stewart, M. P., and Halperin, J. L. (2021). Machine learning and deep learning to predict mortality in patients with spontaneous coronary artery dissection. *Scientific reports*, 11(1):1–10.

[55] Kuhn, M., Johnson, K., et al. (2013). *Applied predictive modeling*, volume 26. Springer.

[56] Lashgari, E., Liang, D., and Maoz, U. (2020). Data augmentation for deep-learning-based electroencephalography. *Journal of Neuroscience Methods*, 346:108885.

[57] Ledoit, O. and Wolf, M. (2012). Nonlinear shrinkage estimation of large-dimensional covariance matrices. *The Annals of Statistics*, 40(2):1024–1060.

[58] Li, R. C., Asch, S. M., and Shah, N. H. (2020). Developing a delivery science for artificial intelligence in healthcare. *NPJ digital medicine*, 3(1):1–3.

[59] Li, Y., Nowak, C. M., Pham, U., Nguyen, K., and Bleris, L. (2021). Cell morphology-based machine learning models for human cell state classification. *NPJ systems biology and applications*, 7(1):1–9.

[60] Liakakis, G., Nickel, J., and Seitz, R. (2011). Diversity of the inferior frontal gyrus—a meta-analysis of neuroimaging studies. *Behavioural brain research*, 225(1):341–347.

[61] Loh, H. W., Ooi, C. P., Palmer, E., Barua, P. D., Dogan, S., Tuncer, T., Baygin, M., and Acharya, U. R.

(2021). Gaborpdnet: Gabor transformation and deep neural network for parkinson's disease detection using eeg signals. *Electronics*, 10(14):1740.

[62] Lopez-Martin, M., Nevado, A., and Carro, B. (2020). Detection of early stages of alzheimer's disease based on meg activity with a randomized convolutional neural network. *Artificial Intelligence in Medicine*, 107:101924.

[63] Lubinski, D. (2004). Introduction to the special section on cognitive abilities: 100 years after spearman's (1904)"'general intelligence,'objectively determined and measured". *Journal of personality and social psychology*, 86(1):96.

[64] Lundberg, S. M. and Lee, S.-I. (2017). A unified approach to interpreting model predictions. In *Proceedings of the 31st international conference on neural information processing systems*, pages 4768–4777.

[65] Mahesh, T., Geman, O., Margala, M., Guduri, M., et al. (2023). The stratified k-folds cross-validation and class-balancing methods with high-performance ensemble classifiers for breast cancer classification. *Healthcare Analytics*, 4:100247.

[66] Matell, M. S., Meck, W. H., and Nicolelis, M. A. (2003). Interval timing and the encoding of signal duration by ensembles of cortical and striatal neurons. *Behavioral neuroscience*, 117(4):760.

[67] Mincholé, A. and Rodriguez, B. (2019). Artificial intelligence for the electrocardiogram. *Nature medicine*, 25(1):22–23.

[68] Moazami-Goudarzi, M., Sarnthein, J., Michels, L., Moukhtieva, R., and Jeanmonod, D. (2008). Enhanced frontal low and high frequency power and synchronization in the resting eeg of parkinsonian patients. *Neuroimage*, 41(3):985–997.

[69] Müller-Nedebock, A. C., Dekker, M. C., Farrer, M. J., Hattori, N., Lim, S.-Y., Mellick, G. D., Rektorová, I., Salama, M., Schuh, A. F., Stoessl, A. J., et al. (2023). Different pieces of the same puzzle: a multifaceted perspective on the complex biological basis of parkinson's disease. *npj Parkinson's Disease*, 9(1):110.

[70] Nakisa, B., Rastgoo, M. N., Rakotonirainy, A., Maire, F., and Chandran, V. (2020). Automatic emotion recognition using temporal multimodal deep learning. *IEEE Access*, 8:225463–225474.

[71] Olde Dubbelink, K. T., Hillebrand, A., Stoffers, D., Deijen, J. B., Twisk, J. W., Stam, C. J., and Berendse, H. W. (2014). Disrupted brain network topology in parkinson's disease: a longitudinal magnetoencephalography study. *Brain*, 137(1):197–207.

[72] Pant, A. and Kumar, A. (2024). Hanning fir window filtering analysis for eeg signals. *Biomedical Analysis*, 1(2):111–123.

[73] Park, Y. and Kellis, M. (2015). Deep learning for regulatory genomics. *Nature biotechnology*, 33(8):825–826.

[74] Patel, D., Kher, V., Desai, B., Lei, X., Cen, S., Nanda, N., Gholamrezanezhad, A., Duddalwar, V., Varghese, B., and Oberai, A. A. (2021). Machine learning based predictors for covid-19 disease severity. *Scientific Reports*, 11(1):1–7.

[75] Pedregosa, F., Varoquaux, G., Gramfort, A., Michel, V., Thirion, B., Grisel, O., Blondel, M., Prettenhofer, P., Weiss, R., Dubourg, V., et al. (2011). Scikit-learn: Machine learning in python. *the Journal of machine Learning research*, 12:2825–2830.

[76] Poewe, W., Seppi, K., Tanner, C. M., Halliday, G. M., Brundin, P., Volkmann, J., Schrag, A.-E., and Lang, A. E. (2017). Parkinson disease. *Nature reviews Disease primers*, 3(1):1–21.

[77] Postuma, R. B. and Berg, D. (2019). Prodromal parkinson's disease: the decade past, the decade to come. *Movement disorders*, 34(5):665–675.

[78] Prottasha, N. J., Murad, S. A., Muzahid, A. J. M., Rana, M., Kowsher, M., Adhikary, A., Biswas, S., and Bairagi, A. K. (2023). Impact learning: A learning method from feature's impact and competition. *Journal of Computational Science*, 69:102011.

[79] Qiu, L., Li, J., Zhong, L., Feng, W., Zhou, C., and Pan, J. (2024). A novel eeg-based parkinson's disease detection model using multiscale convolutional prototype networks. *IEEE Transactions on Instrumentation and Measurement*.

[80] Raschka, S. (2015). *Python machine learning*. Packt publishing ltd.

[81] Rashidi, H. H., Sen, S., Palmieri, T. L., Blackmon, T., Wajda, J., and Tran, N. K. (2020). Early recognition of burn-and trauma-related acute kidney injury: a pilot comparison of machine learning techniques. *Scientific reports*, 10(1):1–9.

[82] Raza, C., Anjum, R., et al. (2019). Parkinson's disease: Mechanisms, translational models and management strategies. *Life sciences*, 226:77–90.

[83] Richhariya, B., Tanveer, M., Rashid, A. H., Initiative, A. D. N., et al. (2020). Diagnosis of alzheimer's disease using universum support vector machine based recursive feature elimination (usvm-rfe). *Biomedical Signal Processing and Control*, 59:101903.

[84] Rizvi, S. Q. A., Wang, G., Khan, A., Hasan, M. K., Ghazal, T. M., and Khan, A. U. R. (2023). Classifying parkinson's disease using resting state electroencephalogram signals and u^{EN}-pdnet. *IEEE Access*.

[85] Rockhill, A. P., Jackson, N., George, J., Aron, A., Swann, N. C., et al. (2020). Uc san diego resting state eeg data from patients with parkinson's disease. *Available:*.

[86] Sato, M., Morimoto, K., Kajihara, S., Tateishi, R., Shiina, S., Koike, K., and Yatomi, Y. (2019). Machine-learning approach for the development of a novel predictive model for the diagnosis of hepatocellular carcinoma. *Scientific reports*, 9(1):1–7.

[87] Schapira, A. H., Chaudhuri, K. R., and Jenner, P. (2017). Non-motor features of parkinson disease. *Nature Reviews Neuroscience*, 18(7):435–450.

[88] Shorten, C., Khoshgoftaar, T. M., and Furht, B. (2021). Text data augmentation for deep learning. *Journal of big Data*, 8:1–34.

[89] Singh, V., Pencina, M., Einstein, A. J., Liang, J. X., Berman, D. S., and Slomka, P. (2021). Impact of train/test sample regimen on performance estimate stability of machine learning in cardiovascular imaging. *Scientific reports*, 11(1):14490.

[90] Smith, N. J. and Kutas, M. (2015). Regression-based estimation of erp waveforms: I. the rerp framework. *Psychophysiology*, 52(2):157–168.

[91] Soltész, F., Szűcs, D., Leong, V., White, S., and Goswami, U. (2013). Differential entrainment of neuroelectric delta oscillations in developmental dyslexia. *PloS one*, 8(10):e76608.

[92] Stam, C. J., Montez, T., Jones, B., Rombouts, S., Van Der Made, Y., Pijnenburg, Y. A., and Scheltens, P. (2005). Disturbed fluctuations of resting state eeg synchronization in alzheimer's disease. *Clinical neurophysiology*, 116(3):708–715.

[93] Strehl, A., Ghosh, J., and Mooney, R. (2000). Impact of similarity measures on web-page clustering. In *Workshop on artificial intelligence for web search (AAAI 2000)*, volume 58, page 64.

[94] Su, Q., Liu, Q., Lau, R. I., Zhang, J., Xu, Z., Yeoh, Y. K., Leung, T. W., Tang, W., Zhang, L., Liang, J. Q., et al. (2022). Faecal microbiome-based machine learning for multi-class disease diagnosis. *Nature Communications*, 13(1):6818.

[95] Subramanian, I., Mathur, S., Oosterbaan, A., Flanagan, R., Keener, A. M., and Moro, E. (2022). Unmet needs of women living with parkinson's disease: gaps and controversies. *Movement Disorders*, 37(3):444–455.

[96] Surmeier, D. J., Obeso, J. A., and Halliday, G. M. (2017). Selective neuronal vulnerability in parkinson disease. *Nature Reviews Neuroscience*, 18(2):101–113.

[97] Swinnen, S. P. (2002). Intermanual coordination: from behavioural principles to neural-network interactions. *Nature Reviews Neuroscience*, 3(5):348–359.

[98] Takakusaki, K., Takahashi, M., Noguchi, T., and Chiba, R. (2023). Neurophysiological mechanisms of gait disturbance in advanced parkinson's disease patients. *Neurology and Clinical Neuroscience*, 11(4):201–217.

[99] Thara, D., PremaSudha, B., et al. (2019). Autodetection of epileptic seizure events using deep neural network with different feature scaling techniques. *Pattern recognition letters*, 128:544–550.

[100] Tolkach, Y., Dohmgörgen, T., Toma, M., and Kristiansen, G. (2020). High-accuracy prostate cancer pathology using deep learning. *Nature Machine Intelligence*, 2(7):411–418.

[101] Tsuboi, T., Satake, Y., Hiraga, K., Yokoi, K., Hattori, M., Suzuki, M., Hara, K., Ramirez-Zamora, A., Okun, M. S., and Katsuno, M. (2022). Effects of mao-b inhibitors on non-motor symptoms and quality of life in parkinson's disease: A systematic review. *npj Parkinson's Disease*, 8(1):75.

[102] Varma, S. and Simon, R. (2006). Bias in error estimation when using cross-validation for model selection. *BMC bioinformatics*, 7(1):1–8.

[103] Vigário, R. N. (1997). Extraction of ocular artefacts from eeg using independent component analysis. *Electroencephalography and clinical neurophysiology*, 103(3):395–404.

[104] Wu, Z., Chen, H., Ke, S., Mo, L., Qiu, M., Zhu, G., Zhu, W., and Liu, L. (2023). Identifying potential biomarkers of idiopathic pulmonary fibrosis through machine learning analysis. *Scientific Reports*, 13(1):16559.

[105] Yang, M., Wu, Y., Yang, X.-b., Liu, T., Zhang, Y., Zhuo, Y., Luo, Y., and Zhang, N. (2023). Establishing a prediction model of severe acute mountain sickness using machine learning of support vector machine recursive feature elimination. *Scientific Reports*, 13(1):4633.

[106] Yu, X., Pang, W., Xu, Q., and Liang, M. (2020). Mammographic image classification with deep fusion learning. *Scientific Reports*, 10(1):1–11.

[107] Zhang, W., Sweeney, J. A., Bishop, J. R., Gong, Q., and Lui, S. (2023). Biological subtyping of psychiatric syndromes as a pathway for advances in drug discovery and personalized medicine. *Nature Mental Health*, 1(2):88–99.

[108] Zhang, Y., Wu, W., Toll, R. T., Naparstek, S., Maron-Katz, A., Watts, M., Gordon, J., Jeong, J., Astolfi, L., Shpigel, E., et al. (2021). Identification of psychiatric disorder subtypes from functional connectivity patterns in resting-state electroencephalography. *Nature biomedical engineering*, 5(4):309–323.

[109] Zhong, Z., Yuan, X., Liu, S., Yang, Y., and Liu, F. (2021). Machine learning prediction models for prognosis of critically ill patients after open-heart surgery. *Scientific Reports*, 11(1):1–10.

CHAPTER

7

INFLUENCE OF TOPOLOGY AND DYNAMICS ON NETWORK RECONSTRUCTION

Influence of topology on network recostruction. Loriz Francisco Sallum, Caroline L. Alves, Francisco Aparecido Rodrigues. Current status: In Preparation.

7.1 Context

Reconstructing complex networks from time series data is a fundamental challenge in various scientific fields, including neuroscience, physics, and engineering. Understanding the underlying connectivity of a system from observed dynamics is essential for inferring interactions in real-world networks (BASSETT *et al.*, 2006; EGUILUZ *et al.*, 2005; WU *et al.*, 2020; CALDARELLI *et al.*, 2013; YANG; YANG, 2008). Several methods have been proposed to estimate functional connectivity, including correlation-based metrics (BARDOSCIA *et al.*, 2021; WANG; HUANG, 2014; LAI *et al.*, 2018), information-theoretic measures (ANTONOPOULOS, 2023; GAO; JIN, 2009; LIANG; WANG, 2008; NOVELLI; LIZIER, 2021), and phase synchronization techniques (ROSENBLUM; PIKOVSKY, 2023; SCHMIDT; GHUMAN; HUPPERT, 2014; BASTOS; SCHOFFELEN, 2016; STAM, 2009; BASTOS; SCHOFFELEN, 2016).

However, the effectiveness of these methods is highly dependent on both the dynamical regime and the underlying network topology. Despite extensive research in network reconstruction (YUAN *et al.*, 2011; ANGULO *et al.*, 2017; RUNGE, 2018; MA *et al.*, 2018; SHANDILYA; TIMME, 2011), a systematic comparison of reconstruction performance across different topologies using multiple connectivity measures remains an open question. This work aims to address this gap by evaluating the impact of the network topology on reconstruction performance using various functional connectivity metrics applied to coupled logistic maps.

7.2 Contributions

This study provides a comprehensive analysis of network reconstruction performance by comparing multiple functional connectivity measures across different network topologies. We assess the effectiveness of Pearson correlation, Spearman correlation, mutual information, phase locking value, and coherence in reconstructing networks from time series data derived form coupled logistic maps.

We investigate how the bifurcation parameter r and the coupling strength ε in coupled logistic maps affects the f1-score of different reconstruction methods, highlighting transitions from periodic to chaotic regimes. Our results show that small-world networks with low rewiring probabilities achieve the highest reconstruction accuracy, reinforcing the role of local clustering and moderate path lengths in making reliable inference. We discuss the challenges of network reconstruction, including the sensitivity to dynamical conditions, and propose future research directions to enhance reconstruction robustness and applicability to real-world datasets.

By providing a detailed comparison of network reconstruction methods, this work contributes to a better understanding of functional connectivity inference and offers information about the appropriate techniques based on network topology and dynamical properties.

Influence of topology on network recostruction

Loriz Francisco Sallum,[1,*] Caroline L. Alves,[2] and Francisco A. Rodrigues[1]

[1] *University of São Paulo (USP), Institute of Mathematical and Computer Sciences (ICMC), São Paulo, Brazil*

[2] *Laboratory for Hybrid Modeling, Aschaffenburg University of Applied Sciences, Aschaffenburg, Bayern, Germany*

Reconstructing complex networks from time series data is a fundamental challenge with applications in neuroscience, finance, and engineering. This study investigates the influence of network topology on reconstruction accuracy by applying functional connectivity metrics to coupled logistic map dynamics. We systematically compare Pearson and Spearman correlation, mutual information, phase locking value (PLV), and coherence across different network models, including Erdős-Rényi (ER), Barabási-Albert (BA), Nonlinear Barabási-Albert (NLBA), and Watts-Strogatz (WS) with varying rewiring probabilities. Our results show that small-world networks (WS) with low rewiring probabilities consistently achieve the highest reconstruction performance, highlighting the role of local clustering and moderate path lengths in facilitating accurate inference. Conversely, ER, BA and NLBA networks exhibit lower accuracy, likely due to their lack of clustering and degree heterogeneity. Among the reconstruction methods, correlation-based measures and coherence perform well at high dynamical regimes, whereas PLV struggles under all conditions. These findings emphasize the interplay between topology, dynamics, and reconstruction methods, providing insights into optimal strategies for network inference.

KEYWORDS: network reconstruction, coupled logistic maps, functional connectivity, phase synchronization, correlation measures

I. INTRODUCTION

Complex networks provide a powerful framework for modeling and understanding the intricate interactions present in diverse systems, ranging from biological and social networks to engineering and technological infrastructures. A fundamental challenge in network science is the reconstruction of the underlying network topology from observed data, especially when only time series of node dynamics are available [1–6]. This problem has significant implications for various fields, such as neuroscience [7, 8], social network [9] and finance [6, 10], where direct access to network structures is often limited.

Several methods have been proposed to address this problem, including analytical approaches that reconstruct network structure from dynamical observations under certain model assumptions [11]. These methods often require prior knowledge of system equations and coupling functions, which may not always be available in real-world applications.

In contrast, functional connectivity measures provide a widely adopted approach for network reconstruction that does not require explicit knowledge of the governing equations. These methods infer statistical or dynamical dependencies between node dynamics [12]. These metrics, including correlation-based [13] and information-theoretic measures [14], aim to approximate the true connections by capturing the interplay between node activities.

Various methods for network reconstruction have been proposed and explored in recent literature. Traditional approaches often rely on correlation-based techniques, such as Pearson [15] and Spearman correlation [16], which measure the similarity between time series data or node interactions. These methods have been widely used for reconstructing static and dynamic networks, but they face limitations in capturing complex, non-linear relationships. More recent techniques, such as mutual information [17–19], phase-locking value [20–22], and coherence [22, 23], have been introduced to address these challenges by capturing nonlinear interactions and synchronization effects, which traditional correlation-based measures may overlook.

While functional connectivity metrics have been used for network reconstruction [22, 24, 25], the systematic investigation of their effectiveness as a function of (i) the choice of metric, (ii) the type of node dynamics, and (iii) the underlying network topology is not fully addressed in the literature. Some studies consider these aspects separately [11, 14, 26–29], but a comprehensive comparison across different functional metrics, dynamics and topologies in a controlled setting remains an open question.

In this study, we examine the influence of different network topologies on the accuracy of reconstruction methods. Specifically, we focus on how varying topological structures—while maintaining constant numbers of vertices and mean degree—can affect the performance of reconstruction techniques. By systematically varying the topological features and applying a range of dynamic models, we aim to identify key factors that contribute to or hinder accurate network reconstruction.

This study contributes by systematically investigating how different functional connectivity metrics perform under varying network topologies; the role of coupling strength and the dynamical regime of logistic maps in

* loriz.sallum@usp.br

influencing reconstruction accuracy; and whether certain network structures lead to systematic biases in inferred connectivity.

II. METHODOLOGY

A. Dynamic Model

The dynamic model chosen for this study is the coupled logistic map, a well-known chaotic system. The coupled logistic map is defined as [30]:

$$x_i(t+1) = (1-\epsilon)f(x_i(t)) + \frac{\epsilon}{b_i}\sum_{j=1}^{N} A_{ij} f(x_j(t-\tau_{ij}))$$

where $x_i(t)$ represents the state of node i at time t, and A_{ij} is the element of the adjacency matrix that indicates the connection between nodes i and j. The parameter ϵ is the coupling strength, which is uniform across the network and determines the influence of neighboring nodes on the dynamics of node i. The function $f(x)$ is defined as $f(x) = rx(1-x)$, where r is the bifurcation parameter that controls the chaotic behavior of the logistic map. The term τ_{ij} represents the delay time in the interaction between the i-th and j-th nodes. However, in this study, no delay was considered. The normalized factor $1/b_i$ ensures that each node receives the same total input from its neighbors, where $b_i = \sum_j A_{ij}$ is the number of neighbors of node i.

Time series of 10^4 steps were generated, with the first $3,000$ points discarded to eliminate dependence on the initial conditions.

B. Network Topologies

Next, we generate networks with different topologies, ensuring that each network has a fixed number of vertices and mean degree. Specifically, each topology consists of networks with 100 nodes and an average degree of 10. For each topology, we generate 10 different network structures to account for variability in network realizations. The topologies considered include the following:

- **Erdős–Rényi (ER) graphs** [31, 32]: Networks with random connections between nodes, where each pair of nodes is connected with a fixed probability. In this model, edges are independently and randomly assigned between nodes, making it a simple and widely studied model for random networks.

- **Barabási-Albert Model (BA)** [33]: A model of scale-free networks, where new nodes attach preferentially to high-degree nodes.

- **Nonlinear Barabási-Albert Model** [34]: A generalization of the Barabási-Albert preferential attachment model, where the probability of a new node connecting to an existing node i is given by $\Pi(k_i) \propto k_i^\alpha$, where k_i is the degree of node i and α controls the strength of preferential attachment. For $\alpha = 1$, the model reduces to the standard **Barabási-Albert (BA) model**, where attachment is strictly linear in degree. For $\alpha < 1$, attachment is sublinear, meaning high-degree nodes are less favored, leading to a more homogeneous degree distribution. For $\alpha > 1$, attachment is superlinear, meaning high-degree nodes are disproportionately favored, where very few nodes dominate the network.

- **Watts-Strogatz Model** [35]: A model of small-world networks that interpolates between a regular lattice ($p = 0$) and a random graph ($p = 1$), where p is the rewiring probability controlling the transition between order and randomness.

C. Network Reconstruction Methods

We then apply different methods to reconstruct the networks from the dynamic processes, such as:

- **Pearson Correlation** [36]: A simple method that measures the linear relationship between pairs of time series to reconstruct the network.

- **Spearman Correlation** [37]: A nonparametric method that assesses the monotonic relationship between time series, useful when the relationship is not necessarily linear.

- **Mutual Information** [38]: A method from information theory that measures the amount of information shared between two time series, capturing both linear and nonlinear dependencies.

- **Phase Locking Value** [39]: A measure that quantifies the consistency of phase synchronization between different signals, assessing how stable their phase difference remains over time. It assumes that two dynamic systems can exhibit phase synchronization even when their amplitudes are not correlated.

- **Coherence** [40]: A method that quantifies the degree of linear correlation between two signals in the frequency domain, measuring the consistency of their phase relationship and the strength of their amplitude coupling across different frequencies. It provides information of how stable their phase difference remains over time and how strongly their amplitude variations are related at specific frequencies.

To ensure consistency in the evaluation across different network topologies, the values of each reconstruction metric were rescaled using Min-Max scaling, mapping them to the range $[0, 1]$. This transformation allows for a fair comparison between different network structures by eliminating potential biases caused by variations in absolute metric values. In addition, a threshold of 0.5 was applied to determine the presence or absence of a connection in the reconstructed networks. Specifically, if the rescaled value was greater than or equal to 0.5, a connection was established between the corresponding nodes; otherwise, no connection was assigned. This threshold approach provides a standardized criterion for all reconstruction methods and network topologies.

We assess the effectiveness of network reconstruction by comparing the reconstructed networks to the original networks using the true positive rate (TPR), false positive rate (FPR), and f1-score.

The TPR quantifies the proportion of correctly identified connections (true positives) relative to the total actual connections in the original network, while the FPR measures the proportion of incorrectly inferred connections (false positives) relative to the total absent connections in the original network. Higher TPR and lower FPR indicate a more accurate reconstruction, meaning that the inferred network closely resembles the true underlying structure.

In addition to TPR and FPR, we also evaluate the reconstruction quality using the f1-score, which provides a balanced measure of precision and recall. The f1-score is defined as:

$$f1 = \frac{2 \cdot \text{Precision} \cdot \text{Recall}}{\text{Precision} + \text{Recall}}$$

where precision is the proportion of correctly inferred connections (true positives) relative to all inferred connections (true positives + false positives), and recall is equivalent to TPR. A higher f1-score indicates a better balance between correctly identifying actual connections and minimizing false positives, making it a useful metric for assessing reconstruction performance in scenarios where both precision and recall are important.

III. RESULTS

Figures 1 to 5 illustrate the network reconstruction performance using Pearson correlation, Spearman correlation, mutual information, phase locking value, and coherence, respectively, with a fixed threshold of 0.5. The f1-score is plotted as a function of the parameter ϵ for different values of r, across various network topologies, including Barabási-Albert (BA), Erdős-Rényi (ER), Nonlinear Barabási-Albert with preferential attachment exponent $\alpha = 1.5$ (NLBA_15), and Watts-Strogatz models with rewiring probabilities $p = 0.01$ (WS_001), $p = 0.1$ (WS_01), $p = 0.3$ (WS_03), and $p = 0.5$ (WS_05). Each line represents a different topology, and the shaded regions indicate the variability in performance. This allows for a comparative analysis of how each method performs under different conditions. The corresponding true positive rate (TPR) and false positive rate (FPR) plots for each metric are provided in Appendix A.

In Figure 1 and 2, for $r = 3.58$, the f1-scores remain relatively low across all values of ϵ, with some topologies showing a slight increase before stabilizing. As r increases to 3.70, there is a noticeable improvement in reconstruction performance, particularly for specific topologies, with a peak occurring at intermediate values of ϵ. At $r = 4.00$, the f1-scores reach their highest values, with a distinct peak around $\epsilon \approx 0.5$, after which performance declines. The WS_001 topology (red line) consistently achieves the best performance at larger values of r, whereas other topologies exhibit more varied behavior.

These results indicate that network reconstruction performance depends not only on r and ϵ but also on the network topology. Different topologies display distinct behaviors across the parameter space, with some achieving higher f1-scores and more stable reconstructions than others. The variation in standard deviation further suggests that the reconstruction reliability differs among topologies, reinforcing the influence of structural properties on performance.

Figure 3 illustrates the network reconstruction performance using mutual information with a fixed threshold of 0.5. The three subplots correspond to different values of r, namely $r = 3.58$, $r = 3.70$, and $r = 4.00$. Each plot depicts the relationship between the f1-score and the parameter ϵ for various network topologies, as indicated in the legend. The shaded regions represent the standard deviation of the f1-score across multiple realizations.

For $r = 3.58$ and $r = 3.70$, the reconstruction performance remains relatively low and stable for most topologies, with 11-scores below 0.2 and little variation across ϵ. However, at $r = 4.00$, there is a significant increase in reconstruction performance, with f1-scores reaching their highest values at intermediate ϵ values. In this case, the WS_001 (red) and WS_05 (pink) topologies exhibit the best performance, achieving 11-scores above 0.8 at optimal ϵ values.

These results suggest that mutual information-based reconstruction is highly dependent on r, with a sharp transition in performance occurring as r increases. Furthermore, the effectiveness of reconstruction varies across network topologies, with small-world networks (WS models) demonstrating the highest f1-scores at larger r values.

Figure 4 presents the network reconstruction performance using PLV as a connectivity measure, with a fixed threshold of 0.5. Each subplot corresponds to different values of r, namely $r = 3.58$ (Figure III), $r = 3.70$ (Figure **??**), and $r = 4.00$ (Figure III), illustrating the relationship between f1-score and the parameter ϵ in various network topologies.

Across all values of r, the f1-scores remain relatively

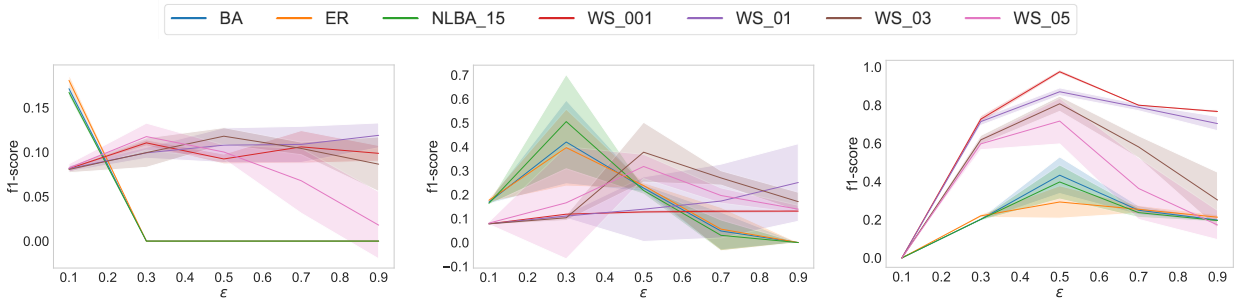

(a) $r = 3.58$ (b) $r = 3.70$ (c) $r = 4.00$

FIG. 1. Network reconstruction performance using Pearson correlation and with a fixed threshold of 0.5. Each plot shows the relationship between f1-score and ϵ for different values of r.

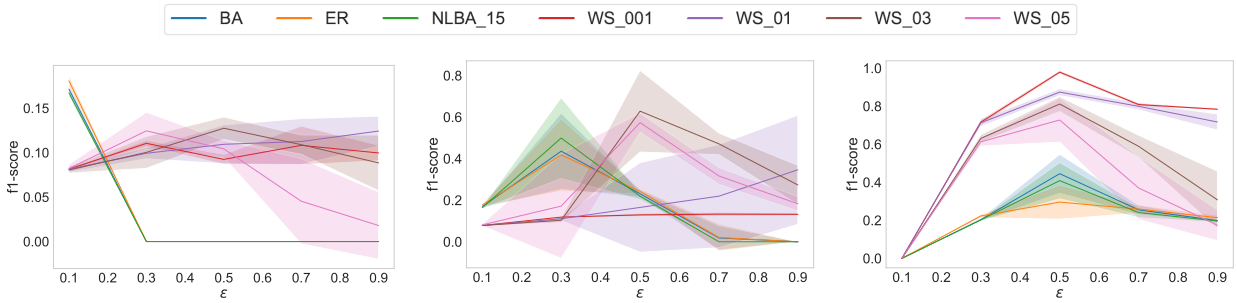

(a) $r = 3.58$ (b) $r = 3.70$ (c) $r = 4.00$

FIG. 2. Network reconstruction performance using Spearman correlation and with a fixed threshold of 0.5. Each plot shows the relationship between f1-score and ϵ for different values of r.

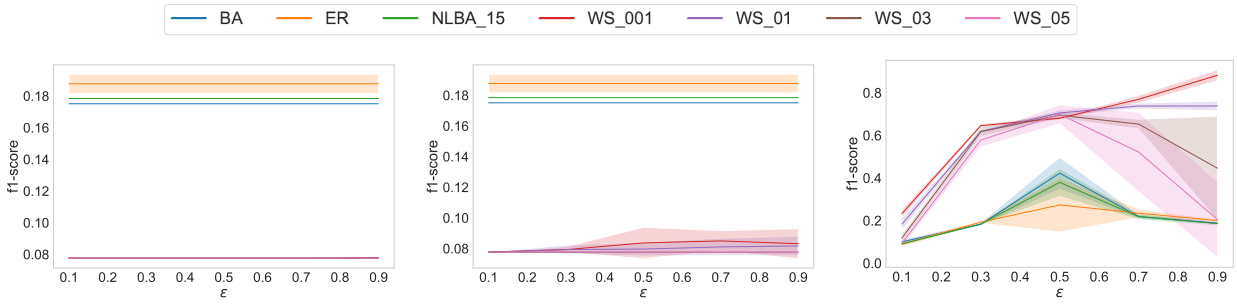

(a) $r = 3.58$ (b) $r = 3.70$ (c) $r = 4.00$

FIG. 3. Network reconstruction performance using mutual information and with a fixed threshold of 0.5. Each plot shows the relationship between f1-score and ϵ for different values of r.

low and nearly constant, showing minimal variation with respect to ϵ. ER, BA and NLBA_15 topologies exhibit slightly higher f1-scores, around 0.17–0.18, compared to other network models. In contrast, small-world networks (WS models) consistently yield the lowest f1-scores, with values close to 0.08, indicating poor reconstruction performance.

In particular, increasing r from 3.58 to 4.00 does not lead to any improvement in accuracy of the reconstruction, suggesting that PLV-based methods struggle to capture a meaningful network structure in this context. Additionally, the relatively narrow shaded regions indicate low variability in performance between multiple realizations. These findings suggest that phase locking value may not be a suitable connectivity measure for effective network reconstruction under the given conditions.

Figure 5 illustrates the network reconstruction performance using coherence as a connectivity measure, with a fixed threshold of 0.5.

For $r = 3.58$ (Figure 5(a)), the f1-score remains relatively low across all ϵ values, with a peak around $\epsilon \approx 0.4$. The performance is generally poor, suggesting that co-

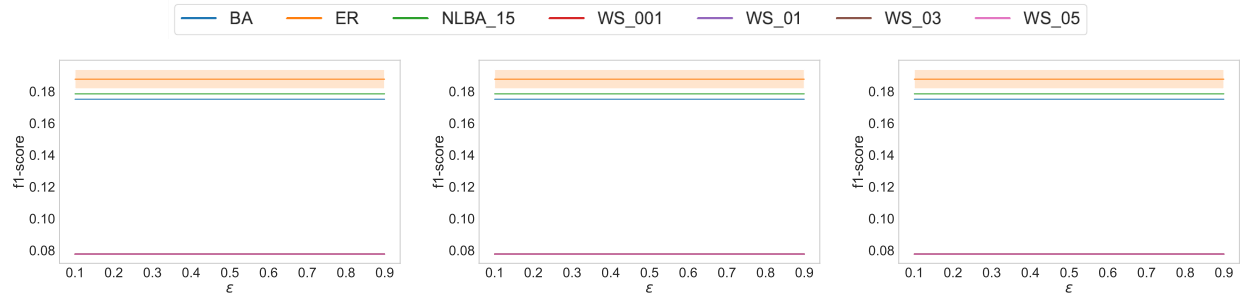

(a) $r = 3.58$ (b) $r = 3.70$ (c) $r = 4.00$

FIG. 4. Network reconstruction performance using phase locking value and with a fixed threshold of 0.5. Each plot shows the relationship between f1-score and ϵ for different values of r.

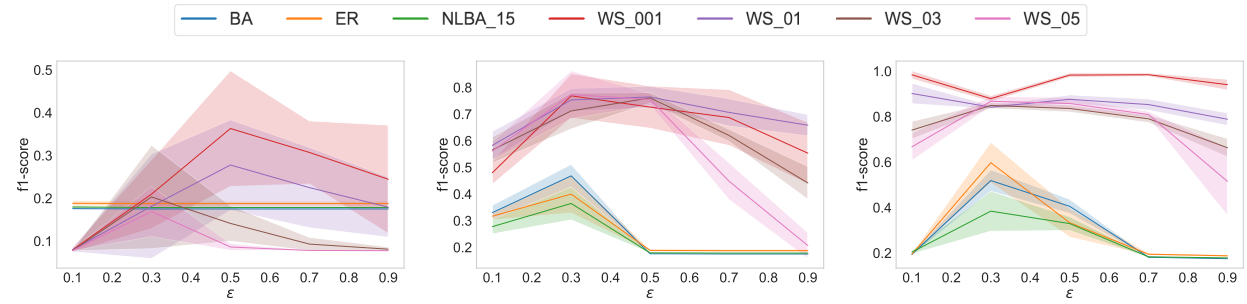

(a) $r = 3.58$ (b) $r = 3.70$ (c) $r = 4.00$

FIG. 5. Network reconstruction performance using coherence and with a fixed threshold of 0.5. Each plot shows the relationship between f1-score and ϵ for different values of r.

herence struggles to accurately reconstruct networks in this regime.

For $r = 3.70$ (Figure 5(b)), there is a noticeable improvement in f1-score, particularly for networks with more structured connectivity (e.g., WS models). The f1-score sharply increases for moderate ϵ values and then declines for larger ϵ, indicating an optimal ϵ range for reconstruction.

For $r = 4.00$ (Figure 5(c)), the performance is significantly higher, particularly for structured networks. The f1-score reaches a peak close to 1.0 for WS_001, while ER and BA networks exhibit lower scores. This suggests that for higher r values, coherence is more effective at capturing the underlying network structure, especially in more regular networks with strong local clustering, rather than in small-world or random networks.

IV. DISCUSSION

A. Reconstruction Method Comparison

The network reconstruction performance varies significantly across different methods, as observed in Figures 1 to 5. While some methods, such as Pearson and Spearman correlations, coherence and mutual information, exhibit strong reconstruction capabilities for higher values of r, others, like PLV, perform poorly across all tested conditions.

Pearson and Spearman correlations display similar trends, with f1-scores improving as r increases. Notably, WS models tend to achieve higher reconstruction accuracy compared to random (ER) or scale-free (BA, NLBA_15) networks. The highest performance is observed for $r = 4.00$ and intermediate values of ϵ, suggesting that an optimal coupling strength is needed to extract meaningful network structures. The effectiveness of these correlation-based approaches diminishes when r is low, as reconstruction remains largely unreliable in that state.

Mutual information shows a sharp transition in reconstruction performance, with negligible f1-score at $r = 3.58$ and $r = 3.70$, followed by a substantial improvement at $r = 4.00$. At this higher r, WS networks, particularly WS_001, achieve f1-score above 0.8 for a high coupling strenght ($\epsilon = 0.9$), indicating that mutual information is highly sensitive to the dynamical regime. This result suggests that when the underlying system is more chaotic, mutual information captures structural dependencies more effectively.

In contrast, PLV-based reconstruction fails to exhibit meaningful variation for all values of ϵ and r and provides consistently low f1-scores, regardless of network topol-

ogy. The narrow shaded regions suggest low variability, reinforcing the conclusion that PLV is not a suitable connectivity measure for this type of network reconstruction. The consistently poor performance, particularly for small-world networks, indicates that PLV does not sufficiently capture the underlying network structure in this context.

Coherence-based reconstruction demonstrates strong performance improvements as r increases, with WS networks showing the highest f1-scores. For $r = 4.00$, coherence achieves near-perfect reconstruction (f1-score close to 1.0) for WS_001, while maintaining relatively lower scores for ER, BA and NLBA_15 networks. This suggests that coherence is particularly effective in identifying structured networks with strong local clustering. Additionally, the presence of an optimal ϵ range reinforces the importance of parameter selection in maximizing the accuracy of the reconstruction.

The influence of the bifurcation parameter r on the reconstruction performance was previously observed in [41]. In this work, incoherent behavior, that is, fully unsynchronized dynamics, allows robust inference while periodic windows and synchronized behavior hinder inference. In the same work [41], the challenges of network inference related to coupling strength are discussed. Strong coupling leads to the emergence of global patterns in the system and as a result, inferring the true network becomes unfeasible. Conversely, for very weak coupling, the system behaves almost as if the units are uncoupled, making it difficult to detect actual connections. Therefore, for successful network inference, the authors observed that the system must be in an intermediate coupling regime.

In general, the results highlight that the choice of reconstruction method significantly affects performance, with correlation-based approaches and coherence performing well at higher r, while PLV remains ineffective under all conditions. Mutual information exhibits a sharp transition in performance, excelling only when the system reaches a sufficiently high value of r. These findings emphasize the interaction between network topology, dynamical regime, and reconstruction method, and highlight the need to select appropriate measures for accurate network inference.

B. Impact of Topology on Reconstruction

The results presented in Figures 1 to 5 highlight the significant influence of network topology on reconstruction performance across different methods. The observed variations in f1-score for different values of r and ϵ underscore the role of structural properties in determining the effectiveness of different reconstruction approaches.

A key observation is that the reconstruction performance improves as the system transitions to more chaotic regimes, with the highest f1-scores occurring at $r = 4.00$. This trend is consistent across all methods, suggesting that increased dynamical complexity enhances the detectability of interactions among nodes. However, the degree of improvement varies depending on the network topology. Particularly, WS_001 and WS_01 consistently outperform other topologies, achieving the highest f1-scores at optimal ϵ values. This suggests that the presence of strong local clustering This suggests that strong local clustering, combined with moderately short path lengths, improve the accuracy of network reconstruction.

ER, BA and NLBA_15 models generally exhibit lower reconstruction performance compared to small-world networks, particularly for larger values of r. ER networks, characterized by random connectivity and the absence of structural organization, exhibit one of the lowest performance across different reconstruction methods. BA networks, characterized by their scale-free degree distribution, also exhibit moderate to low performance, which may be due to the dominance of a few high-degree nodes (hubs), which can introduce biases in the inferred connectivity and reduce reconstruction performance.

The nonlinear Barabasi-Albert model with a preferential attachment exponent $\alpha = 1.5$ (NLBA_15) also displays f1-scores lower than those of WS networks. This can be attributed to its heterogeneous degree distribution and lower local clustering, which may introduce biases in inferred connectivity and worsens the reconstruction performance.

Overall, these results emphasize that network reconstruction is highly dependent on the interplay between the underlying network topology, the dynamical regime, and the reconstruction method employed. Small-world networks with low rewiring probability exhibit the most robust reconstruction performance across all methods, supporting the idea that strong local clustering and moderate path lengths facilitate more accurate connectivity inference. In contrast, random and scale-free networks show reduced performance, likely due to their lack of local clustering or the presence of highly heterogeneous degree distributions, which can be challenging for reconstruction.

V. CONCLUSION

In this study, we evaluated the performance of various network reconstruction methods, including Pearson correlation, Spearman correlation, mutual information, phase locking value, and coherence, across different network topologies and dynamical regimes. Our results demonstrate that reconstruction performance is highly dependent on both the chosen method and the underlying network structure.

Pearson and Spearman correlation exhibited moderate reconstruction performance, with f1-scores improving as the parameter r increased. However, their effectiveness varied across network topologies, with small-world networks generally showing better performance. Mutual information displayed a sharp transition in reconstruction

accuracy, achieving high f1-scores for large r, particularly in small-world networks. In contrast, PLV consistently failed to reconstruct network structures effectively, yielding to low and stable f1-scores across all conditions. Coherence, on the other hand, demonstrated strong reconstruction capability at high r values, with highest performance for WS networks with low rewiring probabilities ($p = 0.01$ and $p = 0.1$).

These findings underscore the importance of selecting an appropriate reconstruction metric based on the network topology and dynamic parameters. The results highlight the influence of the bifurcation parameter r, with higher values generally leading to improved reconstruction accuracy. In addition, the role of coupling strength ϵ was evident, with moderate to high values improving performance.

Despite these findings, some limitations should be acknowledged. The fixed thresholding approach may not be optimal for all methods, and adaptive thresholding strategies could further improve reconstruction performance. Furthermore, while our analysis considered a range of synthetic network topologies, more realistic networks may exhibit more complex dynamics and connectivity patterns, which require further investigation.

Future work could explore alternative connectivity measures, adaptive threshold selection methods, and the application of these techniques to other dynamical regimes. In addition, the inclusion of noise in the time series would provide a more comprehensive understanding of network reconstruction capabilities.

VI. ACKNOWLEDGEMENTS

L.F.S. is indebted to Capes (grant 88887.645667/2021-00) for the financial provided to this research. F.A.R acknowledges CNPq (grant 308162/2023-4) and FAPESP (grants 24/02322-0, 20/09835-1 and 13/07375-0) for the financial support given for his research.

[1] M. Timme and J. Casadiego, Revealing networks from dynamics: an introduction, Journal of Physics A: Mathematical and Theoretical **47**, 343001 (2014).

[2] J. Li, Z. Shen, W.-X. Wang, C. Grebogi, and Y.-C. Lai, Universal data-based method for reconstructing complex networks with binary-state dynamics, Physical Review E **95**, 032303 (2017).

[3] E. S. Ching, P.-Y. Lai, and C. Leung, Reconstructing weighted networks from dynamics, Physical Review E **91**, 030801 (2015).

[4] M. Small, Complex networks from time series: Capturing dynamics, in *2013 IEEE International Symposium on Circuits and Systems (ISCAS)* (IEEE, 2013) pp. 2509–2512.

[5] R. Guimerà and M. Sales-Pardo, Missing and spurious interactions and the reconstruction of complex networks, Proceedings of the National Academy of Sciences **106**, 22073 (2009).

[6] Y. Yang and H. Yang, Complex network-based time series analysis, Physica A: Statistical Mechanics and its Applications **387**, 1381 (2008).

[7] D. S. Bassett, A. Meyer-Lindenberg, S. Achard, T. Duke, and E. Bullmore, Adaptive reconfiguration of fractal small-world human brain functional networks, Proceedings of the National Academy of Sciences **103**, 19518 (2006).

[8] V. M. Eguiluz, D. R. Chialvo, G. A. Cecchi, M. Baliki, and A. V. Apkarian, Scale-free brain functional networks, Physical review letters **94**, 018102 (2005).

[9] K. Wu, X. Hao, J. Liu, P. Liu, and F. Shen, Online reconstruction of complex networks from streaming data, IEEE Transactions on Cybernetics **52**, 5136 (2020).

[10] G. Caldarelli, A. Chessa, F. Pammolli, A. Gabrielli, and M. Puliga, Reconstructing a credit network, Nature Physics **9**, 125 (2013).

[11] S. G. Shandilya and M. Timme, Inferring network topology from complex dynamics, New Journal of Physics **13**, 013004 (2011).

[12] G. Tirabassi, R. Sevilla-Escoboza, J. M. Buldú, and C. Masoller, Inferring the connectivity of coupled oscillators from time-series statistical similarity analysis, Scientific reports **5**, 10829 (2015).

[13] M. Bardoscia, P. Barucca, S. Battiston, F. Caccioli, G. Cimini, D. Garlaschelli, F. Saracco, T. Squartini, and G. Caldarelli, The physics of financial networks, Nature Reviews Physics **3**, 490 (2021).

[14] C. G. Antonopoulos, Network inference combining mutual information rate and statistical tests, Communications in Nonlinear Science and Numerical Simulation **116**, 106896 (2023).

[15] Y. R. Wang and H. Huang, Review on statistical methods for gene network reconstruction using expression data, Journal of theoretical biology **362**, 53 (2014).

[16] M. Lai, M. Demuru, A. Hillebrand, and M. Fraschini, A comparison between scalp-and source-reconstructed eeg networks, Scientific reports **8**, 12269 (2018).

[17] Z. Gao and N. Jin, Complex network from time series based on phase space reconstruction, Chaos: An Interdisciplinary Journal of Nonlinear Science **19** (2009).

[18] K.-C. Liang and X. Wang, Gene regulatory network reconstruction using conditional mutual information, EURASIP Journal on Bioinformatics and Systems Biology **2008**, 1 (2008).

[19] L. Novelli and J. T. Lizier, Inferring network properties from time series using transfer entropy and mutual information: Validation of multivariate versus bivariate approaches, Network Neuroscience **5**, 373 (2021).

[20] M. Rosenblum and A. Pikovsky, Inferring connectivity of an oscillatory network via the phase dynamics reconstruction, Frontiers in network physiology **3**, 1298228 (2023).

[21] B. T. Schmidt, A. S. Ghuman, and T. J. Huppert, Whole brain functional connectivity using phase locking measures of resting state magnetoencephalography, Frontiers in neuroscience **8**, 141 (2014).

[22] A. M. Bastos and J.-M. Schoffelen, A tutorial review of functional connectivity analysis methods and their interpretational pitfalls, Frontiers in systems neuroscience **9**, 175 (2016).
[23] C. J. Stam, From synchronisation to networks: Assessment of functional connectivity in the brain, Coordinated Activity in the Brain: Measurements and Relevance to Brain Function and Behavior , 91 (2009).
[24] R. M. Hutchison, T. Womelsdorf, E. A. Allen, P. A. Bandettini, V. D. Calhoun, M. Corbetta, S. Della Penna, J. H. Duyn, G. H. Glover, J. Gonzalez-Castillo, *et al.*, Dynamic functional connectivity: promise, issues, and interpretations, Neuroimage **80**, 360 (2013).
[25] Y. Du, Z. Fu, and V. D. Calhoun, Classification and prediction of brain disorders using functional connectivity: promising but challenging, Frontiers in neuroscience **12**, 525 (2018).
[26] P. K. Pandey and V. Badarla, Reconstruction of network topology using status-time-series data, Physica A: Statistical Mechanics and its Applications **490**, 573 (2018).
[27] J. Dai, K. Huang, Y. Liu, C. Yang, and Z. Wang, Global reconstruction of complex network topology via structured compressive sensing, IEEE Systems Journal **15**, 1959 (2020).
[28] S. Pajevic and D. Plenz, Efficient network reconstruction from dynamical cascades identifies small-world topology of neuronal avalanches, PLoS computational biology **5**, e1000271 (2009).
[29] P.-Y. Lai, Reconstructing network topology and coupling strengths in directed networks of discrete-time dynamics, Physical Review E **95**, 022311 (2017).
[30] K. Kaneko, Clustering, coding, switching, hierarchical ordering, and control in a network of chaotic elements, Physica D: Nonlinear Phenomena **41**, 137 (1990).
[31] O. ERD and A. Renyi, On random graphs, Publ. Math **6**, 290 (1959).
[32] P. Erdős and A. Rényi, On the strength of connectedness of a random graph, Acta Mathematica Hungarica **12**, 261 (1961).
[33] A.-L. Barabási and R. Albert, Emergence of scaling in random networks, science **286**, 509 (1999).
[34] P. L. Krapivsky, S. Redner, and F. Leyvraz, Connectivity of growing random networks, Physical review letters **85**, 4629 (2000).
[35] D. J. Watts and S. H. Strogatz, Collective dynamics of 'small-world'networks, nature **393**, 440 (1998).
[36] K. Pearson, Vii. note on regression and inheritance in the case of two parents, proceedings of the royal society of London **58**, 240 (1895).
[37] J. Hauke and T. Kossowski, Comparison of values of pearson's and spearman's correlation coefficients on the same sets of data, Quaestiones geographicae **30**, 87 (2011).
[38] T. M. Cover, *Elements of information theory* (John Wiley & Sons, 1999).
[39] J.-P. Lachaux, E. Rodriguez, J. Martinerie, and F. J. Varela, Measuring phase synchrony in brain signals, Human brain mapping **8**, 194 (1999).
[40] G. C. Carter, Coherence and time delay estimation, Proceedings of the IEEE **75**, 236 (1987).
[41] N. Rubido, A. C. Martí, E. Bianco-Martínez, C. Grebogi, M. S. Baptista, and C. Masoller, Exact detection of direct links in networks of interacting dynamical units, New Journal of Physics **16**, 093010 (2014).

Appendix A: Network reconstruction using coupled logistic maps dynamics

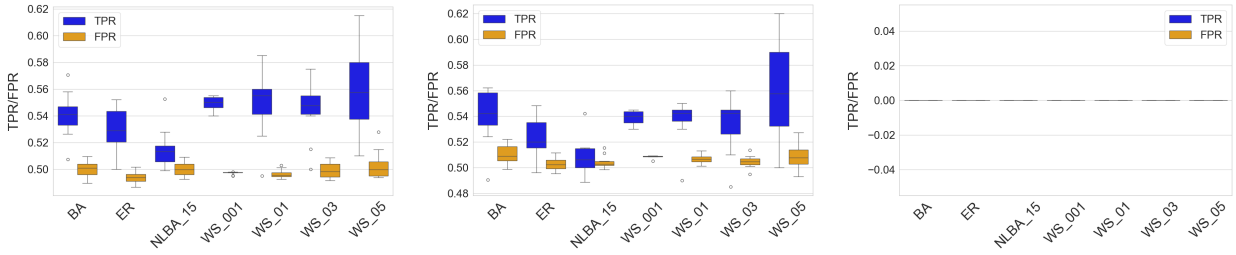

(a) $r = 3.58$, $\epsilon = 0.1$ (b) $r = 3.70$, $\epsilon = 0.1$ (c) $r = 4.00$, $\epsilon = 0.1$

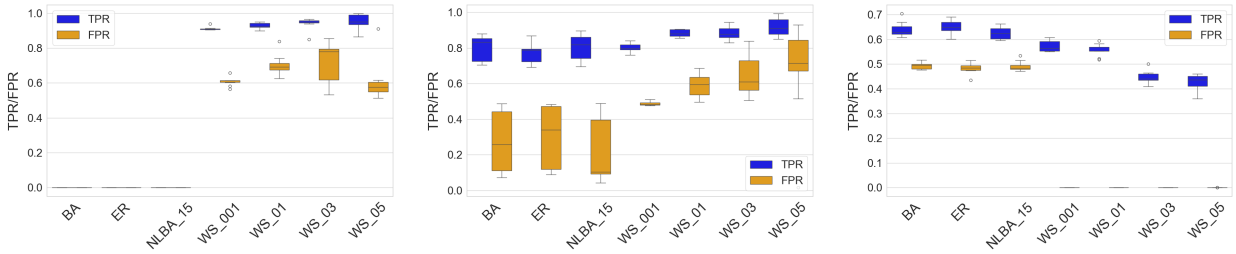

(d) $r = 3.58$, $\epsilon = 0.3$ (e) $r = 3.70$, $\epsilon = 0.3$ (f) $r = 4.00$, $\epsilon = 0.3$

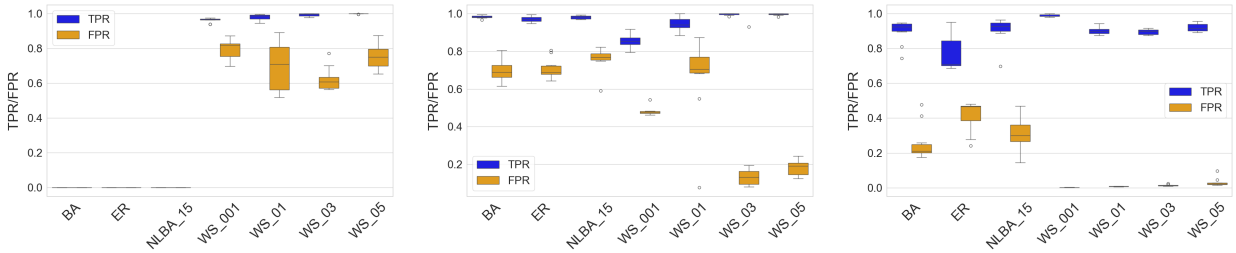

(g) $r = 3.58$, $\epsilon = 0.5$ (h) $r = 3.70$, $\epsilon = 0.5$ (i) $r = 4.00$, $\epsilon = 0.5$

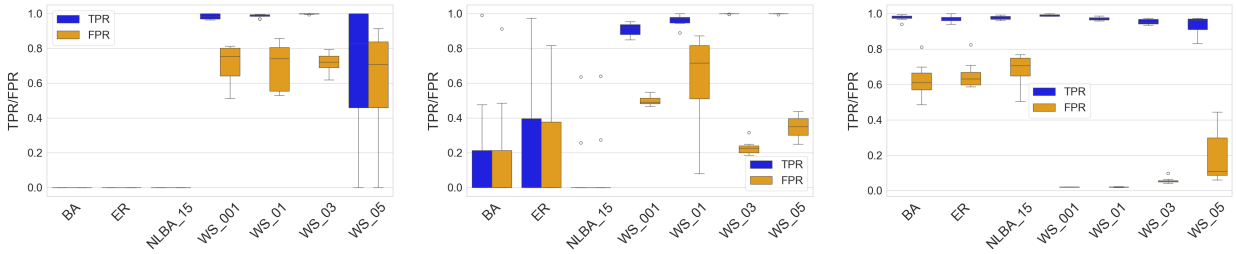

(j) $r = 3.58$, $\epsilon = 0.7$ (k) $r = 3.70$, $\epsilon = 0.7$ (l) $r = 4.00$, $\epsilon = 0.7$

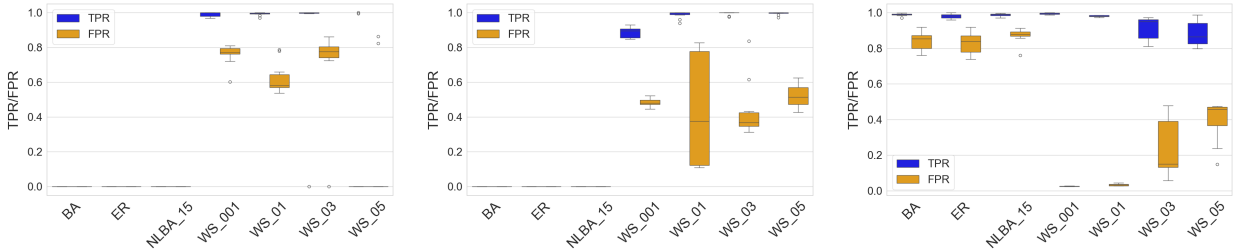

(m) $r = 3.58$, $\epsilon = 0.9$ (n) $r = 3.70$, $\epsilon = 0.9$ (o) $r = 4.00$, $\epsilon = 0.9$

FIG. 6. Box plots illustrating the TPR and FPR using Pearson correlation coefficient for different values of r and ϵ, with a fixed threshold of 0.5. Each row corresponds to a different value of ϵ, while the columns represent different values of r.

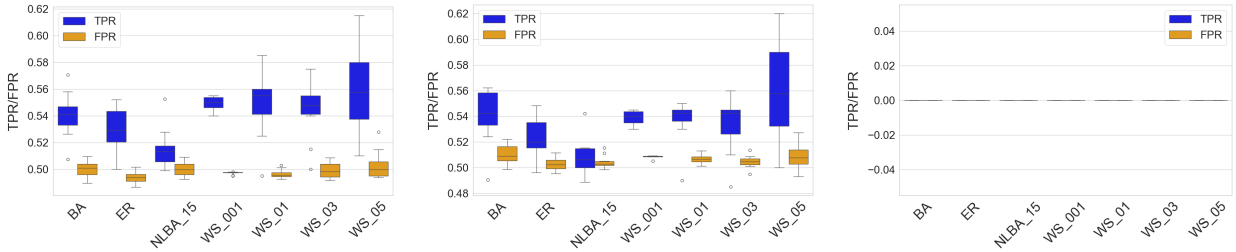

(a) $r = 3.58$, $\epsilon = 0.1$ (b) $r = 3.70$, $\epsilon = 0.1$ (c) $r = 4.00$, $\epsilon = 0.1$

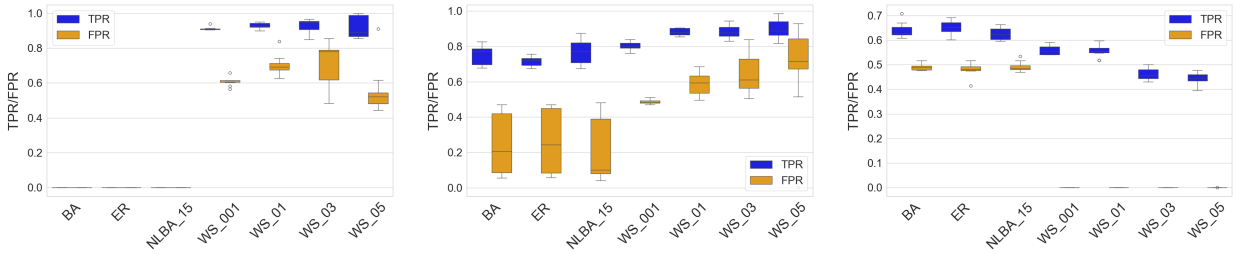

(d) $r = 3.58$, $\epsilon = 0.3$ (e) $r = 3.70$, $\epsilon = 0.3$ (f) $r = 4.00$, $\epsilon = 0.3$

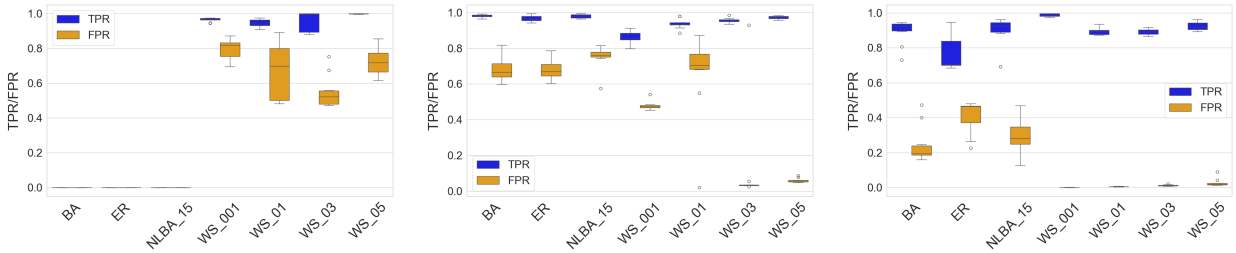

(g) $r = 3.58$, $\epsilon = 0.5$ (h) $r = 3.70$, $\epsilon = 0.5$ (i) $r = 4.00$, $\epsilon = 0.5$

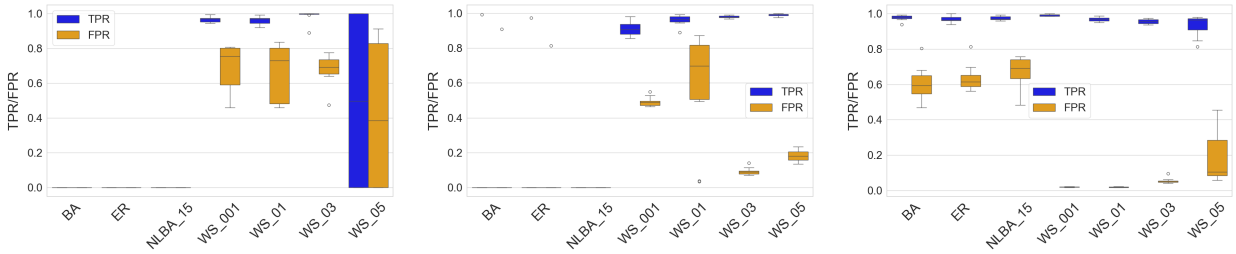

(j) $r = 3.58$, $\epsilon = 0.7$ (k) $r = 3.70$, $\epsilon = 0.7$ (l) $r = 4.00$, $\epsilon = 0.7$

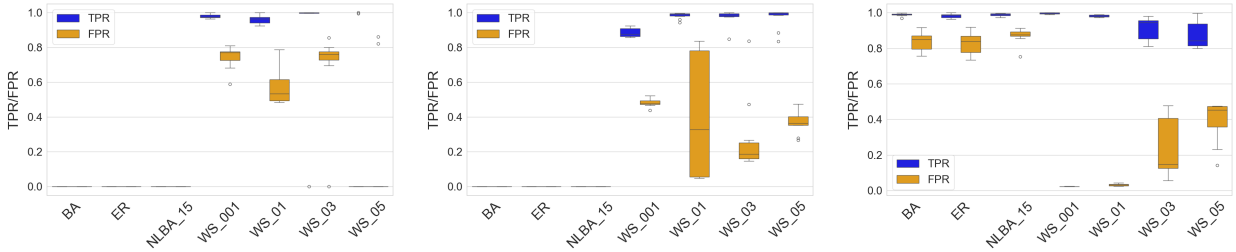

(m) $r = 3.58$, $\epsilon = 0.9$ (n) $r = 3.70$, $\epsilon = 0.9$ (o) $r = 4.00$, $\epsilon = 0.9$

FIG. 7. Box plots illustrating the TPR and FPR using Spearman correlation coefficient for different values of r and ϵ, with a fixed threshold of 0.5. Each row corresponds to a different value of ϵ, while the columns represent different values of r.

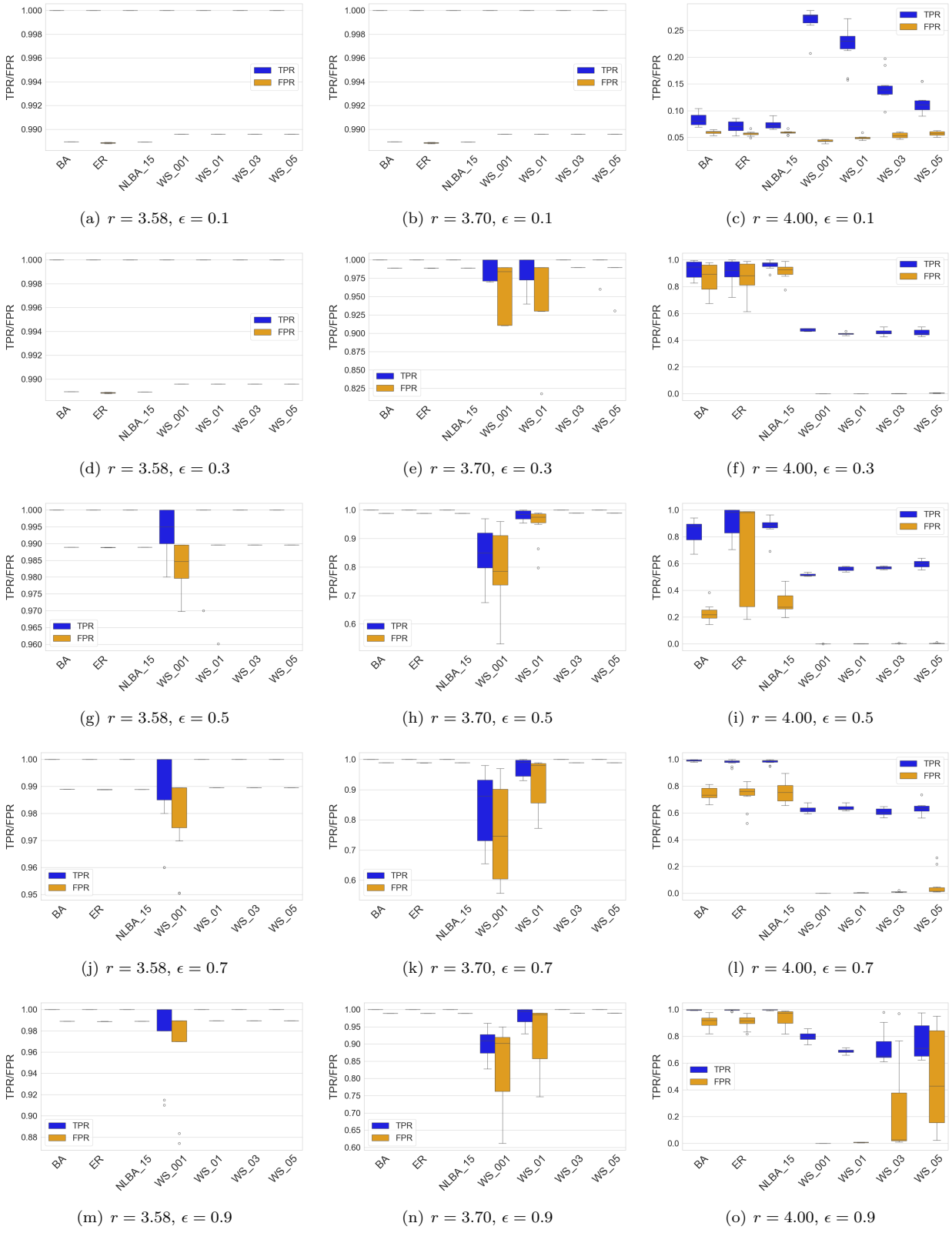

(a) $r = 3.58$, $\epsilon = 0.1$ (b) $r = 3.70$, $\epsilon = 0.1$ (c) $r = 4.00$, $\epsilon = 0.1$

(d) $r = 3.58$, $\epsilon = 0.3$ (e) $r = 3.70$, $\epsilon = 0.3$ (f) $r = 4.00$, $\epsilon = 0.3$

(g) $r = 3.58$, $\epsilon = 0.5$ (h) $r = 3.70$, $\epsilon = 0.5$ (i) $r = 4.00$, $\epsilon = 0.5$

(j) $r = 3.58$, $\epsilon = 0.7$ (k) $r = 3.70$, $\epsilon = 0.7$ (l) $r = 4.00$, $\epsilon = 0.7$

(m) $r = 3.58$, $\epsilon = 0.9$ (n) $r = 3.70$, $\epsilon = 0.9$ (o) $r = 4.00$, $\epsilon = 0.9$

FIG. 8. Box plots illustrating the TPR and FPR using mutual information for different values of r and ϵ, with a fixed threshold of 0.5.

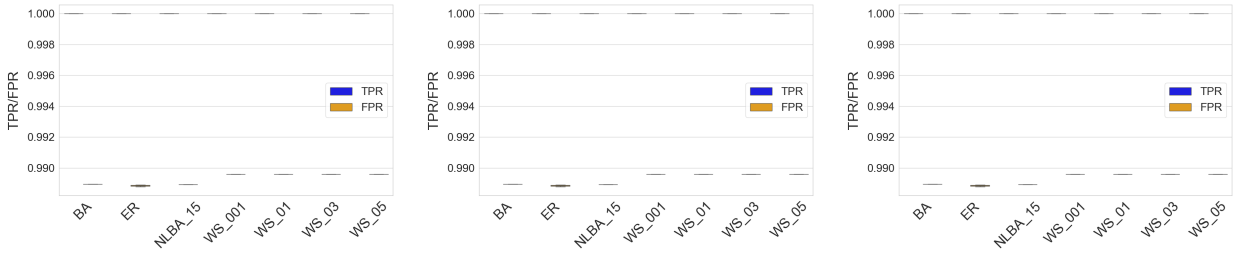

(a) $r = 3.58$, $\epsilon = 0.1$ (b) $r = 3.70$, $\epsilon = 0.1$ (c) $r = 4.00$, $\epsilon = 0.1$

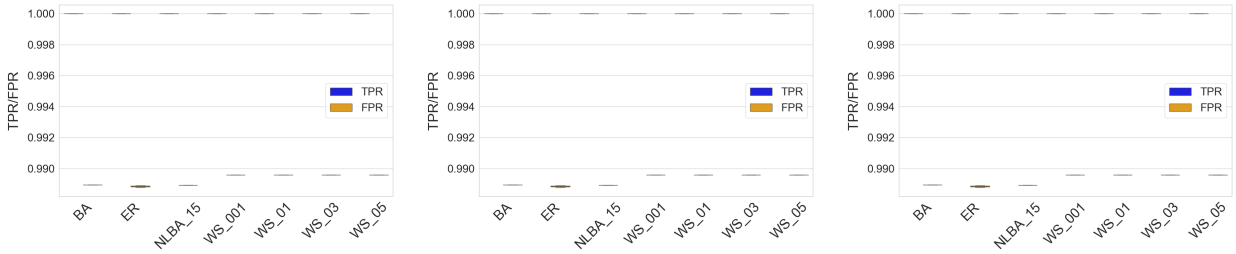

(d) $r = 3.58$, $\epsilon = 0.3$ (e) $r = 3.70$, $\epsilon = 0.3$ (f) $r = 4.00$, $\epsilon = 0.3$

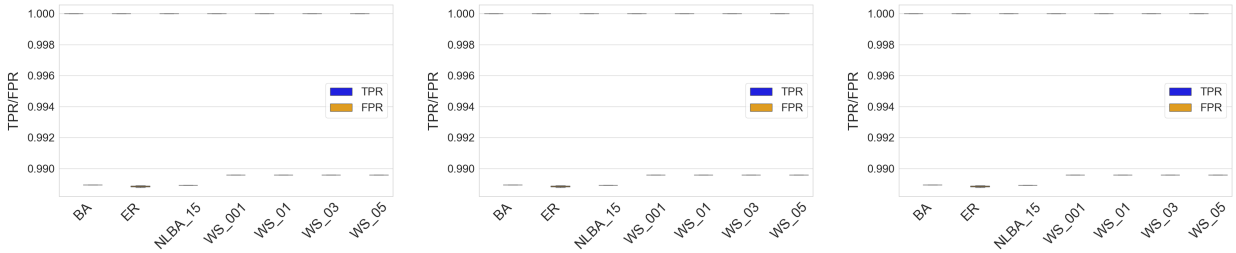

(g) $r = 3.58$, $\epsilon = 0.5$ (h) $r = 3.70$, $\epsilon = 0.5$ (i) $r = 4.00$, $\epsilon = 0.5$

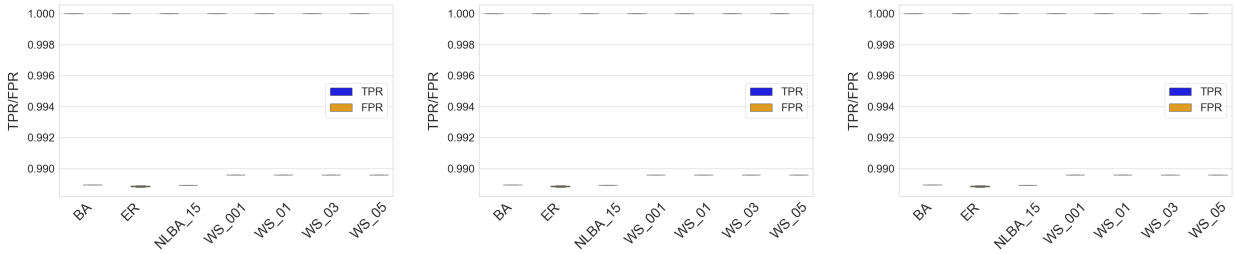

(j) $r = 3.58$, $\epsilon = 0.7$ (k) $r = 3.70$, $\epsilon = 0.7$ (l) $r = 4.00$, $\epsilon = 0.7$

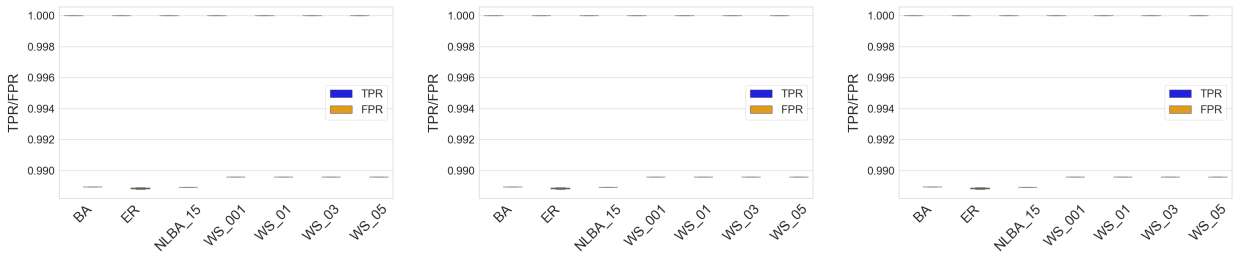

(m) $r = 3.58$, $\epsilon = 0.9$ (n) $r = 3.70$, $\epsilon = 0.9$ (o) $r = 4.00$, $\epsilon = 0.9$

FIG. 9. Box plots illustrating the TPR and FPR using phase-locking value (PLV) for different values of r and ϵ, with a fixed threshold of 0.5.

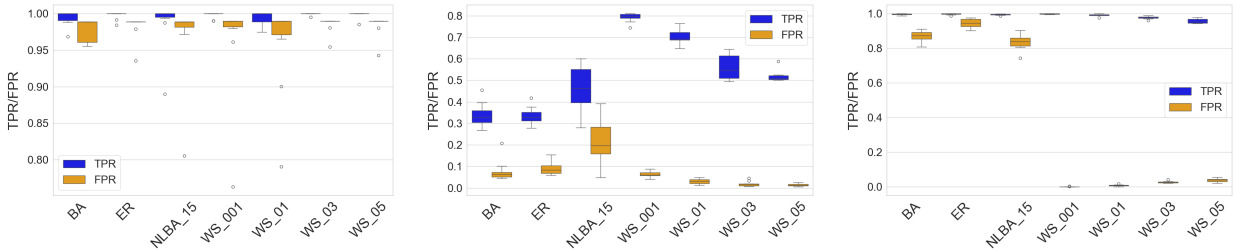

(a) $r = 3.58$, $\epsilon = 0.1$ (b) $r = 3.70$, $\epsilon = 0.1$ (c) $r = 4.00$, $\epsilon = 0.1$

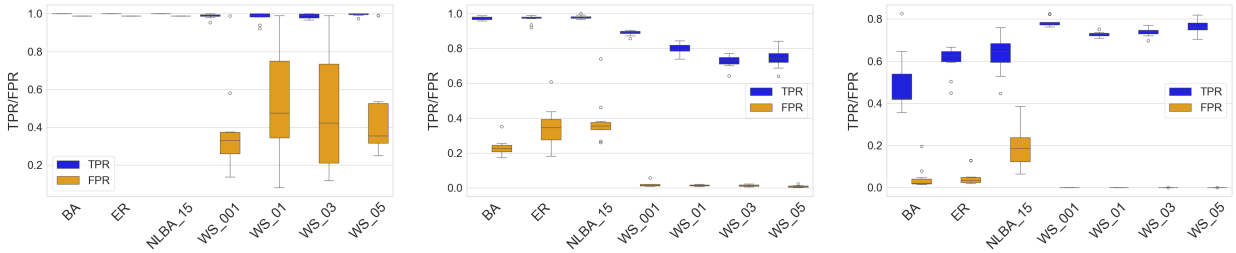

(d) $r = 3.58$, $\epsilon = 0.3$ (e) $r = 3.70$, $\epsilon = 0.3$ (f) $r = 4.00$, $\epsilon = 0.3$

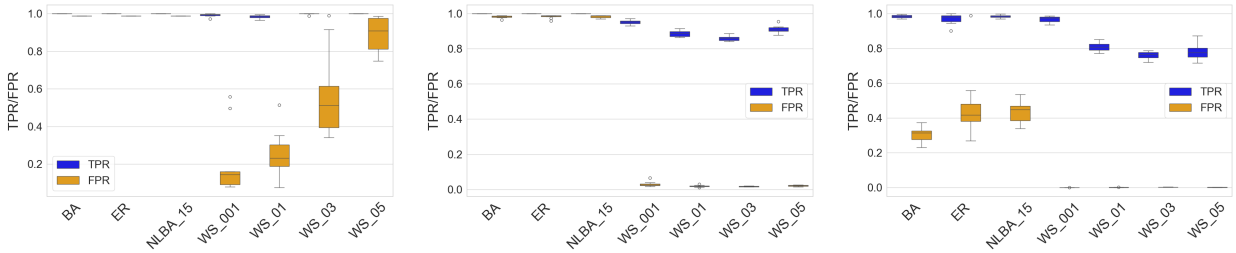

(g) $r = 3.58$, $\epsilon = 0.5$ (h) $r = 3.70$, $\epsilon = 0.5$ (i) $r = 4.00$, $\epsilon = 0.5$

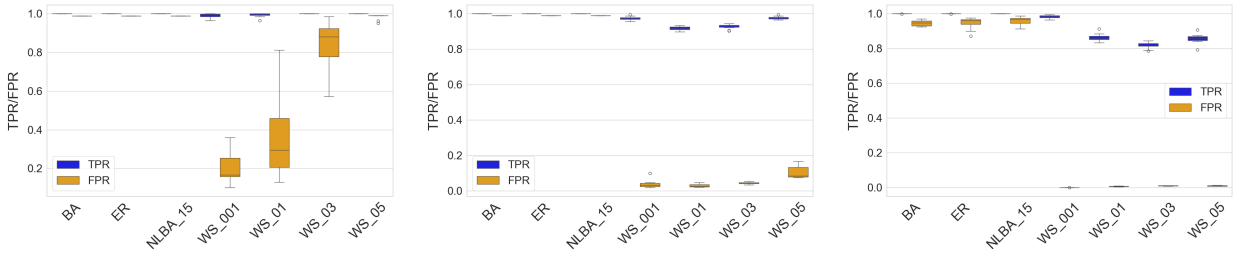

(j) $r = 3.58$, $\epsilon = 0.7$ (k) $r = 3.70$, $\epsilon = 0.7$ (l) $r = 4.00$, $\epsilon = 0.7$

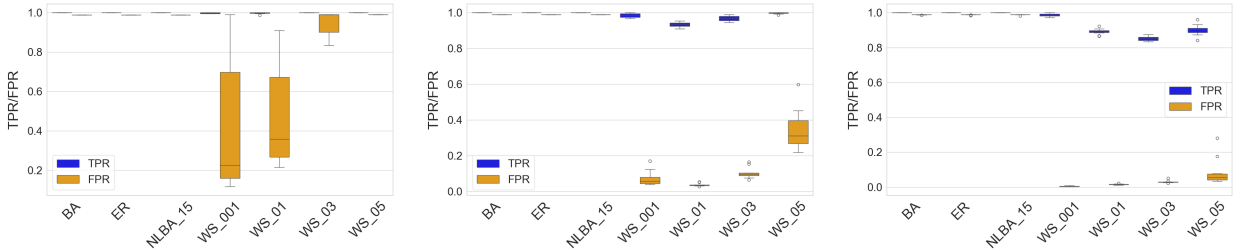

(m) $r = 3.58$, $\epsilon = 0.9$ (n) $r = 3.70$, $\epsilon = 0.9$ (o) $r = 4.00$, $\epsilon = 0.9$

FIG. 10. Box plots illustrating the TPR and FPR using coherence for different values of r and ϵ, with a fixed threshold of 0.5.

CHAPTER

8

CONCLUSION

In this thesis, we explore the application of machine learning and network analysis to various neurological and psychological disorders, aiming to uncover distinct patterns and contributing to more precise diagnostic and therapeutic strategies. Through these investigations, we discovered novel insights into the patterns of brain connectivity of several disorders such as Major Depressive Disorder (MDD), Autism Spectrum Disorder (ASD), Asperger Syndrome (AS), Attention Deficit Hyperactivity Disorder (ADHD), and Parkinson's Disease (PD). Additionally, we examined how the network topology and dynamical states influence the performance of network reconstruction for different connectivity metrics through simulation studies.

In Chapter 3, we examine MDD using machine learning and network-based methodologies, identifying specific biomarkers and connectivity patterns that enhance our understanding of the neural mechanisms underlying MDD. We demonstrated the effectiveness of machine learning algorithms in detecting disruptions in brain networks associated with MDD, particularly in regions involved in emotional regulation and cognitive processing. This study highlights the potential of EEG-based connectivity measures as reliable biomarkers for MDD and underscores the critical role of specific brain regions in the development and progression of the disorder.

Chapter 4 focused on multiclass classification of ASD, ADHD, and TD and contributed to a deeper understanding of these neurodevelopmental disorders. By integrating normalized transfer entropy with effective information, determinism, and degeneracy coefficients, this work provides deeper insight into network segregation and integration under these conditions. The results revealed different neural signatures associated with ASD and ADHD, particularly in regions related to social cognition, decision-making, and sensory processing. Furthermore, network analysis highlights fragmented connectivity in ASD and intermediate network cohesion in ADHD. These findings not only surpass previous benchmarks in classification performance, but also contribute to the development of improved diagnostic tools and clinical decision support systems.

In Chapter 6, we investigated the progression of PD by analyzing temporal patterns of EEG connectivity. Our study presents a novel approach by stratifying patients according to the duration of the disease, revealing a continuum of connectivity alterations across disease stages, and coherence emerged as a key metric for for distinguishing PD patients and underscored how neural connectivity evolves over time. The integration of SHAP values enhanced the interpretability of the ML model, strengthening the reliability and clinical relevance of the results. Despite of some limitations of the dataset, the proposed methodologies achieved high classification accuracy, highlighting the robustness of the methodology used.

Finally, In Chapter 7, we investigate the impact of network topology on reconstruction performance using various functional connectivity measures applied to coupled logistic maps. Our findings highlight that Watts-Strogatz networks with low rewiring probabilities exhibit the highest reconstruction performance using coherence, emphasizing the role of local clustering and moderate path lengths in enabling reliable inference. Furthermore, we demonstrate how the dynamics, ruled by the bifurcation parameter r and the coupling strength ε influence the reconstruction performance. The results highlight the challenges presented by different dynamic conditions and highlight the sensitivity of reconstruction methods to both network structure and system dynamics.

Collectively, this thesis highlights the effectiveness of integrating machine learning with network analysis to elucidate the complex neural architectures underlying various disorders. The insights gained not only a deeper understanding of these conditions, but also provide a basis for the development of targeted, personalized treatment approaches.

Throughout all chapters, the application of machine learning and network analysis to brain data has significantly contributed to our understanding of the complex neural structures associated with different disorders. This thesis demonstrates that these methodologies are not only complementary, but also essential for advancing research in computational neuroscience. The findings presented here establish a foundation for future studies that aim to refine the diagnosis, optimize treatments, and ultimately improve the quality of life of individuals affected by these conditions. Through novel insights and methodologies, this thesis makes a meaningful contribution to the field of computational neuroscience.

8.1 Future works

The primary objective of this thesis is to reconstruct functional connectivity from time series data in neuroscience to classify brain disorders while determining the most appropriate reconstruction metrics and computational algorithms for each disorder studied. Although this thesis provides valuable information for the application of machine learning and network analysis to understanding complex neural disorders, several opportunities remain for future exploration to further refine and extend these findings.

One possible direction is to apply the proposed methodology to other neurological and psychiatric disorders and to assess its generalization and effectiveness in different conditions.

Another important approach is to investigate common patterns and characteristics between different brain disorders, which could improve classification models and provide deeper insights into their underlying mechanisms.

In addition, integrating brain connectivity data with genetic, clinical and other biological information can improve predictive accuracy and uncover more comprehensive biomarkers of neurological disorders, leading to improved diagnostic and treatment strategies.

Finally, computational simulations will be conducted to analyze the influence of topology on network reconstruction using various dynamic models to predict the level of reconstruction achievable in each case. In addition, random noise will be incorporated to evaluate the robustness of reconstruction methods under different levels of external perturbations. This will help determine how sensitive each method is to measurement noise and incomplete data, which are common challenges in real-world applications.

BIBLIOGRAPHY

ABASOLO, D.; ESCUDERO, J.; HORNERO, R.; GÓMEZ, C.; ESPINO, P. Approximate entropy and auto mutual information analysis of the electroencephalogram in alzheimer's disease patients. **Medical & biological engineering & computing**, Springer, v. 46, p. 1019–1028, 2008. Citation on page 31.

ABDELHALIM, K.; SMOLYAKOV, V.; GENOV, R. Phase-synchronization early epileptic seizure detector vlsi architecture. **IEEE transactions on biomedical circuits and systems**, IEEE, v. 5, n. 5, p. 430–438, 2011. Citation on page 33.

ACHARD, S.; SALVADOR, R.; WHITCHER, B.; SUCKLING, J.; BULLMORE, E. A resilient, low-frequency, small-world human brain functional network with highly connected association cortical hubs. **Journal of Neuroscience**, Soc Neuroscience, v. 26, n. 1, p. 63–72, 2006. Citation on page 37.

AHMADLOU, M.; ADELI, H.; ADELI, A. Fuzzy synchronization likelihood-wavelet methodology for diagnosis of autism spectrum disorder. **Journal of neuroscience methods**, Elsevier, v. 211, n. 2, p. 203–209, 2012. Citation on page 104.

AL-HIYALI, M. I.; YAHYA, N.; FAYE, I.; HUSSEIN, A. F. Identification of autism subtypes based on wavelet coherence of bold fmri signals using convolutional neural network. **Sensors**, MDPI, v. 21, n. 16, p. 5256, 2021. Citation on page 104.

ALEXANDER-BLOCH, A. F.; GOGTAY, N.; MEUNIER, D.; BIRN, R.; CLASEN, L.; LALONDE, F.; LENROOT, R.; GIEDD, J.; BULLMORE, E. T. Disrupted modularity and local connectivity of brain functional networks in childhood-onset schizophrenia. **Frontiers in systems neuroscience**, Frontiers Research Foundation, v. 4, p. 147, 2010. Citation on page 37.

ALJALAL, M.; ALDOSARI, S. A.; MOLINAS, M.; ALSHARABI, K.; ALTURKI, F. A. Detection of parkinson's disease from eeg signals using discrete wavelet transform, different entropy measures, and machine learning techniques. **Scientific Reports**, Nature Publishing Group UK London, v. 12, n. 1, p. 22547, 2022. Citation on page 145.

ALVES, C.; THAISE, G. d. O.; AGUIAR, P. de C.; PINEDA, A. M.; ROSTER, K.; THIELEMANN, C.; PORTO, J. A. M.; RODRIGUES, F. A. Diagnosis of autism spectrum disorder based on functional brain networks and machine learning. 2022. Citations on pages 15, 23, 25, 26, and 38.

ALVES, C. L.; CURY, R. G.; ROSTER, K.; PINEDA, A. M.; RODRIGUES, F. A.; THIELEMANN, C.; CIBA, M. Application of machine learning and complex network measures to an eeg dataset from ayahuasca experiments. **Plos one**, Public Library of Science San Francisco, CA USA, v. 17, n. 12, p. e0277257, 2022. Citations on pages 15 and 38.

ALVES, C. L.; PINEDA, A. M.; ROSTER, K.; THIELEMANN, C.; RODRIGUES, F. A. Eeg functional connectivity and deep learning for automatic diagnosis of brain disorders: Alzheimer's disease and schizophrenia. **Journal of Physics: Complexity**, IOP Publishing, v. 3, n. 2, p. 025001, 2022. Citations on pages 15, 16, 25, 26, 35, 38, and 39.

ALVES, C. L.; TOUTAIN, T. G. d. O.; AGUIAR, P. de C.; PINEDA, A. M.; ROSTER, K.; THIELEMANN, C.; PORTO, J. A. M.; RODRIGUES, F. A. Diagnosis of autism spectrum disorder based on functional brain networks and machine learning. **Scientific Reports**, Nature Publishing Group UK London, v. 13, n. 1, p. 8072, 2023. Citation on page 38.

ALVES, C. L.; TOUTAIN, T. G. d. O.; PORTO, J. A. M.; AGUIAR, P. d. C.; PINEDA, A. M.; RODRIGUES, F. A.; SENA, E. P.; THIELEMANN, C. Analysis of functional connectivity using machine learning and deep learning in multimodal data from patients with schizophrenia. **medRxiv**, Cold Spring Harbor Laboratory Press, p. 2022–11, 2022. Citations on pages 37 and 39.

AMOROSO, N.; ROCCA, M. L.; MONACO, A.; BELLOTTI, R.; TANGARO, S. Complex networks reveal early mri markers of parkinson's disease. **Medical image analysis**, Elsevier, v. 48, p. 12–24, 2018. Citation on page 145.

ANGULO, M. T.; MORENO, J. A.; LIPPNER, G.; BARABÁSI, A.-L.; LIU, Y.-Y. Fundamental limitations of network reconstruction from temporal data. **Journal of the Royal Society Interface**, The Royal Society, v. 14, n. 127, p. 20160966, 2017. Citations on pages 15, 16, and 167.

ANIK, I. A.; KAMAL, A.; KABIR, M. A.; UDDIN, S.; MONI, M. A. A robust deep-learning model to detect major depressive disorder utilising eeg signals. **IEEE Transactions on Artificial Intelligence**, IEEE, 2024. Citation on page 41.

ANTONOPOULOS, C. G. Network inference combining mutual information rate and statistical tests. **Communications in Nonlinear Science and Numerical Simulation**, Elsevier, v. 116, p. 106896, 2023. Citation on page 167.

AOE, J.; FUKUMA, R.; YANAGISAWA, T.; HARADA, T.; TANAKA, M.; KOBAYASHI, M.; INOUE, Y.; YAMAMOTO, S.; OHNISHI, Y.; KISHIMA, H. Automatic diagnosis of neurological diseases using meg signals with a deep neural network. **Scientific reports**, Nature Publishing Group UK London, v. 9, n. 1, p. 5057, 2019. Citation on page 38.

ARBABSHIRANI, M. R.; PLIS, S.; SUI, J.; CALHOUN, V. D. Single subject prediction of brain disorders in neuroimaging: Promises and pitfalls. **Neuroimage**, Elsevier, v. 145, p. 137–165, 2017. Citations on pages 65 and 66.

ARICI, M. K.; TUNCBAG, N. Performance assessment of the network reconstruction approaches on various interactomes. **Frontiers in molecular biosciences**, Frontiers Media SA, v. 8, p. 666705, 2021. Citation on page 16.

ARRIDGE, S.; MAASS, P.; ÖKTEM, O.; SCHÖNLIEB, C.-B. Solving inverse problems using data-driven models. **Acta Numerica**, Cambridge University Press, v. 28, p. 1–174, 2019. Citation on page 21.

BALESTRINO, R.; SCHAPIRA, A. Parkinson disease. **European journal of neurology**, Wiley Online Library, v. 27, n. 1, p. 27–42, 2020. Citation on page 145.

BARABÁSI, A.-L.; ALBERT, R. Emergence of scaling in random networks. **science**, American Association for the Advancement of Science, v. 286, n. 5439, p. 509–512, 1999. Citation on page 16.

BARDOSCIA, M.; BARUCCA, P.; BATTISTON, S.; CACCIOLI, F.; CIMINI, G.; GARLASCHELLI, D.; SARACCO, F.; SQUARTINI, T.; CALDARELLI, G. The physics of financial networks. **Nature Reviews Physics**, Nature Publishing Group UK London, v. 3, n. 7, p. 490–507, 2021. Citations on pages 21 and 167.

BARNETT, L.; BOSSOMAIER, T. Transfer entropy as a log-likelihood ratio. **Physical review letters**, APS, v. 109, n. 13, p. 138105, 2012. Citation on page 35.

BARNETT, L.; MUTHUKUMARASWAMY, S. D.; CARHART-HARRIS, R. L.; SETH, A. K. Decreased directed functional connectivity in the psychedelic state. **NeuroImage**, Elsevier, v. 209, p. 116462, 2020. Citation on page 34.

BARRAT, A.; BARTHELEMY, M.; PASTOR-SATORRAS, R.; VESPIGNANI, A. The architecture of complex weighted networks. **Proceedings of the national academy of sciences**, National Acad Sciences, v. 101, n. 11, p. 3747–3752, 2004. Citation on page 15.

BARTTFELD, P.; WICKER, B.; CUKIER, S.; NAVARTA, S.; LEW, S.; SIGMAN, M. A big-world network in asd: dynamical connectivity analysis reflects a deficit in long-range connections and an excess of short-range connections. **Neuropsychologia**, Elsevier, v. 49, n. 2, p. 254–263, 2011. Citation on page 37.

BASSETT, D. S.; BULLMORE, E. T. Human brain networks in health and disease. **Current opinion in Neurology**, NIH Public Access, v. 22, n. 4, p. 340, 2009. Citations on pages 16 and 24.

BASSETT, D. S.; MEYER-LINDENBERG, A.; ACHARD, S.; DUKE, T.; BULLMORE, E. Adaptive reconfiguration of fractal small-world human brain functional networks. **Proceedings of the National Academy of Sciences**, National Academy of Sciences, v. 103, n. 51, p. 19518–19523, 2006. Citations on pages 25 and 167.

BASSETT, D. S.; SPORNS, O. Network neuroscience. **Nature Neuroscience**, Nature Publishing Group, v. 20, n. 3, p. 353–364, 2017. Citations on pages 25, 28, and 34.

BASTOS, A. M.; SCHOFFELEN, J.-M. A tutorial review of functional connectivity analysis methods and their interpretational pitfalls. **Frontiers in systems neuroscience**, Frontiers Media SA, v. 9, p. 175, 2016. Citations on pages 27, 31, and 167.

BENDAT, J. S.; PIERSOL, A. G. **Random data: analysis and measurement procedures**. [S.l.]: John Wiley & Sons, 2011. Citation on page 31.

BINNEWIJZEND, M. A.; ADRIAANSE, S. M.; FLIER, W. M. Van der; TEUNISSEN, C. E.; MUNCK, J. C. D.; STAM, C. J.; SCHELTENS, P.; BERCKEL, B. N. V.; BARKHOF, F.; WINK, A. M. Brain network alterations in alzheimer's disease measured by eigenvector centrality in fmri are related to cognition and csf biomarkers. **Human brain mapping**, Wiley Online Library, v. 35, n. 5, p. 2383–2393, 2014. Citation on page 28.

BOCCALETTI, S.; LATORA, V.; MORENO, Y.; CHAVEZ, M.; HWANG, D.-U. Complex networks: Structure and dynamics. **Physics Reports**, Elsevier, v. 424, n. 4-5, p. 175–308, 2006. Citations on pages 15 and 21.

BORNHOLDT, S. Boolean network models of cellular regulation: prospects and limitations. **Journal of the Royal Society interface**, The Royal Society London, v. 5, n. suppl_1, p. S85–S94, 2008. Citation on page 21.

BORST, A.; THEUNISSEN, F. E. Information theory and neural coding. **Nature neuroscience**, Nature Publishing Group, v. 2, n. 11, p. 947–957, 1999. Citation on page 30.

BOWYER, S. M. Coherence a measure of the brain networks: past and present. **Neuropsychiatric Electrophysiology**, Springer, v. 2, p. 1–12, 2016. Citations on pages 31 and 32.

BRAZIER, M. A. Spread of seizure discharges in epilepsy: anatomical and electrophysiological considerations. **Experimental neurology**, Elsevier, v. 36, n. 2, p. 263–272, 1972. Citation on page 31.

BRUNTON, S. L.; PROCTOR, J. L.; KUTZ, J. N. Discovering governing equations from data by sparse identification of nonlinear dynamical systems. **Proceedings of the national academy of sciences**, National Academy of Sciences, v. 113, n. 15, p. 3932–3937, 2016. Citation on page 22.

BULLMORE, E.; SPORNS, O. Complex brain networks: graph theoretical analysis of structural and functional systems. **Nature reviews neuroscience**, Nature Publishing Group UK London, v. 10, n. 3, p. 186–198, 2009. Citations on pages 17, 24, 25, and 26.

____. The economy of brain network organization. **Nature reviews neuroscience**, Nature Publishing Group UK London, v. 13, n. 5, p. 336–349, 2012. Citation on page 22.

BUTTE, A. J.; KOHANE, I. S. Mutual information relevance networks: functional genomic clustering using pairwise entropy measurements. In: **Biocomputing 2000**. [S.l.]: World Scientific, 1999. p. 418–429. Citation on page 22.

CALDARELLI, G.; CHESSA, A.; PAMMOLLI, F.; GABRIELLI, A.; PULIGA, M. Reconstructing a credit network. **Nature Physics**, Nature Publishing Group UK London, v. 9, n. 3, p. 125–126, 2013. Citation on page 167.

CARLOS-SANDBERG, L.; CLACK, C. D. Incorporation of causality structures to complex network analysis of time-varying behaviour of multivariate time series. **Scientific Reports**, Nature Publishing Group UK London, v. 11, n. 1, p. 18880, 2021. Citation on page 35.

CASADIEGO, J.; NITZAN, M.; HALLERBERG, S.; TIMME, M. Model-free inference of direct network interactions from nonlinear collective dynamics. **Nature communications**, Nature Publishing Group UK London, v. 8, n. 1, p. 2192, 2017. Citation on page 22.

CHAWLA, D.; LUMER, E. D.; FRISTON, K. J. The relationship between synchronization among neuronal populations and their mean activity levels. **Neural Computation**, MIT Press, v. 11, n. 6, p. 1389–1411, 1999. Citation on page 33.

CHEN, C.-C.; HSIEH, J.-C.; WU, Y.-Z.; LEE, P.-L.; CHEN, S.-S.; NIDDAM, D. M.; YEH, T.-C.; WU, Y.-T. Mutual-information-based approach for neural connectivity during self-paced finger lifting task. **Human brain mapping**, Wiley Online Library, v. 29, n. 3, p. 265–280, 2008. Citation on page 31.

CHEN, W.; CAI, Y.; LI, A.; JIANG, K.; SU, Y. Mdd brain network analysis based on eeg functional connectivity and graph theory. **Heliyon**, Elsevier, v. 10, n. 17, 2024. Citation on page 41.

COLLABORATORS, G. . Global burden of disease study 2020 (gbd 2020) results. **Institute for Health Metrics and Evaluation (IHME)**, 2021. Available: <http://www.healthdata.org/gbd>. Citation on page 41.

COLLABORATORS, G. . M. D. *et al.* Global, regional, and national burden of 12 mental disorders in 204 countries and territories, 1990–2019: a systematic analysis for the global burden of disease study 2019. **The Lancet Psychiatry**, Elsevier, v. 9, n. 2, p. 137–150, 2022. Citation on page 16.

CONSTANTINO, J. N.; CHARMAN, T. Diagnosis of autism spectrum disorder: reconciling the syndrome, its diverse origins, and variation in expression. **The lancet neurology**, Elsevier, v. 15, n. 3, p. 279–291, 2016. Citation on page 103.

COSTA, L. d. F.; JR, O. N. O.; TRAVIESO, G.; RODRIGUES, F. A.; BOAS, P. R. V.; ANTIQUEIRA, L.; VIANA, M. P.; ROCHA, L. E. C. Analyzing and modeling real-world phenomena with complex networks: a survey of applications. **Advances in Physics**, Taylor & Francis, v. 60, n. 3, p. 329–412, 2011. Citation on page 15.

COSTA, L. d. F.; RODRIGUES, F. A.; TRAVIESO, G.; BOAS, P. R. V. Characterization of complex networks: A survey of measurements. **Advances in Physics**, Taylor & Francis, v. 56, n. 1, p. 167–242, 2007. Citation on page 15.

COVER, T. M.; THOMAS, J. A. *et al.* Entropy, relative entropy and mutual information. **Elements of information theory**, v. 2, n. 1, p. 12–13, 1991. Citation on page 29.

DAVID, O.; KIEBEL, S. J.; HARRISON, L. M.; MATTOUT, J.; KILNER, J. M.; FRISTON, K. J. Dynamic causal modeling of evoked responses in eeg and meg. **NeuroImage**, Elsevier, v. 30, n. 4, p. 1255–1272, 2006. Citation on page 25.

DILUCA, M.; OLESEN, J. The cost of brain diseases: a burden or a challenge? **Neuron**, Elsevier, v. 82, n. 6, p. 1205–1208, 2014. Citation on page 23.

DIMITRIADIS, S. I.; SIMOS, P. G.; FLETCHER, J. M.; PAPANICOLAOU, A. C. Aberrant resting-state functional brain networks in dyslexia: Symbolic mutual information analysis of neuromagnetic signals. **International Journal of Psychophysiology**, Elsevier, v. 126, p. 20–29, 2018. Citation on page 30.

DING, M.; BRESSLER, S. L.; YANG, W.; LIANG, H. Short-window spectral analysis of cortical event-related potentials by adaptive multivariate autoregressive modeling: data preprocessing, model validation, and variability assessment. **Biological cybernetics**, Springer, v. 83, p. 35–45, 2000. Citation on page 31.

DING, M.; CHEN, Y.; BRESSLER, S. L. Granger causality: basic theory and application to neuroscience. **Handbook of time series analysis: recent theoretical developments and applications**, Wiley Online Library, p. 437–460, 2006. Citation on page 16.

DU, Y.; FU, Z.; CALHOUN, V. D. Classification and prediction of brain disorders using functional connectivity: promising but challenging. **Frontiers in neuroscience**, Frontiers Media SA, v. 12, p. 525, 2018. Citations on pages 17, 36, 65, and 66.

DUDA, M.; HABER, N.; DANIELS, J.; WALL, D. Crowdsourced validation of a machine-learning classification system for autism and adhd. **Translational psychiatry**, Nature Publishing Group, v. 7, n. 5, p. e1133–e1133, 2017. Citation on page 65.

DUDA, M.; MA, R.; HABER, N.; WALL, D. Use of machine learning for behavioral distinction of autism and adhd. **Translational psychiatry**, Nature Publishing Group, v. 6, n. 2, p. e732–e732, 2016. Citation on page 65.

EGUILUZ, V. M.; CHIALVO, D. R.; CECCHI, G. A.; BALIKI, M.; APKARIAN, A. V. Scale-free brain functional networks. **Physical review letters**, APS, v. 94, n. 1, p. 018102, 2005. Citations on pages 25 and 167.

ELAHIAN, B.; YEASIN, M.; MUDIGOUDAR, B.; WHELESS, J. W.; BABAJANI-FEREMI, A. Identifying seizure onset zone from electrocorticographic recordings: a machine learning approach based on phase locking value. **Seizure**, Elsevier, v. 51, p. 35–42, 2017. Citation on page 33.

ELDRIDGE, J.; LANE, A. E.; BELKIN, M.; DENNIS, S. Robust features for the automatic identification of autism spectrum disorder in children. **Journal of neurodevelopmental disorders**, Springer, v. 6, p. 1–12, 2014. Citation on page 104.

EROGLU, D.; TANZI, M.; STRIEN, S. van; PEREIRA, T. Effective networks: a model to predict network structure and critical transitions from datasets. **arXiv preprint arXiv:1907.02416**, 2019. Citation on page 21.

____. Revealing dynamics, communities, and criticality from data. **Physical Review X**, APS, v. 10, n. 2, p. 021047, 2020. Citation on page 22.

ESLAMI, T.; ALMUQHIM, F.; RAIKER, J. S.; SAEED, F. Machine learning methods for diagnosing autism spectrum disorder and attention-deficit/hyperactivity disorder using functional and structural mri: a survey. **Frontiers in neuroinformatics**, Frontiers Media SA, v. 14, p. 575999, 2021. Citations on pages 65 and 66.

FOMBONNE, E. Epidemiology of pervasive developmental disorders. **Pediatric research**, Nature Publishing Group, v. 65, n. 6, p. 591–598, 2009. Citation on page 103.

FORNITO, A.; YOON, J.; ZALESKY, A.; BULLMORE, E. T.; CARTER, C. S. General and specific functional connectivity disturbances in first-episode schizophrenia during cognitive control performance. **Biological psychiatry**, Elsevier, v. 70, n. 1, p. 64–72, 2011. Citation on page 17.

FORNITO, A.; ZALESKY, A.; BREAKSPEAR, M. The connectomics of brain disorders. **Nature Reviews Neuroscience**, Nature Publishing Group UK London, v. 16, n. 3, p. 159–172, 2015. Citation on page 22.

Chapter 1 - an introduction to brain networks. In: FORNITO, A.; ZALESKY, A.; BULLMORE, E. T. (Ed.). **Fundamentals of Brain Network Analysis**. San Diego: Academic Press, 2016. p. 1–35. ISBN 978-0-12-407908-3. Citation on page 27.

Chapter 2 - nodes and edges. In: FORNITO, A.; ZALESKY, A.; BULLMORE, E. T. (Ed.). **Fundamentals of Brain Network Analysis**. San Diego: Academic Press, 2016. p. 37–88. ISBN 978-0-12-407908-3. Citation on page 26.

FREILICH, M. A.; REBOLLEDO, R.; CORCORAN, D.; MARQUET, P. A. Reconstructing ecological networks with noisy dynamics. **Proceedings of the Royal Society A**, The Royal Society Publishing, v. 476, n. 2237, p. 20190739, 2020. Citations on pages 15 and 16.

FRENCH, C. C.; BEAUMONT, J. G. A critical review of eeg coherence studies of hemisphere function. **International Journal of Psychophysiology**, Elsevier, v. 1, n. 3, p. 241–254, 1984. Citation on page 31.

FRISTON, K.; MORAN, R.; SETH, A. K. Analysing connectivity with granger causality and dynamic causal modelling. **Current opinion in neurobiology**, Elsevier, v. 23, n. 2, p. 172–178, 2013. Citations on pages 24, 25, and 35.

FRISTON, K. J. Functional and effective connectivity in neuroimaging: a synthesis. **Human brain mapping**, Wiley Online Library, v. 2, n. 1-2, p. 56–78, 1994. Citations on pages 16, 22, and 24.

FRISTON, K. J.; HARRISON, L.; PENNY, W. Dynamic causal modelling. **Neuroimage**, Elsevier, v. 19, n. 4, p. 1273–1302, 2003. Citations on pages 22 and 25.

FROLOV, N.; HRAMOV, A. Extreme synchronization events in a kuramoto model: The interplay between resource constraints and explosive transitions. **Chaos: An Interdisciplinary Journal of Nonlinear Science**, AIP Publishing, v. 31, n. 6, 2021. Citation on page 24.

FURMAN, D. J.; HAMILTON, J. P.; GOTLIB, I. H. Frontostriatal functional connectivity in major depressive disorder. **Biology of mood & anxiety disorders**, Springer, v. 1, p. 1–11, 2011. Citation on page 17.

GANZETTI, M.; MANTINI, D. Functional connectivity and oscillatory neuronal activity in the resting human brain. **Neuroscience**, Elsevier, v. 240, p. 297–309, 2013. Citation on page 31.

GAO, T.-T.; YAN, G. Data-driven inference of complex system dynamics: A mini-review. **Europhysics Letters**, IOP Publishing, v. 142, n. 1, p. 11001, 2023. Citation on page 22.

GAO, Z.; JIN, N. Complex network from time series based on phase space reconstruction. **Chaos: An Interdisciplinary Journal of Nonlinear Science**, AIP Publishing, v. 19, n. 3, 2009. Citation on page 167.

GHUMAN, A. S.; MCDANIEL, J. R.; MARTIN, A. A wavelet-based method for measuring the oscillatory dynamics of resting-state functional connectivity in meg. **Neuroimage**, Elsevier, v. 56, n. 1, p. 69–77, 2011. Citation on page 33.

GLEREAN, E.; SALMI, J.; LAHNAKOSKI, J. M.; JÄÄSKELÄINEN, I. P.; SAMS, M. Functional magnetic resonance imaging phase synchronization as a measure of dynamic functional connectivity. **Brain connectivity**, Mary Ann Liebert, Inc. 140 Huguenot Street, 3rd Floor New Rochelle, NY 10801 USA, v. 2, n. 2, p. 91–101, 2012. Citation on page 33.

GRANGER, C. W. Investigating causal relations by econometric models and cross-spectral methods. **Econometrica: journal of the Econometric Society**, JSTOR, p. 424–438, 1969. Citations on pages 22 and 34.

GROSS, J.; KUJALA, J.; HÄMÄLÄINEN, M.; TIMMERMANN, L.; SCHNITZLER, A.; SALMELIN, R. Dynamic imaging of coherent sources: studying neural interactions in the human brain. **Proceedings of the National Academy of Sciences**, The National Academy of Sciences, v. 98, n. 2, p. 694–699, 2001. Citation on page 31.

GUPTA, S.; MASTRANTONAS, N.; MASOLLER, C.; KURTHS, J. Perspectives on the importance of complex systems in understanding our climate and climate change—the nobel prize in physics 2021. **Chaos: An Interdisciplinary Journal of Nonlinear Science**, AIP Publishing LLC, v. 32, n. 5, p. 052102, 2022. Citation on page 15.

GYSELS, E.; CELKA, P. Phase synchronization for the recognition of mental tasks in a brain-computer interface. **IEEE Transactions on neural systems and rehabilitation engineering**, IEEE, v. 12, n. 4, p. 406–415, 2004. Citation on page 33.

HAN, X.; SHEN, Z.; WANG, W.-X.; DI, Z. Robust reconstruction of complex networks from sparse data. **Physical review letters**, APS, v. 114, n. 2, p. 028701, 2015. Citation on page 21.

HARIKUMAR, A.; EVANS, D. W.; DOUGHERTY, C. C.; CARPENTER, K. L.; MICHAEL, A. M. A review of the default mode network in autism spectrum disorders and attention deficit hyperactivity disorder. **Brain connectivity**, Mary Ann Liebert, Inc., publishers 140 Huguenot Street, 3rd Floor New . . . , v. 11, n. 4, p. 253–263, 2021. Citations on pages 65 and 66.

HASANZADEH, F.; MOHEBBI, M.; ROSTAMI, R. Graph theory analysis of directed functional brain networks in major depressive disorder based on eeg signal. **Journal of neural engineering**, IOP Publishing, v. 17, n. 2, p. 026010, 2020. Citation on page 41.

HE, Y.; WANG, J.; WANG, L.; CHEN, Z. J.; YAN, C.; YANG, H.; TANG, H.; ZHU, C.; GONG, Q.; ZANG, Y. *et al.* Uncovering intrinsic modular organization of spontaneous brain activity in humans. **PloS one**, Public Library of Science San Francisco, USA, v. 4, n. 4, p. e5226, 2009. Citation on page 37.

HERRGÅRD, M. J.; SWAINSTON, N.; DOBSON, P.; DUNN, W. B.; ARGA, K. Y.; ARVAS, M.; BLÜTHGEN, N.; BORGER, S.; COSTENOBLE, R.; HEINEMANN, M. *et al.* A consensus yeast metabolic network reconstruction obtained from a community approach to systems biology. **Nature biotechnology**, Nature Publishing Group US New York, v. 26, n. 10, p. 1155–1160, 2008. Citation on page 21.

HEUVEL, M. P. V. D.; POL, H. E. H. Exploring the brain network: a review on resting-state fmri functional connectivity. **European neuropsychopharmacology**, Elsevier, v. 20, n. 8, p. 519–534, 2010. Citation on page 37.

HEUVEL, M. P. V. D.; SPORNS, O. Rich-club organization of the human connectome. **Journal of Neuroscience**, Soc Neuroscience, v. 31, n. 44, p. 15775–15786, 2011. Citation on page 25.

HEUVEL, M. P. V. D.; SPORNS, O.; COLLIN, G.; SCHEEWE, T.; MANDL, R. C.; CAHN, W.; GOÑI, J.; POL, H. E. H.; KAHN, R. S. Abnormal rich club organization and functional brain dynamics in schizophrenia. **JAMA psychiatry**, v. 70, n. 8, 2013. Citation on page 17.

HEUVEL, M. P. van den; SPORNS, O. A cross-disorder connectome landscape of brain dysconnectivity. **Nature reviews neuroscience**, Nature Publishing Group UK London, v. 20, n. 7, p. 435–446, 2019. Citation on page 17.

HRAMOV, A. E.; FROLOV, N. S.; MAKSIMENKO, V. A.; KURKIN, S. A.; KAZANTSEV, V. B.; PISARCHIK, A. N. Functional networks of the brain: from connectivity restoration to dynamic integration. **Physics-Uspekhi**, IOP Publishing, v. 64, n. 6, p. 584, 2021. Citations on pages 27 and 29.

IOANNIDES, A.; LIU, L.; KWAPIEN, J.; DROZDZ, S.; STREIT, M. Coupling of regional activations in a human brain during an object and face affect recognition task. **Human brain mapping**, Wiley Online Library, v. 11, n. 2, p. 77–92, 2000. Citation on page 29.

JEONG, J.; GORE, J. C.; PETERSON, B. S. Mutual information analysis of the eeg in patients with alzheimer's disease. **Clinical neurophysiology**, Elsevier, v. 112, n. 5, p. 827–835, 2001. Citation on page 31.

JIANG, D.; WANG, W.; SHI, L.; SONG, H. A compressive sensing-based approach to end-to-end network traffic reconstruction. **IEEE Transactions on Network Science and Engineering**, IEEE, v. 7, n. 1, p. 507–519, 2018. Citation on page 21.

JO, T.; NHO, K.; SAYKIN, A. J. Deep learning in alzheimer's disease: diagnostic classification and prognostic prediction using neuroimaging data. **Frontiers in aging neuroscience**, Frontiers Media SA, v. 11, p. 220, 2019. Citation on page 38.

KAIDERY, N. A.; TARANNUM, S.; THOMAS, B. Epigenetic landscape of parkinson's disease: emerging role in disease mechanisms and therapeutic modalities. **Neurotherapeutics**, Elsevier, v. 10, n. 4, p. 698–708, 2013. Citation on page 145.

KAISER, R. H.; ANDREWS-HANNA, J. R.; WAGER, T. D.; PIZZAGALLI, D. A. Large-scale network dysfunction in major depressive disorder: a meta-analysis of resting-state functional connectivity. **JAMA psychiatry**, American Medical Association, v. 72, n. 6, p. 603–611, 2015. Citation on page 17.

KANA, R. K.; LIBERO, L. E.; MOORE, M. S. Disrupted cortical connectivity theory as an explanatory model for autism spectrum disorders. **Physics of life reviews**, Elsevier, v. 8, n. 4, p. 410–437, 2011. Citation on page 17.

KHARE, S. K.; BAJAJ, V.; ACHARYA, U. R. Detection of parkinson's disease using automated tunable q wavelet transform technique with eeg signals. **Biocybernetics and Biomedical Engineering**, Elsevier, v. 41, n. 2, p. 679–689, 2021. Citation on page 145.

KILZHEIMER, A.; HENTRICH, T.; BURKHARDT, S.; SCHULZE-HENTRICH, J. M. The challenge and opportunity to diagnose parkinson's disease in midlife. **Frontiers in Neurology**, Frontiers Media SA, v. 10, p. 1328, 2019. Citation on page 145.

KLIN, A.; MCPARTLAND, J.; VOLKMAR, F. R. Asperger syndrome. **Handbook of autism and pervasive developmental disorders**, Wiley Online Library, v. 1, p. 88–125, 2005. Citation on page 103.

KOK, F. M.; GROEN, Y.; BECKE, M.; FUERMAIER, A. B.; TUCHA, O. Self-reported empathy in adult women with autism spectrum disorders–a systematic mini review. **PloS one**, Public Library of Science San Francisco, CA USA, v. 11, n. 3, p. e0151568, 2016. Citation on page 103.

KOLAPPA, K.; SEEHER, K.; DUA, T. **Brain health as a global priority**. [S.l.]: Elsevier, 2022. 120326 p. Citation on page 23.

LACHAUX, J.-P.; RODRIGUEZ, E.; MARTINERIE, J.; VARELA, F. J. Measuring phase synchrony in brain signals. **Human brain mapping**, Wiley Online Library, v. 8, n. 4, p. 194–208, 1999. Citations on pages 32 and 33.

LAI, M.; DEMURU, M.; HILLEBRAND, A.; FRASCHINI, M. A comparison between scalp-and source-reconstructed eeg networks. **Scientific reports**, Nature Publishing Group UK London, v. 8, n. 1, p. 12269, 2018. Citation on page 167.

LEE, H.; LEE, D. S.; KANG, H.; KIM, B.-N.; CHUNG, M. K. Sparse brain network recovery under compressed sensing. **IEEE Transactions on Medical Imaging**, IEEE, v. 30, n. 5, p. 1154–1165, 2011. Citations on pages 25 and 28.

LEISTEDT, S. J.; COUMANS, N.; DUMONT, M.; LANQUART, J.-P.; STAM, C. J.; LINKOWSKI, P. Altered sleep brain functional connectivity in acutely depressed patients. **Human brain mapping**, Wiley Online Library, v. 30, n. 7, p. 2207–2219, 2009. Citation on page 38.

LEISTEDT, S. J.; LINKOWSKI, P. Brain, networks, depression, and more. **European neuropsychopharmacology**, Elsevier, v. 23, n. 1, p. 55–62, 2013. Citation on page 38.

LI, X.; ZHANG, X.; ZHU, J.; MAO, W.; SUN, S.; WANG, Z.; XIA, C.; HU, B. Depression recognition using machine learning methods with different feature generation strategies. **Artificial intelligence in medicine**, Elsevier, v. 99, p. 101696, 2019. Citation on page 41.

LI, Y.; SHEN, M.; STOCKTON, M. E.; ZHAO, X. Hippocampal deficits in neurodevelopmental disorders. **Neurobiology of learning and memory**, Elsevier, v. 165, p. 106945, 2019. Citation on page 65.

LIANG, K.-C.; WANG, X. Gene regulatory network reconstruction using conditional mutual information. **EURASIP Journal on Bioinformatics and Systems Biology**, Springer, v. 2008, p. 1–14, 2008. Citation on page 167.

LIANG, X.; WANG, J.; YAN, C.; SHU, N.; XU, K.; GONG, G.; HE, Y. Effects of different correlation metrics and preprocessing factors on small-world brain functional networks: a resting-state functional mri study. **PloS one**, Public Library of Science San Francisco, USA, v. 7, n. 3, p. e32766, 2012. Citation on page 27.

LIU, J.; LI, M.; PAN, Y.; LAN, W.; ZHENG, R.; WU, F.-X.; WANG, J. *et al.* Complex brain network analysis and its applications to brain disorders: a survey. **Complexity**, Hindawi, v. 2017, 2017. Citation on page 37.

LIZIER, J. T.; HEINZLE, J.; HORSTMANN, A.; HAYNES, J.-D.; PROKOPENKO, M. Multivariate information-theoretic measures reveal directed information structure and task relevant changes in fmri connectivity. **Journal of computational neuroscience**, Springer, v. 30, p. 85–107, 2011. Citation on page 36.

LOH, H. W.; OOI, C. P.; PALMER, E.; BARUA, P. D.; DOGAN, S.; TUNCER, T.; BAYGIN, M.; ACHARYA, U. R. Gaborpdnet: Gabor transformation and deep neural network for parkinson's disease detection using eeg signals. **Electronics**, MDPI, v. 10, n. 14, p. 1740, 2021. Citation on page 145.

LORD, C.; ELSABBAGH, M.; BAIRD, G.; VEENSTRA-VANDERWEELE, J. Autism spectrum disorder. **The lancet**, Elsevier, v. 392, n. 10146, p. 508–520, 2018. Citation on page 65.

LOWET, E.; ROBERTS, M. J.; BONIZZI, P.; KAREL, J.; WEERD, P. D. Quantifying neural oscillatory synchronization: a comparison between spectral coherence and phase-locking value approaches. **PloS one**, Public Library of Science San Francisco, CA USA, v. 11, n. 1, p. e0146443, 2016. Citation on page 33.

LÜ, L.; ZHOU, T. Link prediction in complex networks: A survey. **Physica A: statistical mechanics and its applications**, Elsevier, v. 390, n. 6, p. 1150–1170, 2011. Citation on page 16.

LUI, S.; WU, Q.; QIU, L.; YANG, X.; KUANG, W.; CHAN, R. C.; HUANG, X.; KEMP, G. J.; MECHELLI, A.; GONG, Q. Resting-state functional connectivity in treatment-resistant depression. **American Journal of Psychiatry**, American Psychiatric Publishing Arlington, VA, v. 168, n. 6, p. 642–648, 2011. Citation on page 17.

LUNDBERG, S. A unified approach to interpreting model predictions. **arXiv preprint arXiv:1705.07874**, 2017. Citation on page 146.

LYNN, C. W.; BASSETT, D. S. The physics of brain network structure, function and control. **Nature Reviews Physics**, Nature Publishing Group UK London, v. 1, n. 5, p. 318–332, 2019. Citations on pages 25, 27, 34, and 36.

MA, C.; CHEN, H.-S.; LAI, Y.-C.; ZHANG, H.-F. Statistical inference approach to structural reconstruction of complex networks from binary time series. **Physical Review E**, APS, v. 97, n. 2, p. 022301, 2018. Citation on page 167.

MAHATO, S.; PAUL, S. Classification of depression patients and normal subjects based on electroencephalogram (eeg) signal using alpha power and theta asymmetry. **Journal of medical systems**, Springer, v. 44, p. 1–8, 2020. Citation on page 41.

MAHONE, E. M.; WARSCHAUSKY, S.; ZABEL, T. A. Introduction to the jins special issue: Neurodevelopmental disorders. **Journal of the International Neuropsychological Society**, Cambridge University Press, v. 24, n. 9, p. 893–895, 2018. Citation on page 65.

MAJDANDZIC, A.; PODOBNIK, B.; BULDYREV, S. V.; KENETT, D. Y.; HAVLIN, S.; STANLEY, H. E. Spontaneous recovery in dynamical networks. **Nature Physics**, Nature Publishing Group UK London, v. 10, n. 1, p. 34–38, 2014. Citation on page 21.

MARCOT, B. G.; PENMAN, T. D. Advances in bayesian network modelling: Integration of modelling technologies. **Environmental modelling & software**, Elsevier, v. 111, p. 386–393, 2019. Citation on page 22.

MARZETTI, L.; BASTI, A.; CHELLA, F.; D'ANDREA, A.; SYRJÄLÄ, J.; PIZZELLA, V. Brain functional connectivity through phase coupling of neuronal oscillations: a perspective from magnetoencephalography. **Frontiers in neuroscience**, Frontiers Media SA, v. 13, p. 964, 2019. Citation on page 33.

MCGRATH, J. J.; AL-HAMZAWI, A.; ALONSO, J.; ALTWAIJRI, Y.; ANDRADE, L. H.; BROMET, E. J.; BRUFFAERTS, R.; ALMEIDA, J. M. C. de; CHARDOUL, S.; CHIU, W. T. *et al.* Age of onset and cumulative risk of mental disorders: a cross-national analysis of population surveys from 29 countries. **The Lancet Psychiatry**, Elsevier, v. 10, n. 9, p. 668–681, 2023. Citation on page 16.

MEDAGLIA, J. D.; LYNALL, M.-E.; BASSETT, D. S. Cognitive network neuroscience. **Journal of cognitive neuroscience**, MIT Press One Rogers Street, Cambridge, MA 02142-1209, USA journals-info . . . , v. 27, n. 8, p. 1471–1491, 2015. Citation on page 27.

MENG, C.; BRANDL, F.; TAHMASIAN, M.; SHAO, J.; MANOLIU, A.; SCHERR, M.; SCHWERTHÖFFER, D.; BÄUML, J.; FÖRSTL, H.; ZIMMER, C. *et al.* Aberrant topology of striatum's connectivity is associated with the number of episodes in depression. **Brain**, Oxford University Press, v. 137, n. 2, p. 598–609, 2014. Citation on page 38.

MENG, C.; JIANG, X. S.; WEI, X. M. Scrn: A complex network reconstruction method based on multiple time series. **Journal of Circuits, Systems and Computers**, World Scientific, v. 29, n. 13, p. 2050213, 2020. Citation on page 21.

MICHELOYANNIS, S.; PACHOU, E.; STAM, C. J.; BREAKSPEAR, M.; BITSIOS, P.; VOURKAS, M.; ERIMAKI, S.; ZERVAKIS, M. Small-world networks and disturbed functional connectivity in schizophrenia. **Schizophrenia research**, Elsevier, v. 87, n. 1-3, p. 60–66, 2006. Citation on page 37.

MIGUEL, M. S.; JOHNSON, J. H.; KERTESZ, J.; KASKI, K.; DÍAZ-GUILERA, A.; MACKAY, R. S.; LORETO, V.; ERDI, P.; HELBING, D. Challenges in complex systems science. **The European Physical Journal Special Topics**, Springer, v. 214, n. 1, p. 245–271, 2012. Citations on pages 15 and 16.

MIJALKOV, M.; PEREIRA, J. B.; VOLPE, G. Delayed correlations improve the reconstruction of the brain connectome. **PloS one**, Public Library of Science San Francisco, CA USA, v. 15, n. 2, p. e0228334, 2020. Citation on page 25.

MORIDIAN, P.; GHASSEMI, N.; JAFARI, M.; SALLOUM-ASFAR, S.; SADEGHI, D.; KHODATARS, M.; SHOEIBI, A.; KHOSRAVI, A.; LING, S. H.; SUBASI, A. *et al.* Automatic autism spectrum disorder detection using artificial intelligence methods with mri neuroimaging: A review. **Frontiers in Molecular Neuroscience**, Frontiers Media SA, v. 15, p. 999605, 2022. Citations on pages 65 and 66.

MORMANN, F.; LEHNERTZ, K.; DAVID, P.; ELGER, C. E. Mean phase coherence as a measure for phase synchronization and its application to the eeg of epilepsy patients. **Physica D: Nonlinear Phenomena**, Elsevier, v. 144, n. 3-4, p. 358–369, 2000. Citation on page 32.

MOVAHED, R. A.; JAHROMI, G. P.; SHAHYAD, S.; MEFTAHI, G. H. A major depressive disorder classification framework based on eeg signals using statistical, spectral, wavelet, functional connectivity, and nonlinear analysis. **Journal of Neuroscience Methods**, Elsevier, v. 358, p. 109209, 2021. Citation on page 41.

MÜLLER-NEDEBOCK, A. C.; DEKKER, M. C.; FARRER, M. J.; HATTORI, N.; LIM, S.-Y.; MELLICK, G. D.; REKTOROVÁ, I.; SALAMA, M.; SCHUH, A. F.; STOESSL, A. J. *et al.* Different pieces of the same puzzle: a multifaceted perspective on the complex biological basis of parkinson's disease. **npj Parkinson's Disease**, Nature Publishing Group UK London, v. 9, n. 1, p. 110, 2023. Citation on page 145.

MUNGO, L.; BRINTRUP, A.; GARLASCHELLI, D.; LAFOND, F. Reconstructing supply networks. **Journal of Physics: Complexity**, IOP Publishing, v. 5, n. 1, p. 012001, 2024. Citation on page 16.

MYERS, L.; SIROIS, M. J. Spearman correlation coefficients, differences between. **Encyclopedia of statistical sciences**, Wiley Online Library, v. 12, 2004. Citation on page 28.

MYSZCZYNSKA, M. A.; OJAMIES, P. N.; LACOSTE, A. M.; NEIL, D.; SAFFARI, A.; MEAD, R.; HAUTBERGUE, G. M.; HOLBROOK, J. D.; FERRAIUOLO, L. Applications of machine learning to diagnosis and treatment of neurodegenerative diseases. **Nature Reviews Neurology**, Nature Publishing Group UK London, v. 16, n. 8, p. 440–456, 2020. Citation on page 39.

NA, S. H.; JIN, S.-H.; KIM, S. Y.; HAM, B.-J. Eeg in schizophrenic patients: mutual information analysis. **Clinical Neurophysiology**, Elsevier, v. 113, n. 12, p. 1954–1960, 2002. Citations on pages 29 and 30.

NATU, M.; BACHUTE, M.; GITE, S.; KOTECHA, K.; VIDYARTHI, A. *et al.* Review on epileptic seizure prediction: machine learning and deep learning approaches. **Computational and Mathematical Methods in Medicine**, Hindawi, v. 2022, 2022. Citation on page 39.

NEWMAN, M. E. The structure and function of complex networks. **SIAM review**, SIAM, v. 45, n. 2, p. 167–256, 2003. Citation on page 21.

NOBAKHSH, B.; SHALBAF, A.; ROSTAMI, R.; KAZEMI, R. Graph-based analysis to predict repetitive transcranial magnetic stimulation treatment response in patients with major depressive disorder using eeg signals. **Basic and Clinical Neuroscience**, Basic and Clinical Neuroscience, v. 15, n. 2, p. 199–210, 2024. Citation on page 41.

NOGAY, H. S.; ADELI, H. Machine learning (ml) for the diagnosis of autism spectrum disorder (asd) using brain imaging. **Reviews in the Neurosciences**, De Gruyter, v. 31, n. 8, p. 825–841, 2020. Citations on pages 65 and 66.

NOLTE, G.; BAI, O.; WHEATON, L.; MARI, Z.; VORBACH, S.; HALLETT, M. Identifying true brain interaction from eeg data using the imaginary part of coherency. **Clinical neurophysiology**, Elsevier, v. 115, n. 10, p. 2292–2307, 2004. Citation on page 31.

NOVELLI, L.; LIZIER, J. T. Inferring network properties from time series using transfer entropy and mutual information: Validation of multivariate versus bivariate approaches. **Network Neuroscience**, MIT Press One Rogers Street, Cambridge, MA 02142-1209, USA journals-info . . . , v. 5, n. 2, p. 373–404, 2021. Citations on pages 36 and 167.

NUCKOLS, C. C.; NUCKOLS, C. C. The diagnostic and statistical manual of mental disorders,(dsm-5). **Philadelphia: American Psychiatric Association**, 2013. Citation on page 103.

PALLAGROSI, M.; FONZI, L.; PICARDI, A.; BIONDI, M. Association between clinician's subjective experience during patient evaluation and psychiatric diagnosis. **Psychopathology**, S. Karger AG Basel, Switzerland, v. 49, n. 2, p. 83–94, 2016. Citation on page 41.

PALVA, J. M.; PALVA, S.; KAILA, K. Phase synchrony among neuronal oscillations in the human cortex. **Journal of Neuroscience**, Society for Neuroscience, v. 25, n. 15, p. 3962–3972, 2005. Citation on page 33.

PERON, T. K. D.; COSTA, L. da F.; RODRIGUES, F. A. The structure and resilience of financial market networks. **Chaos: An Interdisciplinary Journal of Nonlinear Science**, American Institute of Physics, v. 22, n. 1, p. 013117, 2012. Citation on page 15.

PIKOVSKY, A. S.; ROSENBLUM, M. G.; OSIPOV, G. V.; KURTHS, J. Phase synchronization of chaotic oscillators by external driving. **Physica D: Nonlinear Phenomena**, Elsevier, v. 104, n. 3-4, p. 219–238, 1997. Citation on page 32.

POEWE, W.; SEPPI, K.; TANNER, C. M.; HALLIDAY, G. M.; BRUNDIN, P.; VOLKMANN, J.; SCHRAG, A.-E.; LANG, A. E. Parkinson disease. **Nature reviews Disease primers**, Nature Publishing Group, v. 3, n. 1, p. 1–21, 2017. Citation on page 145.

POSTUMA, R. B.; BERG, D. Prodromal parkinson's disease: the decade past, the decade to come. **Movement disorders**, Wiley Online Library, v. 34, n. 5, p. 665–675, 2019. Citation on page 145.

QIU, L.; LI, J.; ZHONG, L.; FENG, W.; ZHOU, C.; PAN, J. A novel eeg-based parkinson's disease detection model using multiscale convolutional prototype networks. **IEEE Transactions on Instrumentation and Measurement**, IEEE, 2024. Citation on page 145.

RASHID, B.; CALHOUN, V. Towards a brain-based predictome of mental illness. **Human brain mapping**, Wiley Online Library, v. 41, n. 12, p. 3468–3535, 2020. Citations on pages 39, 65, and 66.

RAZA, C.; ANJUM, R. *et al.* Parkinson's disease: Mechanisms, translational models and management strategies. **Life sciences**, Elsevier, v. 226, p. 77–90, 2019. Citation on page 145.

RIZVI, S. Q. A.; WANG, G.; KHAN, A.; HASAN, M. K.; GHAZAL, T. M.; KHAN, A. U. R. Classifying parkinson's disease using resting state electroencephalogram signals and u en-pdnet. **Ieee access**, IEEE, 2023. Citation on page 145.

ROEBROECK, A.; FORMISANO, E.; GOEBEL, R. Mapping directed influence over the brain using granger causality and fmri. **Neuroimage**, Elsevier, v. 25, n. 1, p. 230–242, 2005. Citation on page 35.

ROMMELSE, N. N.; GEURTS, H. M.; FRANKE, B.; BUITELAAR, J. K.; HARTMAN, C. A. A review on cognitive and brain endophenotypes that may be common in autism spectrum disorder and attention-deficit/hyperactivity disorder and facilitate the search for pleiotropic genes. **Neuroscience & Biobehavioral Reviews**, Elsevier, v. 35, n. 6, p. 1363–1396, 2011. Citation on page 65.

ROSENBLUM, M.; PIKOVSKY, A. Inferring connectivity of an oscillatory network via the phase dynamics reconstruction. **Frontiers in network physiology**, Frontiers Media SA, v. 3, p. 1298228, 2023. Citation on page 167.

ROSENBLUM, M. G.; PIKOVSKY, A. S.; KURTHS, J. Phase synchronization of chaotic oscillators. **Physical review letters**, APS, v. 76, n. 11, p. 1804, 1996. Citation on page 32.

RUBIDO, N.; MARTÍ, A. C.; BIANCO-MARTÍNEZ, E.; GREBOGI, C.; BAPTISTA, M. S.; MASOLLER, C. Exact detection of direct links in networks of interacting dynamical units. **New Journal of Physics**, IOP Publishing, v. 16, n. 9, p. 093010, 2014. Citations on pages 22 and 23.

RUBINOV, M.; KNOCK, S. A.; STAM, C. J.; MICHELOYANNIS, S.; HARRIS, A. W.; WILLIAMS, L. M.; BREAKSPEAR, M. Small-world properties of nonlinear brain activity in schizophrenia. **Human brain mapping**, Wiley Online Library, v. 30, n. 2, p. 403–416, 2009. Citation on page 37.

RUBINOV, M.; SPORNS, O. Complex network measures of brain connectivity: uses and interpretations. **Neuroimage**, Elsevier, v. 52, n. 3, p. 1059–1069, 2010. Citations on pages 25 and 36.

RUNGE, J. Causal network reconstruction from time series: From theoretical assumptions to practical estimation. **Chaos: An Interdisciplinary Journal of Nonlinear Science**, AIP Publishing, v. 28, n. 7, 2018. Citation on page 167.

SAEEDI, M.; SAEEDI, A.; MAGHSOUDI, A. Major depressive disorder assessment via enhanced k-nearest neighbor method and eeg signals. **Physical and Engineering Sciences in Medicine**, Springer, v. 43, p. 1007–1018, 2020. Citation on page 41.

SAKKALIS, V. Review of advanced techniques for the estimation of brain connectivity measured with eeg/meg. **Computers in biology and medicine**, Elsevier, v. 41, n. 12, p. 1110–1117, 2011. Citation on page 32.

SAKKALIS, V.; GIURCANEANU, C. D.; XANTHOPOULOS, P.; ZERVAKIS, M. E.; TSIARAS, V.; YANG, Y.; KARAKONSTANTAKI, E.; MICHELOYANNIS, S. Assessment of linear and nonlinear synchronization measures for analyzing eeg in a mild epileptic paradigm. **IEEE Transactions on Information Technology in Biomedicine**, IEEE, v. 13, n. 4, p. 433–441, 2008. Citation on page 33.

SAUSENG, P.; KLIMESCH, W. What does phase information of oscillatory brain activity tell us about cognitive processes? **Neuroscience & Biobehavioral Reviews**, Elsevier, v. 32, n. 5, p. 1001–1013, 2008. Citation on page 33.

SAVVA, A. D.; MITSIS, G. D.; MATSOPOULOS, G. K. Assessment of dynamic functional connectivity in resting-state fmri using the sliding window technique. **Brain and behavior**, Wiley Online Library, v. 9, n. 4, p. e01255, 2019. Citation on page 31.

SCHAPIRA, A. H.; CHAUDHURI, K. R.; JENNER, P. Non-motor features of parkinson disease. **Nature Reviews Neuroscience**, Nature Publishing Group UK London, v. 18, n. 7, p. 435–450, 2017. Citation on page 145.

SCHMIDT, B. T.; GHUMAN, A. S.; HUPPERT, T. J. Whole brain functional connectivity using phase locking measures of resting state magnetoencephalography. **Frontiers in neuroscience**, Frontiers Media SA, v. 8, p. 141, 2014. Citations on pages 33 and 167.

SCHREIBER, T. Measuring information transfer. **Physical review letters**, APS, v. 85, n. 2, p. 461, 2000. Citations on pages 22, 35, and 36.

SHANDILYA, S. G.; TIMME, M. Inferring network topology from complex dynamics. **New Journal of Physics**, IOP Publishing, v. 13, n. 1, p. 013004, 2011. Citation on page 167.

SHANNON, C. E. A mathematical theory of communication. **The Bell system technical journal**, Nokia Bell Labs, v. 27, n. 3, p. 379–423, 1948. Citation on page 29.

SHEN, Z.; WANG, W.-X.; FAN, Y.; DI, Z.; LAI, Y.-C. Reconstructing propagation networks with natural diversity and identifying hidden sources. **Nature communications**, Nature Publishing Group UK London, v. 5, n. 1, p. 4323, 2014. Citation on page 16.

SIMONOFF, E.; PICKLES, A.; CHARMAN, T.; CHANDLER, S.; LOUCAS, T.; BAIRD, G. Psychiatric disorders in children with autism spectrum disorders: prevalence, comorbidity, and associated factors in a population-derived sample. **Journal of the American Academy of Child & Adolescent Psychiatry**, Elsevier, v. 47, n. 8, p. 921–929, 2008. Citation on page 65.

SINGH, M. K.; KESLER, S. R.; HOSSEINI, S. H.; KELLEY, R. G.; AMATYA, D.; HAMILTON, J. P.; CHEN, M. C.; GOTLIB, I. H. Anomalous gray matter structural networks in major depressive disorder. **Biological psychiatry**, Elsevier, v. 74, n. 10, p. 777–785, 2013. Citation on page 38.

SIULY, S.; ZHANG, Y. Medical big data: neurological diseases diagnosis through medical data analysis. **Data Science and Engineering**, Springer, v. 1, p. 54–64, 2016. Citation on page 24.

SPEARMAN, C. The proof and measurement of association between two things. Appleton-Century-Crofts, 1961. Citation on page 28.

SPORNS, O. The human connectome: origins and challenges. **Neuroimage**, Elsevier, v. 80, p. 53–61, 2013. Citation on page 24.

____. Structure and function of complex brain networks. **Dialogues in clinical neuroscience**, Taylor & Francis, 2022. Citation on page 36.

SPORNS, O.; TONONI, G. Structural determinants of functional brain dynamics. **Handbook of Brain Connectivity**, Springer Berlin, p. 117–148, 2007. Citations on pages 24 and 25.

SRINIVASAN, R.; WINTER, W. R.; DING, J.; NUNEZ, P. L. Eeg and meg coherence: measures of functional connectivity at distinct spatial scales of neocortical dynamics. **Journal of neuroscience methods**, Elsevier, v. 166, n. 1, p. 41–52, 2007. Citation on page 31.

STAM, C. Use of magnetoencephalography (meg) to study functional brain networks in neurodegenerative disorders. **Journal of the neurological sciences**, Elsevier, v. 289, n. 1-2, p. 128–134, 2010. Citations on pages 25 and 26.

STAM, C. J. From synchronisation to networks: Assessment of functional connectivity in the brain. **Coordinated Activity in the Brain: Measurements and Relevance to Brain Function and Behavior**, Springer, p. 91–115, 2009. Citation on page 167.

____. Modern network science of neurological disorders. **Nature Reviews Neuroscience**, Nature Publishing Group UK London, v. 15, n. 10, p. 683–695, 2014. Citation on page 16.

STAM, C. J.; REIJNEVELD, J. C. Graph theoretical analysis of complex networks in the brain. **Nonlinear biomedical physics**, Springer, v. 1, p. 1–19, 2007. Citation on page 36.

STAM, C. v.; STRAATEN, E. V. The organization of physiological brain networks. **Clinical neurophysiology**, Elsevier, v. 123, n. 6, p. 1067–1087, 2012. Citation on page 36.

STROGATZ, S. H. Exploring complex networks. **nature**, Nature Publishing Group UK London, v. 410, n. 6825, p. 268–276, 2001. Citations on pages 16 and 21.

SU, C.; XU, Z.; PATHAK, J.; WANG, F. Deep learning in mental health outcome research: a scoping review. **Translational Psychiatry**, Nature Publishing Group UK London, v. 10, n. 1, p. 116, 2020. Citation on page 39.

SUBRAMANIAN, I.; MATHUR, S.; OOSTERBAAN, A.; FLANAGAN, R.; KEENER, A. M.; MORO, E. Unmet needs of women living with parkinson's disease: gaps and controversies. **Movement Disorders**, Wiley Online Library, v. 37, n. 3, p. 444–455, 2022. Citation on page 145.

SUN, S.; LI, X.; ZHU, J.; WANG, Y.; LA, R.; ZHANG, X.; WEI, L.; HU, B. Graph theory analysis of functional connectivity in major depression disorder with high-density resting state eeg data. **IEEE Transactions on Neural Systems and Rehabilitation Engineering**, IEEE, v. 27, n. 3, p. 429–439, 2019. Citation on page 41.

TASS, P.; ROSENBLUM, M.; WEULE, J.; KURTHS, J.; PIKOVSKY, A.; VOLKMANN, J.; SCHNITZLER, A.; FREUND, H.-J. Detection of n: m phase locking from noisy data: application to magnetoencephalography. **Physical review letters**, APS, v. 81, n. 15, p. 3291, 1998. Citation on page 32.

THAPA, R.; GARIKIPATI, A.; CIOBANU, M.; SINGH, N.; BROWNING, E.; DECURZIO, J.; BARNES, G.; DINENNO, F.; MAO, Q.; DAS, R. Machine learning differentiation of autism spectrum sub-classifications. **Journal of Autism and Developmental Disorders**, Springer, v. 54, n. 11, p. 4216–4231, 2024. Citation on page 104.

THAPAR, A.; COOPER, M.; RUTTER, M. Neurodevelopmental disorders. **The Lancet Psychiatry**, Elsevier, v. 4, n. 4, p. 339–346, 2017. Citation on page 65.

THOMPSON, W. H.; FRANSSON, P. The frequency dimension of fmri dynamic connectivity: Network connectivity, functional hubs and integration in the resting brain. **Neuroimage**, Elsevier, v. 121, p. 227–242, 2015. Citation on page 28.

____. The mean–variance relationship reveals two possible strategies for dynamic brain connectivity analysis in fmri. **Frontiers in human neuroscience**, Frontiers Media SA, v. 9, p. 398, 2015. Citation on page 28.

TIMME, M.; CASADIEGO, J. Revealing networks from dynamics: an introduction. **Journal of Physics A: Mathematical and Theoretical**, IOP Publishing, v. 47, n. 34, p. 343001, 2014. Citations on pages 15, 16, 22, and 25.

TIMME, N. M.; LAPISH, C. A tutorial for information theory in neuroscience. **eneuro**, Society for Neuroscience, v. 5, n. 3, 2018. Citations on pages 29 and 30.

TIRABASSI, G.; SEVILLA-ESCOBOZA, R.; BULDÚ, J. M.; MASOLLER, C. Inferring the connectivity of coupled oscillators from time-series statistical similarity analysis. **Scientific reports**, Nature Publishing Group UK London, v. 5, n. 1, p. 10829, 2015. Citation on page 23.

TOWBIN, K. E. Pervasive developmental disorder not otherwise specified. **Handbook of autism and pervasive developmental disorders**, Wiley Online Library, v. 1, p. 165–200, 2005. Citation on page 103.

TSONIS, A. A.; WANG, G.; SWANSON, K. L.; RODRIGUES, F. A.; COSTA, L. d. F. Community structure and dynamics in climate networks. **Climate Dynamics**, Springer, v. 37, n. 5, p. 933–940, 2011. Citation on page 15.

TSUBOI, T.; SATAKE, Y.; HIRAGA, K.; YOKOI, K.; HATTORI, M.; SUZUKI, M.; HARA, K.; RAMIREZ-ZAMORA, A.; OKUN, M. S.; KATSUNO, M. Effects of mao-b inhibitors on non-motor symptoms and quality of life in parkinson's disease: A systematic review. **npj Parkinson's Disease**, Nature Publishing Group UK London, v. 8, n. 1, p. 75, 2022. Citation on page 145.

TURNBULL, L.; HÜTT, M.-T.; IOANNIDES, A. A.; KININMONTH, S.; POEPPL, R.; TOCKNER, K.; BRACKEN, L. J.; KEESSTRA, S.; LIU, L.; MASSELINK, R. *et al.* Connectivity and complex systems: learning from a multi-disciplinary perspective. **Applied Network Science**, SpringerOpen, v. 3, n. 1, p. 1–49, 2018. Citation on page 16.

UDDIN, L. Q.; SUPEKAR, K.; LYNCH, C. J.; KHOUZAM, A.; PHILLIPS, J.; FEINSTEIN, C.; RYALI, S.; MENON, V. Salience network–based classification and prediction of symptom severity in children with autism. **JAMA psychiatry**, American Medical Association, v. 70, n. 8, p. 869–879, 2013. Citation on page 104.

UDDIN, M.; WANG, Y.; WOODBURY-SMITH, M. Artificial intelligence for precision medicine in neurodevelopmental disorders. **NPJ digital medicine**, Nature Publishing Group UK London, v. 2, n. 1, p. 112, 2019. Citation on page 65.

USTA, M. B.; KARABEKIROGLU, K.; SAHIN, B.; AYDIN, M.; BOZKURT, A.; KARAOSMAN, T.; ARAL, A.; COBANOGLU, C.; KURT, A. D.; KESIM, N. *et al.* Use of machine learning methods in prediction of short-term outcome in autism spectrum disorders. **Psychiatry and Clinical Psychopharmacology**, Taylor & Francis, v. 29, n. 3, p. 320–325, 2019. Citation on page 104.

VENKATESH, M.; JAJA, J.; PESSOA, L. Comparing functional connectivity matrices: A geometry-aware approach applied to participant identification. **NeuroImage**, Elsevier, v. 207, p. 116398, 2020. Citation on page 36.

VICENTE, R.; WIBRAL, M.; LINDNER, M.; PIPA, G. Transfer entropy—a model-free measure of effective connectivity for the neurosciences. **Journal of computational neuroscience**, Springer, v. 30, n. 1, p. 45–67, 2011. Citations on pages 34, 35, and 36.

WANG, W.-X.; LAI, Y.-C.; GREBOGI, C. Data based identification and prediction of nonlinear and complex dynamical systems. **Physics Reports**, Elsevier, v. 644, p. 1–76, 2016. Citation on page 21.

WANG, Y. R.; HUANG, H. Review on statistical methods for gene network reconstruction using expression data. **Journal of theoretical biology**, Elsevier, v. 362, p. 53–61, 2014. Citation on page 167.

WANG, Z.; XIN, J.; WANG, Z.; YAO, Y.; ZHAO, Y.; QIAN, W. Brain functional network modeling and analysis based on fmri: a systematic review. **Cognitive neurodynamics**, Springer, v. 15, p. 389–403, 2021. Citations on pages 23, 25, and 26.

WANG, Z.-M.; ZHOU, R.; HE, Y.; GUO, X.-M. Functional integration and separation of brain network based on phase locking value during emotion processing. **IEEE Transactions on Cognitive and Developmental Systems**, IEEE, v. 15, n. 2, p. 444–453, 2020. Citation on page 33.

WASHINGTON, P.; WALL, D. P. A review of and roadmap for data science and machine learning for the neuropsychiatric phenotype of autism. **Annual review of biomedical data science**, Annual Reviews, v. 6, n. 1, p. 211–228, 2023. Citations on pages 65 and 66.

WASS, S. Distortions and disconnections: disrupted brain connectivity in autism. **Brain and cognition**, Elsevier, v. 75, n. 1, p. 18–28, 2011. Citation on page 17.

WATTS, D. J.; STROGATZ, S. H. Collective dynamics of 'small-world'networks. **nature**, Nature Publishing Group, v. 393, n. 6684, p. 440–442, 1998. Citation on page 16.

WEIN, S.; DECO, G.; TOMÉ, A. M.; GOLDHACKER, M.; MALLONI, W. M.; GREENLEE, M. W.; LANG, E. W. Brain connectivity studies on structure-function relationships: A short survey with an emphasis on machine learning. **Computational intelligence and neuroscience**, Hindawi, v. 2021, 2021. Citation on page 25.

WIBRAL, M.; WOLLSTADT, P.; MEYER, U.; PAMPU, N.; PRIESEMANN, V.; VICENTE, R. Revisiting wiener's principle of causality—interaction-delay reconstruction using transfer entropy and multivariate analysis on delay-weighted graphs. In: IEEE. **2012 Annual International Conference of the IEEE Engineering in Medicine and Biology Society**. [S.l.], 2012. p. 3676–3679. Citation on page 35.

WING, L.; GOULD, J.; GILLBERG, C. Autism spectrum disorders in the dsm-v: better or worse than the dsm-iv? **Research in developmental disabilities**, Elsevier, v. 32, n. 2, p. 768–773, 2011. Citation on page 103.

World Health Organization. **Mental Disorders Fact Sheet**. 2023. Accessed: 2025-02-21. Available: <https://www.who.int/news-room/fact-sheets/detail/mental-disorders>. Citation on page 16.

WU, K.; HAO, X.; LIU, J.; LIU, P.; SHEN, F. Online reconstruction of complex networks from streaming data. **IEEE Transactions on Cybernetics**, IEEE, v. 52, n. 6, p. 5136–5147, 2020. Citation on page 167.

XIA, M.; ZHANG, Y.; WU, Y.; WANG, X. An end-to-end deep learning model for eeg-based major depressive disorder classification. **IEEE Access**, IEEE, v. 11, p. 41337–41347, 2023. Citation on page 41.

YAN, Y.; LIU, G.; CAI, H.; WU, E. Q.; CAI, J.; CHEOK, A. D.; LIU, N.; LI, T.; FAN, Z. A review of graph theory-based diagnosis of neurological disorders based on eeg and mri. **Neurocomputing**, Elsevier, p. 128098, 2024. Citation on page 16.

YANG, Y.; YANG, H. Complex network-based time series analysis. **Physica A: Statistical Mechanics and its Applications**, Elsevier, v. 387, n. 5-6, p. 1381–1386, 2008. Citation on page 167.

YIN, Z.; LI, J.; ZHANG, Y.; REN, A.; MENEEN, K. M. V.; HUANG, L. Functional brain network analysis of schizophrenic patients with positive and negative syndrome based on mutual information of eeg time series. **Biomedical Signal Processing and Control**, Elsevier, v. 31, p. 331–338, 2017. Citation on page 30.

YU, R.; QIAO, L.; CHEN, M.; LEE, S.-W.; FEI, X.; SHEN, D. Weighted graph regularized sparse brain network construction for mci identification. **Pattern recognition**, Elsevier, v. 90, p. 220–231, 2019. Citation on page 25.

YUAN, Y.; STAN, G.-B.; WARNICK, S.; GONCALVES, J. Robust dynamical network structure reconstruction. **Automatica**, Elsevier, v. 47, n. 6, p. 1230–1235, 2011. Citation on page 167.

ZALESKY, A.; FORNITO, A.; EGAN, G. F.; PANTELIS, C.; BULLMORE, E. T. The relationship between regional and inter-regional functional connectivity deficits in schizophrenia. **Human brain mapping**, Wiley Online Library, v. 33, n. 11, p. 2535–2549, 2012. Citation on page 27.

ZBILI, M.; RAMA, S. A quick and easy way to estimate entropy and mutual information for neuroscience. **Frontiers in Neuroinformatics**, Frontiers Media SA, v. 15, p. 596443, 2021. Citation on page 30.

ZENG, H. Mesoscale connectomics. **Current opinion in neurobiology**, Elsevier, v. 50, p. 154–162, 2018. Citation on page 24.

ZHANG, B.; YAN, G.; YANG, Z.; SU, Y.; WANG, J.; LEI, T. Brain functional networks based on resting-state eeg data for major depressive disorder analysis and classification. **IEEE Transactions on Neural Systems and Rehabilitation Engineering**, IEEE, v. 29, p. 215–229, 2020. Citation on page 41.

ZHANG, H.-Y.; WANG, S.-J.; LIU, B.; MA, Z.-L.; YANG, M.; ZHANG, Z.-J.; TENG, G.-J. Resting brain connectivity: changes during the progress of alzheimer disease. **Radiology**, Radiological Society of North America, Inc., v. 256, n. 2, p. 598–606, 2010. Citation on page 24.

ZHANG, Y.; PAN, X.; WANG, R.; SAKAGAMI, M. Functional connectivity between prefrontal cortex and striatum estimated by phase locking value. **Cognitive neurodynamics**, Springer, v. 10, p. 245–254, 2016. Citation on page 33.

ZHOU, Q.; XU, Z.; YEN, N. Y. User sentiment analysis based on social network information and its application in consumer reconstruction intention. **Computers in Human Behavior**, Elsevier, v. 100, p. 177–183, 2019. Citation on page 21.


ICMC
USP
SÃO CARLOS